DOT/FAA/PM-87/19

Program Engineering
and Maintenance Service
Washington, D.C. 20591

Design of Overlays for Rigid Airport Pavements

Raymond S. Rollings

Geotechnical Laboratory

DEPARTMENT OF THE ARMY
Waterways Experiment Station
Corps of Engineers
P.O. Box 631, Vicksburg, Miss 39180-0631

April 1988

Final Report

U.S Department of Transportation
Federal Aviation Administration

NOTICE

This document is disseminated under the sponsorship of the US Department of Transportation in the interest of information exchange. The United States Government assumes no liability for its contents or use thereof.

The United States Government does not endorse products of manufacturers. Trade or manufacturers' names appear herein solely because they are considered essential to the object of this report.

Technical Report Documentation Page

1. Report No.	2. Government Accession No.	3. Recipient's Catalog No.
DOT/FAA/PM-87/19		

4. Title and Subtitle	5. Report Date
DESIGN OF OVERLAYS FOR RIGID AIRPORT PAVEMENTS	April 1988
	6. Performing Organization Code
	8. Performing Organization Report No.
7. Author(s) Raymond S. Rollings	
9. Performing Organization Name and Address US Army Engineer Waterways Experiment Station Geotechnical Laboratory PO Box 631 Vicksburg, MS 39180-0631	10. Work Unit No. (TRAIS) DTFA01-81-Y-10523 11. Contract or Grant No.
12. Sponsoring Agency Name and Address US Department of Transportation Federal Aviation Administration 800 Independence Avenue, SW Washington, DC 20591	13. Type of Report and Period Covered Final Report January 1982 to June 1987 14. Sponsoring Agency Code

15. Supplementary Notes
The US Army Engineer Waterways Experiment Station conducted this study sponsored by the Federal Aviation Administration under Inter-Agency Agreement No. DTFA01-81-Y-10523.

16. Abstract

Existing rigid and flexible overlay pavement design methods are empirical, and they use specified level of cracking or visual deflection as the defined failure condition. The existing empirical designs are based on tests run 30 years ago, and current analytical models provide greatly improved abilities to examine the overlay pavement structure. Emphasis by many agencies on life-cycle cost analysis and more sophisticated maintenance and rehabilitation strategies require methods of predicting pavement performance rather than simply developing safe designs. A layered-elastic analytical model was selected to evaluate stresses from applied loads in the pavement structure. Pavement performance was measured in terms of a structural condition index (SCI) which related the type, degree, and severity of pavement cracking and spalling on a scale of 0 to 100. Models were developed to represent the effect of cracking in base slabs under the overlay, to account for fatigue damage of previous traffic on the base pavement, and to account for the effects of substandard load transfer at slab joints. The predicted performance of rigid overlays and pavements using this analysis was checked against the results of full-scale accelerated traffic tests conducted by the Corps of Engineers and against current overlay design methods and was found to provide reasonable agreement. The design methodology for rigid overlays uses the layered-elastic analytical model and the analysis of fatigue cracking in the base slab to predict rigid overlay deterioration in terms of a SCI. Predictive models for reflective cracking are not currently available so that

(Continued)

17. Key Words		18. Distribution Statement
Concrete fatigue	Pavement	This document is available to the public through the National Technical Information Service, Springfield, Virginia 22161.
Concrete pavements	Pavement design	
Layered elastic analysis	Pavement performance	
Overlays		

19. Security Classif. (of this report)	20. Security Classif. (of this page)	21. No. of Pages	22. Price
Unclassified	Unclassified	267	

Form DOT F 1700.7 (8-72) Reproduction of completed page authorized

16. Abstract (Continued).

application of the methodology to flexible overlays is more limited. The proposed design approach for flexible overlays is to (a) prevent cracking in an uncracked base slab to avoid reflective cracking from base slab cracks, (b) minimize further cracking in an already cracked base slab to reduce future reflective cracking, and (c) check asphalt tensile strain and subgrade vertical strain.

METRIC CONVERSION FACTORS

Approximate Conversions to Metric Measures

Symbol	When You Know	Multiply by	To Find	Symbol
		LENGTH		
mm	millimeters	0.04	inches	in
cm	centimeters	0.4	inches	in
m	meters	3.3	feet	ft
m	meters	1.1	yards	yd
km	kilometers	0.6	miles	mi
		AREA		
cm^2	square centimeters	0.16	square inches	in^2
m^2	square meters	1.2	square yards	yd^2
km^2	square kilometers	0.4	square miles	mi^2
ha	hectares (10,000 m^2)	2.5	acres	
		MASS (weight)		
g	grams	0.036	ounces	oz
kg	kilograms	2.2	pounds	lb
t	tonnes (1000 kg)	1.1	short tons	
		VOLUME		
ml	milliliters	0.03	fluid ounces	fl oz
l	liters	2.1	pints	pt
l	liters	1.06	quarts	qt
l	liters	0.26	gallons	gal
m^3	cubic meters	35	cubic feet	ft^3
m^3	cubic meters	1.3	cubic yards	yd^3
		TEMPERATURE (exact)		
°C	Celsius temperature	9/5 (then add 32)	Fahrenheit temperature	°F

°F: −40, 0, 32, 40, 80, 98.6, 120, 160, 200, 212

°C: −40, −20, 0, 20, 37, 40, 60, 80, 100

Approximate Conversions to Metric Measures

Symbol	When You Know	Multiply by	To Find	Symbol
		LENGTH		
in	inches	* 2.5	centimeters	cm
ft	feet	30	centimeters	cm
yd	yards	0.9	meters	m
mi	miles	1.6	kilometers	km
		AREA		
in^2	square inches	6.5	square centimeters	cm^2
ft^2	square feet	0.09	square meters	m^2
yd^2	square yards	0.8	square meters	m^2
mi^2	square miles	2.6	square kilometers	km^2
	acres	0.4	hectares	ha
		MASS (weight)		
oz	ounces	28	grams	g
lb	pounds	0.45	kilograms	kg
	short tons (2000 lb)	0.9	tonnes	t
		VOLUME		
tsp	teaspoons	5	milliliters	ml
Tbsp	tablespoons	15	milliliters	ml
fl oz	fluid ounces	30	milliliters	ml
c	cups	0.24	liters	l
pt	pints	0.47	liters	l
qt	quarts	0.95	liters	l
gal	gallons	3.8	liters	l
ft^3	cubic feet	0.03	cubic meters	m^3
yd^3	cubic yards	0.76	cubic meters	m^3
		TEMPERATURE (exact)		
°F	Fahrenheit temperature	5/9 after subtracting 32)	Celsius temperature	°C

* 1 in. = 2.54 (exactly). For other exact conversions and more detailed tables see NBS Misc. Publ. 286, Units of Weights and Measures, Price $2.25, SD Catalog No. C13.10:286

PREFACE

This report was sponsored by the US Department of Transportation, Federal Aviation Administration (FAA) under Inter-Agency Agreement No. DTFA01-81-Y-10523, "Update Overlay Thickness Criteria." The fieldwork was performed by the Pavement Systems Division (PSD), Geotechnical Laboratory (GL), US Army Engineer Waterways Experiment Station (WES), Vicksburg, Miss., during the period January 1982 to June 1987. Dr. A. McLaughlin was the FAA Technical Monitor.

This study was conducted under the general supervision of Dr. W. F. Marcuson III, Chief, GL, and Mr. H. H. Ulery, Jr., Chief, PSD. Mr. E. J. Alford, Mr. P. S. McCaffrey, Jr. and Mr. D. D. Mathews, PSD, assisted in conducting the slab tests described in Effective Modulus for Cracked Slabs section. Mr. S. Kohn and Ms. S. Heath, formally with PSD, and Mr. D. Pittman, PSD, assisted in the calculations in the Load Transfer section and Appendixes A and C, and Dr. M. W. Witczak, University of Maryland, provided advice and guidance on this work. Dr. R. S. Rollings, PSD, prepared the report. The report was edited by Ms. Odell F. Allen, Information Products Division, Information Technology Laboratory.

COL Dwayne G. Lee, CE, was the Commander and Director of WES during the preparation and publication of this report. Dr. Robert W. Whalin was Technical Director.

CONTENTS

CONTENTS (Continued)

LIST OF FIGURES

LIST OF TABLES

INTRODUCTION

A design of rigid and flexible concrete overlays to upgrade existing concrete base pavements for airport pavements today use the same techniques that were developed by the US Army Corps of Engineers (CE) over 30 years ago. Although current methods of concrete pavement design have developed into a blend of theory, laboratory investigation, field testing, and modifications based on observed field behavior, overlay design continues to be purely empirical and is based on a limited number of tests conducted during the 1940's and 1950's. The need for rehabilitation of existing pavement facilities is more important than ever before, and continued reliance on an empirical design approach for such a basic rehabilitation technique as pavement overlays needs to be reevaluated.

An analysis of in-service pavements revealed that the current methods of concrete pavement design have proven adequate in the past for selecting new airfield pavement thickness[39,33]. However, similar analysis of in-service overlays comparing their performance with a design method has not been performed. A group of consultants reviewed to the Waterways Experiment Station (WES) the existing CE overlay design method and their review is summarized by Chou[14]. The group identified a number of problems with the current overlay design approach. Inconsistent failure definitions and inadequate empirical equations are major limitations of the design method. Future requirements for life-cycle cost analysis and improved methods for pavement rehabilitation will need an improved mechanistic analysis approach. A review of concrete overlays by Hutchinson[31] also suggested replacing the current empirical approach with a new theoretical design procedure.

Pavement design procedures may either develop a safe design which will not fail under future traffic, or they may attempt to predict future pavement performance. The current concrete pavement and overlay design methods use the safe design approach wherein thicknesses of pavement are selected for some specified design traffic to keep the surface pavement above a predefined failure level in terms of slab cracking. The current approaches have been found to be generally adequate for structural design of new concrete pavements but have been strongly questioned for overlay design.

In recent years numerous Government agencies have placed new emphasis on life-cycle cost analyses, growing pavement rehabilitation requirements, and effective pavement management. This change in emphasis requires design methods capable of predicting pavement performance, and previous safe design approaches are no longer totally satisfactory. Witczak[84] stated that

> However, this approach (safe design approach), while sound for other engineering designs, leads to excessive costs and, furthermore, provides little, if any, ability to predict deterioration and, hence, performance with time. In the author's opinion, this latter concept (design predicting performance) is absolutely mandatory if pavement design is to ever achieve a

'higher step' in rational design concepts. As a result, the overall interaction of initial fracture prediction, rate of crack propagation, subsequent distress-to-performance relationships, and a failure level based upon functional concepts is considered necessary in order to truly define a procedure that can predict future pavement performance.

The need for an improved overlay design method has been noted by a number of investigators including Hutchinson[31] and the WES consultants[14]. Furthermore, this improved method should use a mechanistic approach and be capable of predicting pavement performance rather than simply providing a safe design. The ability to predict performance allows a realistic appraisal of alternate strategies of rehabilitation and maintenance of pavements. The objective of this study is to develop a mechanistically based design procedure for overlays of an existing concrete base pavement. This design procedure will predict deterioration of the pavement as a function of applied traffic. The design procedure for rigid overlays will be developed first and then will be extended to flexible overlays.

APPROACH

This study will evaluate potential analytical models to calculate stresses within the overlay system and select one that best represents the layered structure of the overlay system that can reasonably model the interactions of aircraft loads, pavement geometry, and material properties. Methods of quantitatively measuring the pavement performance will be developed, and predictive performance models compatible with the analytical model will be established. A design methodology will be developed that will use analytically determined stresses to predict the deterioration of the base pavement and overlay under traffic. This design methodology will then be checked against the Corps of Engineers accelerated traffic test sections and design methods to evaluate the approach.

BACKGROUND

CURRENT AIRPORT RIGID PAVEMENT DESIGN

At present, thickness designs for concrete airport pavements use a fatigue analysis. Tensile stresses in the bottom of the slab from a selected design aircraft are calculated and then related to passes of the design aircraft through a fatigue relationship. The most widely used concrete airfield design procedures in the United States were developed originally by the CE[65] and the Portland Cement Association (PCA)[57]. The CE approach is used by the US Army, the US Air Force, and the Federal Aviation Administration (FAA). The PCA approach is used by the US Navy and a number of commercial designers. These two approaches differ primarily in the analytical models and fatigue relationships used, but each individual agency also modifies these basic approaches to reflect its specific needs and experiences.

In order to implement any design approach, the aircraft traffic on the pavement must be analyzed; the real pavement structure and aircraft loads must be idealized so that tensile stresses may be calculated by an analytical model; these stresses must be compared with some fatigue criterion to determine the number of load cycles the pavement can withstand, and the field performance of pavements designed with these idealizations must be evaluated to make adjustments in the design approach. The following sections present in more detail some of the specific idealizations and assumptions used in current airport design approaches.

AIRCRAFT TRAFFIC

Aircraft do not traverse the same point on a pavement with each pass of the aircraft. Studies of aircraft traffic at airfields[9,28] developed the concept of using a normal distribution to develop a pass-to-coverage ratio that represents the variable pattern of aircraft traffic. Brown and Thompson's[9] observations found that 75 percent of the traffic on a channelized traffic area such as a primary taxiway or runway was concentrated within a 70-in.[a] wander width. For less channelized traffic areas such as runway interiors or parking aprons, a representative wander width was 140 in. For an aircraft gear with a single wheel, the pass-to-coverage ratio is the inverse of the maximum probability of the wheel passing over a point within the traffic lane or as shown in equation 1:

$$\frac{P}{C} = \frac{1}{C_x W_t} \tag{1}$$

[a] A table of factors for converting non-SI units of measurement to SI (metric) units is presented on page v.

where

P/C = pass-to-coverage ratio

C_x = maximum ordinate of the normally distributed curve of the applied traffic

$$= \frac{C_Z}{\sigma_x}$$

C_Z = maximum ordinate of the standard normal distribution curve (tabulated values found in Harr[22])

σ_x = standard deviation of the applied traffic distribution

W_t = width of the tire

However, if the gear contains a second wheel, the distribution of each wheel must be added together to determine a composite distribution and equation 1 becomes

$$\frac{P}{C} = \frac{1}{C_{xc} W_t} \tag{2}$$

where

C_{xc} = maximum ordinate of the composite distribution found by summing the individual wheel distribution curves

For instance, a 70-in. wander width which is defined to include 75 percent of the total traffic has a standard deviation of 30.43 in. The maximum ordinate from the standard normal distribution for a single wheel is 0.399. Therefore

$$C_x = \frac{C_Z}{\sigma_x} = \frac{0.399}{30.43} = 0.0131 \tag{3}$$

The B-727 has two 13.5-in.-wide tires spaced 34 in. apart. When the distribution curves of these two tires are added together, the maximum ordinate C_{xc} of the composite curve is 0.0228, and the pass-to-coverage ratio becomes

$$\frac{P}{C} = \frac{1}{C_{xc} W_t} = \frac{1}{0.0228 \times 13.5} \tag{4}$$

$$= 3.25$$

The maximum tensile stress is normally underneath the tire of the B-727. Consequently, the number of coverages on a concrete pavement is the maximum number of stress repetitions to which the concrete is subjected. Certain twin-tandem gears such as the B-747 develop only a single maximum stress between the forward and trailing wheels. These trailing wheels are not counted in determining a pass-to-coverage ratio for rigid pavements as they are for flexible pavements. Brown and Thompson[9] identify these aircraft and tabulate pass-to-coverage ratios of 70- and 140-in. wander widths for a variety of current civil and military aircraft.

The actual traffic at an airport will almost always consist of a mixture of different sizes of aircraft with varying gear configurations. Not only does the pattern of traffic cause difficulty in formulating the problem, but also the mixture of aircraft with each aircraft type causing a different stress level must be considered in the analysis. Furthermore, aircraft of the same type operate at varying loads, sometimes at only 70 to 80 percent of the maximum gross load.

Landing aircraft are often thought to impart an impact load on the pavement, but this is unsubstantiated. Tests conducted by the CE during World War II found that a dynamic load could only be measured during intentionally hard landings that often resulted in mechanical damage to the aircraft[77]. Later more extensive tests were conducted jointly by the FAA and the CE[43]. These tests found that concrete pavements tended to show relatively flat pressure and deflection responses to a wide variety of aircraft operations. The responses were a maximum for the stationary aircraft loads but decreased somewhat for taxiing, landing, and rotation. Flexible pavements showed much sharper and more pronounced peak measurements for the static loads compared with other aircraft operations than did the concrete pavement.

The actual traffic at an airport is a complex combination of varying aircraft types, gear configurations, and loads following diverse patterns of traffic at varying speeds. To reduce this situation to manageable proportions, airfields are usually designed only for departing aircraft on the assumption that the lighter landing aircraft have little effect. Simplicity aircraft are assumed to operate at maximum load in the absence of more detailed information. Agencies such as the CE or the FAA include in their published design procedures[23,78] methods to convert a mixture of aircraft into equivalent passes of the single, most severe aircraft loading in the mixture.

ANALYTICAL MODELS

The first analytical models for theoretical analysis of concrete pavements were developed by Westergaard[82,83]. These models characterized the pavement as a thin elastic plate supported on a bed of independent springs. Three stress solutions were developed: (a) a load in the interior of a slab infinite in horizontal directions, (b) a load adjacent to an edge of a slab infinite in the other three horizontal directions, and (c) a load on a corner of a slab infinite in the other two horizontal directions. These solutions are as follows:

Interior Loading

$$\sigma_i = \frac{3P(1+\nu)}{2\pi h^2}\left[\ln\left(\frac{2\ell}{a}\right) + 0.5 - \gamma\right] + \frac{3P(1+\nu)}{64\,h^2}(a/\ell)^2$$

Edge Loading

$$\sigma_e = \frac{3(1+\nu)P}{\pi(3+\nu)\,h^2}\left[\ln\left(\frac{Eh^3}{100ka^4}\right) + 1.84 - \frac{4\nu}{3} + \frac{1-\nu}{2} + 1.18\,(1+2\nu)\,(a/\ell)\right]$$

Corner Loading

$$\sigma_c = \frac{3P}{h^2}\left[1 - \left(\frac{a_1}{\ell}\right)^{0.6}\right]$$

where

σ_i = tensile stress for interior loading

P = total applied load

ν = Poisson's ratio

h = slab thickness

ℓ = radius of relative stiffness

$$= \left[\frac{E\,h^3}{12(1-\nu^2)k}\right]^{1/4}$$

E = modulus of elasticity

k = modulus of subgrade reaction

a = radius of circular load

a_1 = distance to point of action of resultant along corner angle bisector

$$= \sqrt{2}\,a$$

γ = Euler's constant

= 0.5722...

σ_e = tensile stress for edge loading

σ_c = tensile stress for corner loading

Ioannides, Thompson, and Barenberg[34] present a detailed description of the origins and various forms of these equations including other load shapes (elliptical, semicircle, and square), simplified forms, and the inclusion of a special theory adjustment for cases where the radius of the loaded area is less than 1.724 times the pavement thickness. A number of modifications have been proposed for the corner load by other investigators, and these modifications are discussed by Ioannides, Thompson, and Barenberg[34]. They considered the above forms of the equations for interior and edge loading to be the most correct and complete. Based on comparisons with finite element analysis, they concluded that the ratio of the smallest horizontal slab dimension to the radius of relative stiffness must be at least 3.5, 5.0, and 4.0 to meet the infinite or semi-infinite Westergaard assumptions for the interior, edge, and corner loading cases.

The concrete pavement slab in these models is characterized with the elastic material properties of a modulus of elasticity and a Poisson's ratio, and the supporting layers of the base course and subgrade materials are represented by a spring constant k termed modulus of subgrade reaction with units of pounds per square inch per inch. Westergaard[82] referred to this spring constant k as "an empirical makeshift, which however has been found in the past to give usable results." Terzaghi[76] discussed extensively the applications and limitations of the plate load tests used to determine the value of k. The idealization of all the supporting layers as a simple linear spring is generally the major objection to the Westergaard model. Major drawbacks to this idealization include the difficulty of determining a k value during design since this determination requires an in situ field test and the poor idealization by a single number for the real layered base course and subgrade structure. If one or more of these layers is stabilized, representing the structure with only a spring constant is particularly poor.

Pickett and Ray[62] developed solutions to the Westergaard equations in terms of influence charts that simplified the required calculations. Computerized solutions were also presented later for the interior load problem[57] and for the edge load problem[40]. A regression equation to calculate the Westergaard free edge stress was developed by Witczak, Uzan, and Johnson[85] and later modified slightly at the WES. This modified regression equation is

$$\sigma_e = \left[a_o + a_1 \ln \ell + a_2 (\ln \ell)^2\right] \frac{P}{h^2} \qquad (5)$$

where

a_o, a_1, a_2 = regression constants dependent on individual aircraft gear and tire properties (tabulated values published by Rollings[63]

P = gear load, lb

The limitations in the Westergaard model's representation of the materials under the concrete slab led to interest in using the layered-elastic analytical model to calculate stresses. The widespread use of nondestructive pavement testing equipment that analyze pavement properties by comparing field measured deflection basins with those calculated by the layered elastic theory has also contributed greatly to the interest in layered elastic solutions for pavement evaluation and design. The CE and the FAA recently developed an airfield rigid pavement layered-elastic design procedure[59] that is accepted by the CE as an alternative to the Westergaard based-design procedures.

The layered elastic model idealizes the pavement structure as a sequence of continuous, horizontally uniform, homogeneous, isotropic layers each characterized by a modulus of elasticity and a Poisson's ratio. The interface between the layers can be full slip, no slip, or some specified intermediate level slip. The formulation of the problem of a circular load on a layered elastic system is usually expressed with one or more stress functions for each layer. For instance the vertical displacement, v_z, and stress, σ_{zz}, in a layer can be expressed as

$$U_z = \frac{2(1-\nu^2)}{E} \nabla^2\phi - \frac{1+\nu}{E} \frac{\partial^2\phi}{\partial z^2} \tag{6}$$

$$\sigma_{zz} = \frac{\partial}{\partial z}\left\{(2-\nu)\nabla^2\phi - \frac{\partial^2\phi}{\partial z^2}\right\} \tag{6a}$$

where

$$\nabla^2 = \text{Laplace operator} = \frac{\partial^2}{\partial r^2} + \frac{1}{r}\frac{\partial}{\partial r} + \frac{1}{r^2}\frac{\partial^2}{\partial \theta^2} + \frac{\partial^2}{\partial z^2}$$

ϕ = stress function in r, θ, and z

The stress function ϕ can be transformed with the Hankel transformation by

$$T_n(\phi) = \int_0^\infty r\,\phi\,J_o(m,r)\,dr \tag{7}$$

where

$T_n(\phi)$ = Hankel transform of ϕ

$J_o(m,r)$ = Bessel function of the first kind and of zero order

m = Hankel transform parameter

Neglecting body forces, equilibrium, and compatibility are met if

$$\Delta^4 \phi = 0$$

The general solution to this equation in the Hankel transform of the stress function becomes

$$T_n(\phi) = Ae^{mz} + Bme^{-mz} + mCe^{mz} + zDe^{-mz}$$

The four constants, A, B, C, and D are evaluated for each layer from the layer boundary conditions. The stress function is found by inverting the transformed solution by the Hankel inversion theorem:

$$\phi = \int_0^\infty m\, T_n(\phi)\, J_n(m,r)\, dm$$

Displacement stresses and strains in the layer can then be found from the stress function.

Complete derivations of generalized forms of the layered elastic model have been presented by Schiffman[67], Peutz and Kempen[60], Jong, Peutz, and Korswagen[37], and Cauwelaert, Lequeux, and Delaunois[13]. The integrals in the layered elastic model cannot be solved analytically and must be evaluated numerically. Some solutions are available for specific numbers of layers and assumptions of material properties[10,36]; however, computers are the only practical method of solving the general layered elastic model. Several computer programs are available, and they differ primarily in the numerical methods used to evaluate the integrals.

The limitations of the Westergaard and layered elastic models have led to interest in numerical methods using discretization such as finite element or finite difference methods. Of these approaches, finite element analysis has generated the most interest, but the Westergaard models remain the most widely used for calculating stresses in published design procedures and in practice for airfield pavements. The PCA[58] and the US Navy[25] use the

Westergaard interior load model, and the CE[24], the US Air Force, and the FAA[79] use the Westergaard edge load model.

FATIGUE RELATIONSHIPS

Airfield rigid pavement thickness design is normally based on a fatigue analysis of the concrete. The fatigue strength of plain concrete is that proportion of the static strength that can withstand a specified number of load cycles. It is usually considered to be the same in compression, tension, and flexure. In general, the modulus of elasticity decreases and the strains increase with increasing load repetitions.

If concrete is subjected to fluctuating levels of stress, the ratio of the minimum stress level to the maximum stress level affects the fatigue strength. This is illustrated by the stress-fatigue life curves in Figure 1[4] for plain concrete beams tested in flexure. The ratio of maximum applied stress to concrete flexural strength that supports a given number of load cycles increases dramatically if the ratio of the minimum stress to the maximum stress applied to the test beam increases from 0.15 to 0.75. There is considerable scatter in fatigue test results for concrete, thus, it is common to show the probability of sample failure as presented in Figure 1 for the minimum-maximum stress ratio of 0.15. Tepfers[74] and Tepfers and Kutti[75] have proposed a concrete fatigue relation to include the effect of the minimum-maximum stress ratio as

$$\frac{\sigma_{max}}{f} = 1 - \beta (1 - A) \log N \qquad (8)$$

where

σ_{max} = maximum applied stress

f = compressive or tensile strength of concrete

β = a coefficient with a proposed value of 0.0685

A = stress ratio $\sigma_{min}/\sigma_{max}$

N = number of load cycles to produce failure

An in-service pavement exists under fluctuating stress conditions. Temperature and moisture gradients in the pavement slab change with time and result in varying stress conditions in the slab upon which are added periodic load induced stresses. Domenichini and Marchionna[17] studied the effects of temperature variation for the concrete pavement in the American Association of State Highway Officials (AASHO) road test. Their data show that the stress ratio of minimum temperature stress to the sum of the temperature and load stresses for AASHO road test slabs 6.5 to 9.5 in. thick varied from 0.16 to 0.60 depending on the time of day and season of the year. The analysis by Domenichini and Marchionna[17] only considered the daytime condition of the surface of the slab to be warmer than the bottom and neglected other potential

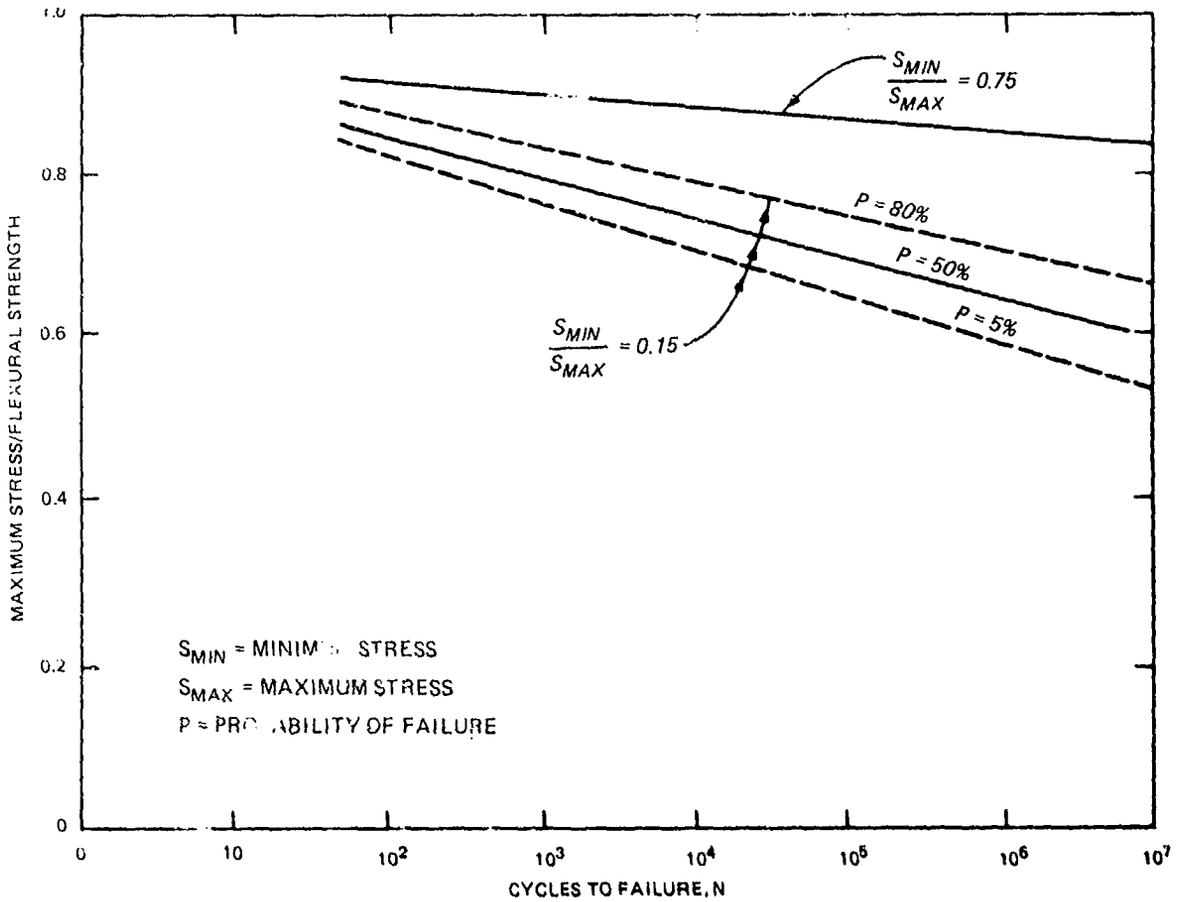

Figure 1. Representative concrete fatigue curves

stresses such as those caused by a moisture gradient. Nevertheless, their work clearly shows that the stress ratio that exists in pavements is not a constant. The fluctuating stress ratio in pavements implies that there is not a unique concrete fatigue relationship for concrete pavements.

The effect of varying magnitudes of loading is usually handled by Miner's hypothesis[49] which states that failure occurs when the summation of n_i/N_i equals 1,

where

n_i = the number of cycles applied at a particular stress level

N_i = the number of cycles that would cause failure at the same stress level

The effect of varying magnitudes of cyclic loading has not been adequately investigated, and Miner's hypothesis does not always give conservative results. Initial loads near 90 percent of the ultimate static strength reduce

fatigue life, whereas initial loads below 50 to 55 percent increase fatigue life[84]. Consequently, Miner's hypothesis would appear to be unsafe for high loads and conservative for low loads[38].

Pavements are subject to varying frequencies of loading and have rest periods of varying length between loadings. Laboratory tests have shown that these factors can have significant effect on the fatigue performance of concrete. If the applied cyclic stress is less than 0.75 of the ultimate strength, frequencies of loading in the range of 70 to 900 cycles per minute do not have much effect on fatigue performance. However, at higher stress level frequency has significant effect on fatigue performance of concrete[4]. Also, periodic rest periods between loadings appear to improve fatigue life significantly[38].

There are two basic approaches to developing a concrete fatigue relationship for use in pavement design. The first is to use a conservative interpretation of laboratory beam tests conducted at a low minimum to maximum stress ratio. The PCA[57] fatigue relationship is probably the most widely used relation of this type. The second approach is to use full-scale accelerated traffic tests of concrete pavements to develop field fatigue relationships. The CE has conducted large-scale accelerated traffic tests using aircraft size loads and gear assemblies, and the AASHO road test provided similar information for truck-sized axle loads. Full-scale tests have the advantages of testing actual slab and joint systems, testing the concrete under actual multiaxial stress conditions, and including to some extent, temperature and moisture stresses. As illustrated in the previous discussion, a number of factors such as stress ratios, rest periods, relative load magnitude, and load frequency can affect the fatigue performance of concrete. Field tests include some of these effects, but they have the disadvantages of high cost and difficulty in defining applied stress levels.

Figure 2 shows a comparison of several concrete fatigue relationships used or proposed for use in the design of concrete pavements. The ordinate of this figure is plotted as the design factor which is the concrete flexural strength divided by the applied stress. This factor is used by the CE for pavement fatigue analysis and will be used for the remainder of this report rather than its inverse which is commonly used by the PCA[57] and the American Concrete Institute (ACI)[4]. The PCA relation is a very conservative interpretation when compared with the ACI[4] curves for 5 and 50 percent probability of failure at a minimum to maximum stress ratio of 0.15. The other curves in Figure 2 are based on field tests and are different from these laboratory developed curves.

The problem of defining the applied stress level in field tests is illustrated in Figure 2 by the two CE relationships. Both CE fatigue relationships are based on the same field tests, but one relation uses the layered-elastic analytical model to calculate the stresses under the test load, and the other uses the Westergaard edge load model. Each model calculates a different numerical value for the stress with the layered-elastic

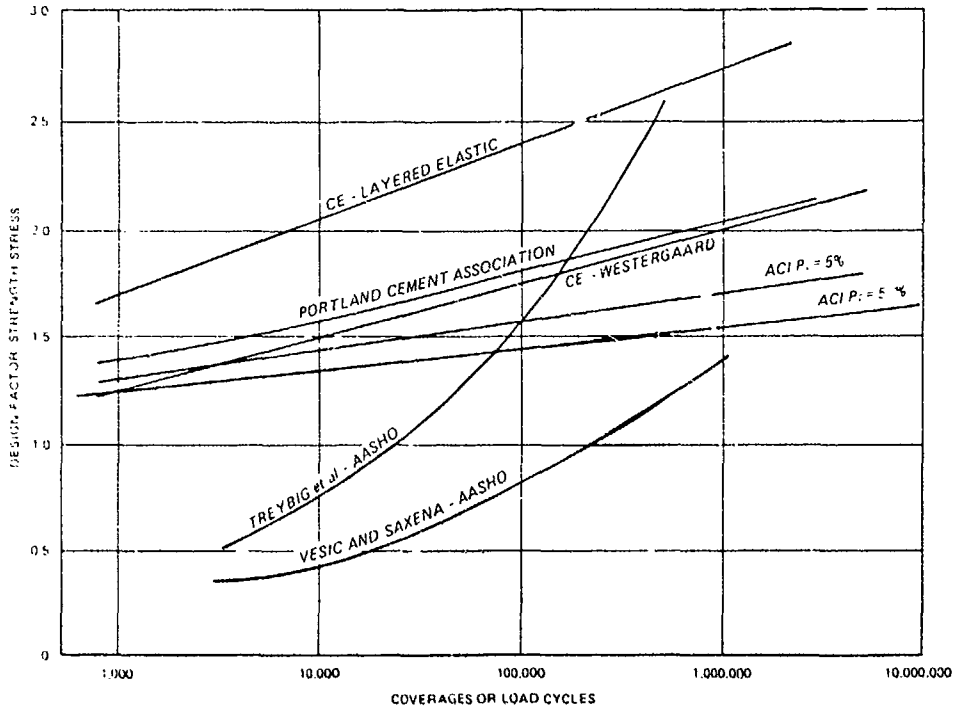

Figure 2. Fatigue curves for pavement design

calculated stress always being lower. Consequently, the resulting fatigue relation for each analytical model is different. The same effect is shown for the AASHO road test results in Figure 2 where Treybig et al.[77] used the layered elastic model and Vesic and Saxena[81] used the Westergaard edge load analytical model. The actual stresses in the slabs in the field are actually variable depending on the placement of the load, rate of loading, load transfer of joints, temperature conditions, and moisture gradient. Therefore, the stresses calculated from the analytical models are nominal stresses reflecting the relative effect of imposed traffic loads rather than actual stresses.

The fatigue relationships based on field tests must define some condition of failure for the test sections. The CE tests defined failure as occurring when one-half or more of the trafficked slabs have one or more structural cracks. Vesic and Saxena[81] defined failure as a pavement serviceability index (PSI) of 2.5. As a comparison, the CE failure criteria would represent a PSI of 3.0 to 3.3. The relationship developed by Treybig et al.[77] defined failure as the development of class 3 cracking in an AASHO road test section. A class 3 crack is a "crack opened or spalled at the surface to a width of 1/4 in. or more over a distance equal to at least one-half of the crack length"[68].

Fatigue relationships based on field tests will vary depending on the analytical model used to calculate stresses and on the defined failure level, but the shape of relationships based on the AASHO road tests is very different from other fatigue relationships. The ACI and both CE curves in Figure 2 are straight lines on a semilogarithmic plot whereas the AASHO relationships are sharply curved. This difference is probably due to extensive pumping that developed at the AASHO road test. Consequently, AASHO road test relationships actually include the damage from both concrete fatigue and the pumping. Pumping is a severe problem in highway pavements but less so in airfields.

DESIGN METHODS

The most common airport pavement design procedures are the PCA and CE design methods or some modification of these methods. The basic steps in the design are to convert the actual pattern of aircraft traffic to cycles of stress or coverages, calculate the load-induced stresses using an analytical model, and then determine the number of coverages of this load that could be sustained by the pavement using one of the fatigue relationships.

The PCA uses a Westergaard interior load analytical model for its stress calculations neglecting the effects of higher stresses at the joints. The higher stresses at the joints and the other additional environmental stresses are accounted for indirectly by use of a factor of safety of 1.5 to 2.0 with concrete flexural strength and the conservative interpretation of laboratory fatigue test results previously shown in Figure 2.

The CE design method using the Westergaard edge load model with 25 percent load transfer is widely used and has been adopted by the US Army, the US Air Force, and the FAA. This design method does not use any factor of safety directly. The assumptions on loads are conservative, and the use of field test that developed fatigue relations includes some thermal and moisture related stress in the performance criteria. CE construction specifications require that 80 percent of the quality control flexural tests fall above the specified design flexural strength. The practical effect of this requirement is that the contractor usually produces a concrete that is well above the design flexural strength. The CE now uses the Westergaard or layered-elastic fatigue relationships shown in Figure 2. However, earlier CE and the current FAA design methods used fatigue relationship defined in terms of percent standard thickness. The concepts are similar and have little effect on the results. The background of the percent standard thickness fatigue relationships is described by Rollings[63] and Parker et al.[59].

Soon after the first version of the CE design method was produced in World War II, a long-term pavement performance monitoring program began that produced modifications to the design procedure to reflect field performance of pavements. One of the early observations was that the ends of concrete runways were failing before the runway interior. This observation in conjunction with the study of traffic at military airfields led to the definition of four types of pavement at military airfields. Type A areas are runway ends and primary taxiways that are subject to highly channelized, slow moving aircraft and are designed for 70-in. wander widths and full aircraft loads. Type B areas are parking and similar areas where traffic is more widely distributed. These areas are designed for full aircraft load and 140-in. wander widths.

Type C areas are runway interiors and are designed for 75 percent of the aircraft load and 140-in. wander widths. Type D areas are seldom trafficked areas like the outside edges of the runway and are designed for reduced weight, a limited number of aircraft passes, and 140-in. wander widths.

Traffic at commercial airports is more complex in mixture and pattern than military airfields; therefore, the FAA adopts a different approach. Full design thickness is used for areas subject to departing aircraft. Areas such as high speed turnoffs that are used primarily by arriving aircraft may be reduced 10 percent from the full design thickness. Seldom trafficked areas analogous to the military Type D areas can be reduced 30 percent in thickness.

The CE pavement performance monitoring program and test sections found that the Westergaard model did not adequately reflect the effect of subgrade strength on observed pavement performance. The modulus of subgrade reaction k appears in Westergaard stress calculations as a fourth root in the denominator of the radius of relative stiffness ℓ for the edge and interior load stress calculations. Taking the natural logarithm of the radius of relative stiffness in several of the equations further reduces the effect of k. Consequently, the subgrade support as measured by the k value has a relatively small effect on the calculated stresses. Pavements on high- and low- strength subgrades were observed to crack approximately as predicted by the CE criteria, but at this point their performance diverged. Pavements on low-strength subgrades rapidly deteriorated with additional cracking, faulting, and spalling, but the pavements on high strength subgrades deteriorated at a much slower rate. Consequently, the CE reduces the required pavement thickness on high-strength subgrades as shown in Table 1 to take advantage of this improved postcracking behavior. The FAA does not use this reduction for high-strength subgrade in its design.

Table 1

Reduction in Pavement Thickness for High-Strength Foundations

Subgrade Modulus, k lb/in.^{2}/in.	Reduction in Thickness, %
200	0.0
300	4.6
400	10.6
500	19.2

The existing design methods are essentially fatigue analyses that are modified by agency and organization experience. A number of idealizations are used to reduce the real field problems of aircraft operating on pavements so

that these analyses can be performed. Much of each method is based on past experience; therefore, modifications, changes, and substitutions in the design procedures cannot be performed blindly. To obtain reliable results with any of these design methods, the complete method must be used as the agency specifies.

CURRENT RIGID OVERLAY DESIGN METHODS

CE DESIGN METHOD

The most widely used overlay design methods are the empirical relations developed by the CE. The required overlay thickness is determined by the overlay equation:

$$h_o^n = h_e^n - Ch_b^n \tag{9}$$

where

h_o = thickness of overlay

h_e = required thickness for a new pavement to support the design traffic planned for the overlay

C = condition factor for existing base pavement values summarized in Table 2

h_b = original thickness of existing pavement to be overlaid

n = a power deperdent on the bond condition between base pavement and overlay

= 1.0 fully bonded overlay

= 1.4 partially bonded overlay

= 2.0 unbonded overlay

An overlay is considered to be unbonded if there is a separation layer of asphalt concrete or other material between the overlay and base slab so that no bond can develop. If the overlay is cast directly on the base slab, it is considered a partially bonded overlay. If the surface is well prepared by cold milling or similar techniques and a bonding grout is used between the overlay and the base slab, the overlay is considered to be fully bonded.

If the flexural strength of the overlay and the base pavement are substantially different; this difference may be included by replacing h_b with

$$\frac{h_{eo}}{h_{eb}} \times h_b \tag{10}$$

where

h_{eo} = required thickness for a new pavement to support the overlay design traffic determined with the overlay concrete flexural strength

h_{eb} = required thickness for a new pavement to support the overlay design traffic determined with the existing base pavement concrete flexural strength

h_b = original thickness of pavement to be overlaid

This adjustment is used by the CE but not by the FAA.

Table 2

Condition Factor Values

C Factor	Base Pavement Condition
1.0	Existing pavement is in good structural condition with little or no structural cracking.
0.75	Existing pavement has some initial structural cracking but little progressive distress such as spalling and multiple cracks.
0.35	Existing pavement is badly cracked and may show multiple cracking, shattered slabs, spalling, and faulting.

The origin of the concept relating an overlay slab and a base slab to an equivalent slab by a summation of the thicknesses raised to a power is unclear. Older[56] used a square relation (n=2 and C=1) to evaluate a monolithic structure of bricks bonded to a concrete base slab for the Bates road test, and this reference to equation 9 is the earliest that has been found. Arms, Aaron, and Palmer[5] suggested that this relation with n equal to 2 came into general use for overlay design with the recognition that it was not technically accurate. The ACI Committee 325 on concrete pavements states that "for many years" concrete overlays have been designed on the "assumption" that the strength of a base and overlay slab is equal to that of a single slab with a thickness that is equal to the square root of the sum of the squares of the base and overlay slab thicknesses[3].

During the 1940's and 1950's the CE conducted a series of accelerated traffic tests of overlay test items. Many of these tests were never

adequately documented, but summaries of the results were published by Hutchinson and Wathen[32] and Mellinger[47]. The Engineering Manual EM 1110-45-303[23] from this period stated that:

> The results of the traffic testing at Lockbourne No. 1 and No. 2 and Sharonville No. 2 indicated that the above relationship (n=2 and C=1 in equation 1) was approximately correct when a leveling course, cushion course, or bond-breaking course was placed between the two slabs, and that the relationship was too conservative when the overlay was placed directly on the base slab without purposely destroying the bond between the slabs.

As shown in Figure 3,[a] the CE accelerated traffic testing suggested that the power in the overlay design equation should be 1.4 instead of 2.0 when partial bond was allowed between the overlay and the base slab. Fully bonded overlays (n = 1 and C = 1) should behave monolithically with the base pavement. However, problems of constructing adequate joints in the overlay capable of load transfer have not been solved, and fully bonded overlays are now considered most appropriate in airfield work for solving surface problems such as scaling or smoothness rather than for pavement structural upgrade[31].

The CE overlay design equations are widely used, but their derivation and basis are poorly documented and incomplete.

OTHER DESIGN METHODS

Problems with the CE developed empirical overlay design equations have led to examinations of other approaches to overlay design. Martin[46] used the results of the AASHO road test to establish allowable maximum deflections and propose a design procedure based on measured deflections. The use of allowable deflections has generally been applied to flexible overlays over a rigid pavement rather than to rigid overlays.

The weakness of the Westergaard models for evaluating layered overlay systems led other investigations to examine approaches using stronger analytical models. The layered elastic model does a better job of modeling the multiple layers of the overlay geometry than any of the Westergaard models. Several investigators used the layered elastic model or a hybrid finite element model to calculate tensile stresses which were related to performance through one of the fatigue relationships discussed earlier. Smith et al.[72] and Hutchinson[31] provided summaries of current overlay design practice and described the characteristics of some of the proposed design procedures using

---

[a]This figure was provided by M. Ronald Hutchinson (CE, retired, previously at the Ohio River Division Laboratories and Chief of the PSD at the WES) from his personal files. To this author's knowledge it was not published previously in the CE overlay reports.

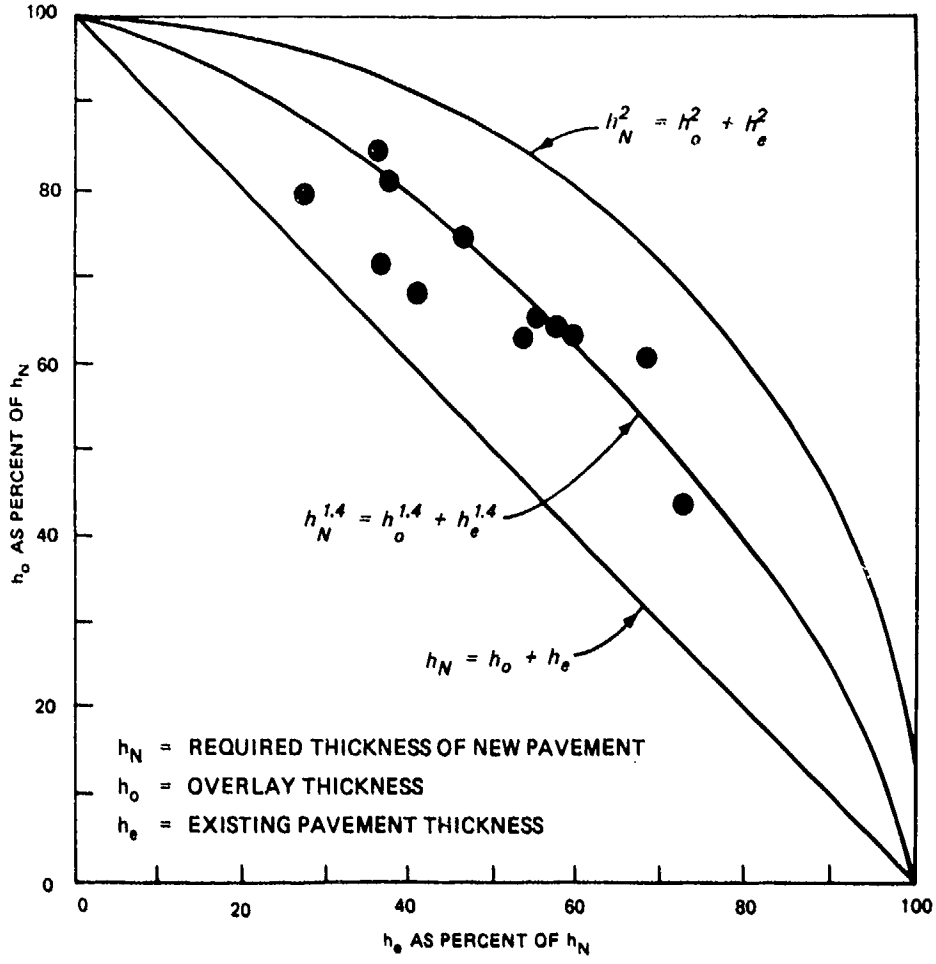

Figure 3. Corps of Engineers overlay test data results

stronger analytical models. Tayabji and Okamoto[73] developed a design procedure for bonded and unbonded overlays using a finite element plate element model to represent the concrete slabs and a spring foundation to represent the underlying layers. No attempt was made to evaluate partially bonded overlays.

Several approaches to overlay design summarized by Smith et al.[72] and Hutchinson[31] have been studied to try to improve the CE equation. Most of these have been oriented toward highways rather than airfields. Major problems encountered in these investigations have included problems in evaluating the condition of the base pavement, establishing design performance criteria, and adequately modeling slab joints and interface conditions.

BASIC OVERLAY RELATIONSHIPS

Simple beam theory can be used to derive equations for unbonded overlays and an equivalent slab that are in a form similar to the CE overlay design equation given earlier. An overlay slab and a base slab can be considered to

be structurally equal to an equivalent slab such as shown in Figure 4. If a thin slice of unit width b from this equivalent slab is subjected to a moment M_e the curvature of the beam is

$$\frac{1}{\rho_e} = \frac{M_e}{E_e I_e} \tag{11}$$

where

ρ_e = radius of curvature

M_e = moment

E_e = modulus of elasticity

I_e = moment of inertia

If the overlay and base slab are subject to an equivalent moment such that $M_e = M_1 + M_2$, compatibility requires the radius of curvature of the base and the overlay slabs to be equal so that

$$\frac{1}{\rho} = \frac{M_1}{I_1 E_1} = \frac{M_2}{I_2 E_2} \tag{12}$$

There are three potential ways of defining an equivalent slab: (a) the equivalent slab must have the same rigidity as the overlay and base slab, i.e., $E_e I_e = E_1 I_1 + E_2 I_2$, (b) the tensile stress in the equivalent slab σ_e must be equal to the tensile stress in the base slab σ_2, i.e., $\sigma_e = \sigma_2$, (c) the tensile stress in the equivalent slab must be equal to the tensile stress in the overlay σ_1, i.e., $\sigma_e = \sigma_1$.

Substituting the formula for the moment of inertia of a rectangular cross section ($bh^3/12$) into the requirement that the equivalent slab's moment of inertia must equal the sum of the moment of inertia of the base and the overlay results in the relation:

$$E_e h_e^3 = E_1 h_1^3 + E_2 h_2^3 \tag{13}$$

Now if an equivalent slab and the base slab thickness are known and all modulus values are equal, then the required overlay thickness to meet this definition would be

$$h_1^3 = h_e^3 - h_2^3 \tag{14}$$

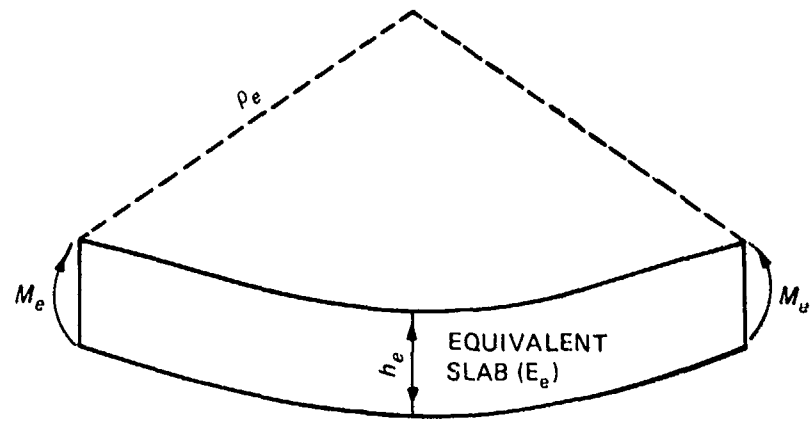

EQUIVALENT SLAB

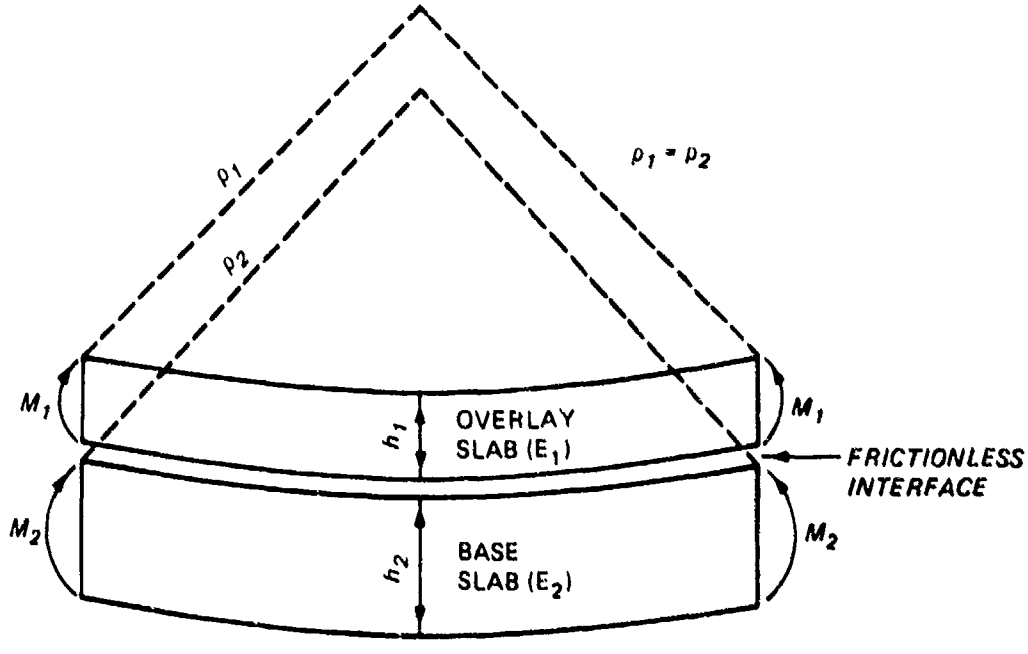

Figure 4. Base, overlay, and equivalent slabs

This relation is analogous to the current unbonded overlay equation except the power relation is a cube rather than a square. Although this approach provides a system of equal rigidity, it does not provide any information on stresses.

In a simple, linearly elastic beam the extreme fiber stress may be determined as

$$\sigma = \frac{Mc}{I} \tag{15}$$

where

σ = extreme fiber stress

M = applied moment

c = centroidal distance = h/2

I = moment of inertia

The stress in the equivalent slab and the base slab can be represented as

$$\sigma_e = \frac{M_e \frac{h_e}{2}}{I_e} = \frac{6M_e}{h_e^2}$$

$$\sigma_2 = \frac{M_2 \frac{h_2}{2}}{I_2} \tag{16}$$

Noting from equation 12 that the radius of relative stiffness of the overlay and the base slab must be equal, and the equivalent moment equaling to the sum of M_1 and M_2 leads to

$$\frac{1}{\rho_1} = \frac{M_1 E_1}{I_1} = \frac{1}{\rho_2} = \frac{M_2 E_2}{I_2}$$

$$M_1 = \frac{I_1 E_1}{I_2 E_2} M_2$$

$$M_e = \frac{I_1 E_1}{I_2 E_2} M_2 + M_2 = M_2 \left(1 + \frac{E_1 h_1^3}{E_2 h_2^3} \right) \tag{17}$$

Expressing M_2 in terms of M_e followed by substituting into the expression for stress in the base slab leads to

$$\sigma_2 = \frac{M_3}{1 + \frac{E_1 h_1^3}{E_2 h_2^3}} \cdot \frac{E_2}{E_1} \cdot \frac{\frac{h_2}{2}}{I_2} = \frac{6 M_e E_2 h_2^3}{E_2 h_2^3 + E_1 h_1^3} \tag{18}$$

Requiring that σ_e and σ_2 must be equal in the second definition of an equivalent slab and setting the expressions for each equal to one another will simplify to

$$E_2 h_2 h_e^2 = E_2 h_2^3 + E_1 h_1^3 \tag{19}$$

If the equivalent slab and the base slab are known, the required overlay thickness to keep the stresses in the base slab and equivalent slab equal becomes

$$h_1^3 = \frac{E_2}{E_1} \left(h_2 h_e^2 - h_2^3 \right) \tag{20}$$

A similar analysis with the requirement that the equivalent slab stress and overlay slab stress σ_1 are equal results in the third case in the relation

$$h_1^3 = h_1 h_e^2 - \frac{E_2}{E_1} h_2^3 \tag{21}$$

Since h_1 appears on both sides of equation 21, it can be found most easily by an iterative solution process.

Figure 5 shows each of the equations for the three definitions of equivalent slab (equal rigidity, overlay slab stress equals equivalent slab stress, and base slab stress equals equivalent slab stress) plotted together if the overlay and base slab moduli of elasticity are equal. Also shown is the CE

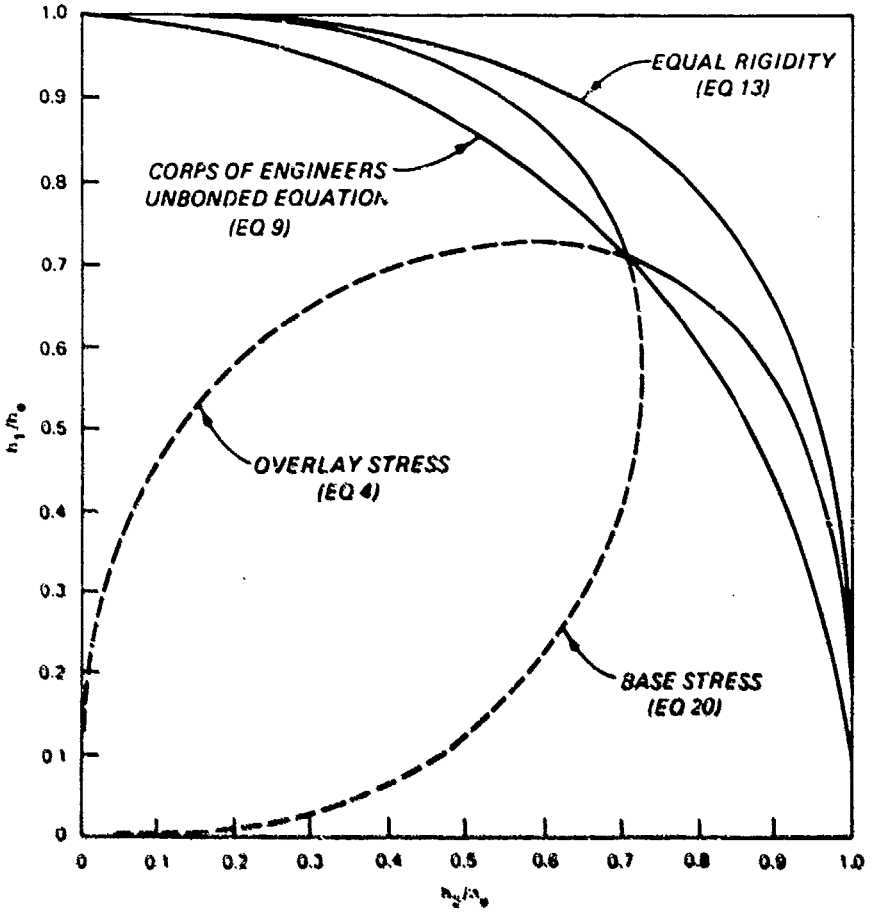

Figure 5. Overlay equation for different definitions of equivalent slab

unbonded overlay equation. Each axis has been normalized by h_e, and they are expressed in terms of h_1/h_e and h_2/h_e. The CE equation, the overlay stress equation, and the base slab all intersect when

$$\frac{h_1}{h_e} = \frac{h_2}{h_e} = \sqrt{1/2} = 0.707 \tag{22}$$

Each value of h_2/h_e has two solutions in the base stress equation. As the thickness of the base slab term h_2/h_e increases toward $\sqrt{1/2}$, relatively thick overlays are required to maintain the stress in the base equal to the stress in the equivalent slab without increasing the stress in the overlay above the value for the equivalent slab. If the lower value of h_1/h_e is

selected for any given h_2/h_e value, the overlay stress equation shows that the stress in the overlay exceeds that of the equivalent slab. When the h_2/h_e value exceeds $\sqrt{1/2}$, the overlay stress equation controls. The CE equation keeps stresses in the overlay or the base higher than the equivalent slab in all cases except the point $h_1/h_e = h_2/h_e = 1/\sqrt{2}$. The equal rigidity equation keeps the stresses in both the overlay and the base slab below that of the equivalent slab for all values.

Simple beam theory can derive forms of overlay design equations similar to the CE overlay design equation depending on how the equivalent slab is defined. The definitions of equivalent slab on the basis of stress show there are different regions where stress in the overlay and stress in the base slab control. Which stress controls depends on the ratio of base slab thickness to equivalent slab thickness.

BASIS FOR IMPROVED OVERLAY DESIGN PROCEDURE

An improved rigid pavement overlay design procedure will require developing a method of measuring performance of the concrete pavement to replace the current defined failure level approach. An analytical model will be needed to calculate stresses, strains, deflections, or some combination of design parameters to replace the current empirical overlay relationships. This analytical model will have to be able to represent two layers of concrete with various possible interface conditions as well as model the underlying base and subgrade materials. The existing base pavement to be overlaid may have suffered some deterioration from past traffic, and a method of measuring or accounting for this damage is needed. A complete methodology for an improved overlay design procedure must address each of these concepts.

PERFORMANCE CRITERIA

Current prescriptive definitions of pavement failure in specific terms such as percentage of cracked slabs are not adequate to monitor or predict pavement performance. A pavement is either failed or not failed by such definitions. There is no way to express how well or how poorly a pavement is performing or how fast it is deteriorating. Once the defined state of failure is reached, the pavement is still functional, but there is no way to express this postfailure performance. Defining pavement performance by a specified failure condition will not meet the objective of this study.

The AASHO road test introduced the concept of Present Serviceability Index (PSI) to express the condition of a pavement numerically. A PSI of 5.0 represents a perfect pavement, and a 0.0 rating would be an unusable pavement. This concept was originally developed by Carey and Irick[12] and is a measurable function of roughness, cracking, and patching. Longitudinal roughness is the primary controlling factor that affects the PSI value. The PSI is an improvement over the previous defined failure levels, but it is oriented toward highway usage. However, it is not directly applicable to airports.

The US Army Construction Engineering Research Laboratory developed a system of rating airport pavement for the US Air Force[69]. This system is known as the pavement condition index (PCI) and has been adopted by the US Air Force, the US Navy, and the FAA[69,79,26]. Further work has extended this system as a rating and management tool for roads and streets for municipalities, Army posts, and similar organizations.

The PCI varies from 0 to 100. Qualitative pavement ratings and corresponding PCI ranges are shown in Table 3. The PCI is a simple, reproducible method of obtaining a numerical rating of a pavement that would equal the subjective rating of a panel of experienced pavement engineers.

The PCI recognizes the 31 types of distress listed in Table 4. Deduct values are assigned depending on the type of distress, its severity, and the amount or density of the distress in the pavement. The PCI is described by the equation:

$$PCI = 100 - a\sum_{i=1}^{m}\sum_{j=1}^{n} f(T_i, S_j, D_{ij}) \quad (23)$$

where

a = an adjustment factor depending on the number of distress types with deduct values in excess of 5 points (this factor was necessary to match the original engineer panel's ratings)

m = total number of distress types

n = total number of severity levels for each distress type

$f(T_i,S_j,D_{ij})$ = deduct value for distress type T_i at severity level S_j existing at density D_{ij}

Table 3

Descriptive Rating of the PCI

PCI Rating	Descriptive Rating
86-100	Excellent
71-85	Very good
56-70	Good
41-55	Fair
26-40	Poor
11-25	Very poor
0-10	Failed

The PCI may conceptually also be considered as follows:

$$PCI = 100 - D_S - D_E - D_M - D_C - D_O \quad (24)$$

where

D_S = structural deduct due to distress types, severities, and densities associated with loads (e.g., distress No. R12 shattered slab)

D_E = environmental deduct due to distresses associated with environmental effects (e.g., distress No. F12 raveling, weathering)

D_M = materials deduct due to distress associated with materials used in construction (e.g., distress No. R8 popouts)

D_C = construction deduct due to distress associated with construction procedures (e.g., distress No. F2 bleeding)

D_O = operations deduct due to distress associated with operations and maintenance of the pavement (e.g., distress No. R7 patching/utility cuts)

In many cases, the distress types identified in Table 4 may be caused by different factors. For example, distress No. R3, longitudinal/transverse/diagonal cracking, may be caused by structural loads, or it may be caused by environmentally induced thermal stresses. Distress No. R10, scaling, may be due to poor construction procedures or to certain siliceous aggregates undergoing an alkali-aggregate reaction.

Many of the distress types used in the PCI are caused by factors that are not reflected in analytical models (e.g., durability cracking distress type No. R4 in concrete). This kind of damage in pavements has usually been controlled by construction and material specifications that control how pavements are constructed and what materials are allowed to be used in the pavement. The PCI system as it currently exists includes distress types that cannot be evaluated with current analytical models; therefore, some modifications to the PCI is needed.

A structural condition index (SCI) from the PCI can be defined as:

$$SCI = 100 - a \sum_{i=1}^{m} \sum_{j=1}^{n} f(T_i, S_j, D_{ij}) \tag{25}$$

with variables as defined previously, but T_i is now limited to only those distress types associated with structural deterioration caused by loads. It also follows that

$$PCI = SCI - \text{all other deducts} \tag{26}$$

Thickness design of concrete pavement for fatigue is based on the load-induced tensile stresses in the slab. Available analytical models are capable of calculating the magnitudes of these stresses by using various idealizations of the pavement structure. There are some other load-caused distresses in pavements which are not directly related to the tensile stress in the slab. The most important of these is pumping which is a function of soil type, availability of moisture, and load magnitude and frequency. Pumping forms

Table 4

PCI Distress Types

Pavement Type	Distress Number	Name	Number of Recognized Severity Levels
Rigid	1	Blowup	3
Rigid	2	Corner break	3
Rigid	3	Longitudinal/transverse/diagonal cracking	3
Rigid	4	Durability cracking	3
Rigid	5	Joint seal damage	3
Rigid	6	Small patch	3
Rigid	7	Patching/utility cut defect	3
Rigid	8	Popouts	1
Rigid	9	Pumping	1
Rigid	10	Scaling	3
Rigid	11	Settlement	3
Rigid	12	Shattered slab	3
Rigid	13	Shrinkage cracks	1
Rigid	14	Spalling along joints	3
Rigid	15	Spalling corner	3
Flexible	1	Alligator cracking	3
Flexible	2	Bleeding	1
Flexible	3	Block cracking	3
Flexible	4	Corrugation	3
Flexible	5	Depression	3
Flexible	6	Jet blast erosion	1
Flexible	7	Joint reflective cracking	3
Flexible	8	Longitudinal and transverse cracking	3
Flexible	9	Oil spillage	1
Flexible	10	Patching and utility cut	3
Flexible	11	Polished aggregate	1
Flexible	12	Raveling, weathering	1
Flexible	13	Rutting	3
Flexible	14	Shoving of flexible pavement by PCC[a] slabs	3
Flexible	15	Slippage cracking	1
Flexible	16	Swell	3

[a]PCC = portland cement concrete.

voids under the pavement resulting in loss of support and accelerated deterioration. These other load-related problems such as pumping are not directly considered in pavement thickness design. Instead, protection such as requiring pumping resistant base courses or stabilization, is specified. Pumping is usually a highway rather than an airfield problem and is a special topic. The SCI for this study is limited to considering only those distress types associated with load-induced tensile stresses that result in fatigue damage to pavements.

Table 5 shows the PCI distress types that have been selected to be used with rigid pavements to determine the SCI value. Distress No. 13, shrinkage cracking, is included in the SCI because this distress type would include a tight, load-related crack that does not extend across the entire width or length of the slab as well as the conventional shrinkage cracking because of improper curing procedures. With further traffic this crack, if caused by loads, will propagate across the slab into a Type 3 longitudinal/transverse/diagonal crack of low severity with a higher deduct value. For the SCI value, this distress will be counted only when it is caused by load and not if it is a result of improper concrete curing practice.

Table 5

PCI Rigid Pavement Distress Types Used with the SCI

Number	Name	Associated Severity Levels
2	Corner break	3
3	Longitudinal/transverse/diagonal cracking	3
12	Shattered slab	3
13	Shrinkage cracks[a] (cracking partial width of the slab)	1
14	Spalling along joints	3
15	Spalling corner	3

[a]Used only to describe a load induced crack that extends only part way across a slab. In the SCI it does not include conventional shrinkage cracks due to curing problems.

The SCI allows a much more precise and reproducible rating of a pavement's condition than previous methods. Table 6 shows six examples of the range of SCI values that could be obtained by pavements all meeting the traditional CE initial crack failure criterion. The results in Table 6 illustrate the greater precision possible using the SCI to describe pavement performance compared with the prescribed failure definitions such as the CE initial crack criterion.

Table 6

Example SCI Values Meeting the Corps of Engineers' Initial Failure Definition

Example No.	Density, %	Severity[a]	Type	SCI
1	50	L	No. 3 L/T/D cracking[b]	80
2	50	M	No. 3 L/T/D cracking	55
3	25	L	No. 3 L/T/D cracking	61
	25	M	No. 3 L/T/D cracking	
4	15	L	No. 3 L/T/D cracking	45
	20	M	No. 3 L/T/D cracking	
	15	H	No. 3 L/T/D cracking	
5	25	L	No. 3 L/T/D cracking	70
	25	L	No. 12 shattered slab	
6	15	L	No. 3 L/T/D cracking	55
	15	M	No. 3 L/T/D cracking	
	10	L	No. 12 shattered slab	
	10	M	No. 12 shattered slab	

[a] L = low; M = medium; H = high.
[b] PCI rigid pavement Type No. 3 with L/T/D (longitudinal/transverse/diagonal) cracking.

ANALYTICAL MODEL

WESTERGAARD MODELS

As discussed previously, the Westergaard free edge load or the Westergaard interior load models form the basis of most current airport design methods. The major limitation of either of these models is the characterization of all material below the slab as a spring with a nonvariable spring constant. The inability for this kind of model to consider the layered structure of an overlay slab resting on a base slab led to the original development of the current empirical overlay design equations. To avoid the empirical approach, either the base slab must be included with the underlying materials as part of the spring system supporting the overlay slab or the base slab and the overlay slab must be added together to form an equivalent slab. Neither approach was considered satisfactory for this study.

FINITE ELEMENT MODELS

Finite element analysis is a powerful numerical method that is capable of solving engineering problems with complex material properties and geometry.

In this method the continuum to be analyzed is represented as a collection of finite elements connected only at their nodes; a displacement function is assumed over the region of the element; an element stiffness matrix is determined reflecting the assumed displacement function, geometry of the element, and material properties; a global stiffness matrix is assembled for the continuum from the individual element stiffness matrices; unknown nodal displacements are determined from the global stiffness matrix and load vector; and finally element stresses and strains are calculated from the nodal displacement. Obviously this technique must be computerized.

A variety of finite element computer programs is available and offers a broad selection of element types, displacement functions, material models, and special functions such as friction or slip surfaces. As the programs become more sophisticated and generalized, their cost for input preparation, computer support, and output analysis and their demand for accurate material characterization increase dramatically. Also, finite element solutions for a problem can seldom be performed in a single step but must include sensitivity studies to determine factors such as an adequate finite element mesh or appropriate number of loading steps for some material models.

The most generalized finite element solutions available are the three-dimensional codes that allow complex modeling of material variation and structural geometry in all planes, but their application is prohibitively expensive for routine pavement design and analysis. Some work has been done with prismatic solid elements for analysis of pavements, but these have also been too expensive for general pavement work. The plane strain, plane stress, and axisymmetric finite element programs use idealizations that seldom, if ever, are applicable to rigid pavement problems. A group of hybrid finite element codes has been developed that are simpler and more economical than the three-dimensional and solid prismatic solutions. These codes appear to have more immediate potential for pavement design and analysis than those mentioned previously.

These hybrid codes typically use a four-node thin plate finite element to represent the rigid concrete pavement surface and either a spring or layered elastic representation of the remaining pavement structure[30,15,29,35,45]. Overlays and stabilized layers are analyzed by transforming the surface slab and the base slab or stabilized layer into an equivalent thickness of plain concrete assuming either no bond or complete bond between the layers. Individual slabs are analyzed as an assemblage of the four-node thin plate finite elements, and load transfer between slabs can be included in the analysis by such methods as assigning joint deflection efficiencies, treating dowel bars as beam elements, or using springs to model load transfer across the joint.

LAYERED ELASTIC MODEL

Layered-elastic analytical models idealize the pavement system as a sequence of homogeneous, elastic, horizontally uniform layers subject to circular uniform loads. The formulation of the solution to stresses, strains, and deflections to this problem was originally set forth by Burmister[10]. The solution requiring the integration of Bessel functions which, except for

two- or three-layer systems, is done numerically. A variety of computer programs has been developed to solve the layered elastic problem, and they differ primarily in the methods and accuracy of these numerical procedures. Crawford and Katona[16] and Parker et al.[59] provide some comparisons and evaluations of several of these commonly available programs.

The bond between layers may be treated as unbonded (frictionless), fully bonded (full friction), or intermediate between the two. The fully bonded case requires that the horizontal displacements on either side of the boundary between layers be equal. For the unbonded case, the interface is considered a principal plane, and shear stresses at the interface are set equal to zero. These two cases are the most common idealizations for pavement analysis. Usually, the interface between a rigid pavement and the underlying layer is considered unbonded or frictionless, and almost all other pavement interfaces are considered fully bonded.

The generally recognized existence of partially bonded rigid overlays makes it desirable to treat cases intermediate between fully bonded and unbonded. One approach, originally proposed by Westergaard[82], assumes that the shear stress of a layer above an interface is a function of the difference between the horizontal displacement of the layer above the interface and the horizontal displacement of the layer below the interface. This approximation does not meet the elasticity compatibility equations and has led to another intermediate friction solution based on making the horizontal displacement of the layer above an interface a function of the horizontal displacement of the layer below the interface[13].

The BISAR layered elastic program uses the Westergaard approximation for intermediate bond conditions at interfaces. Cauwelaert, Lequeux, and Delaunois[13] have developed an initial version of a layered elastic program FLIP which solves the intermediate bond condition as noted. Initial checks of this program indicate that it matches the fully bonded and unbonded deflections of BISAR, and it is currently undergoing further study and testing at the WES. A wide variety of other programs such as CHEVRON, CHEVIT, ELSYM5, CIRCLY, and CRANLAY is available to solve either the fully bonded or unbonded interface cases. Parker et al.[59] recommended the BISAR layered elastic program for use with rigid pavements because of problems encountered with erratic deflection basins with some other programs when the ratio of the concrete modulus to the subgrade modulus was very large. There was little difference in calculated concrete pavement tensile stress between the programs. The FLIP program may eventually offer an alternate intermediate bond interface model.

MODEL SELECTION

Most of the analytical models discussed above use linear elastic material properties. Much more powerful material models are available for use with some finite element techniques, but they have not found much application in pavement work. To date, the input data required for these models and the increased effort involved in this type of modeling have not produced results that can be analyzed effectively. More research is required in this area before these types of models will become usable. The Westergaard models and

the hybrid finite element models that use the spring subgrade describe all material below the pavement surface with a single value spring constant. Representing each of these lower layers separately with linear elastic material properties as with the layered elastic model or some of the finite element models offers the advantage of modeling the effects of different layers of material with varying stiffness within the pavement structure.

The Westergaard edge-loaded model, the hybrid finite element codes, and the three-dimensional finite element codes offer the best geometric models of actual pavement slabs and can directly include the effect of slab joints in the analysis. The inability of the layered elastic model to include the effect of joints in the pavement is a major limitation of its usefulness in analysis of concrete pavements. However, the layered elastic model offers an excellent representation of th_ layered overlay structure with variable interface conditions between layers. The joint limitation can be overcome by the use of empirical correlations and adjustment factors.

The layered elastic model and some of the more complex finite element models include methods of accounting for different levels of bond or friction between layers. The hybrid finite element programs handle no bond and complete bond by transforming the surface and base slab into an equivalent slab but are unable to examine intermediate levels of bonding. A similar approach of transforming the slab to an equivalent slab could be used with the Westergaard models. The existence of the partially bonded overlay concept suggests that the effect of various levels of friction and bonding between the overlay and base slab is important in developing an effective overlay analysis technique.

Input time, computer support, and overall cost of analysis of the different models vary. The Westergaard and layered elastic models are readily solved on current levels of microcomputers. Rapidly increasing capacity of these machines suggests that some of the simpler finite element programs will soon be available on microcomputer. At the present time, finite element analysis at sufficient detail to be used for pavements requires the support of a mainframe computer. The cost of analysis is lowest for the Westergaard solutions followed in increasing order of cost by layered elastic, hybrid finite element with spring subgrade, axisymmetric finite element, hybrid finite element with layered elastic subgrade, prismatic solid, and three-dimensional finite element programs.

The layered elastic model solved with the BISAR computer program will be used for this program. Selection of this model is based on (a) reasonable modeling accuracy which can represent the layered structure and variable interface condition that exist in an overlay with appropriate material models. The inability to model joints and effects of nonstandard load transfer is a major disadvantage of this approach, (b) costs and computer support which has reasonable input, computer, and analysis costs. It can be supported on current generations of microcomputers, and (c) compatible with other systems in which layered elastic models are currently being used at the WES and in other agencies for flexible and rigid pavement design and analysis and are widely used for evaluation of nondestructive pavement tests.

PREVIOUS TRAFFIC DAMAGE

Figure 6 illustrates some of the interactions between the base slab and an overlay slab. A base slab subjected to traffic from t_0 to t_1 will undergo some deterioration. If nothing is done, continued traffic would allow the pavement to deteriorate as shown by the dashed line. If, however, the slab is overlaid at t_1, the stresses in the base slab are reduced. As traffic is applied to the overlay slab, the base slab will continue to deteriorate as shown by the solid line but at a reduced rate from before.

At traffic t_1 the base slab is capable of providing a certain amount of support to the new overlay slab. Since the base slab has undergone some deterioration from t_0 to t_1, it will not provide the same support as a brand new slab. For this amount of support the traffic on the overlay will develop a certain stress level which will result in deterioration of the overlay slab. However, at traffic t_2 the base slab has deteriorated further; its support value has decreased; the stress in the overlay, therefore, has increased; and the deterioration of the overlay slab is faster than would be predicted from the conditions at t_1. Similarly, at t_3 base slab deterioration has continued with the same result of accelerating deterioration in the overlay. Any predictive performance model for the overlay slab must recognize and account for the acceleration of the deterioration of the overlay slab as the base slab deteriorates with continuously decreasing support to the overlay.

METHODOLOGY

The objective of this research study is to develop a mechanistic method of designing concrete overlays for rigid pavements that will predict the performance of the overlay. The layered elastic model has been selected as the analytical basis for this study. The SCI has been defined as the measure of performance of the pavement. Prediction of performance of an overlay will require (a) determining pavement properties, (b) base slab analysis, and (c) overlay slab analysis. A layered elastic analysis requires that each material be described by a modulus of elasticity and a Poisson's ratio. Modulus values can be determined for in-place materials by standard nondestructive testing, destructive sampling and testing, or construction data. If nondestructive testing techniques are not used, modulus values for soil and aggregates are usually estimated by correlations with standard pavement tests such as modulus of subgrade reaction or California Bearing Ratio (CBR), but they can also be determined from laboratory tests such as the resilient modulus test. The concrete modulus for the proposed overlay can be estimated from local historical construction data, or it can be determined before construction as part of the mixture proportioning studies. Layered elastic calculations are relatively insensitive to Poisson's ratio, and these values are usually taken as 0.15 to 0.20 for concrete and 0.3 to 0.5 for aggregates and soils. The interface conditions between each layer must also be selected. The interface between concrete and soil or aggregate is commonly modeled as frictionless, and most other soil or aggregate interfaces are modeled as fully bonded. The appropriate bond condition between the concrete overlay and base

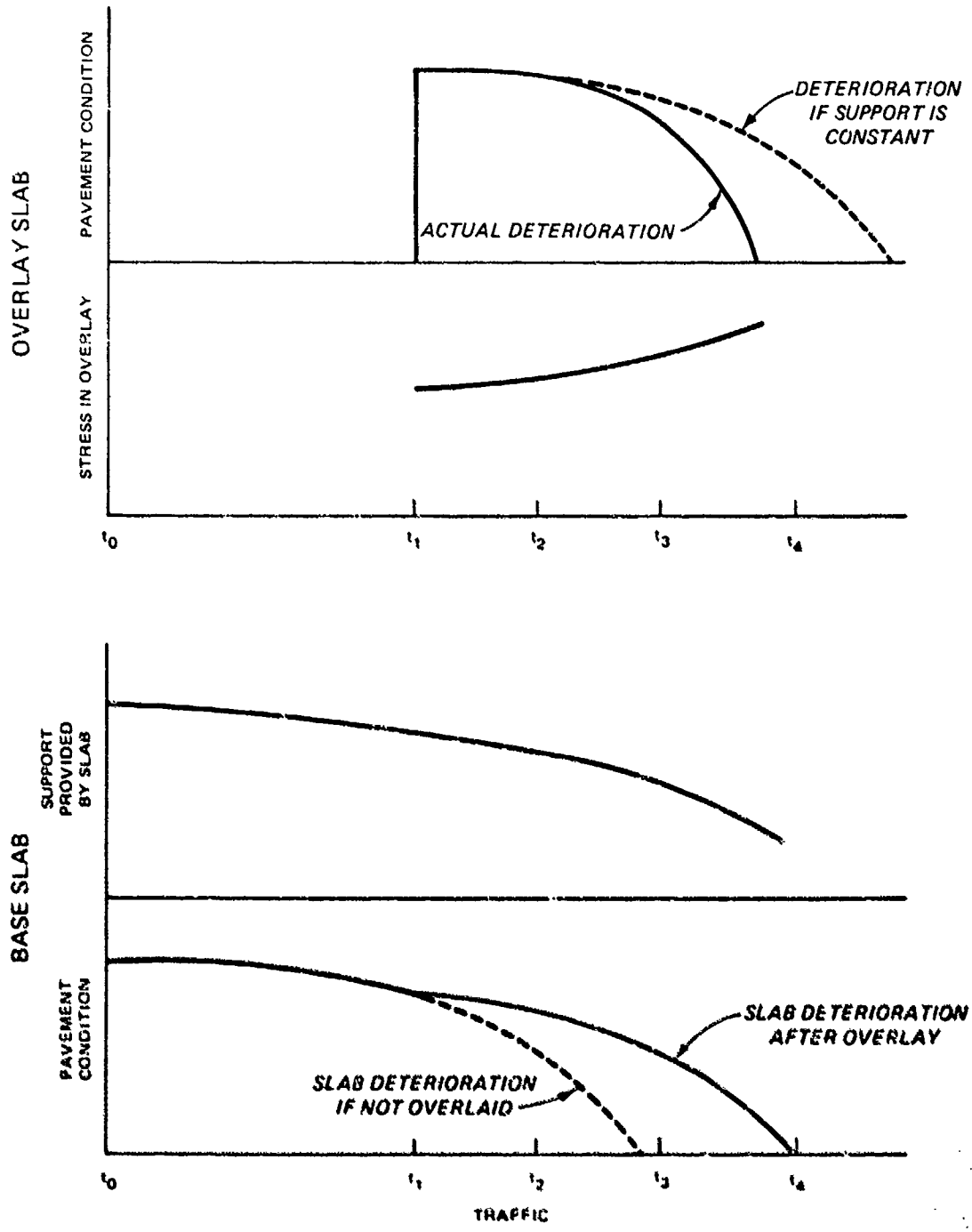

Figure 6. Conceptual deterioration of a pavement and overlay

pavement needs to be determined. The condition of the base slab to be overlaid must be determined. The effect of previous traffic before overlay on the base slab's remaining fatigue life must be evaluated. Its support provided to the overlay slab must be quantified in terms usable with the layered elastic model. Similarly, if the existing base slab load transfer is substandard, this must be expressed in some manner usable with the layered elastic model. As the base slab deteriorates, its supporting value to the overlay slab must be determined. This effect will be accounted for by dividing the traffic into intervals, determining the reduction in support value provided by the base slab during that interval of traffic, calculating the stress in the overlay for this changed support condition, and then calculating the loss in the SCI of the overlay during that traffic interval.

In order to carry out this type of analysis, a model will be needed to describe the deterioration of a concrete pavement in terms of the SCI as load repetitions are applied. Substandard load transfer between slabs in the base pavement must be expressed in terms that are usable with the layered elastic model. A method of quantifying the change in support provided by the base slab as it deteriorates is also needed. Once these models are available this concept of analysis can be checked against available overlay test section data and compared with current design methods.

The most extensive historic controlled trafficking data using full-scale aircraft loads are the CE accelerated trafficking tests conducted at Lockbourne Air Force Base, Sharonville, and the WES. These were the only tests conducted with full aircraft size loads and include tests with weights up to the current B-747 and C-5 aircraft. Sixty-seven test sections were built and tested during this test program that originally started in World War II. These tests used full-size concrete slabs for testing and applied traffic with full-size aircraft gear and gear loads. A summary of all these tests is given by Parker et al.[59].

TEST SECTION DATA

The new rigid pavement performance models developed for this research study are based on a reevaluation of the accelerated traffic tests conducted by the CE. The analysis of these test sections used the original test reports and supplemented this information with photographs, work logs, minutes of meetings, and any related correspondence that could be located in the files at WES. Table 7 lists 67 test sections that were part of this test program. These data are divided into classes, I, II, and III. The class III data were not used in the analysis because of a lack of information needed for the analysis, no deterioration under traffic, failure conditions such as severe pumping that are not included in the SCI, test slabs that had no load transfer or peculiar joint construction no longer in use, and the inadequacy of the quality or spread of the data to determine performance (e.g., at one point SCI = 100, many repetitions later SCI = 0 with no information between these points). Lockbourne No. 1, test sections R-2, R-3, S-2, S-3, T-2, and T-3 are also included as type III data. These sections failed inexplicably. With high design factors they reached shattered conditions in as little as 1.5 coverages. These test sections have been excluded in past analyses of these data because of their peculiar behavior and have also been excluded from this analysis. The remaining data are divided into classes I and II. The class I data are the best quality data. Class II data include tests that may have had slight pumping that could have influenced test results, data that had a poor spread in values which made the data difficult to interpret, or tests that had a large amount of unusual distress such as extensive joint spalling without any cracking.

Most test section reports include a crack map taken at either specific traffic intervals or the traffic coverage level at which a crack formed is indicated on the map. This map is usually supplemented with written descriptions and photographs in the report. Additional information in the form of photographs, work logs, and briefing papers are also available for some test sections.

The PCI procedures as published by the FAA were used to develop the test section SCI, except only the five distress types listed in Table 5 were used. Each of these distress types has a description and photographs that describe its severity level. Charts provide a deduct value for each distress type depending on its severity level and density. These deduct values are summed and then adjusted if more than one distress type exists. The damage

Table 7

Available Rigid Pavement Field Test Data

Test Series	Item Designation: Parker et al.[59] a	Item Designation: Original Test	Quality	Remarks
Lockbourne No. 1	A-1	A2.60	II	Poor data spread
	A-2	A1.60	II	Poor data spread
	B-1	B2.66L	II	One slab
	B-2	B1.66L	II	Unusual failure
	C-1	C2.66L	I	--
	C-2	C1.66S	I	--
	D-1	D2.66	I	--
	D-2	D1.66	I	--
	E-1	E2.66M	III	No deterioration
	E-2	E1.66M	I	--
	F-1	F2.80	III	No deterioration
	F-2	F1.80	III	Unusable data spread
	K-3	K2.100	III	Unusual failure
	K-2	K1.100	III	Unusual failure
	N-2	N1.86	I	--
	N-3	N2.86	II	Poor data spread
	O-2	O1.106	I	--
	O-3	O2.106	I	--
	P-2	P1.812	III	Unusable data spread

(Continued)

[a] Parker et al.[59] summary of test information used a shortened designation for test items in Lockbourne Test Nos. 1 and 2.

(Sheet 1 of 4)

Table 7 (Continued)

Test Series	Item Designation: Parker et al.[59]	Item Designation: Original Test	Quality	Remarks
Lockbourne No. 1 (Continued)	P-3	P2.812	III	Unusable data spread
	Q-2	Q1.102	III	Unusable data spread
	Q-3	Q2.102	I	--
	R-2	R1.612	III	
	R-3	R2.612	III	R-2 through T-3 had unusually rapid failure. These sections have been deleted in past studies
	S-2	S1.66	III	
	S-3	S2.66	III	
	T-2	T1.60	III	
	T-3	T2.60	III	
	U-2	U1.60	II	Poor data spread
	U-3	U2.60	III	Unusable data spread
	A-Rec	A-Rec	III	Insufficient data
Lockbourne No. 2	E-1	a	III	Bad load transfer condition
	E-2	a	III	Poor data
	E-3	a	III	Bad load transfer condition
	E-4	a	III	Bad load transfer condition
	E-5	a	III	Bad load transfer condition
	E-6	a	II	Poor data spread

(Continued)

(Sheet 2 of 4)

Table 7 (Continued)

Test Series	Item Designation: Parker et al.[59]	Item Designation: Original Test	Quality	Remarks
Lockbourne No. 2 (Continued)	E-7	a	III	No deterioration
	M-1	a	I	--
	M-2	a	II	Poor data spread
	M-3	a	III	No deterioration
Lockbourne No. 3	--	--	III	Insufficient data
Sharonville Channelized	--	57	III	No detailed data ever published on Sharonville Channelized Test Sections
	--	58	III	
	--	59	III	
	--	60	III	
	--	61	III	--
	--	62	III	--
Sharonville Heavy Load	--	71	III	No failure
	--	72	III	Poor data, unusual deterioration
	--	73	II	Unusual deterioration
Multiple Wheel Wheel Heavy Gear Load (MWHGL)	--	1-C5	I	--
	--	2-C5	III	Severe pumping
	--	3-C5	III	Severe pumping
	--	4-C5	II	Slight pumping
	--	2-DT	I	--
	--	3-DT	I	--

(Continued)

(Sheet 3 of 4

Table 7 (Concluded)

Test Series	Item Designation: Parker et al.[59]	Item Designation: Original Test	Quality	Remarks
Keyed Longitudinal Joint Study	--	1-C5	II	Slight pumping
	--	2-C5	I	--
	--	3-C5	II	Possible damage from instrumentation traffic
	--	4-C5	III	Pumping
	--	4-DT	I	--
Soil Stabilization Pavement Study	--	3-200	I	--
	--	3-240	III	Damaged by static test
	--	4-200	I	--
	--	4-240	II	Possible damage by adjacent traffic

descriptions and deduct curves used to compute the SCI can be found in the FAA publication describing the PCI[79]. Table 8 shows an example SCI calculation for one test section.

Judging the severity level of a distress from the available records was often very difficult. It was particularly difficult to separate low- and medium-severity type 3 longitudinal/transverse/diagonal cracking. This separation is based on spalling along the joint, crack width, or formation of a second crack. During trafficking, observers watched for cracks and generally noted when the first crack occurred. This crack was undoubtedly a tight, low-severity crack. However, the working of this crack which leads to widening and spalling may not have been recorded, and photographs are not available to show adequate details. The transition between low- and medium-severity cracks then cannot be clearly identified in the tests. Therefore, all cracks were assumed to be low-severity cracks unless information was available to indicate otherwise. Applying this rule, a slab would be assigned a low-severity crack rating when the initial crack forms. It is raised to a medium severity level when a second crack forms and divides the slab into three pieces. When additional cracks divide the slab into four or five pieces, the rating becomes a low-severity shattered slab. This ratio is raised to medium severity when the slab is further subdivided into six pieces. As multiple cracks occur, they usually begin to work and almost invariably spalling is noted in the report text, marked on the crack map, or as shown in the photographs. Consequently, it is usually possible to appropriately class a shattered slab's severity level on the basis of the severity of the cracks in addition to its number of pieces.

The SCI is a function of the density or amount of distress that occurs in a test section. Commonly, a test section consisted of four slabs, but some had only two slabs. On an actual pavement the large number of slabs would be expected to deteriorate gradually, providing a smooth curve. Test section data will tend to be rougher because of the limited number of slabs that lead to large, abrupt changes in the density measurement associated with distresses.

Another problem existed with the Lockbourne No. 1 tests. These sections were built during World War II, and joint design was one of the test variables. A test section was typically 20 by 40 ft and separated from preceding and following test sections by transition slabs. Each test section was divided into four 10- by 20-ft slabs by contraction joints. One longitudinal edge joint was a keyed joint with an adjacent test section. The other longitudinal edge was free. One transverse joint at the end of the test section was a doweled expansion joint, and the other end had a free expansion joint with no provisions for load transfer. Since the layered elastic model was used for stress calculations, it cannot accurately account for varying load transfer levels. Only slabs that represent current construction methods with reasonable joint load transfer were used to develop the performance models. In the Lockbourne No. 1 tests, only the two slabs adjacent to the doweled construction joint can be used for calculation of the SCI. Some of the Lockbourne test items also applied traffic to within 2 ft of the free edge longitudinal joint. For these sections only the single slab adjacent to the doweled expansion joint and the keyed longitudinal joint could be used in the analysis.

Table 8

Example SCI Calculations for Keyed Longitudinal Joint Test Section, Item 2-C5

Traffic Coverage	Distress					Summed Deduct	Adjusted Deduct	SCI
	Number	Description	Severity	Density, %	Deduct			
0	--	--	--	--	--	--	--	100
144	3	L/T/D cracking[a]	Low	25	15	15	15	85
344	3	L/T/D cracking	Low	50	20	20	20	80
504	3	L/T/D cracking	Low	25	15	--	--	--
	12	Shattered slab	Med	25	43	58	50	50
688	3	L/T/D cracking	Low	25	15	--	--	--
	12	Shattered slab	Med	25	43	103	87	13
1696	3	L/T/D cracking	Med	25	32	--	--	--
	12	Shattered slab	Med	25	42	--	--	--
			High	50	77	151	100+	0

[a] L/T/D cracking = longitudinal/transverse/diagonal cracking.

Appendix A presents the detailed summary of the analysis of the CE test sections. The thickness and material properties for each item are tabulated for each test series. These data were taken from the original CE test reports listed in the bibliography and references or from the test summary by Parker et al.[59]. The calculated SCI values for the test items in each test series are tabulated with the calculated C_0 and C_F values, the specific slabs analyzed for the test item, and the size of the load. The SCI values are shown for each coverage level for which there was a map of cracking, photographs, or written description that allowed the SCI to be calculated. The final table in Appendix A presents the stresses and design factors calculated for each test item.

TEST SECTION PERFORMANCE

PROPOSED DETERIORATION MODEL

Test section deterioration data show a great deal of scatter as shown in Figure 7. Fatigue analysis used the logarithm of stress cycles or coverages, and when this is used for the abscissa of the test section deterioration plots, the scatter of the data is greatly reduced. Figure 8 shows the test items from Figure 7 replotted with SCI as a function of the logarithm of coverages. The relation for each test item is essentially linear with the logarithm of coverages.

Rigid pavements and the CE test items generally go through a period of little or no deterioration, and then, as shown in Figure 8, they deteriorate in a linear form as a function of the logarithm of coverages. This allows for the definition of the proposed rigid pavement performance model shown in Figure 9. A rigid pavement suffers no structural fatigue related deterioration until the point identified as C_0 in Figure 9 is reached. During this period the SCI is 100. From C_0 to C_F where the SCI is zero, the pavement deteriorates linearly as a function of the logarithm of coverages. C_0 represents the onset of structural deterioration, and C_F is essentially complete or absolute failure with an SCI of zero.

Some test sections (e.g., multiple wheel heavy gear load (MWHGL) Item 1-C5 in Figure 8) show a gradual upper curve into the linear deterioration behavior rather than the abrupt deterioration in the proposed model. This is probably true of actual pavements also. As noted earlier, the test section data have relatively few slabs, so the damage density values used to calculate the SCI for test items show sudden large increases as slabs begin to deteriorate. In actual pavements this increase in damage density would be progressive resulting probably in a smooth curve. The major deterioration occurs along the line defined by C_0 and C_F, and the minor deterioration that may occur along the upper curve line in Figure 9 does not significantly affect the usefulness of the proposed model.

The structural fatigue deterioration of a rigid pavement can be uniquely described by two parameters, C_0 and C_F. The pavement undergoes no deterioration until C_0 is reached and thereafter deteriorates linearly as a

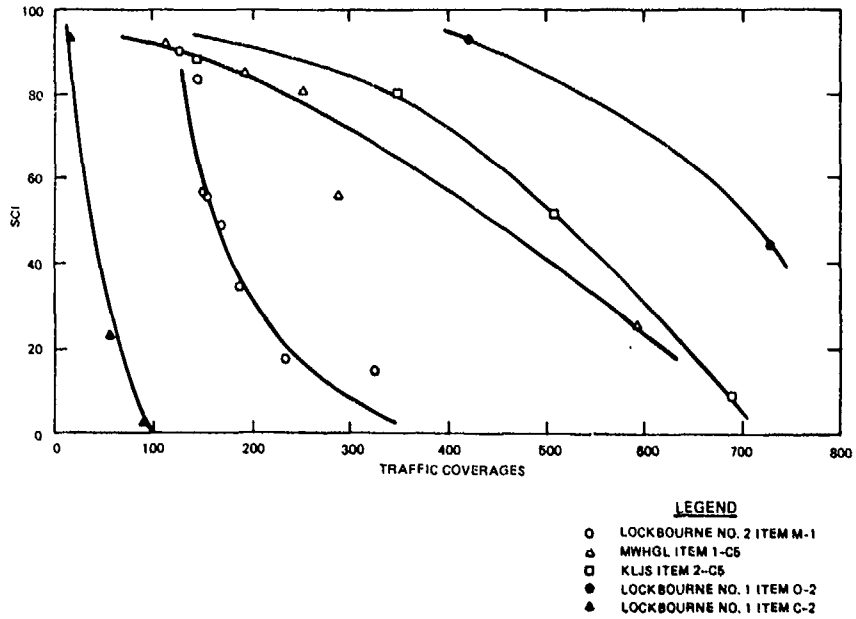

Figure 7. Sample SCI coverage relationships

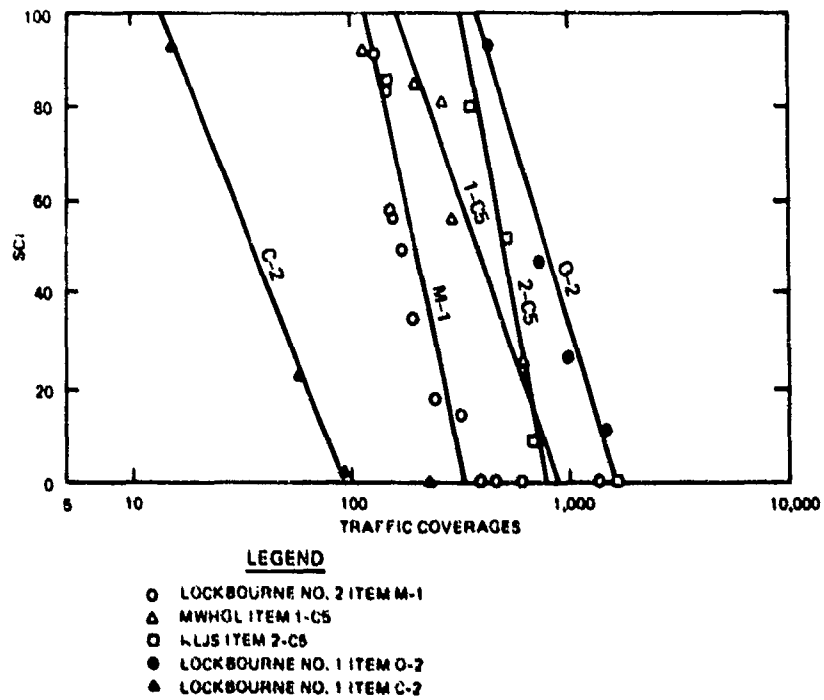

Figure 8. Sample SCI logarithm coverage relationships

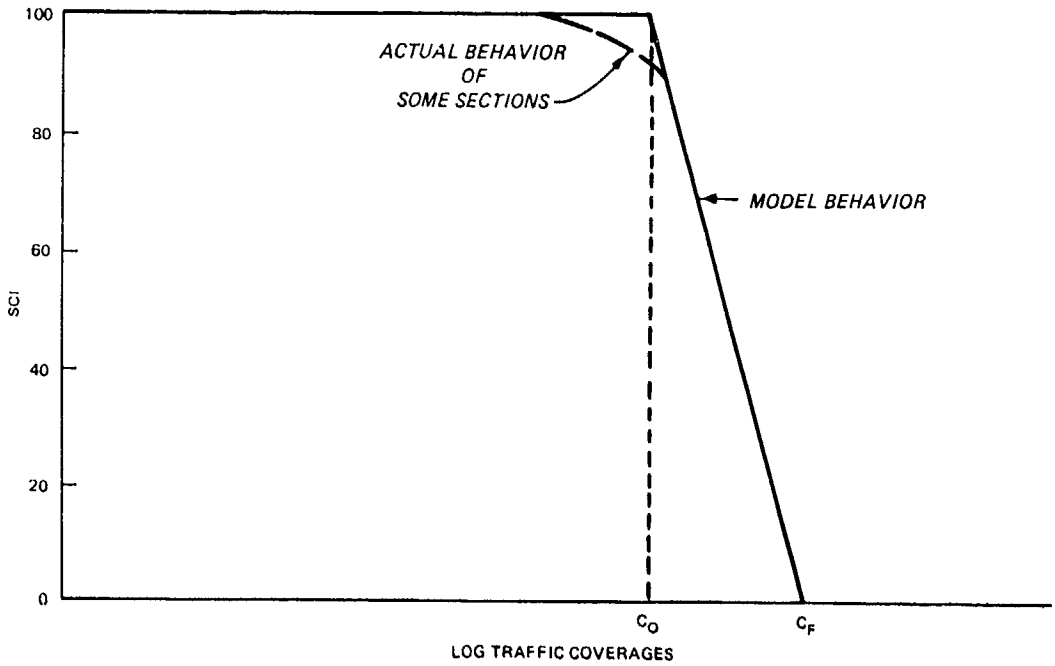

Figure 9. Proposed performance model

function of the logarithm of coverages until C_F is reached. If these two parameters can be predicted for a rigid pavement, then the SCI at any given coverage level can also be predicted.

DETERMINATION OF MODEL PARAMETERS

The C_0 and C_F values were calculated for each CE test item by fitting a least-square regression straight line to the SCI and coverage data of each item. The C_0 value was found by setting SCI equal to 100, and C_F value was found by setting the SCI equal to zero. Table 9 summarizes the results of this analysis for each test item rated as having Type I or II quality data. Not all the SCI-coverage data points were used in the analysis as indicated in Table 9. Excluded data points fell into three groups. When the SCI was equal to 100, the data point was on the horizontal portion of the model in Figure 9 and had not reached C_0. Generally, this kind of point was excluded from the analysis. When a data point had an SCI of zero, it has a similar problem since it can be past C_F and on the horizontal portion of the model in Figure 9. Also, as noted in Figure 9, some test items have a slightly curved upper portion from the SCI of 100 horizontal line to the straight line deterioration. These points have SCI values of 80 to 100 at coverage levels before C_0 is reached. This type of point was excluded from the data points used to determine C_0 and C_F. The correlation coefficient

Table 9

C_0 and C_F Values for Test Sections

Test Section	Quality	C_0	C_F	Number of Data Points	Correlation Coefficient r^2
Lockbourne No. 1					
A-1	II	225	10,084	2	--
A-2	II	13	59	2	--
B-1	II	59	522	3	0.88
B-2	II	3	96	4(3)[a]	0.99
C-1	I	48	636	4	0.93
C-2	I	13	92	3	0.99
D-1	I	289	3,776	3	0.96
D-2	I	6	104	3	0.95
E-2	I	50	212	3	0.95
N-2	I	105	284	4(3)[a]	0.99
N-3	II	6	32	2	--
O-2	I	347	1,606	4	0.97
O-3	I	41	155	4(3)[a]	0.99
Q-3	I	36	209	4	0.92
U-2	II	123	488	3(2)[a]	--
Lockbourne No. 2					
E-6	II	1,342	13,083	2	--
M-1	I	93	353	9	0.87
M-2	II	1,693	6,774	3(2)[a]	--
Sharonville Heavy Load					
73	II	668	7,054	4	0.83
Multiple Wheel Heavy Gear Load Test					
1-C5	I	150	936	5(4)[a]	0.93
4-C5	II	165	258	2	--
2-DT	I	128	476	4(3)[a]	0.99
3-DT	I	177	960	5(4)[a]	0.95
Keyed Longitudinal Joint Study (KLJS)					
1-C5	II	16	683	4	0.91
2-C5	I	292	783	4(3)[a]	0.97
3-C5	II	11	395	4	0.94
4-DT	I	228	1,094	4	0.95

(Continued)

[a]Number in parentheses is number of points actually used to determine C_0 and C_F.

Table 9 (Concluded)

Test Section	Quality	C_0	C_F	Number of Data Points	Correlation Coefficient r^2
Soil Stabilization Pavement Study (SSPS)					
3-200	I	937	4,258	5(4)[a]	0.93
4-200	I	1,179	5,934	3	0.95
4-240	II	22	377	4	0.99

values in Table 9 indicate that the data used to determine C_0 and C_F were reasonably linear as idealized by the model in Figure 9.

Figure 10 shows three relationships developed for C_0 as a function of the design factor (DF). The DF is the concrete flexural strength divided by the layered elastic calculated stress. The C_0 values for each test item are from Table 9. The DF's for each test item were calculated using stresses from layered elastic theory and are tabulated in Appendix A. The first relation was developed for the class I test sections identified in Table 7. The second relation identified as class IIa includes four data points that were listed as class II because of poor data spread that made calculation of C_0 uncertain. These points gave results in line with the class I data. The third relation identified as class II includes all class I and class II data.

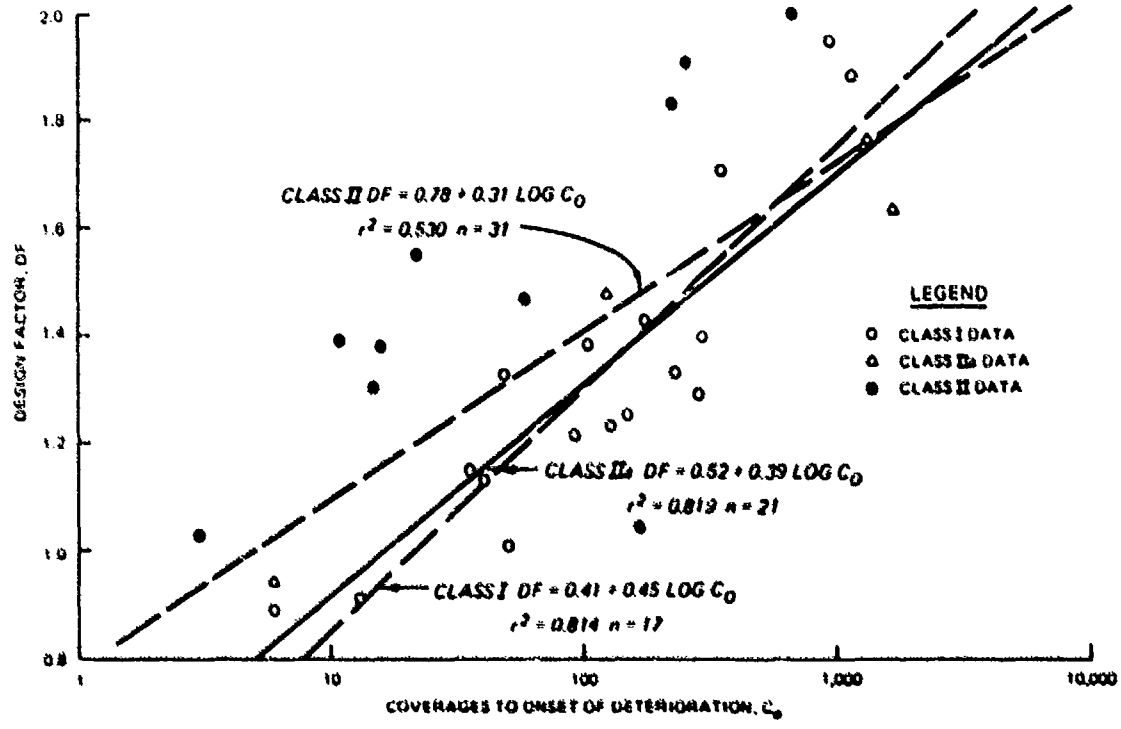

Figure 10. Relationship between DF and C_0

All but one of the class II data, exclusive of the four points shown as IIa, have positive residuals for any of the relationships. These positive residuals suggest that a systematic error may exist. In this case, the poor data spread in most of these test items has resulted in underestimating C_0. The one section that has a negative residual is item 4-C5 of the NWHGL test

that was classified as class II data because slight pumping occurred during the test.

The four class IIa data points change the slope of the relationship between DF and C_0 significantly. The addition of these four data points appears reasonable relative to the class I data. The class IIa relationship slope of 0.39 is also similar in magnitude to the 0.35 developed earlier by Parker et al.[59] for conventional initial failure design with layered elastic models. Overall, the class IIa relationship appears to be the best relation available for the quality and quantity of data available, and it is recommended for predicting the C_0 value.

Figure 11 shows three relations developed for C_F for the data divisions as before. The residuals for the class II data do not show the pattern of being all positive that they did for C_0. The class II and IIa relations are parallel lines, and the class I line once again has an appreciably larger slope. There does not appear to be any reason to exclude any of the data points in Figure 11, and the relation for all of the class II data is the most appropriate for use.

In this analysis, it has been assumed that C_0 and C_F are functions only of the design factor. As previously noted, this assumption may not be completely true. Postcracking behavior of slabs may also be a function of the subgrade support. The CE recognized this effect by the high-strength subgrade thickness reduction used with the traditional CE design method. However, attempts to use subgrade strength with the DF to obtain better C_0 and C_F relationships were unsuccessful because the test sections were almost universally built on low-strength subgrades. Therefore, insufficient data exist to examine the effect of high-strength subgrade influence on postcracking behavior of the pavements. Also, the use of an elastic modulus value with a layered-elastic analytical model may simply reflect the contributions of the subgrade better than the Westergaard model with the subgrade spring constant. As discussed, the Westergaard stress calculation is not very sensitive to the modulus of subgrade reaction.

MODEL EVALUATION

COMPARISON WITH OTHER CRITERIA

The relations developed for the two parameters C_0 and C_F allow the prediction of a pavement's SCI value for any specific traffic coverage if the DF is known. The DF is calculated from the concrete flexural strength and layered elastic stresses. These relations for C_0 and C_F are in effect fatigue relations, and they follow the same linear form as other concrete fatigue relations. These relations for C_0 and C_F are based on tests with relatively small magnitudes of traffic. However, their extrapolation to larger coverage levels is supported by the linear concrete fatigue relations found in beam fatigue tests.

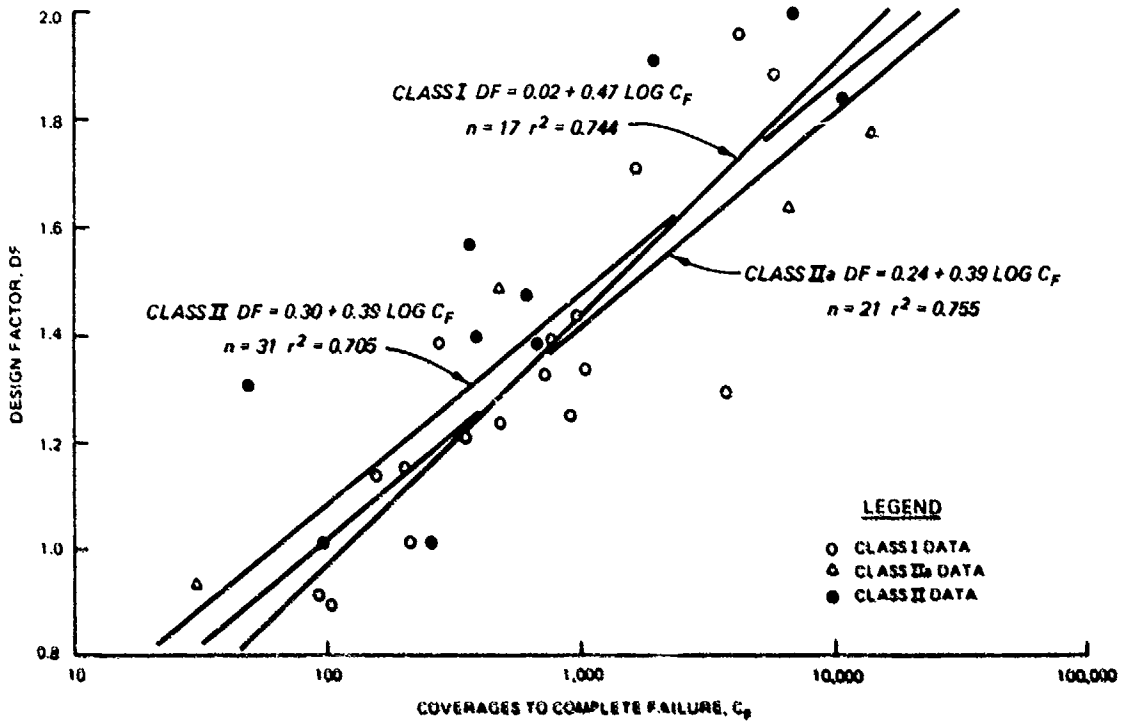

Figure 11. Relationship between DF and C_F

The current CE fatigue relationship for Westergaard edge load model calculated stresses and the fatigue relationship developed by Parker et al.[59] for layered-elastic model calculated stresses use the same form as the C_0 and C_F relations. The DF is expressed as a linear function of the logarithm of coverages. The relationships for C_0 and C_F and Parker et al.[59] relationship use the same analytical model to calculate stresses for determining the DF. Parker et al.[59] used the CE definition of rigid pavement failure to determine their relationship. As noted in Table 6, the CE definition of failure could have SCI values that reasonably range from 55 to 80 depending on the amount and severity of cracking in the test slabs. As shown in Figure 12, the relationships for C_0 and C_F bracket the Parker et al.[59] relationship within the ranges of traffic used in the CE test sections. Since the C_0 and C_F relationships are for an SCI of 100 and 0 and the Parker et al.[59] is for some range of SCI values between these extremes, the relative positions of the three relations are consistent.

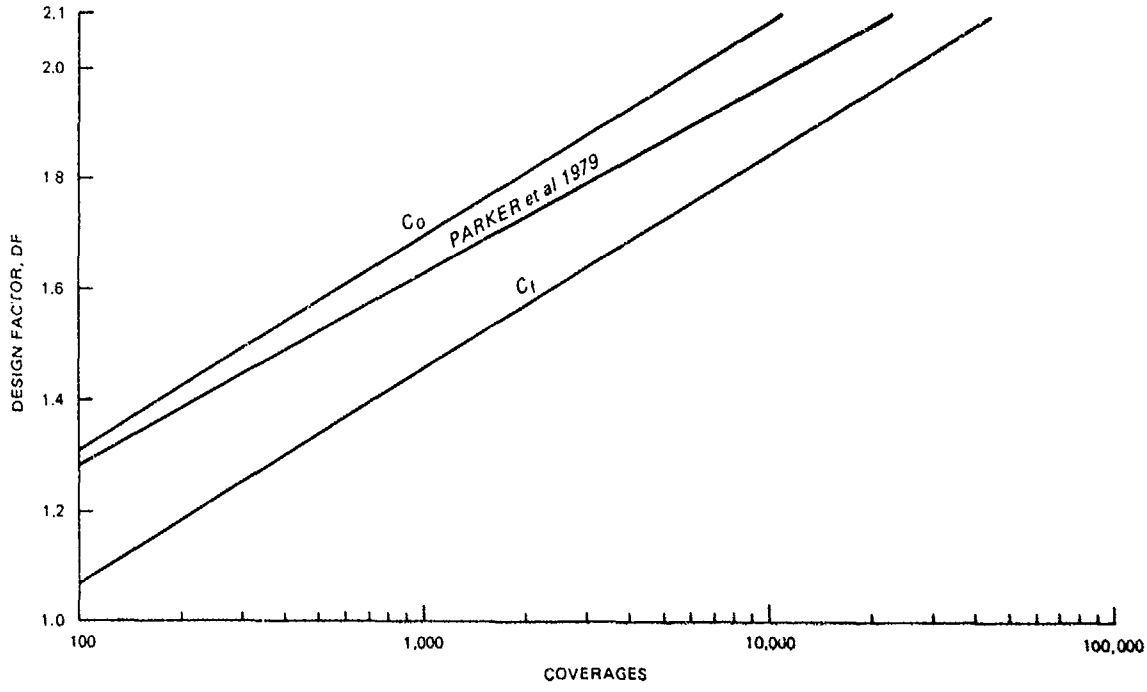

Figure 12. Relationship between C_O and C_F and the criterion of Parker et al.[59]

RATE OF DETERICRATION

The relationships for C_O and C_F have the same form as other concrete fatigue relationships and appear consistent with other concrete pavement criteria. However, the logarithmic form of the C_O and C_F relationships indicates that once deterioration begins the rate of deterioration decreases with increasing coverages.

The deterioration of a test section can also be examined using a normalized coverage factor C_N defined as

$$C_N = \frac{C - C_O}{C_F - C_O} \tag{27}$$

where C is the coverage level at which a specific SCI is calculated. The relation between C_N factor and SCI in Figure 13 is a measure of the rate of structural deterioration at a given coverage level. Normalizing the traffic

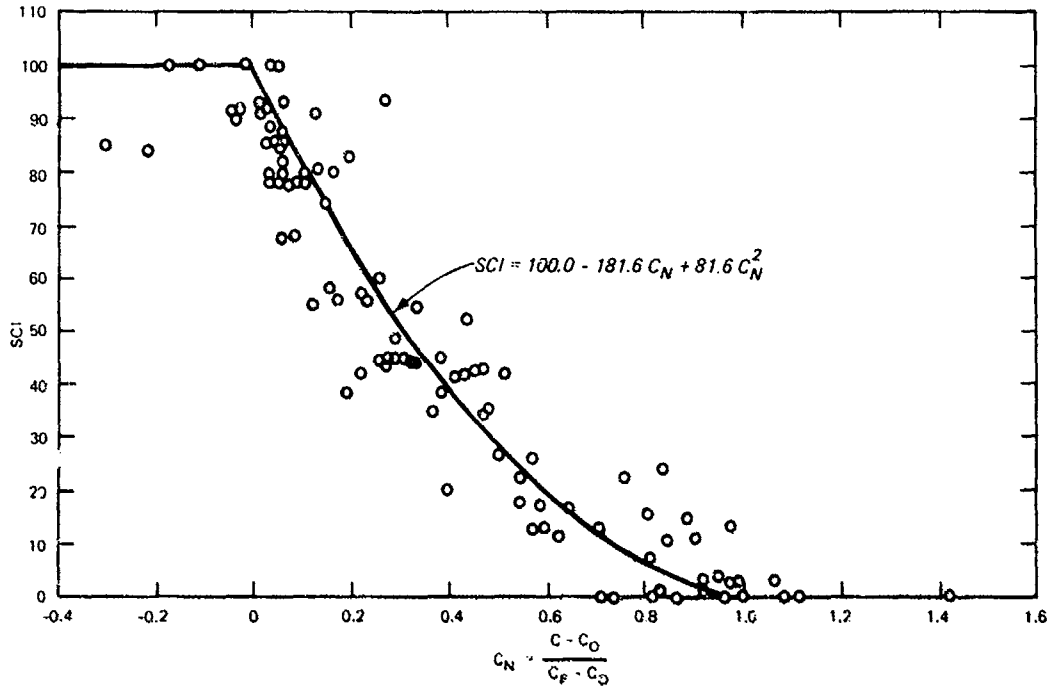

Figure 13. SCI C_N relationship

coverage data using the calculated C_O and C_F values effectively collapses the data.

By definition, when C is equal to C_O, the normalized factor C_N should be zero, and when C is equal to C_F, C_N should be 1. The relation in Figure 13 passes through these points. Negative C_N values with SCI values less than 100 are due to the initial curved deterioration some test sections showed as was shown in Figure 9.

The decrease in the rate of deterioration is not consistent with some of the results reported from the field performance of pavements. Shahin, Darter, and Kohn[70] found that Air Force airfield pavements up to 35 years old showed a slightly convex relationship between PCI and the pavement's age in years. This is an increase in the rate of deterioration with age and implies that if the annual traffic rate is approximately constant then the rate of pavement deterioration increases with coverage level as opposed to decreasing with coverage level implied in Figure 13.

This discrepancy is due to several factors. First, the PCI includes all forms of distress and not just the structural deducts used by the SCI. Some of the distress, particularly those associated with durability or maintenance, will become more pronounced with age regardless of loading. The assumption of constant equivalent annual traffic is probably erroneous. Although the Air Force has not seen the same increase in traffic volume that has occurred in civil aviation, aircraft have become progressively larger and heavier with increasing structural loading of the pavement. The addition of the other PCI

deducts not included in the SCI and increasing aircraft loading will tend to accelerate the rate of deterioration of in-service pavements.

As a pavement begins to structurally deteriorate, its ability to carry load through bending decreases. When carried to the extreme, the pavement is cracked into small blocks that are pushed into the subgrade with negligible bending. Consequently, in badly deteriorated pavements further progression of deterioration will depend less on fatigue tensile related cracking than it will on spalling and faulting. Also, deteriorated pavement will allow water to penetrate to the subgrade thereby weakening it and reducing the pavement support. The C_0 and C_F relationships are based on accelerated traffic tests that, although they include field effects such as temperature or moisture warping or nonuniform subgrade support, generally do not last long enough to provide information on water penetration and subgrade weakening that may occur over years as a pavement deteriorates.

The rate of deterioration of the SCI predicted by the C_0 and C_F relationships is reasonable for the data and limitations upon which the relations are based. An in-service pavement will have additional deterioration besides that predicted by the SCI loss from the C_0 and C_F relations.

UNFAILED TEST SECTIONS

Four test items in Table 7 had SCI values of 100 at the end of traffic testing. Table 10 shows the predicted performance of each of these sections along with the coverage level at the end of trafficking. Only one test section exceeded its predicted C_0 value where deterioration would have been expected to start. The other three test sections stopped traffic before reaching their C_0 values and, as predicted by the model, showed no deterioration.

Table 10

Predicted Performance of Unfailed Test Item

Test Series	Test Item	Predicted Performance C_0	Predicted Performance C_F	Unfailed Coverages
Lockbourne No. 1	E2.66M	252	1,024	556
	F2.80	2,708	11,253	550
Lockbourne No. 2	E-7	74,791	325,068	2,2204
Sharonville Heavy Load	71	7.142×10^6	32.653×10^6	9,680

U-TAPAO AIRBASE

During the Vietnam War, three pavement features failed under B-52 traffic at U-Tapao Airbase, Thailand. It is generally very difficult to assess field performance of in-service pavements because the actual number of

aircraft using the feature and their actual weights are seldom known. However, since these were bomber aircraft on combat missions, departing aircraft were probably at or near their maximum weights. Also, the military operations were concentrated in a relatively short period from 1967 to 1972. These pavement features were subject to predominately B-52 traffic which is such a severe aircraft when fully loaded that traffic by unloaded B-52 aircraft or other types of aircraft is insignificant. The failed U-Tapao features offer the opportunity to check the proposed performance models against in-service pavement performance.

Pavement condition surveys by Lambiotte and Chapman[42] and Lambiotte[41] provide the basis for this analysis. Properties drawn from these reports are shown in Table 11. The SCI values were estimated from the condition survey reports. The C_0 and C_F values were calculated using the performance models presented earlier. About 14 percent of Hardstand Taxiway 2 (the south end) failed and was rebuilt after only 74 coverages. The remainder continued to be used with the estimated SCI deteriorating from 88 to 76 over the next few years. Access Taxiway 2 failed after 1,230 coverages and was rebuilt. No condition information was available other than the pavement failed. Access Taxiway 1 failed after 9,820 coverages and was abandoned. At this point, it had an estimated SCI of 36.

Figure 14 shows the performance of the three U-Tapao pavement features predicted by the C_0 and C_F values from Table 4. Also shown are estimates of the SCI values for Hardstand Taxiway 1 and Access Taxiway 1. The predicted performance curves reflect the relative performance of the actual pavements, i.e,. Access Taxiway 1 significantly outperformed Access Taxiway 2, which in turn outperformed Hardstand Taxiway 1.

The best traffic and condition data were available for Access Taxiway 1, and its SCI of 36, when it was replaced with an adjacent bypass taxiway, agrees well with the predicted performance. Access Taxiway 2 failed sooner than would be predicted. The rapid failure of one end of Hardstand Taxiway 1 at 74 coverages is probably not representative. The fact that one end failed rapidly and the remaining 86 percent of the feature continued to perform leads to the suspicion that moisture or subgrade conditions in this area were worse than reported or that construction problems may have resulted in low-strength concrete. Although pavement condition data for the remainder of the feature were reported to allow estimates of the SCI in 1968, 1969, and 1971, there are no reliable traffic data. If the 74 coverages that caused failure after several months are considered typical for one-third of a year, then there were about 250,500, and 1,000 coverages as is plotted in Figure 14. If it is considered typical for two months, then the coverage levels would be about 500, 1,000, and 1,500. The rapid failure of the south end of Hardstand Taxiway 1 no doubt caused considerable concern, and evaluation of the structural capacity of the pavement recognized that this pavement was not capable of sustained B-52 traffic[42]. In all likelihood traffic on this feature was reduced as much as possible, and all the constant rate of accumulation traffic estimates are

Table 11

Failed Pavements at U-Tapao Airbase

Feature	h in.	R[a] lb/in.^{2}	Subgrade k lb/in.^{2}/in.	Subgrade E lb/in.^{2}	Pavement SCI[b]	Predicted Behavior C_O	Predicted Behavior C_F	Predicted Behavior Coverages At Failure
Hardstand TW 1	16	580	300	39,400	76-88	538	1,486	c
Access TW 1	16	645	400	57,000	36	5,285	19,427	9,820
Access TW 2	16	615	350	48,000	Failed	1,731	6,309	1,230

[a] Concrete flexural strength.

[b] SCI was estimated by percentage of cracked slabs and joint spalls reported. One half of each damage type was assumed to be of low severity, and one half was assumed to be of medium severity.

[c] Five hundred feet on south end failed and was rebuilt in 1967 shortly after opening, approximately 74 coverages. The remaining approximately 3,000 feet remained in use without repair, and some condition survey data were reported for 1968, 1969, and 1971 inspections.

erroneous. Lambiotte and Chapman[42] noted the following on Hardstand Taxiway 1:

> Traffic intensity, however, is far lighter than on either of the access Taxiways (1 and 2) or other primary facilities. Thus the prognosis for this pavement section is that it (deterioration) will probably occur more gradually than other pavement failures experienced to date on the station.

Overall, the performance models did an excellent job predicting the performance of Access Taxiway 1, overestimated the performance of Access Taxiway 2, and in light of the uncertainties concerning traffic levels, made a reasonable estimate of the performance of Hardstand Taxiway 1. The relative predicted performance of each feature was consistent with the relative actual pavement performance.

SUMMARY

Concrete pavement fatigue deterioration can be described by a model using the two performance factors, C_0 and C_F. Until traffic coverages reach C_0, there is no significant structural deterioration, and the pavement SCI is 100. Between the coverage levels of C_0 and C_F, the pavement SCI value decreases linearly with the logarithm of coverages until an SCI value of zero is reached at C_F. Conceptually, C_0 is the onset of deterioration, and C_F is complete failure. The two performance factors, C_0 and C_F, may be determined from the following relationships:

$$DF = 0.5234 + 0.3920 \text{ Log } C_0$$

$$DF = 0.2967 + 0.3881 \text{ Log } C_F \qquad (28)$$

where

DF = design factor
= concrete flexural strength ÷ layered elastic calculated stress

The relations for C_0 and C_F are essentially layered elastic based on field fatigue curves from accelerated traffic field tests. They account for fatigue damage from applied loads and indirectly include factors such as temperature and moisture induced stresses and nonuniform subgrade support because they are based on full-scale field tests. Actual in-service pavements will show additional deterioration due to factors not related to fatigue loading. Some of these other factors include durability problems such as D cracking, deterioration caused by maintenance problems such as failed joint sealant or environmental effects such as subgrade weakening from moisture infiltration through cracked pavements or improperly sealed joints.

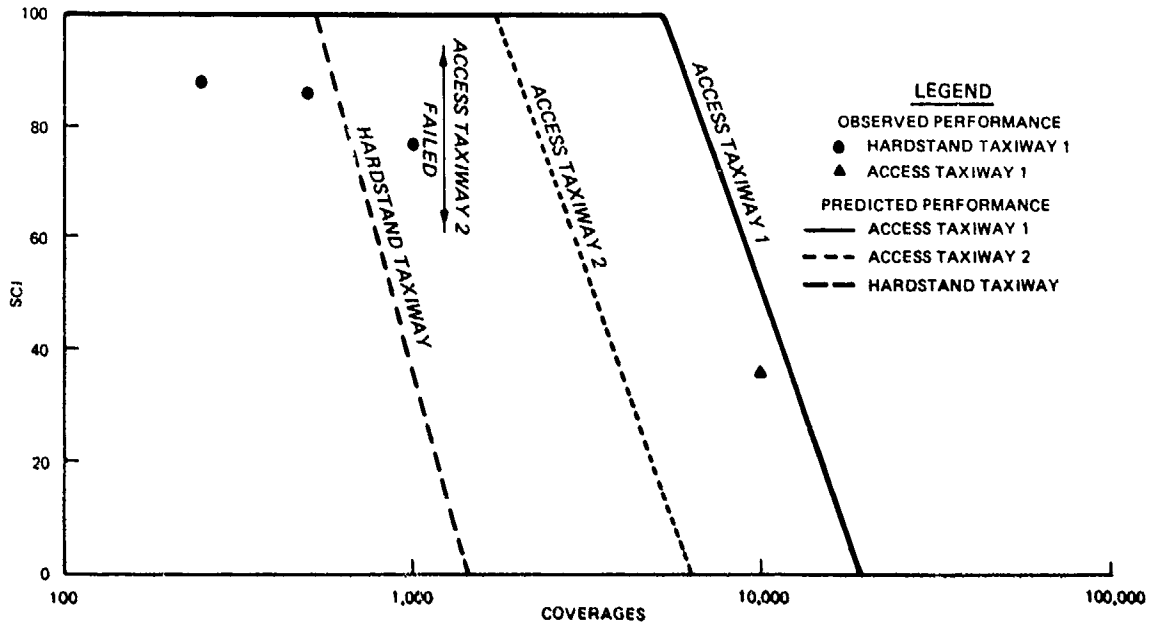

Figure 14. Predicted performance of U-Tapao Airbase pavements

The C_0 and C_F relations are developed from full-scale field tests, and the data show appreciable scatter. However, this variability is common in fatigue testing in both the laboratory and field. The relationships presented for C_0 and C_F appear to be the most appropriate for the available data. They are consistent with other criteria and follow the same form as other fatigue relationships. When these relations were used with unfailed test items and the U-Tapao Airbase in-service pavements, they gave reasonably good agreement between actual and predicted pavement performance.

The pavement performance model based on C_0 and C_F parameters predicts the SCI of a specific pavement system for any coverage level. This is a major departure from conventional pavement design criteria that use a specific failure condition as their basis. The model with the C_0 and C_F factors has no specified failure level; but if the final predicted SCI value is between 55 and 80 at the end of the design traffic, then the design will be consistent with the current CE failure criterion.

EFFECTIVE MODULUS FOR CRACKED SLABS

When a plain concrete pavement slab cracks, its ability to transmit load through bending is reduced. Generally such a crack in a pavement is unable to transmit moment, although aggregate interlock across the crack can transmit shear. This shear transfer across the crack decreases with further application of load repetitions or opening of the crack.

The progressive cracking and decreasing load-carrying capacity of a slab must be modeled for overlay design. The performance relations for concrete pavements developed in the previous section require that the supporting layers be characterized by a thickness, a modulus of elasticity, a Poisson's ratio, and an interface condition. When a concrete base slab is overlaid, the base slab can continue to crack and deteriorate under traffic loads, and the support provided to the overlay is decreased as the base slab deteriorates. Consequently, the support provided to an overlay slab by the base pavement is a variable and not a constant.

Within the limitations of the layered elastic model there are two potential ways to represent this decreasing support. The base slab thickness used in the stress calculations can be replaced with a decreased or effective thickness or the base slab concrete modulus of elasticity can be reduced. Of these two approaches, the use of a reduced effective modulus of elasticity for the cracked concrete was selected as the preferable approach for this study. Thickness is almost the only pavement parameter that can physically be measured with confidence. The concepts of linear elasticity and the concrete modulus of elasticity used for analysis are artificial constraints placed on a real, nonlinear system to make it analyzable. Therefore, it was felt that the thickness should not be varied and that an effective modulus of elasticity was a more reasonable adjustment.

EXISTING MODELS

A design study for an overlay at Diego Garcia by Lyon Associates, Inc.[44] used 200 falling weight deflectometer tests on cracked slabs to develop a correlation between the CE visual condition or C factor in Table 2 and the effective modulus of cracked slabs. This relation was expressed as

$$E_r = 67.8\ C + 22.9 \qquad (29)$$

where

E_r = ratio of the effective modulus of the cracked slab to the modulus of the uncracked slabs as a percent

C = CE visual condition factor from Table 2

One of the criticisms of the CE C factor has been that it is subjective and poorly defined. Figure 15 shows a range of possible SCI values for

the available definitions of the C factor. An approximate relation within this band is shown in Figure 15 and is described by

$$C = -0.076 + 1.073\ (SCI) \tag{30}$$

where

C = CE visual condition factor

SCI = structural condition index

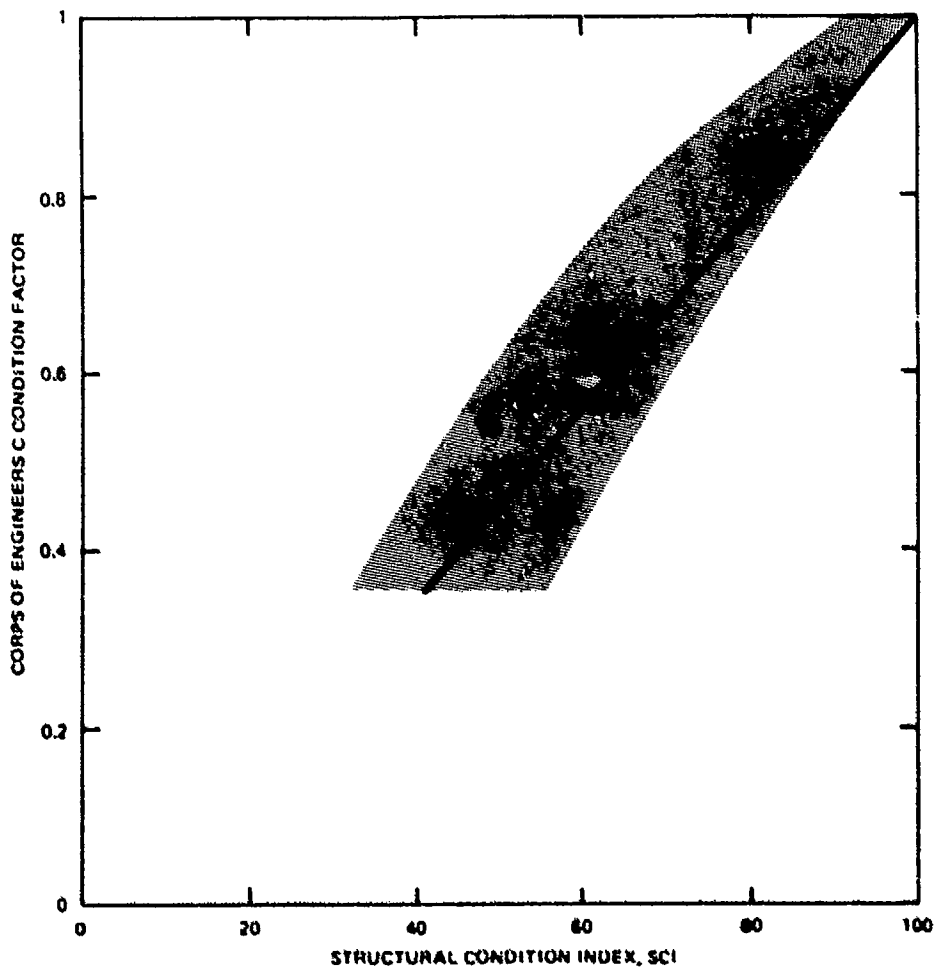

Figure 15. Relationship between CE visual C factor and SCI

This relation can be substituted into the Diego Garcia expression to provide an estimate of the effective modulus in terms of SCI as follows:

$$E_r = 0.177 + 0.00727\ (SCI) \qquad (31)$$

Two other relations for C versus effective modulus and for nominal size of portland cement concrete (PCC) slab fragment versus the effective modulus ratio are shown in Figures 16 and 17[2]. The relation between C and SCI can be used to convert the relation in Figure 16 into a relation between SCI and E-ratio. Table 12 lists some sample calculations to show one possible form of the SCI and E-ratio relation derived from Figure 17. The assumptions on damage used in developing the relation between SCI and nominal slab fragment length obviously affect the results, and the curve in Figure 17 is one of a family of possible curves.

The AASHTO, Diego Garcia, and slab fragment developed relations between SCI and E-ratio are plotted in Figure 18. The Diego Garcia relation was based on data where the C factor varied from 0.35 to 0.95 or a SCI of approximately 41 to 95. The E-ratio should go to 1.0 as the SCI goes to 100 although the mathematics of the regression analysis does not do so. The relation developed from the nominal slab fragment size could be replaced with a family of possible curves developed by changing assumptions of initial slab size and damage density. The relations show reasonable agreement with one another, even though the Diego Garcia relation begins to deviate from the others as the SCI decreases. Information in the lower regions of SCI values for any of the curves is missing. These relations are not adequate to develop a usable model for the effective modulus of cracked concrete, so tests were conducted at the WES to provide additional data on the effective modulus of elasticity for cracked concrete slabs.

SLAB TESTS

TEST SLABS

Six concrete slabs were located at WES that could be tested to develop data for the SCI and E-ratio relationships. Test Slabs 1 and 2 were located in the Mobility Division test vehicle parking area. They were 21 by 27.8 ft in plan, 7.3 in. thick, and reinforced with wire mesh. Both slabs had been cast directly on the native loess (classified as CL by the Unified Soil Classification System) subgrade. Slab 1 had several discontinuous contraction shrinkage cracks. Slab 2 had similar contraction shrinkage cracks that quartered the slab. The slab dimensions in plan are such that contraction cracking would be expected for slabs of this thickness. The location of the cracks at the approximate slab edge centerpoints of Slab 2 supports this conclusion. These slabs in the past have only been subject to light traffic of unloaded Mobility Division test vehicles going to an adjacent wash rack. All indications are that the existing cracks in Slabs 1 and 2 before the test are from initial contraction induced stresses and overly large plan dimensions rather than load related stresses.

Test Slabs 3 and 4 were located in Hanger No. 4 and had been used previously for parking. The slabs were 15 by 16 ft in plan, 5.6 in. thick, and reinforced with wire mesh. Both slabs had been cast directly on the native loess subgrade and had corner breaks. These outside corner breaks had been

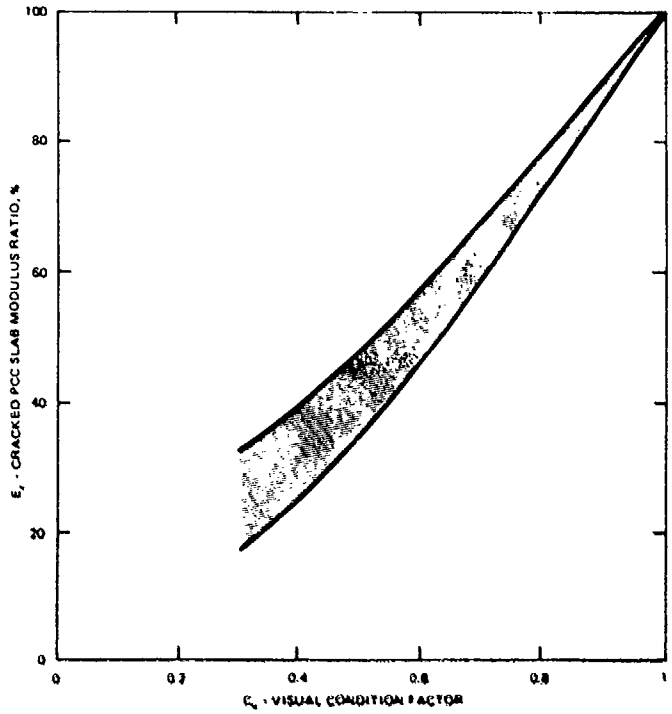

Figure 16. AASHTO relation between visual C factor and E-ratio[2]

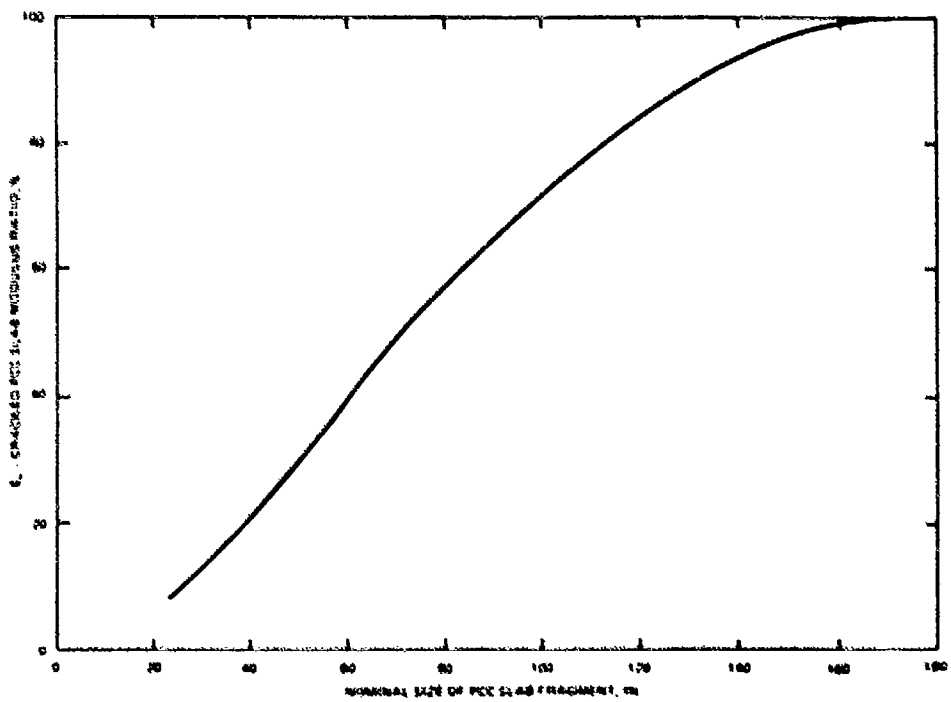

Figure 17. Relationship between nominal slab fragment and E-ratio[2]

Table 12

Sample Calculations for Determining SCI and E-Ratio from Nominal Slab Fragment Size

Slab Condition	SCI[a]	Nominal Slab Fragment, in.	E_r[b]	Effective Length[c]	E_r[d]
Intact	100	240 × 240	1.0	240	1.0
Initial Crack	80	120 × 240	0.83	170	0.98
3 to 4 pieces	55	60 × 60	0.40	60	0.40
6 pieces	39	30 × 60	0.13	42	0.23
9 pieces	23	15 × 30	0.05[e]	21	0.08[e]

[a] Assumes 50 percent damage density.
[b] Calculated from Figure 17 using least dimension of nominal slab fragment.
[c] Square root of area of slab fragment.
[d] Calculated from Figure 17 using effective length.
[e] Extrapolated.

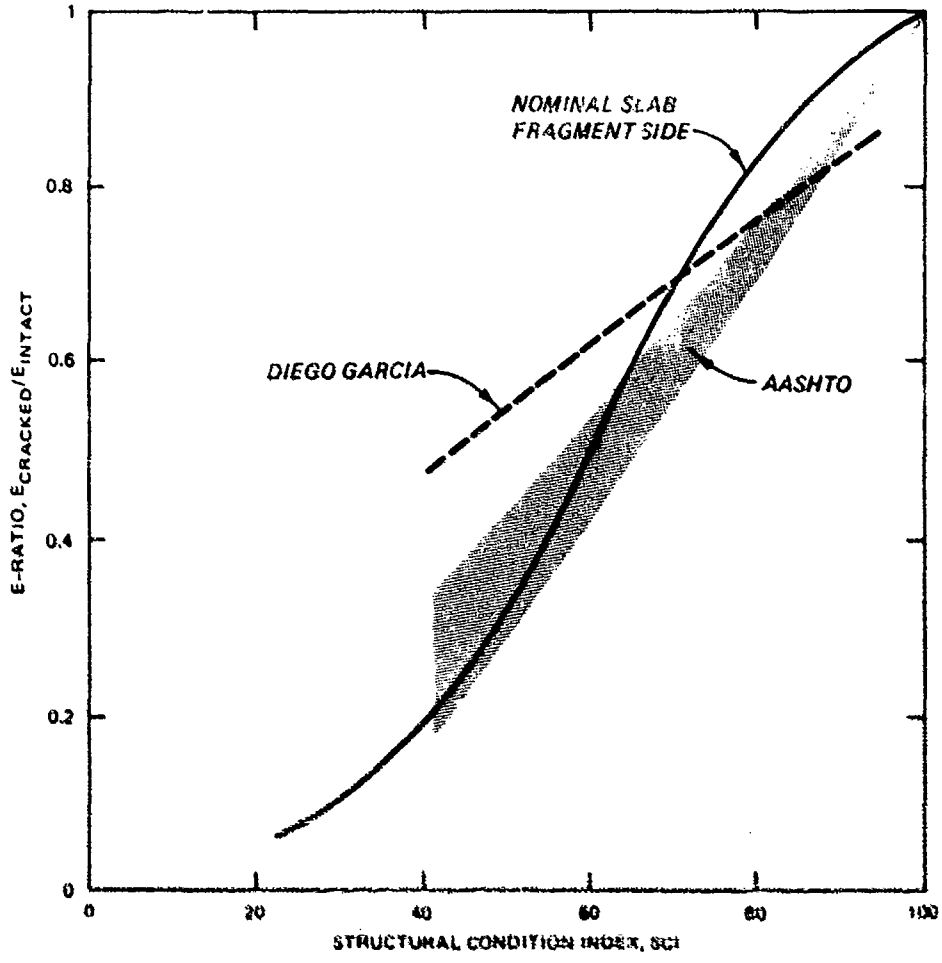

Figure 18. Existing relationships between SCI and E-ratio

caused during previous nearby tests when the wheels of the MX Transporter had inadvertently traversed the outside edges of the slabs.

Test Slabs 5 and 6 were located on the WES Poorhouse Property. Slab 5 was 13.5 by 17.9 ft in plan, and Slab 6 was 16.25 by 17.9 ft in plan. The slabs had been originally cast as a single slab, but a contraction crack divided the original slab into two slabs. Both slabs were 18.1 in. thick and had been cast directly on the native loess subgrade. These slabs had been originally used to test security sensors. Each slab had slots approximately 1.5 in. wide and 2 in. deep cut across the width of the slabs. Security sensor cable had been placed in these slots, and then the slots had been filled with flexible polymeric materials.

TEST PROCEDURES AND LIMITATIONS

Data for the SCI and E-ratio relationships were developed by progressively cracking each of the slabs, rating the slab SCI at each stage of cracking, and measuring the elastic response of the slab at each stage.

Cracking was done by dropping a headache ball from a crane at selected points to try to obtain controlled cracking. A falling weight deflectometer was used to measure the slab's deflection under load.

The contraction cracks in Slab 2 essentially acted as contraction joints dividing the original slab into four slabs. Each of these was considered to be a separate effective slab. All deflection tests were run away from the sides of Slabs 3 and 4 that had the corner cracks. Consequently, the effect of these corner cracks on the elastic deflection of the slab should have been minor, and they were ignored in computing the SCI for these slabs. The sensor slots in Slabs 5 and 6 could not be avoided and would have some effect on the stiffness of the slab. However, their small size in relation to the overall slab dimensions and the fact that they were filled suggested that their overall effect on deflection would be minor. However, they would probably affect crack location significantly.

Slabs 1 through 4 were all lightly reinforced. Airfield pavement slabs and most highway pavement slabs are not usually reinforced. Reinforcing in pavements is placed at middepth of the pavement to hold any cracks that form tightly closed and to prevent opening and working of the crack. Reinforcing in pavements is not intended to handle tensile strains as it is in structural concrete. Its location at or near the midpoint of the slab should be near enough to the neutral axis of bending that any effect on deflection by the reinforcing steel should be slight, but it was ignored for this test. Because the steel will tend to hold cracks tightly closed, all cracking in these slabs can be expected to be low severity.

Concrete cracking from the impact of the dropped weight is due to shock waves. Fatigue cracking develops slowly from repeated load application. However, research has found no difference in cracks caused by slow or fast loading[8], and the cracking from this test's impact loads should affect deflection measurements in the same manner as would fatigue cracking.

Deflection measurements were made using the Dynatest Falling Weight Deflectometer, model 8000. This machine uses a weight dropped onto an 11.812-in.-diam steel plate to impart an impulse load to the pavement and cause the pavement to deflect. A hard plastic pad followed by a hard rubber pad are attached to the bottom of the plate. Four drop heights are available so that the level of impact load can be selected to be within the range of approximately 8,000 to 23,000 lb. The actual load applied to the plate for each test drop is measured by a load cell. Velocity transducers are used to measure surface deflections up to 79×10^{-3} in. in magnitude. Deflections were measured radially in a straight line at 0, 12, 24, 36, 48, 60, and 72 in. from the center of the plate for this test. The 0-in. transducer measures the deflection through a hole in the center of the plate. All data are automatically recorded and stored for future analysis. Typically four drops were made at any one station. The first drop generally gave the highest deflection readings probably because of the seating of the plate under load. The first readings were not used for analysis. The next three drops were checked for consistency of results, and one typical set of readings was selected for analysis.

The deflection basin measured by the velocity transducers was used to determine modulus values of the concrete and subgrade. Modulus values were varied until the calculated basin matched the measured basin as closely as possible. Deflections were calculated using the layered elastic model solved with the BISAR computer code. The iterations of matching the calculated and measured deflection basins were done using the computer program BISDEF developed by Dr. Walter Barker of WES. BISDEF uses BISAR as a subroutine to calculate deflections. The calculation of modulus values from deflection basins is a standard WES pavement evaluation and analysis procedure described in detail by Bush[11].

The input requirements and selected constants for each BISDEF calculation are shown in Figure 19. The 1 million-psi modulus material at 20 ft was found necessary in previous work to obtain accurate surface deflection predictions[59]. The computer program BISDEF varies the concrete pavement and subgrade modulus (or one of them can be set to a specified value) until the computed deflection basin matches the measured one as closely as possible.

Deflection basins were measured at three locations on each slab. The location of deflection basin measurements and initial slab conditions are shown in Figures 20, 21, and 22. Each falling weight test position is identified as position 100, 200, or 300 on each slab. In general position 100 is located at the center of the slab, position 200 is adjacent to a joint, and position 300 is at a slab quarter point. The contraction cracking in Slab 2 required some modification of this positioning as shown in Figure 20. The third digit in the position number indicates the series of cracking. For example, test 100 is an initial falling weight test at position 100 before any cracking. Test 101 is a falling weight test at position 100 after the first set of cracks have been formed, Test 102 is a falling weight test at position 100 after the second set of cracks have been formed, etc. As the tests were conducted on Slab 1, modifications to test positions were made. The position 100.5 was established immediately north of the crack so that the plate and sensors would be on the same side of the crack. Tests were run at both position 100 and 100.5, and tests were subsequently numbered 101, 101.5, 102, 102.5. After the final cracks were made in Slab 1, deflections at position 300 were very large because of extensive cracking in the area; therefore, another location was tested. This position is shown as 300.5 in Figure 22, and the test was numbered 304.5. Test 3 at position 300 was rerun the next day and is identified as test 304R. All deflection basins that were collected during these tests are recorded in Appendix B.

INITIAL MODULUS VALUES

The results of falling weight tests and predicted modulus values for the concrete and subgrade of each slab and test position before beginning the cracking of slabs are shown in Table 13. When evaluating a concrete pavement to determine modulus values, it is the general practice to run the test at the center of an intact slab so that the conditions of continuous, homogenous, linearly elastic layers assumed in the analytical model to calculate deflections will be as nearly valid as possible. Position 100 on all slabs most nearly corresponds to this condition. The lowest deflections were recorded at position 100 on all slabs and the highest at position 200 adjacent to a joint or crack. The only exception is Slab 2 where position 300 in the corner

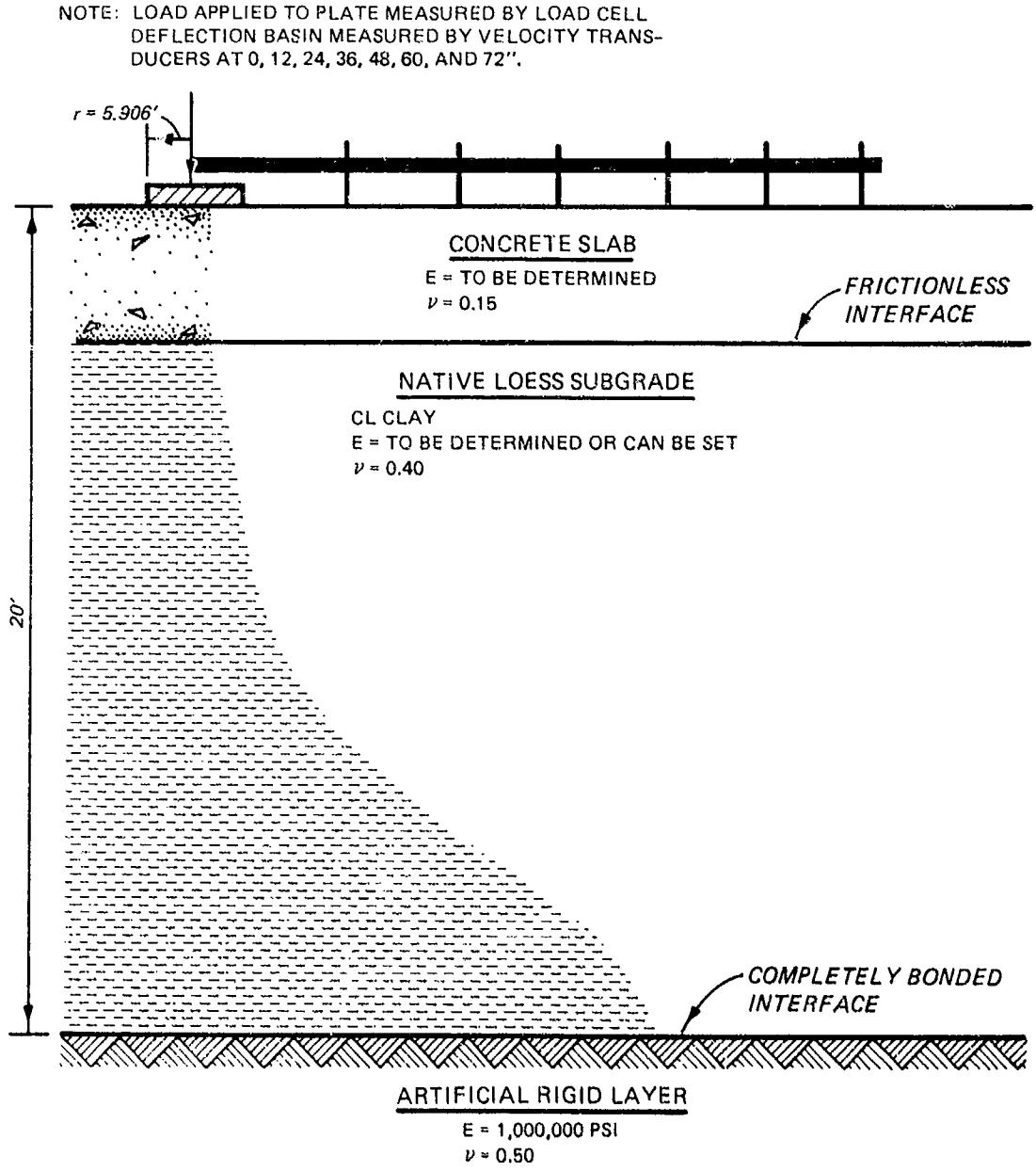

Figure 19. Deflection basin analysis model

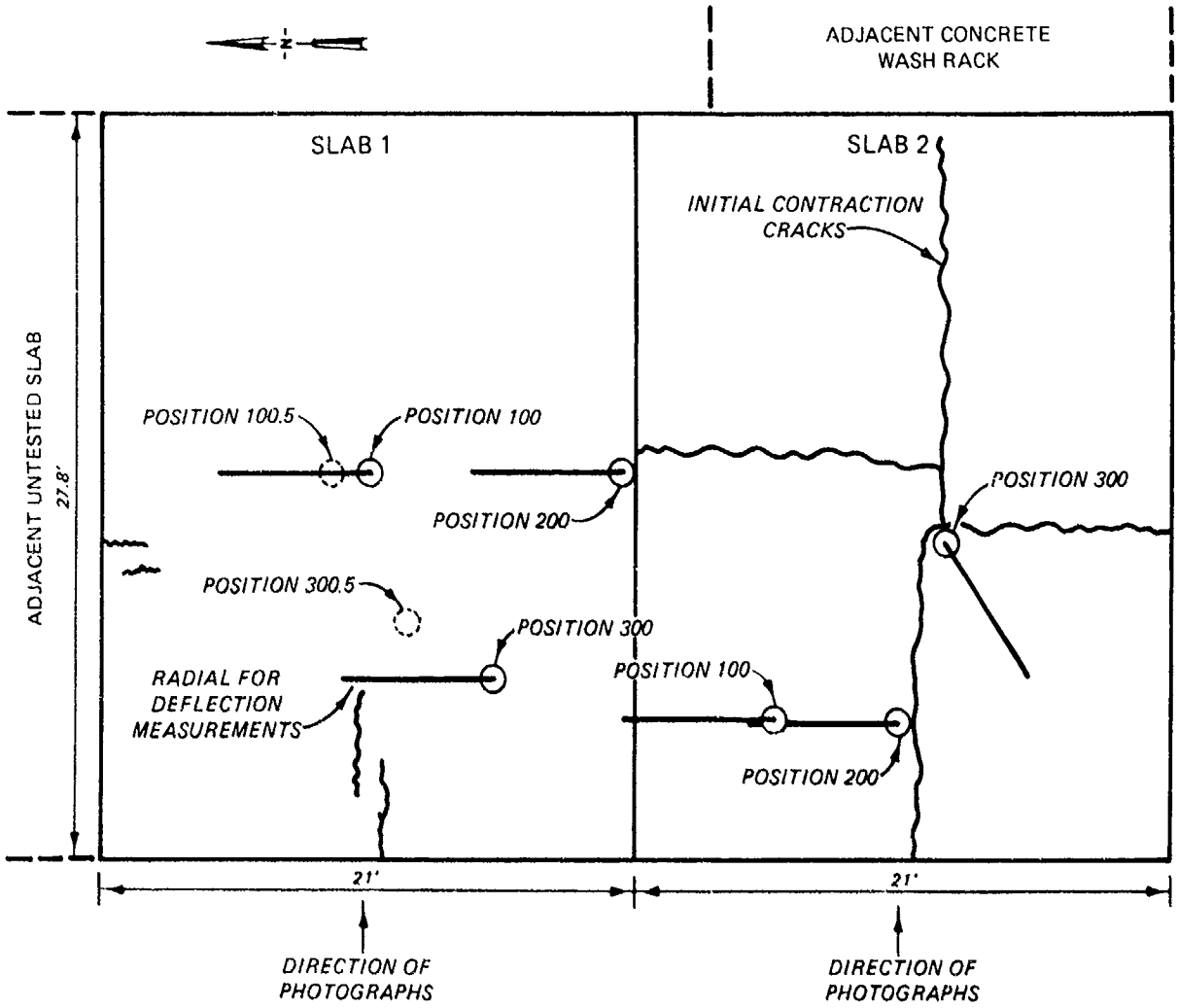

Figure 20. Position of falling weight tests for Slabs 1 and 2

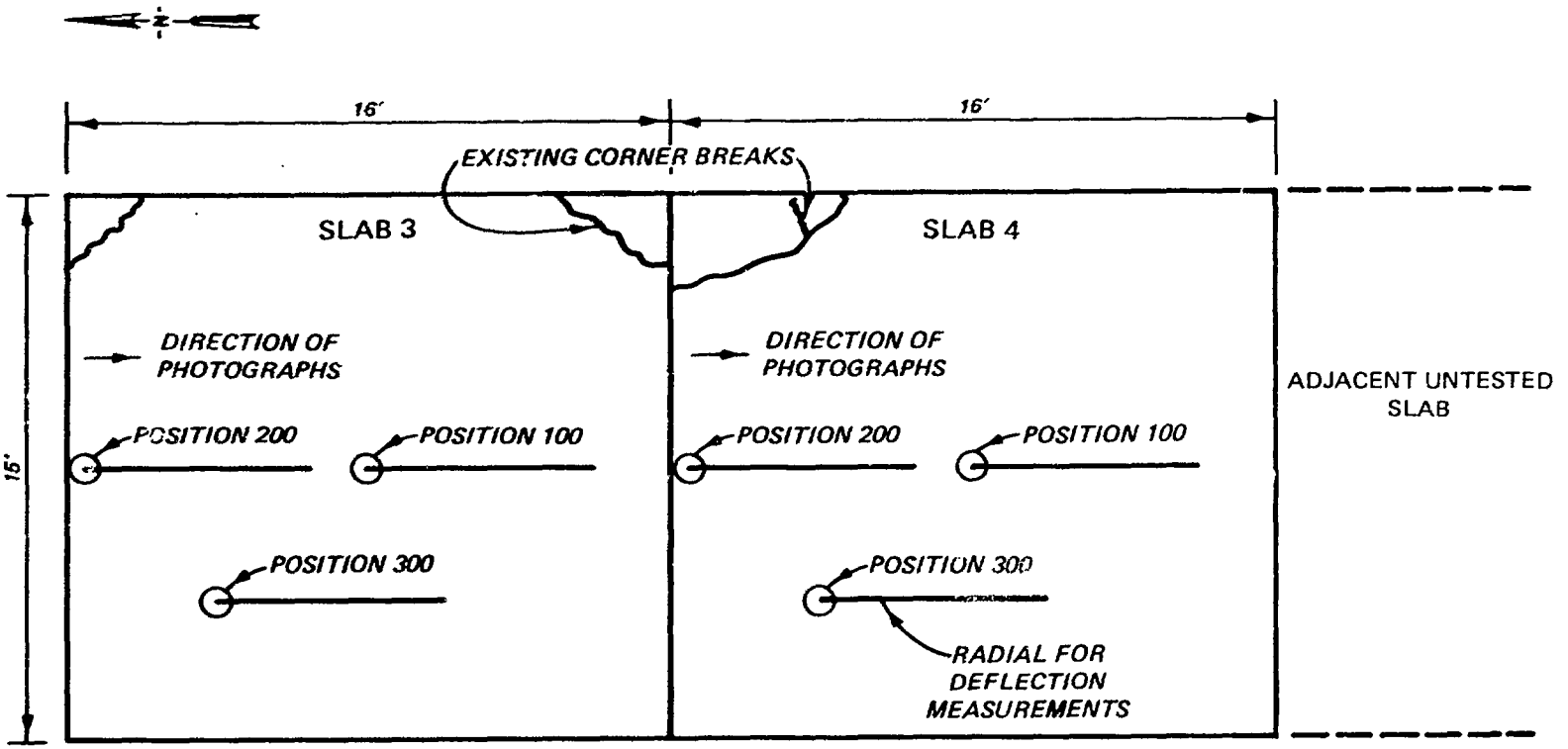

Figure 21. Position of falling weight tests for Slabs 3 and 4

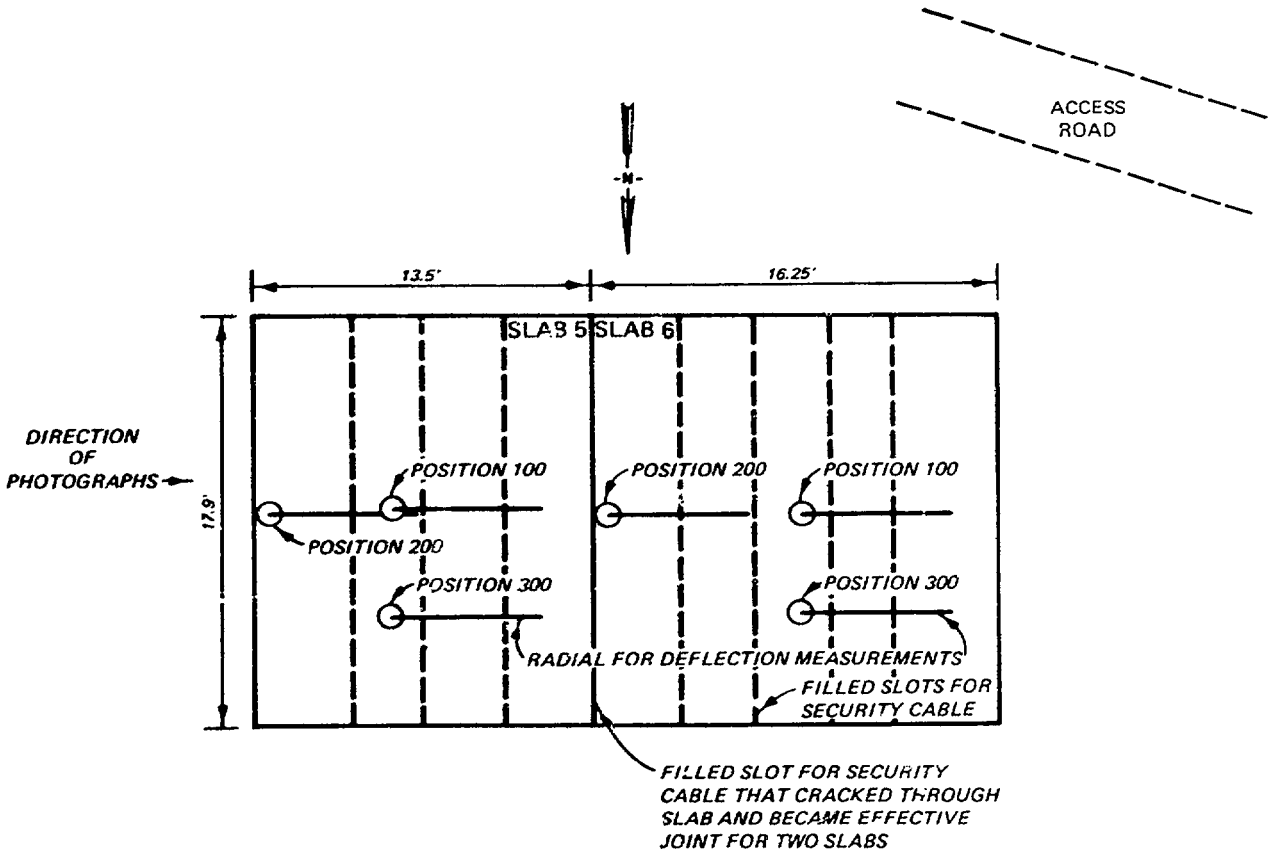

Figure 22. Position of falling weight tests for Slabs 5 and 6

Table 13

Predicted Initial Modulus Values Before Cracking

Slab	Test	Measured Deflection ($\times 10^{-3}$ in.) D0[a]	D12[a]	D24[a]	D36[a]	D48[a]	D60[a]	D72[a]	Load (lb)	Predicted Modulus lb/in.^{2} Concrete	Sub-grade	Error in Matching Basin Absolute[b]	Arithmetic[c]
1	100	27.3	23.6	18.0	13.5	10.0	7.5	5.6	22,437	1,953,000	10,540	14.58	3.32
	200	32.0	25.5	19.0	14.1	9.8	7.6	5.6	23,470	1,452,000	10,960	30.50	6.47
	300	30.6	26.2	20.0	14.9	11.0	8.1	5.9	21,992	1,620,000	9,530	11.21	1.60
2	100	26.3	23.7	18.9	14.9	11.5	9.0	6.8[d]	22,920	2,690,000	9,680	29.37	29.37
	100A	Same as above but D72 sensor not used								2,758,000	9,360	8.90	6.54
	200	26.6	25.0	19.5	15.0	11.1	8.5	6.5	22,800	2,372,000	9,750	22.07	21.57
	300	27.3	23.4	18.2	14.0	8.8	8.3	6.3	22,528	2,062,000	10,370	44.25	7.80
3	100	21.1	19.1	15.7	11.9	7.4	6.5	4.8	23,016	5,862,000	13,020	35.13	5.23
	200	39.8	30.5	21.0	14.3	9.5	7.1	5.0	22,400	1,478,000	10,740	4.37	29.40
	300	28.4	24.9	17.3	11.9	8.1	6.6	5.0	22,632	2,709,000	12,700	42.05	28.79

(Continued)

[a] Sensor location D0 = sensor at 0 in.; D12 = sensor at 12 in.; D24 = sensor at 24 in.
[b] Absolute error = sum of the absolute value of the percent error.
Percent error = (measured deflection - calculated deflection)/(measured deflection).
[c] Arithmetic error = arithmetic sum of percent error taking into account the sign of the error.
[d] Sensor on adjacent slab.

Table 13 (Concluded)

Slab	Test	Measured Deflection ($\times 10^{-3}$ in.) D0[a]	D12[a]	D24[a]	D36[a]	D48[a]	D60[a]	D72[a]	Load (lb)	Predicted Modulus, lb/in.^{2} Concrete	Sub-grade	Error in Matching Basin Absolute[b]	Arithmetic[c]
4	100	17.9	15.9	12.8	10.0	7.6	5.9	4.4	22,897	2,489,000	16,070	190.53	20.58
	200	52.0	38.9	24.6	16.3	10.6	7.0	5.0	22,262	1,000,000	9,420	24.65	-10.49
	300	20.5	17.9	14.1	10.6	7.5	5.8	4.4	22,770	5,884,000	13,870	15.44	2.61
5	100	4.5	4.2	3.7	3.4	3.0	2.6	2.2	21,152	3,959,000	21,990	9.77	3.58
	100A	Same as above except E-subgrade set = 1							1,660	10,286,000	11,660	66.58	-18.53
	200	9.2	8.1	7.0	6.1	5.2	4.3	3.5	20,776	1,295,000	14,870	6.87	-0.08
	300	5.6	5.2	4.9	4.5	4.1	3.7	3.4	20,896	4,995,000	11,660	4.40	-0.12
6	100	3.9	3.7	3.6	3.4	3.2	3.1	2.9	21,072	15,216,000	8,340	6.64	1.18
	100A	Same as above except E-subgrade set = 1							3,250	8,606,000	13,250	26.04	9.52
	100B	Same as above except E-subgrade set = 2							1,990	4,632,000	21,990	56.99	79.62
	200	7.5	7.1	5.5	4.6	3.9	3.4	2.8	20,544	13,935,000	19,559	20.19	-1.95
	300	4.7	4.5	4.4	4.3	4.0	4.0	3.9	20,832	20,000,000	4,130	9.65	0.31

[a] Sensor location D0 = sensor at 0 in.; D12 = sensor at 12 in.; D24 = sensor at 24 in.
[b] Absolute error = sum of the absolute value of the percent error.
Percent error = (measured deflection - calculated deflection)/(measured deflection).
[c] Arithmetic error = arithmetic sum of percent error taking into account the sign of the error.

between cracks had the highest deflection. Position 200 on all slabs and position 300 on Slab 2 are the least satisfactory tests to try to determine an initial, uncracked concrete modulus of elasticity because the presence of discontinuities distorts the deflection basin by violating the basic assumptions of the analytical model used to calculate deflections. All tests at each position were run with the plate and the velocity transducers in the same position.

The predicted subgrade modulus for Slabs 1 and 2 varied from approximately 9,500 to 10,500 lb/in.^{2}. These elastic modulus values correspond to a modulus of subgrade reaction k of approximately 100 to 110 lb/in.^{2}/in. This is toward the lower end of the range of values to be expected from this soil type. However, this subgrade was originally poorly prepared before concrete placement, and the slabs are located adjacent to a washrack and between the washrack and a drainage ditch. The subgrade soil under the slabs probably remains wet since the washrack is in frequent use. Therefore, subgrade soil modulus values appear to be reasonable for Slabs 1 and 2. A plate load test run at Slab 1 approximately 2-1/2 months after these deflection tests found the k value to be 167 lb/in.^{2}/in. This value is in reasonable agreement with the predicted values from the falling weight tests considering the approximate nature of all correlations between modulus of subgrade reaction and elastic modulus and considering the elapsed time between tests.

The predicted concrete modulus values for Slabs 1 and 2 vary from approximately 1.6 to 2.8 million. These modulus values are unusually low for concrete; however, the quality of the concrete in Slabs 1 and 2 is very poor. The concrete tended to crush rather than crack when struck by the headache ball. The same was true even when the ball was dropped from only a few feet above the pavement surface. An examination of the crushed concrete found intact aggregate and a soft matrix that could often be broken by hand. Immediately after crushing there was a distinct odor that was generally described by observers as green. Although the concrete modulus values are low, the concrete quality appears to be poor, and the values are therefore not unreasonable.

Test 300 on Slab 1 was taken as the most representative test position to serve as a base for further analysis as the slab was cracked. The error in matching this basin was smaller than position 100, and as will be discussed later, during initial cracking a crack formed between the plate at position 100 and the first sensor and thus made interpretation of the deflection basin more difficult using an elastic layer analytical model. Position 200, as discussed earlier, is the least desirable position to use as a base for further analysis. For Slab 2, Test 100A in Table 2 was selected as the base for further analysis. This test is the same as Test 100 except the 72-in. sensor deflection was not used in the basin matching because the sensor was located across the joint on Slab 1. Removing this sensor from the analysis significantly reduced the error in matching the basin when compared with Test 100, and the error is significantly lower than Tests 200 or 300.

The soil modulus of elasticity values for Slabs 3 and 4 vary from approximately 13,000 to 16,000 lb/in.^{2}, neglecting position 200 on each slab.

This corresponds to a modulus of subgrade reaction k of about 110 to 150 lb/in.^{2}/ in. which is reasonable for this soil. A plate load test run at Slab 3 approximately 2-1/2 months after the deflection tests found a modulus of subgrade reaction of 122 lb/in.^{2}/ in. The length of time between the original falling weight test and the plate load test probably had a minimal effect since the slabs are located inside a hanger and are protected from weather. The modulus of concrete for Slabs 3 and 4 ranges from 2.5 to 5.9 million lb/in.^{2}. Test 100 on Slab 3 and Test 300 on Slab 4 were selected as the best choices for further analysis because they had the lowest errors and most consistent and reasonable soil and concrete modulus values.

The concrete and soil modulus values for Slabs 5 and 6 in Table 13 are much less satisfactory than those calculated for Slabs 1 through 4. A major part of this problem is the small magnitude of the deflections that could be obtained on the 18-in.-thick slabs using the falling weight deflectometer. Small errors in deflection measurements cause by lack of instrument sensitivity greatly affect the basin and resulting calculations when the deflection magnitudes are so small. Concrete modulus values of 10 to 20 million are completely unrealistic. The concrete modulus values of 4 to 5 million for Tests 100 and 300 on Slab 5 are much more reasonable. However, the subgrade elastic modulus values for these two tests are approximately 22,000 and 11,700 lb/in.^{2}. These values correspond to modulus of subgrade reaction k values of about 190 and 120 lb/in.^{2}/in. The value of 190 lb/in.^{2}/in. is toward the upper end of values to be expected for this type of soil. These slabs are located on the soil surface at the top of a well-drained hill. No information on site preparation before construction could be located. At the time of these tests, Vicksburg, Miss., was in the midst of an extended drought. The combination of good site drainage and extended dry weather make it plausible that the elastic modulus values for this site could be on the order of 22,000 lb/in.^{2}. More expected values for this soil under moist conditions would be 10,000 to 15,000 psi as at position 300. This position also gave the smallest errors for matching the deflection basin on Slab 5. When the deflection Test 100B was run with the same subgrade modulus as Test 300, the predicted concrete modulus was 10 million which is too high to be acceptable. The concrete modulus at position 100 on Slab 6 was calculated with assigned subgrade modulus values of 13,250 lb/in.^{2} (Test 100A) and 21,990 lb/in.^{2} (Test 100B). Results are shown in Table 13. The predicted concrete modulus value of 8.6 million for 100A remains suspiciously high. When the high-strength subgrade modulus was used in 100B, the predicted concrete modulus was 4.6 million, which is within reasonable ranges for concrete and is in agreement with the predicted concrete modulus values Tests 100 and 300 on Slab 5. Test 100 on Slab 5 and Test 100B on Slab 6 were selected as the most reasonable results to use as a base for further analysis for (a) the center of the slab, position 100, provides the closest physical agreement with the layered elastic model, (b) slab 5, position 100, gives reasonably small agreement errors between the calculated and measured deflection basins, (c) the relatively high subgrade modulus of 21,990 lb/in.^{2} gives consistent and reasonable predicted concrete modulus values for both Slab 5, Test 100,

and Slab 6, Test 100B, (d) the subgrade modulus value of 21,990 lb/in.^{2} is reasonable, even though it is somewhat high for the site, weather, and soil conditions, (e) lower subgrade modulus values gave unrealistically high predicted concrete modulus values for Slab 5, position 100B, and Slab 6, position 100A.

CRACKED SLAB SCI ANALYSIS

After the initial uncracked falling weight deflection data were collected for a slab, the headache ball was used to develop various levels of cracking, and then the SCI at each level of cracking was determined. The SCI calculations assumed that the test slab was representative of a pavement feature with a 50 percent distress density. At each level of cracking with accompanying SCI calculation, falling weight deflection data were collected for each position on each slab. Generally, all falling weight tests and cracking were performed one day for each slab.

Photographs and crack maps for each slab at the different stages of cracking are contained in Appendix B. Slab 2 was effectively broken into four slabs by contraction cracking, and the slab considered in the analysis was the northwest corner of the original slab. This slab, for analysis, is bordered by the west edge of the slab, the joint between Slabs 1 and 2 and two contraction cracks.

The calculations of the SCI for each stage of cracking on each slab are summarized in Table 14. The guidelines for SCI calculations were used for determining the SCI for these slabs with two limitations. Since only one slab was available, all SCI calculations assume a 50 percent damage density. This test slab would be considered as representative of an entire pavement feature to be evaluated. The SCI value of zero was assigned when the area immediately around the test position was divided into multiple fragments by extensive cracking as for Slab 1, Test 104 shown in Appendix B.

DETERMINING CRACKED CONCRETE MODULUS

A concrete modulus was calculated for each stage of cracking, as described earlier, by matching the falling weight deflection basin as closely as possible. Table 15 shows the results of these calculations for Slab 1 at positions 100, 200, and 300 at each stage of cracking. For the calculations for Slab 1, the subgrade modulus of elasticity was set equal to 10,000 lb/in.^{2} for all positions. Results for the initial Tests 100, 200, and 300 appear reasonable. However, once cracking starts (Tests 101, 201, etc.) calculated concrete modulus values decrease rapidly, and the error in matching the basin increases dramatically. Figures 23 through 25 show the measured and calculated basins at each position and degree of cracking on Slab 1. From these figures, it is apparent that layered elastic theory can do a reasonable job of matching the deflection basin of an intact slab. Once cracking begins, differences between the measured and predicted basins become more pronounced.

Since the cracked slab deflection basin could not be matched acceptably by layered elastic theory, the effective modulus of concrete was defined to be that modulus which would give the same deflection under the center of the loaded plate using layered elastic theory as was measured in the falling

Table 14

Summary of SCI Calculations for Test Slabs

Slab	Test	Damage Type	Density, %	Severity	Deduct	SCI
1	300	None	0	--	0	100
	301	Type 3, L/T/D cracking[a]	50	Low	20	80
	302	Type 12, shattered slab	50	Low	42	58
	303	Type 12, shattered slab	50	High	77	23
	304	Closely spaced cracks	--	--	100	0
2	100	None	0	--	0	100
	101	Type 3, L/T/D cracking	50	Low	20	80
	102	Type 3, L/T/D cracking	50	Low	20	80
	103	Type 12, shattered slab	50	Med.	61	39
	104	Type 12, shattered slab	50	High	77	23
3	100	None	0	--	0	100
	101	Type 12, shattered slab	50	Med.	61	39
	102	Type 12, shattered slab	50	High	77	23
4	300	None	0	--	0	100
	301	Type 12, shattered slab	50	Low	42	58
	302	Type 12, shattered slab	50	High	77	23
5	100	None	0	--	0	100
	101	Type 12, shattered slab	50	Med.	61	39
	102	Type 12, shattered slab	50	High	77	23
	103	Closely spaced cracks	--	--	100	0
6	100	None	0	--	0	100
	101	Type 3, L/T/D cracking	50	Med.	45	55
	102	Type 12, shattered slab	50	High	77	23
	103	Closely spaced cracks	--	--	100	0

[a] L/T/D cracking = longitudinal/transverse/diagonal cracking.

Table 15

Predicted Concrete Modulus from Slab 1

by Matching Deflection Basins

Position	Predicted Concrete Modulus, psi[a]	Absolute Error[b]	Arithmetic Error[c]
100	2,266,000	3.1	-2.6
101	545,000	11.2	9.9
102	50,000	31.4	31.4
103	50,500	30.3	30.0
104	10,200	35.2	35.2
200	1,870,000	5.5	-4.3
201	467,000	10.7	10.7
202	153,000	22.1	22.1
203	312,000	11.7	11.6
204	10,000	25.9	18.2
300	1,504,000	2.0	2.0
301	783,000	25.0	-5.4
302	500,000	17.3	11.3
303	215,000	24.7	24.3
304R[d]	20,136	29.5	29.5

[a] Subgrade modulus for all runs set at E = 10,000 psi.
[b] Arithmetic error = sum of the percent error.
[c] Absolute error = sum of the absolute values of percent error. Percent error = (measured deflection - calculated deflection)/(measured deflection).
[d] Retested next day, original test overranged sensors for lowest load.

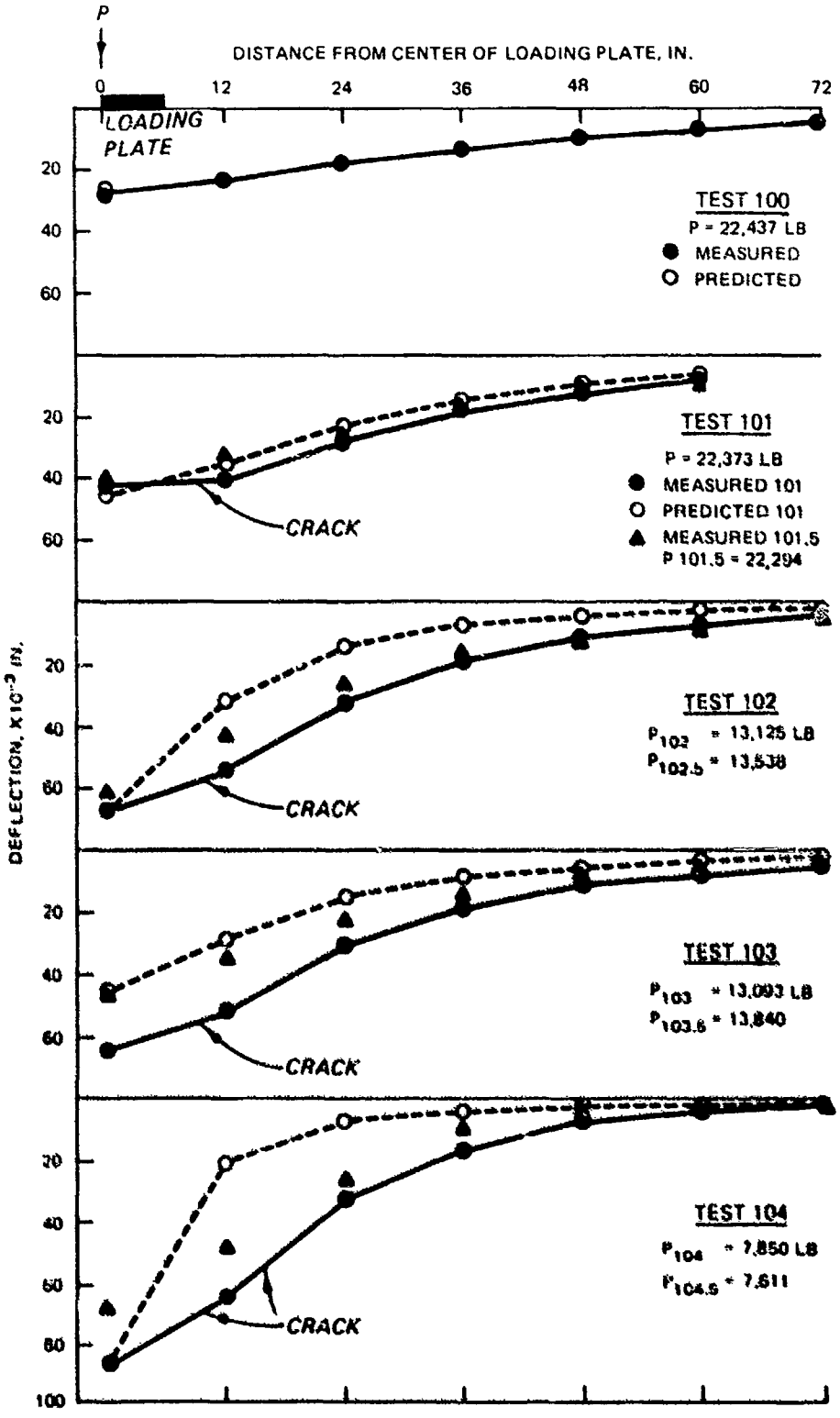

Figure 23. Deflection basins for Slab 1, position 100

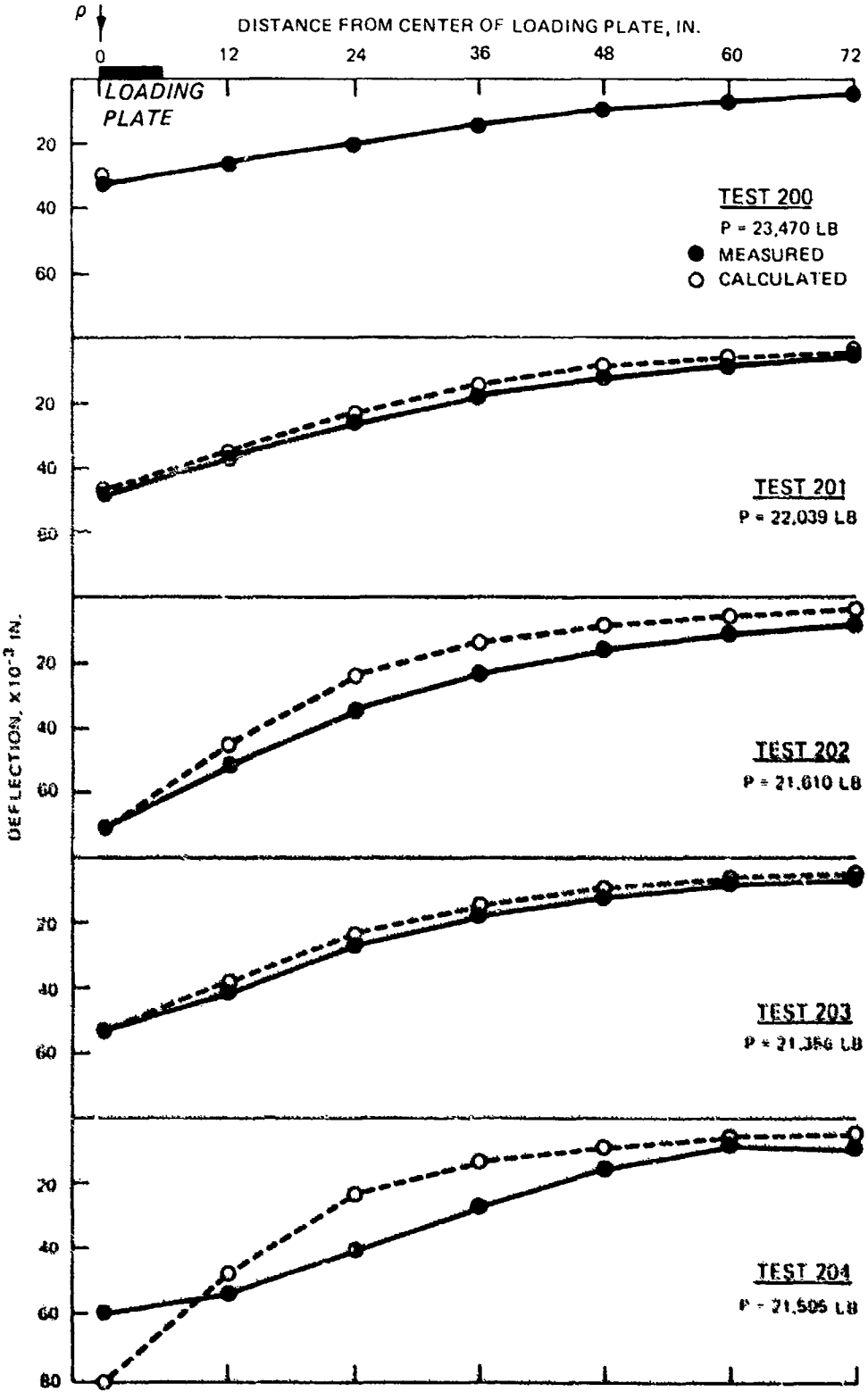

Figure 24. Deflection basins for Slab 1, position 200

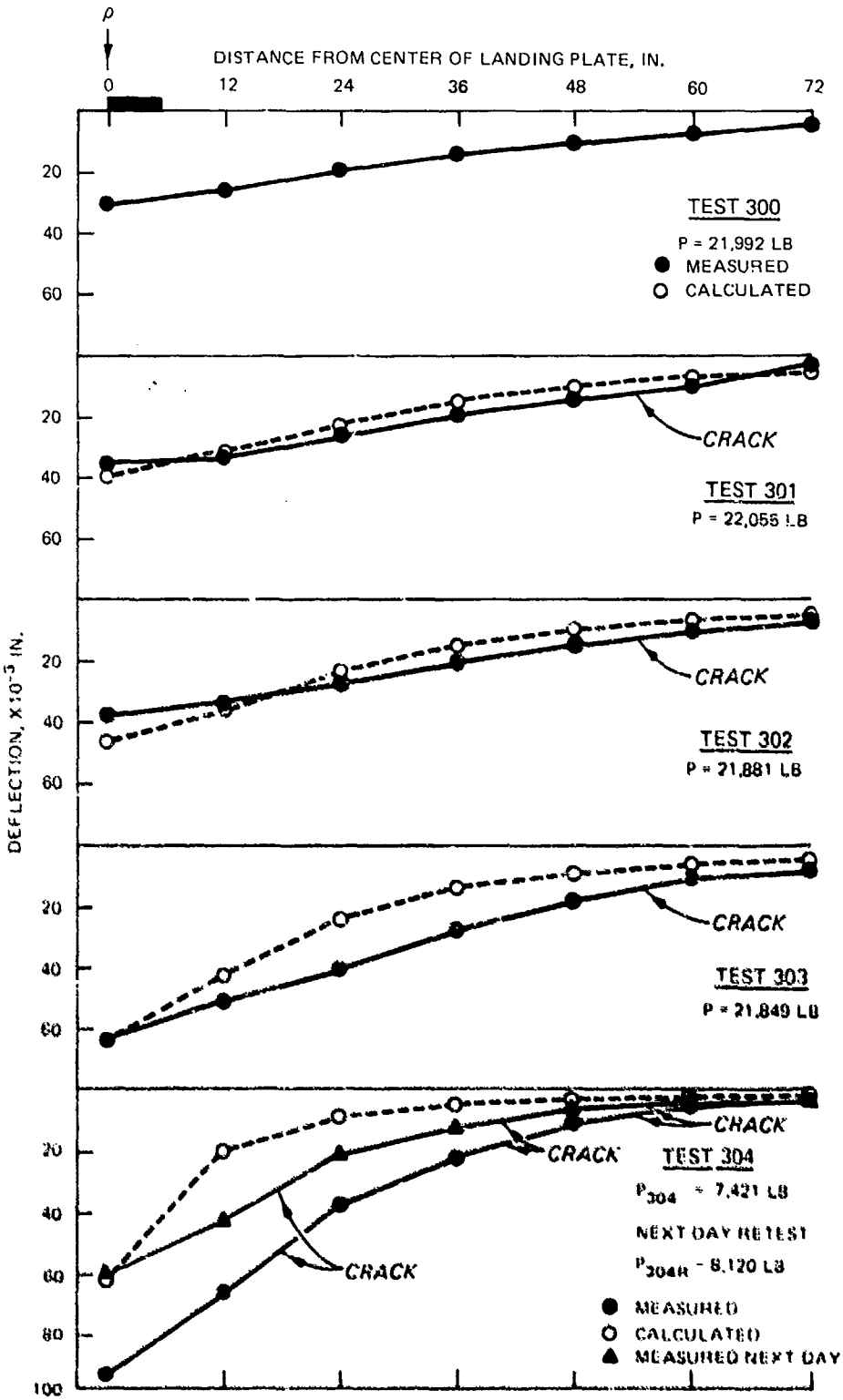

Figure 25. Deflection basins for Slab 1, position 300

weight test. The representative positions, initial concrete modulus, and subgrade modulus for uncracked concrete slabs were selected earlier. For each test at subsequent levels of cracking, the measured field center deflection from the falling weight test was matched by varying the concrete modulus and holding the subgrade modulus the same as for the initial uncracked condition. The BISAR layered elastic computer code was used for all calculations. Table 16 summarizes the calculations of effective concrete modulus for each level of cracking of each slab.

CRACKED SLAB MODEL

Figure 26 shows the data in Table 16 plotted with the original estimated relationships of the E-ratio and SCI from Figure 18. The best fit second order polynomial least squares regression for these data is described by the equation:

$$\text{E-ratio} = 0.0198 + 0.0064\ (\text{SCI}) + (0.00575 \times \text{SCI})^2$$

$$n = 24$$

$$r^2 = 0.95$$

$$\text{Standard error of regression} = 0.083 \qquad (32)$$

At the SCI value of 100, the predicted E-ratio is 0.99. The coefficients of the above equation were adjusted slightly so that at the SCI of 100, the predicted E-ratio is 1.00. The form of this final recommended equation is plotted in Figure 26 as

$$\text{E-ratio} = 0.02 + 0.0064\ (\text{SCI}) + (0.00584 \times \text{SCI})^2 \qquad (33)$$

This equation appears to be a reasonable relationship. It is in agreement with trends suggested by existing relationships in Figure 26. It also appears to do a reasonable job of agreeing with the data developed in the WES slab tests. At the SCI value of zero the predicted E-ratio is 0.02. For a common concrete modulus of elasticity of 4 million psi, the effective modulus of elasticity of the concrete slab when completely broken up would be predicted to be 80,000 psi. This value is in the range of modulus values used for analysis of granular base courses and would be a reasonable representative value of a badly broken up concrete slab. For the information currently available, the formula for E_r given above appears to be the best and most reasonable one available.

Table 16

Effective Concrete Modulus Using Center Deflections

Slab	Test Position	Concrete Modulus, psi	E-Ratio[a]	SCI
1	300	1,620,000[b]	1.000	100
	301	1,180,000	0.728	80
	302	985,000	0.608	58
	303	258,000	0.159	23
	304	24,250	0.015	0
2	100A	2,758,000[b]	1.000	100
	100	1,950,000	0.707	80
	102	1,724,000	0.625	80
	103	466,000	0.169	39
	104	306,000	0.111	23
3	100	5,862,000[b]	1.000	100
	101	2,650,000	0.452	39
	102	1,110,000	0.189	23
	300	5,884,000[b]	1.000	100
4	301	4,350,000	0.739	58
	302	1,210,000	0.206	23
5	100	3,959,000[b]	1.000	100
	101	950,000	0.240	39
	102	496,000	0.125	23
	103	135,000	0.034	0
6	100B	4,632,000[b]	1.000	100
	101	2,000,000	0.432	55
	102	995,000	0.215	23
	103	313,000	0.068	0

[a] E-Ratio = effective E of concrete slab/initial E of concrete slab.
[b] Taken from Table 13.

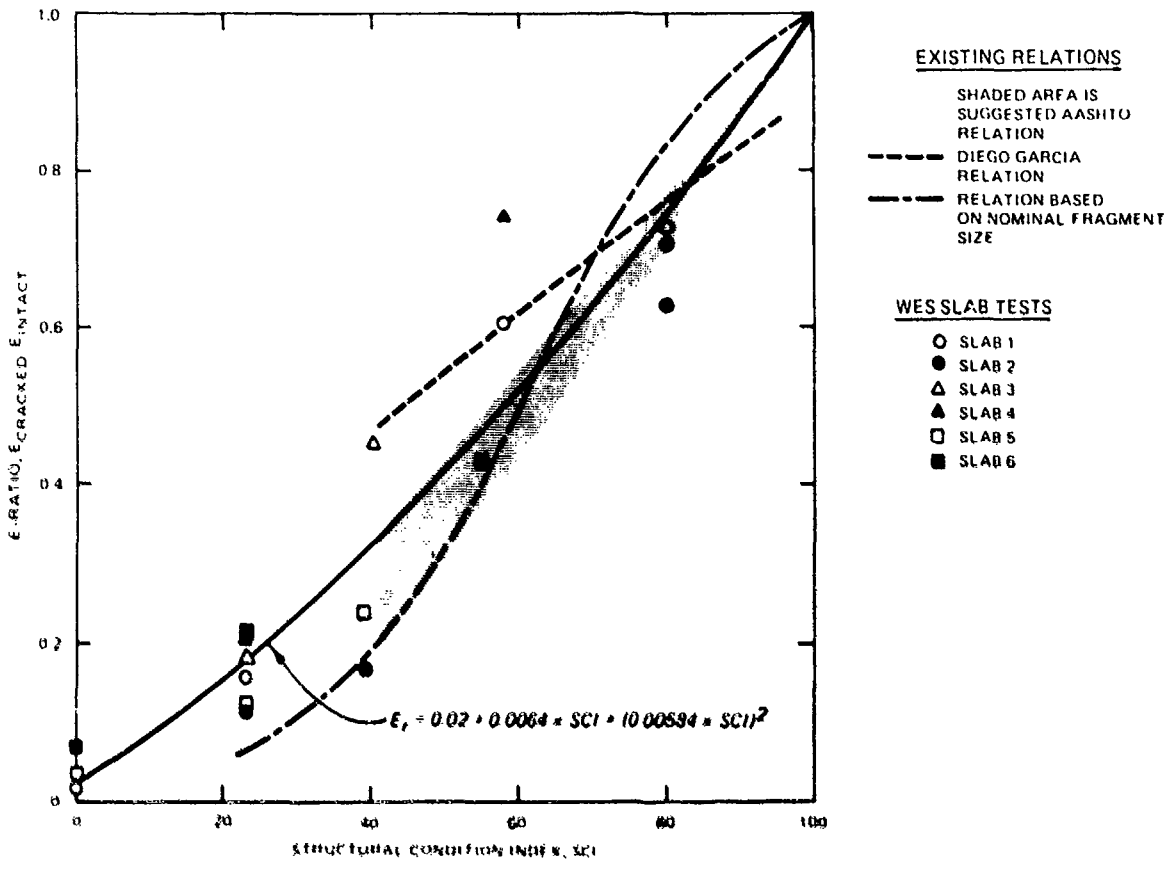

Figure 26. SCI and E-ratio model

LOAD TRANSFER

MEASURED LOAD TRANSFER

When a load is placed on the edge of an airfield pavement slab, some portion of that load is carried to the adjacent slab by the dowel bars, keys, or aggregate interlock between the slabs. This additional support provided by the adjacent slab is load transfer. It is usually expressed as a percent of the total load applied (e.g. 25 percent load transfer means that 25 percent of the load is carried by the adjacent slab). In an analysis using the Westergaard free edge model, the effect of load transfer can be included directly by assuming that some percentage of the applied load is supported by the adjacent slab. Because the system is linear, a 25 percent reduction in load results in a 25 percent reduction in stress, as can be verified by examining the Westergaard equations. The CE and FAA design procedures assume that 25 percent of the load applied to the edge of a slab is supported by the adjacent slab.

As discussed earlier, the layered elastic analytical model is unable to account for the load transfer effect directly. All the performance models and relationships developed in this study have been based on test sections that have used doweled or keyed construction joints and contraction joints on short joint spacings that develop good aggregate interlock. Consequently, all of the relationships in the proposed design procedure are only valid for pavements that use these standard joints and develop typical levels of load transfer.

The actual value of load transfer across a joint is a variable rather than a constant. It will be influenced by a variety of factors such as construction quality, magnitude of joint opening from temperature and moisture fluctuations, load magnitude, and number of repetitions of traffic.

Load transfer can be determined in the field by comparing strains or deflections measured on the loaded and unloaded side of a joint. Data of this type reported by Grau[19], Ahlvin et al.[1], and Ohio River Division Laboratories[51,52,54] were analyzed to obtain load transfer values for different joint types. Load transfer from strain data was computed as the ratio of strains from the unloaded side of the joint to the strains on the loaded side of the joint. Grau[19] gives more detail on this type of analysis.

The joint efficiency measured as the ratio of the deflection on the unloaded side of the joint to the deflection on the loaded side of the joint can be related to the stress load transfer or percent maximum edge stress as indicated by the two relations in Figure 27. The regression equation fitted to Chou's[14] data in Figure 27 should pass through the 50, 1.0, 100, and 0.0 points for percent maximum edge stress and joint efficiency; however, the mathematics of the regression does not meet this requirement. Most of the deflection data to be analyzed fall in the intermediate joint efficiency ranges where the regression equation provides good agreement with Chou's[14] results, and this equation was used to convert reported deflection joint efficiency data into edge percent maximum stress. A comparison between

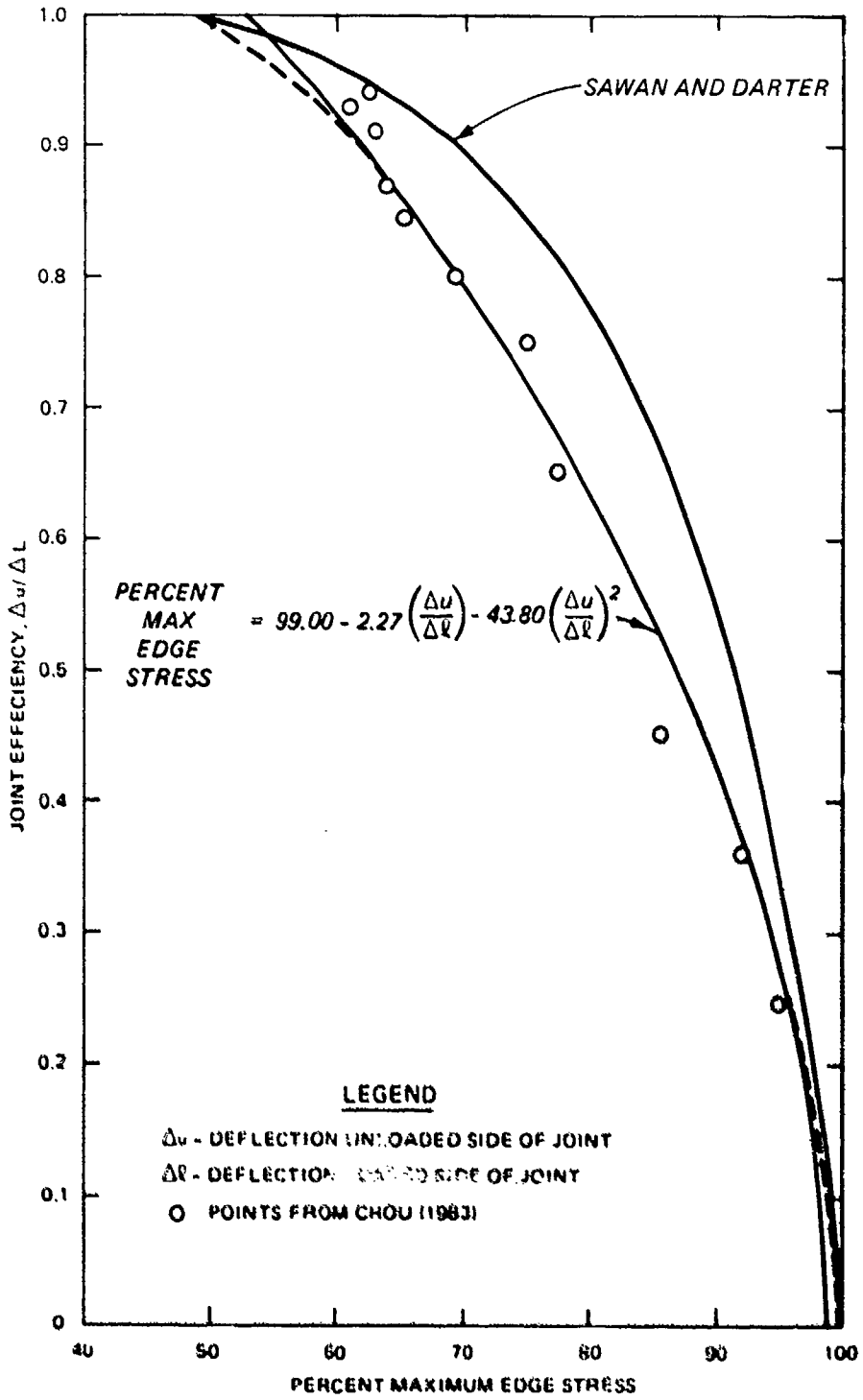

Figure 27. Relation between joint efficiency and edge stress

Chou's[14] results and the relation suggested by Sawan and Darter[66] shows differences of up to approximately 8 percent in the estimate of percent maximum edge stress for a given joint efficiency.

Table 17 shows the results of the analyses of the deflection and strain data reported by Grau[19], Ahlvin et al.[1] and Ohio River Division Laboratories[51,52,55]. Doweled joints and contraction joints with aggregate interlock achieved high mean values of load transfer that exceeded the common 25 percent assumption while the keyed joint mean load transfer barely met this assumption. The free joint that was used at the Lockbourne tests consisted of a piece of redwood board the full depth of the slab which provided high variable and low levels of load transfer. This joint is not a standard joint, and deterioration in test items that used this joint usually started around these joints. For this reason the earlier analyses did not include test item slabs with this joint.

Table 17

Load Transfer for Different Joint Types

Type of Joint	Number of Data Points	Load Transfer Range	Load Transfer Mean	Coefficient of Variation, %
Doweled Construction Joint	195	0.0-50.0	30.6	38.0
Doweled Expansion Joint	15	15.4-42.6	30.5	24.4
Contraction Joint with Aggregate Interlock	46	15.6-50.0	37.2	19.2
Keyed Joint	61	5.6-49.0	25.4	41.4
Lockbourne "Free" Joint	8	5.8-24.5	15.5	40.9

A joint, particularly if overloaded, will deteriorate with increasing traffic repetitions. Figure 28 shows that the initially high load transfer of 45.2 percent of a keyed joint deteriorated under C-5A traffic to levels of 15.4 and 11.1 percent. Reductions in load transfer with traffic repetitions have also been reported for other types of joints[6].

This loss of load transfer with traffic is of particular importance for overlay analysis. The base pavement is often being overlaid because of structural damage from past traffic. Consequently, an integral part of any overlay design must be the assessment of the existing load transfer at the joints in the base pavement. If these joints are not achieving at least the 25 percent load transfer commonly assumed for standard joints, then adjustments to the proposed design method must be made. These adjustments can be made by developing a factor to increase the stresses calculated by the layered elastic model if substandard load transfer is found in the joints of the base pavement.

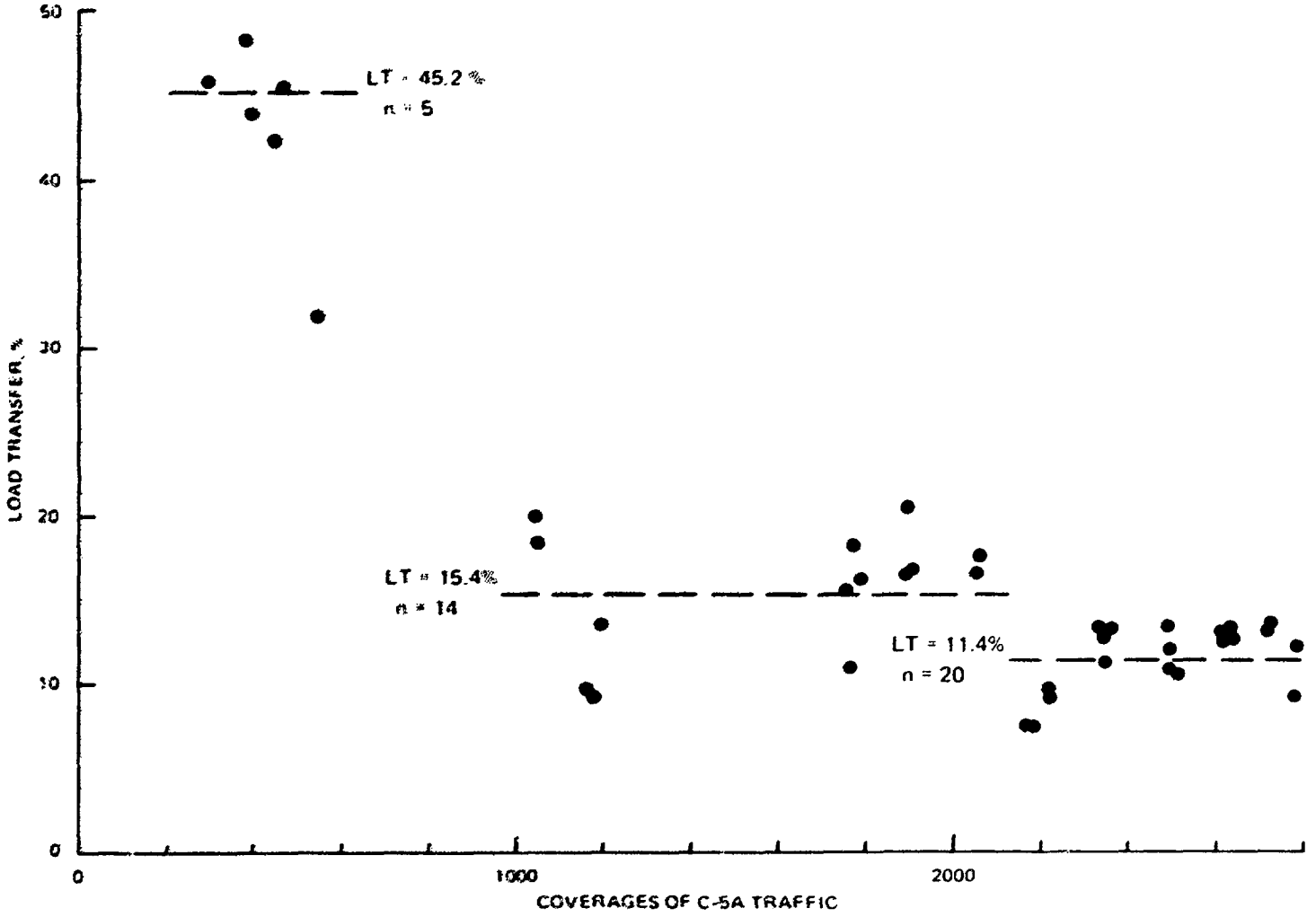

Figure 28. Deterioraion of load transfer with traffic for a keyed construction joint (based on data reported by Ahlvin et al.[1])

MODIFICATIONS FOR LAYERED ELASTIC THEORY

Parker et al.[59] observed that the relation between stresses for rigid pavement test sections calculated using the Westergaard edge loaded model and the layered elastic model was approximately linear. To obtain additional information on the relation between Westergaard and layered elastic stresses, both stresses were calculated for an additional 60 cases to supplement the 60 test sections analyzed by Parker et al.[59]. These additional cases included F-4, B-707, B-727, B-747, and C-141 aircraft with modulus of subgrade reactions from 50 to 400 lb/in.^{2}/in. and thicknesses of 6 to 40 in. These calculations along with the Parker et al.[59] stress calculations are tabulated in Appendix C.

Several different least square regression relations were tried for these 120 total cases. As can be seen in Figure 29, a simple power relationship did better than the linear relationship suggested by Parker et al.[59]. The scatter of the data is larger at high levels of stress. However, in the range of stresses encountered in normal design the scatter is much less. This power relationship can be expressed as

$$\gamma\sigma_{LE} = 0.64(\beta\sigma_w)^{0.972} \tag{34}$$

where

γ = equivalent proportion of layered elastic stress to account for load transfer in the Westergaard stress

σ_{LE} = stress from layered elastic analytical model

β = the proportion of the Westergaard stress used in design to account for load transfer, i.e., 1.0 - α

σ_w = stress from Westergaard edge loaded analytical model

α = load transfer to adjacent slab

It is apparent that γ is simply β raised to the 0.972 power. All the models and relationships developed for use with the proposed design procedures are based on joints meeting the common 25 percent load transfer assumption. Normalizing the relation between γ and β for the standard 25 percent load transfer results in a multiplier X for the layered elastic stress as shown in Figure 30. The equation for the multiplier X is

$$X = \frac{(1 - \alpha)^{0.972}}{0.7561} \tag{35}$$

where α is load transfer.

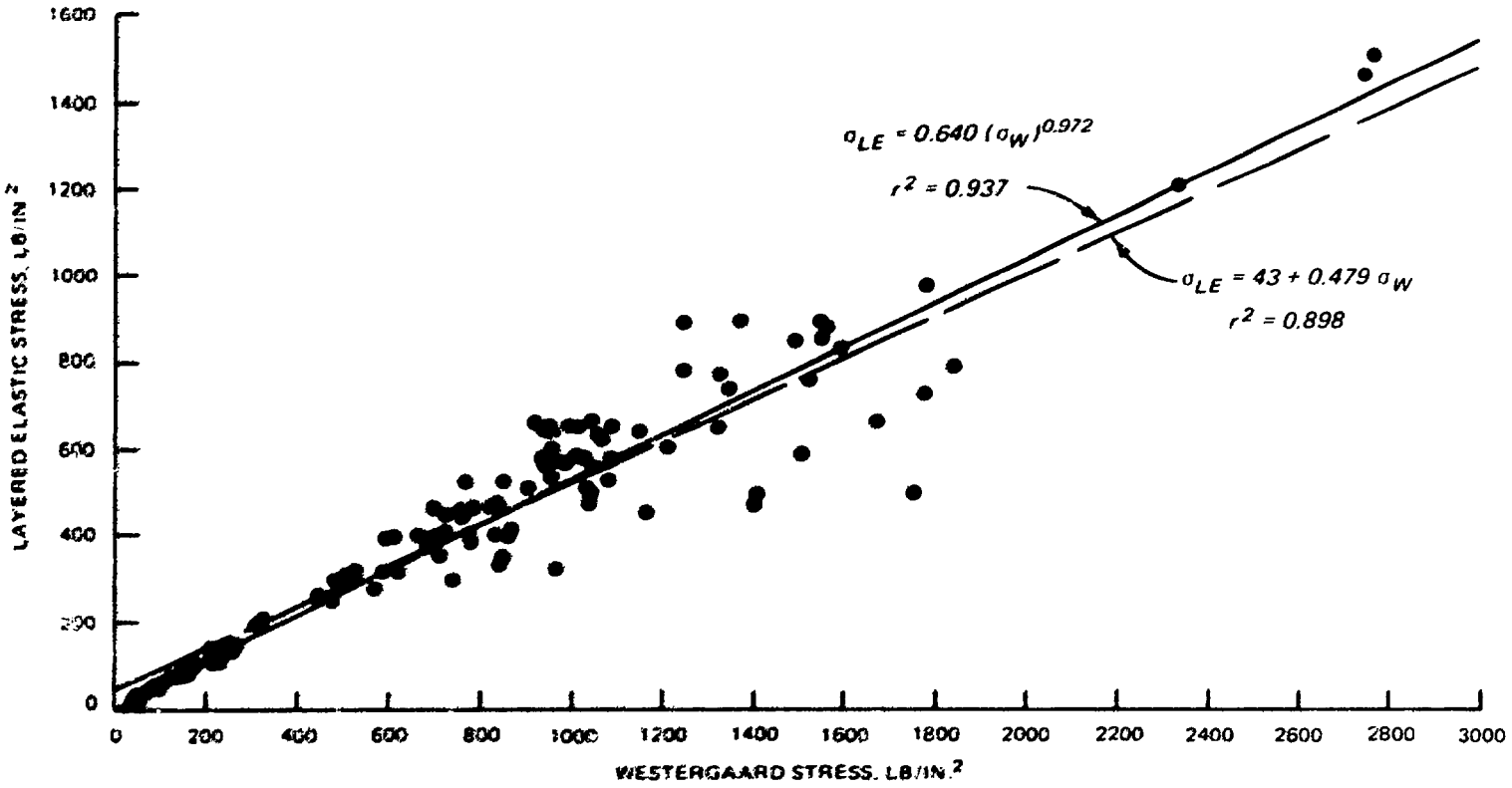

Figure 29. Relation between Westergaard and layered elastic calculated stresses

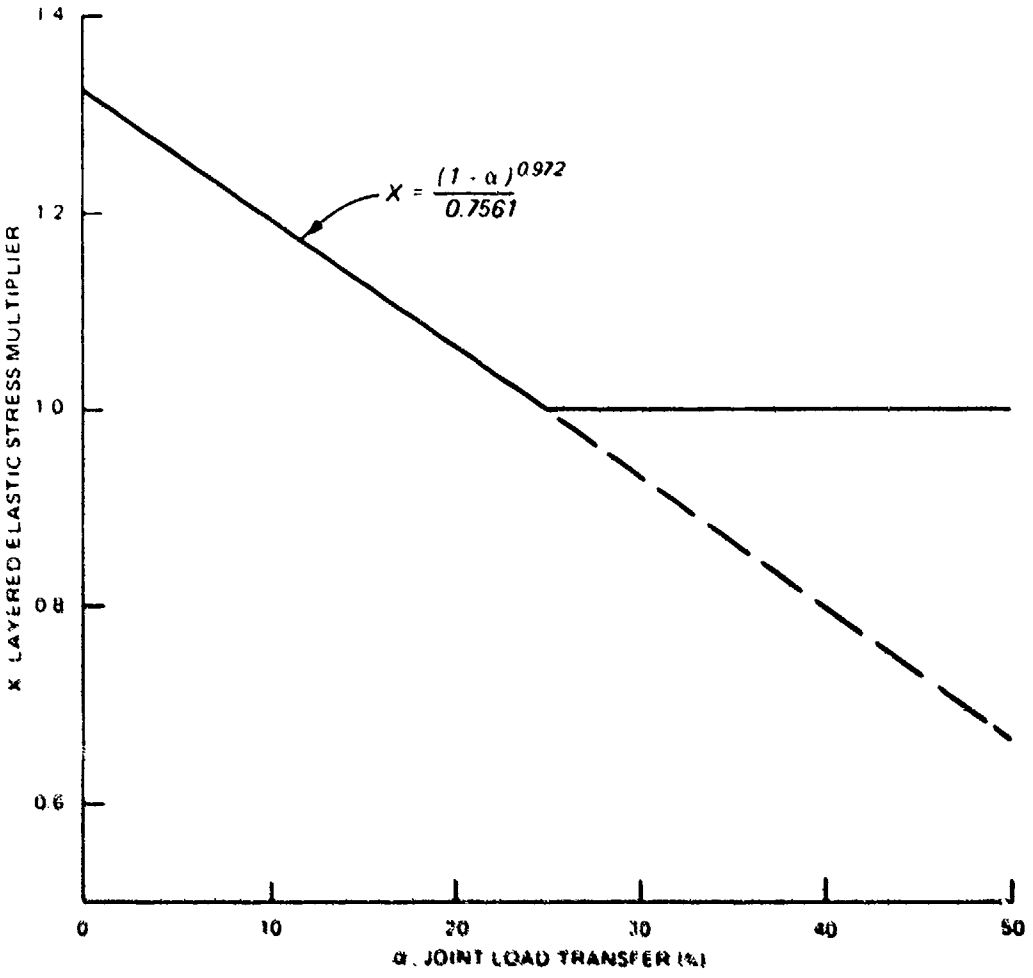

Figure 30. Multiplier for layered elastic stresses to account for load transfer

This multiplier accounts for load transfer different from that used to develop the models and relations in the proposed design procedure.

The average joint load transfer of a base pavement can be found using Figure 27 from the ratio of the deflection on the unloaded and loaded side of a joint. If this load transfer meets or exceeds 25 percent, then no adjustment in stresses should be made. If the load transfer is lower than this value, the layered elastic calculated stresses in the base slab should be increased by multiplying them by the appropriate X from Figure 30.

PROPOSED DESIGN PROCEDURE

METHODOLOGY

The models for predicting pavement performance, representing the reduced structural support of a base slab as it cracks, and accounting for substandard load transfer were developed in the preceding sections and can be incorporated in a new design procedure for overlays. This proposed design procedure will use the layered elastic analytical model to calculate load induced tensile stress in the base pavement and overlay. These stresses are used to predict deterioration of the base and overlay in terms of a SCI varying from 0 to 100. Effects of fatigue damage to the base pavement prior to placing the overlay, progressive cracking in the base pavement and substandard load transfer at the pavement joints are included in the analysis. The steps in the proposed design procedure are shown in Figure 31 and will be discussed and illustrated with a design example in the following sections.

MATERIAL PROPERTIES

Each layer in the pavement must be described by a modulus of elasticity and a Poisson's ratio. A very effective method of estimating the modulus of elasticity for the existing base pavement and underlying layers is to calculate the modulus values from the deflection basin of a falling weight as was done for the six slabs described earlier and as is described by Bush[11]. The modulus value for the overlay concrete could be determined in the laboratory as part of the mixture proportioning studies; or it could be conservatively estimated as 4,000,000 lb/in.^{2} as is currently done for the CE and FAA pavement design curves. Another option would be to estimate it from typical laboratory or nondestructive test values from recently completed local projects that used concrete mixture proportions similar to that anticipated for the overlay. Poisson's ratio is seldom measured for pavement analysis. Instead, it is commonly estimated to be 0.15 to 0.20 for concrete, 0.30 for granular materials, and 0.40 to 0.50 for cohesive soil materials.

If falling weight deflectometer or similar nondestructive tests are not used to determine modulus values, laboratory tests can be run on samples taken from the base pavement and underlying layers to determine modulus values. This is relatively simple for the concrete in the base pavement or for samples of stabilized material. On the other hand, laboratory resilient modulus tests on undisturbed or representative recompacted soil samples are expensive and often difficult to interpret properly.

Modulus values for soils are often estimated from correlations with existing tests. For example, the CBR is often used to estimate modulus values if no more detailed information is available. An approximate relation suggested by Dorman and Klomp[18] is

$$E = 1,500 \times CBR \qquad (36)$$

where

E = modulus of elasticity, $lb/in.^2$

CBR = the California Bearing Ratio, percent

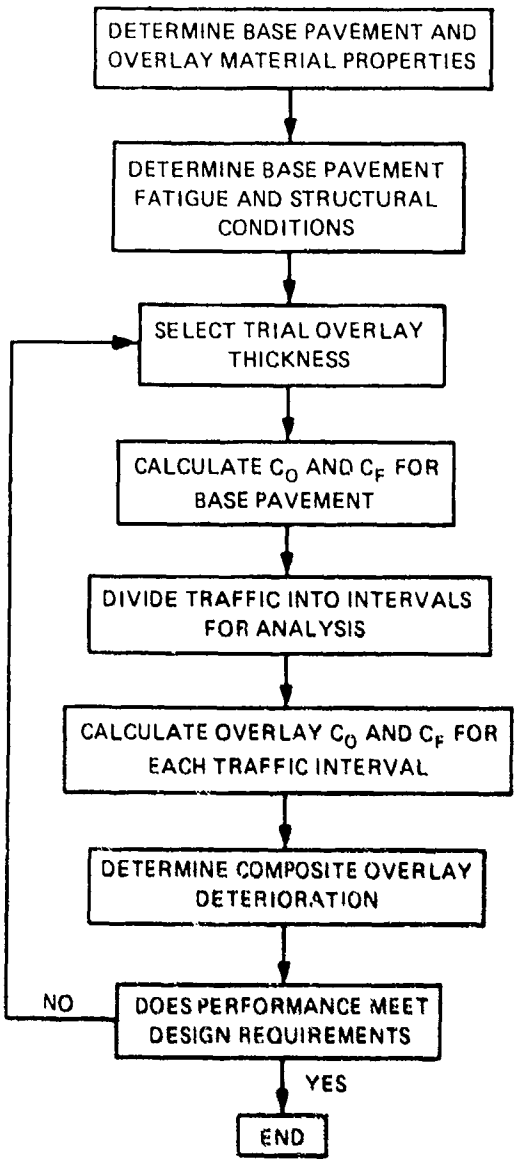

Figure 31. Steps in the proposed design procedure

Parker et al.[59] have suggested the following relationship

$$\text{Log } E = 1.415 + 1.284 \log k \qquad (37$$

where

E = modulus of elasticity, lb/in.^{2}

k = modulus of subgrade reaction, lb/in.^{2}/in.

If no other data are available, the modulus values could be estimated from the soil classification, but this is obviously the least accurate approach. Table 18 shows some typical modulus of elasticity values. The values vary widely and reflect variations due to temperature, state of stress, load frequency and duration, age and composition of materials, and strain level. Selection of modulus values for design is a critical step. More detailed information on determining modulus values for paving materials to be used with layered elastic analysis can be found in Parker et al.[59], Barker and Brabston[7], and Green[20].

Table 18

Typical Modulus of Elasticity Values

Material	Typical ranges, lb/in.^{2}
Portland Cement Concrete	$3.5 - 6.0 \times 10^6$
Asphalt Concrete	100,000 - 1,000,000 (highly temperature dependent)
Highly Plastic Clay or Silt (CH, MH)[a]	<15,000
Clays and Silts of low plasticity, Silty Clays (CL, ML)[a]	5,000 - 20,000
Sands, Sandy Clays, Clayey Sands (SP, SW, SM, SC)[a]	15,000 - 40,000
Natural Gravels (GP, GW, GM, GC)[a]	15,000 - 100,000
Crushed Well-Graded Stone (GM, GW)[a]	30,000 - 150,000
Stabilized Base Course Materials	200,000 - 1,000,000

[a]Unified Soil Classification Symbols.

A problem arises if the modulus of subgrade reaction, k , is used to estimate the elastic modulus values for a granular base over a subgrade. A 30-in.-diam plate is used to determine a composite k on the surface of the base that, unless the base is exceptionally thick, includes the influence of both the base and subgrade. This is the k that would be used in

conventional design. For the proposed design procedure it would be appropriate to conduct plate load tests (or CBR tests) on the subgrade as well as on the surface of the base course to get better estimates of modulus values. If a relatively thin granular base on the order of 4 to 6 in. thick rests on a clay subgrade, the composite k may give a reasonable estimate of the modulus of elasticity. Such thin layers in a pavement may not actually act independently and are very difficult to compact if they are on a resilient subgrade. Consequently, these thin bases may not obtain very high modulus values. If, on the other hand, the base is relatively thick, any modulus value estimated from the composite k will not adequately reflect the lower modulus of the subgrade. Each structural layer in the pavement must have its modulus value evaluated. Tests with the falling weight deflectometer or similar device are the best method of characterizing the pavement properties under these conditions.

Flexural strength has a major impact on concrete pavement performance. Consequently, the best possible estimate of flexural strength is needed. The flexural strength of the overlay concrete should be determined as part of the mixture proportioning studies. The flexural strength of the base pavement may be determined from historical data, flexural beams cut from the base pavement, or approximate correlations between flexural strength and tests run on cores taken from the base pavement. Flexural strength is often estimated by the relation

$$f_f = K_1 \sqrt{f'_c} \tag{38}$$

where

f_f = flexural strength, lb/in.^{2}

K_1 = a constant varying from 8 to 10

f'_c = compressive strength, lb/in.^{2}

Also, Hammitt[21] has suggested the relationships

$$f_f = \frac{f'_c + 2123}{10.02}$$

$$n = 189 \text{ tests}$$

$$r^2 = 0.77$$

$$f_f = 210 + 1.017\, f_{st} \tag{39}$$

$$n = 199 \text{ tests}$$

$$r^2 = 0.73$$

where

f'_c = compressive strength, lb/in.^{2}

f_f = flexural strength, lb/in.^{2}

f_{st} = splitting tensile strength, lb/in.^{2}

There is no unique correlation between flexural strength and compressive or splitting tensile strengths. The actual relationship varies depending on the aggregates and mixture proportions used in the concrete. Even though cores are far easier to obtain from an existing pavement than beams, the estimate of flexural strength from compressive or splitting tensile tests on the cores may not be very reliable.

The interface conditions between layers must also be described. In general all pavement interfaces except those with concrete have been treated as fully bonded in most layered elastic analyses of pavements. The interface between concrete and other materials is usually treated as frictionless. Obviously, the interface for a fully bonded overlay with special surface preparation and bonding grouts should be treated as fully bonded, whereas the unbonded overlay interface with a distinct bond breaking course would be more appropriately treated as frictionless. The partially bonded overlay is more of a problem, and an appropriate friction factor will be developed from the CE overlay test section data that appear later in this report.

The condition of the base pavement at the time of overlay often determines the bonding condition used for the overlay. Any crack or joint in the base pavement will reflect through the overlay soon after placement unless there is a positive bond breaker between the overlay and base pavements. Therefore, joints in the overlay are matched with the base pavement joints for fully bonded or partially bonded overlays. Also, their use is usually limited to overlay of pavements that are in sound structural condition. Fully bonded overlays are used only on uncracked pavements or pavements with cracked slabs that are replaced prior to placement of the overlay. Partially bonded overlays are sometimes placed on pavements with some minor load related cracking. The pavement SCI should be 70 or better if a partially bonded overlay is to be used. However, slabs showing multiple cracks or spalling or raveling cracks should be replaced prior to placement of the overlay.

The bond breaking course used with unbonded overlays is generally thin and will not normally need to be modeled in the layered elastic analytical model. Typical examples of bond breakers include polyethylene, heavy applications of curing compound, building paper, applications of sprayed bitumen and sand or gravel, or thin asphalt concrete layers. Sometimes thicker bond breaker layers of asphalt concrete, roller compacted concrete, or econocrete may be used as leveling courses or to make major grade changes. If these

layers are 1-in. or more in thickness, it will probably be necessary to include them in the layered elastic model.

BASE PAVEMENT CONDITIONS

Previous traffic on the base pavement has consumed some of its fatigue capacity. If it has begun to structurally deteriorate from this traffic, an SCI can be determined from the PCI procedures in the FAA[79], Department of the Navy[25], or Shahin, Darter, and Kohn[69] using the specific distress types listed in Table 5. The ratio between the effective modulus of elasticity and the initial undamaged modulus of elasticity can be determined for any SCI from the slab test relationship:

$$E_r = 0.02 + 0.0064 \times SCI + (0.00584 \times SCI)^2 \quad (40)$$

Since the initial concrete modulus was determined in the previous step, the effective concrete modulus to use in the layered elastic model can be determined. The initial modulus of elasticity should be determined from intact concrete. For example, falling weight deflectometer tests should be run at the center of intact slabs. Certain durability related distress problems such as severe D cracking or crazing due to alkali aggregate reaction affect the concrete modulus of elasticity, and this may need to be included in the analysis. If the falling weight is used to determine the initial modulus of the concrete from an intact slab that is undergoing alkali aggregate reaction, the alkali aggregate reaction damage is already included in the initial modulus estimate. No adjustment would then be needed. However, if the initial modulus was determined from historical construction records or estimated, then it would be appropriate to include the PCI deducts for crazing because of alkali aggregate reaction in calculating the SCI. However, minor crazing caused by plastic shrinkage cracking from improper curing has little or no effect on the concrete modulus and should not be considered in any adjustment to modulus values. Each case needs to be analyzed individually.

If the pavement to be overlaid has an SCI of 100, the amount and type of past traffic on the base pavement must be determined. Records of this type are often poor, but the best possible estimate of this must be made so that fatigue damage to the base pavement can be calculated later. A mixture of aircraft types can be converted to equivalent passes of a single selected type of aircraft using the FAA[79] or the Department of the Army[24] method.

The effective load transfer at the joints of the base pavement needs to be determined. This may be done by determining the ratio of the deflections on the loaded to the unloaded side of a joint and using the relationship in Figure 27 to estimate load transfer. If the effective load transfer is below 25 percent, then a stress multiplier from Figure 30 needs to be selected. This multiplier will be used in a later step to adjust the calculated stresses in the base. Presumably, no adjustment will normally be needed for the overlay since conventional joint construction would be used. Load transfer is a variable rather than a constant, and it also often decreases with increasing traffic repetition. Consequently, consistent substandard load transfer

measurement in the base pavement might conservatively be treated as no load transfer to recognize the potential for future deterioration.

TRIAL THICKNESS

This design method is an iterative process. A trial thickness of overlay is selected, and its condition in terms of SCI at the end of the design traffic is predicted. If this SCI is unacceptably low, then a thicker overlay is tried. If, on the other hand, the initial trial overlay thickness is capable of supporting much more traffic than necessary, a thinner overlay can be tried. The models used in this proposed design procedure only represent the deterioration of a concrete pavement due to cyclic fatigue damage caused by repetitive loading. Other causes of pavement deterioration such as pumping or D cracking must be guarded against by other means.

BASE PAVEMENT PERFORMANCE

The base pavement performance factors C_0 and C_F before overlay must be calculated for the traffic load applied before the overlay is placed. Next, these factors must be recalculated for the base after the overlay is placed using the traffic load to be applied after overlay. These factors are determined from the following equation

$$DF = 0.5234 + 0.3920 \log C_0$$

$$DF = 0.2967 + 0.3881 \log C_F \qquad (41)$$

where

DF = design factor = flexural strength ÷ calculated stress

C_0 = coverage level at which SCI begins to decrease from 100

C_F = coverage level at which SCI becomes 0

If the base pavement has not begun to deteriorate before overlay, the fatigue damage f from this previous traffic can be calculated as

$$f = \frac{C}{C_{ob}} \qquad (42)$$

where

f = fatigue damage

C = coverage of traffic applied before overlay

C_{ob} = base performance factor C_0 calculated for traffic load applied before overlay

The equivalent amount of traffic that this represents after overlay is determined by

$$C_E = f \times C_0 \tag{43}$$

where

C_E = the equivalent amount of traffic after overlay that would do the same fatigue damage to the base pavement as was done by the traffic before the overlay was placed

C_0 = base performance factor C_0 after overlay calculated using trial overlay thickness and the overlay traffic load

If the joint load transfer has been found to be substandard, the appropriate stress multiplier X selected earlier should be used to increase the calculated stresses used to determine the base C_0 and C_F factors.

TRAFFIC INTERVALS

The design traffic to be applied to the overlay is divided into intervals so that the stresses from the varying base slab support during each interval can be determined. The first interval of traffic is up to the base C_0 value calculated after overlay, and the last interval is all traffic past C_F. If some equivalent traffic has been applied before overlay, these traffic coverages must be subtracted from C_0 and C_F because this damage has already occurred.

During the initial traffic interval the full uncracked concrete modulus is used for the base slab to calculate the stresses in the overlay. During the last interval the SCI is 0, and the appropriate reduced base concrete modulus is used to calculate the stresses in the overlay.

Between C_0 and C_F the traffic is divided into intermediate intervals for analysis. This study used four intermediate intervals and used the appropriate reduced modulus for SCI values of 80, 60, 40, and 20 for the intervals. The intervals of traffic were from C_0 to the coverage level at which the SCI was 70, from this last point to the coverage level at which the SCI was 50, from this last point to the coverage level at which the SCI was 30, and from this last point to C_F.

If there has been fatigue damage, these traffic intervals must be reduced by the equivalent traffic. If the base pavement has begun to deteriorate before the overlay is placed, the base SCI value at the time of overlay determines the initial support conditions. If applied traffic before the

overlay is placed exceeds the C_{ob} value (possibly because of limits of the model, poor traffic estimates, or inaccurate material or load parameters), the equivalent traffic can be set equal to C_0 after overlay. Doing so is equivalent to assuming that the base pavement will begin to deteriorate with the first coverage of traffic on the overlay.

OVERLAY PERFORMANCE FOR EACH INTERVAL

During each interval of traffic the damage suffered by the overlay during that interval is assumed to be controlled by the performance factors, C_0 and C_F, calculated for the overlay stresses for that interval. Each interval of traffic results in a decrease in the modulus of the concrete in the base pavement. This causes higher tensile stresses in the overlay with a corresponding decrease in the overlay performance factors, C_0 and C_F. Once these overlay performance factors are calculated for the stresses in each interval of traffic, the fatigue damage during an interval of traffic can be determined by

$$f_i = \frac{C_i}{C_{oi}} \tag{44}$$

where

f_i = overlay fatigue damage during the i^{th} interval of traffic

C_i = coverages of traffic during the i^{th} interval

C_{oi} = the overlay C_0 performance factor calculated using the appropriate base pavement modulus of elasticity for the i^{th} traffic interval

COMPOSITE OVERLAY DETERIORATION

The damage suffered by the overlay during each interval of traffic must be combined to determine a composite overlay deterioration. The first step is to determine the coverage level at which overlay deterioration begins. This coverage level is essentially the overlay composite, C_0. During the first interval of traffic (i.e., the traffic up to the point where the base slab begins to deteriorate and support to where the overlay decreases), the fatigue damage f_i during the first interval can be calculated as noted before. Because of this fatigue damage, the C_0 for the next interval needs to be adjusted as follows:

$$C^*_{o,i+1} = (1 - f_i)\, C_{o,i+1} \tag{45}$$

where

$C^*_{o,i+1}$ = C_o factor for interval i+1 adjusted for fatigue damage from the preceding interval

f_i = fatigue damage from the preceding traffic interval

$C_{o,i+1}$ = C_o factor calculated from the stress for traffic interval i+1

This process is continued until traffic applied during an interval exceeds the adjusted C_o value. When traffic reaches this adjusted C_o value, the overlay is assumed to begin to deteriorate. The loss in SCI over the remaining traffic interval is assumed to be the same as the loss in SCI for the same amount of traffic past C_o on the original unadjusted $C_o - C_F$ line of the traffic interval. The loss in SCI for the next interval of traffic will be the same as the loss along that interval's $C_o - C_F$ line. This is continued until the SCI is zero.

The discussion up to this point assumed that the base cracked under the overlay traffic. Under some conditions of load, overlay geometry, and material properties, the base will not crack before the overlay. For this case, the composite overlay performance is simply the unadjusted $C_o - C_F$ relationship for the first interval of traffic.

DESIGN REQUIREMENTS

The composite overlay deterioration curve tells how much structural deterioration is expected for a given overlay thickness at any traffic level. If the rate of deterioration results in an unacceptable SCI at the end of the design traffic, then a thicker overlay needs to be tried. If it has more capacity than needed, a thinner overlay can be tried.

EXAMPLE CALCULATIONS

The overlay design procedure will be illustrated by analyzing overlay test item A 2.7-60 from the Lockbourne No. 1 tests.

MATERIAL PROPERTIES

Figure 32 shows the model of item A 2.7-60. Material properties were reported by the Ohio River Division Laboratories original test report of construction[51] and are also summarized by Parker et al.[59]. Concrete modulus of elasticity was determined in the laboratory from field cast cylinders. Concrete flexural strength was determined from field cast beams, and Poisson's ratio was estimated as 0.15. The modulus of elasticity of the clay subgrade was estimated using the relation developed by Parker et al.[59] from the modulus of subgrade reaction. The modulus of subgrade reaction was determined from field plate load tests. The Poisson's ratio for the clay subgrade was estimated. The inclusion of the rigid boundary at a depth of 20 ft follows the recommendation of Parker et al.[59].

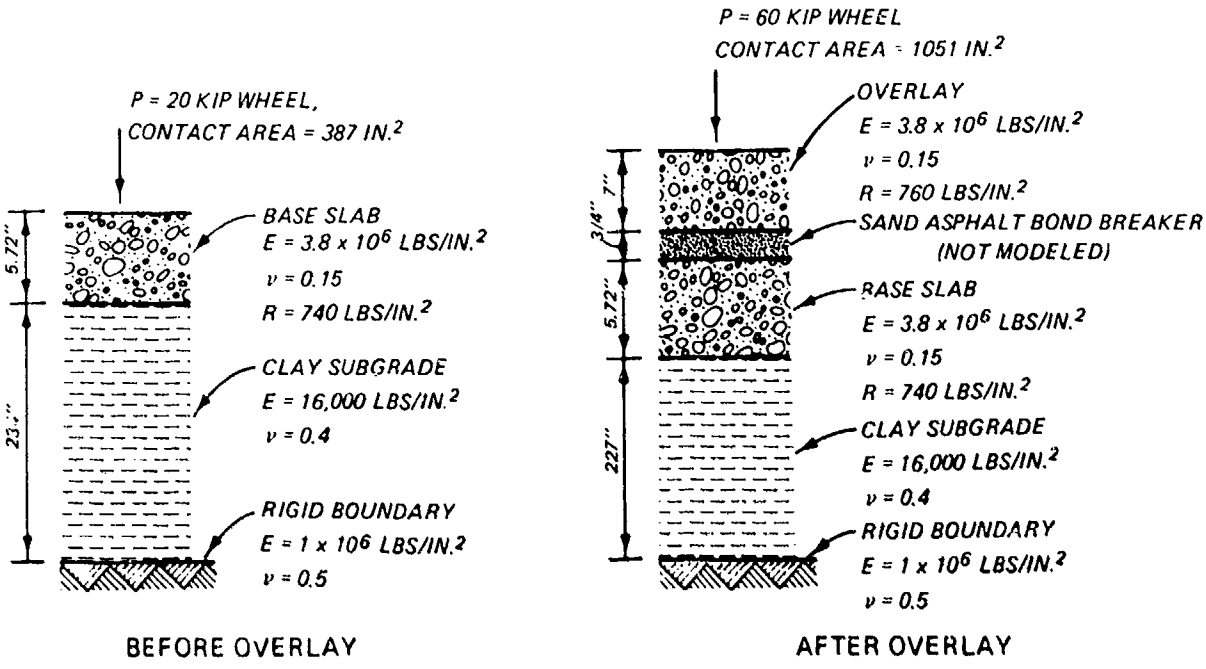

Figure 32. Model of Lockbourne No. 1, Item A 2.7-60

The bond between the overlay and base pavement was treated as unbonded. The 3/4-in.-thick sand asphalt bond breaker was not modeled directly. If the bond breaker was much thicker, it would probably be necessary to include the bond breaker in the model. This bond breaker must be stable under loading. The cutback asphalt actually used in the sand asphalt bond breaker did not cure, and it pumped up through cracks and joints. This unstable material led to premature failure of the overlay, illustrating that pavement failure can arise from factors other than the fatigue damage considered in this study.

BASE PAVEMENT CONDITION

Prior to the overlay placement, the base slab was subjected to 520 coverages of a 20,000-lb wheel load. At the end of this traffic the base pavement had an SCI of 100. All joints for this example meet the basic 25 percent load transfer.

TRIAL THICKNESS

The trial thickness for this example calculation is the actual 7-in.-thick overlay.

BASE PAVEMENT PERFORMANCE

A 20,000-lb wheel trafficked the base pavement before the overlay, and a 60,000-lb wheel trafficked the overlay afterwards. The calculated stresses under these loads and the equivalent C_0 and C_F factors are shown in

Table 19. The fatigue damage from the 20,000-lb wheel load traffic slab can be calculated by

$$f = \frac{C}{C_{O(20\ kip)}} = \frac{520}{2117} = 0.2456 \tag{46}$$

Table 19

Base Slab Stresses and Performance Factors

Calculated stresses for base slab
Before overlay (20-kip wheel) = 405 lb/in.^{2}
After overlay (60-kip wheel) = 395 lb/in.^{2}
Performance Factors C_O and C_F for base slab
C_O before overlay (20-kip wheel) = 2,117
C_O after overlay (60-kip wheel) = 2,779
C_F before overlay (20-kip wheel) = 8,779
C_F after overlay (60-kip wheel) = 11,552

The equivalent traffic is

$$C_E = f\ C_{O(60\ kip)} = 0.2456 \times 2779 = 682 \text{ coverages} \tag{47}$$

The 520 coverages of 20,000 lb wheel before the overlay caused the same damage as 682 coverages of 60,000 lb wheel would cause to the base pavement after the overlay was in place.

TRAFFIC INTERVALS

Figure 33 illustrates the effect of the traffic prior to the overlay placement and the decrease in the support provided by the base slab after it begins to deteriorate. The traffic on the overlay is divided into six intervals as shown in Figure 34. During each interval of traffic on the overlay the SCI of the base is assumed to be constant, and the modulus of elasticity of the base during the interval is assumed to be equal to the value

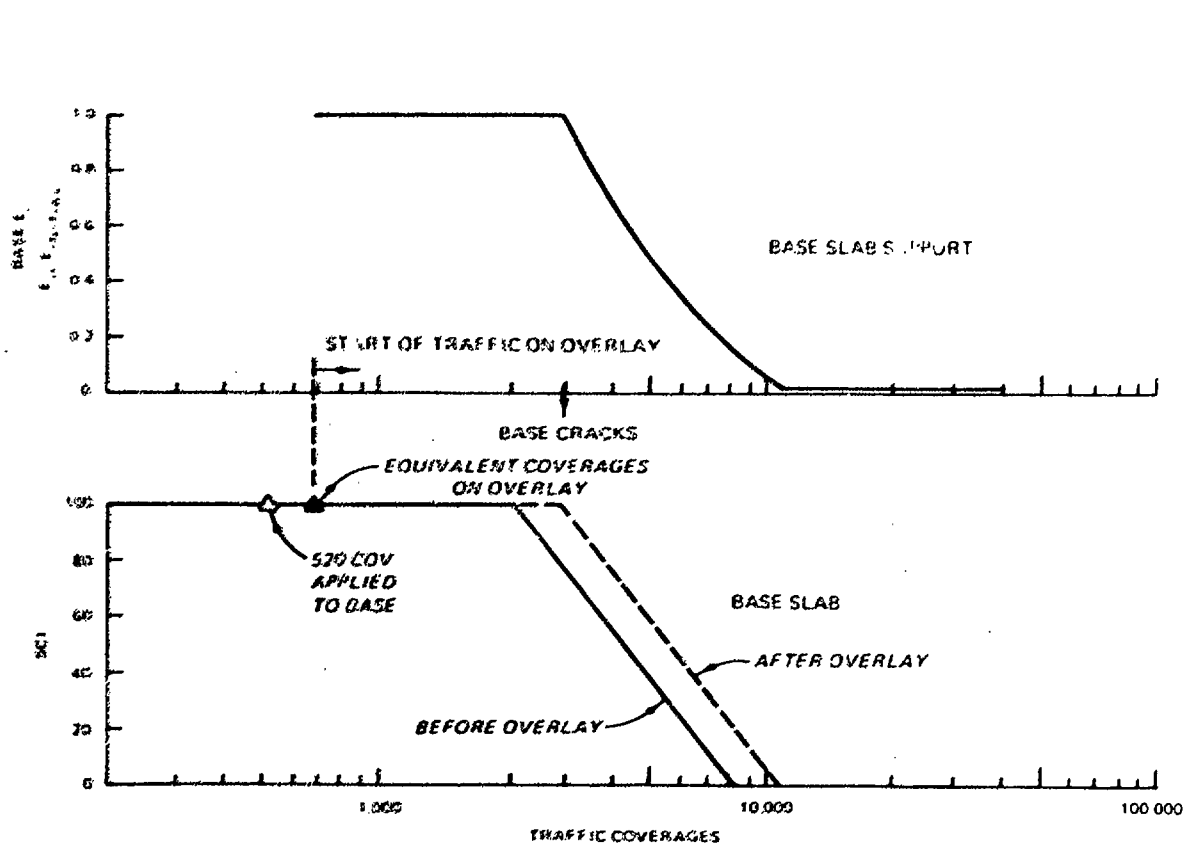

Figure 33. Equivalent traffic and base slab support for Item A 2.7-60

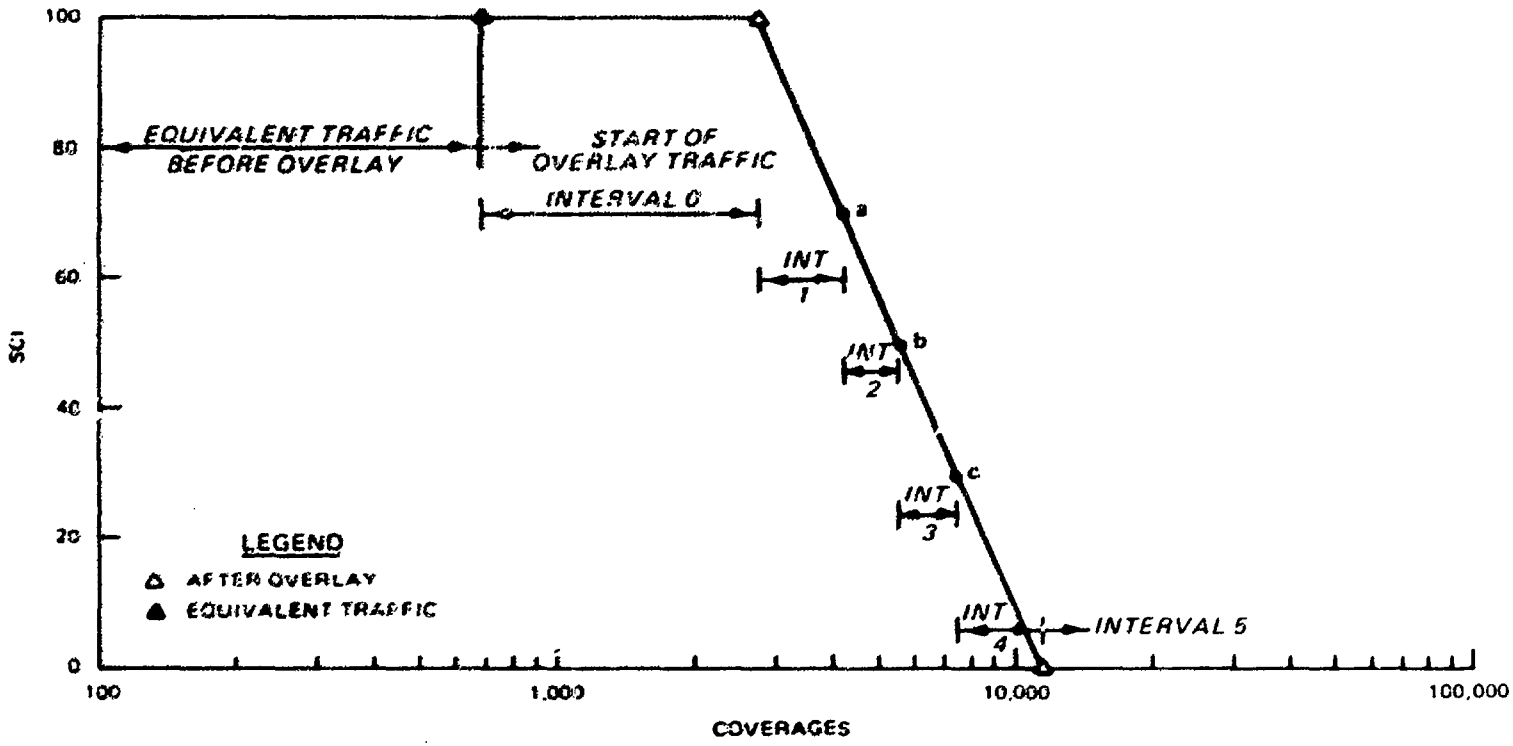

Figure 34. Traffic intervals for Item A 2.7-60 analysis

corresponding to a constant SCI value. The SCI values for this analysis are 100 for interval 0, 80 for interval 1, 60 for interval 2, 40 for interval 3, 20 for interval 4, and 0 for interval 5. The dividing point between intervals 1, 2, 3, and 4 are points a, b, and c in Figure 34 which corresponds to the coverage level where the base SCI is 70, 50, and 30. The equivalent traffic has already been applied to the base.

OVERLAY PERFORMANCE FOR EACH INTERVAL

The stresses in the overlay and the corresponding C_0 and C_F performance factors for interval of traffic are shown in Table 20.

COMPOSITE OVERLAY DETERIORATION

The first step in developing the composite overlay deterioration is to determine the coverage level where the overlay begins to deteriorate. This is in effect the composite C_0 performance factor. During interval zero of traffic the fatigue damage to the overlay can be calculated as

$$d_i = \frac{C_i}{C_{0i}}$$

$$d_o = \frac{C_0}{C_{0o}} = \frac{2,097}{11,254} = 0.186$$

where

d_i = overlay fatigue damage during interval i

C_i = coverages of traffic applied during traffic interval i

C_{0i} = overlay C_0 performance factor for interval i

The next traffic interval's C_0 value adjusted for this fatigue damage can be calculated as

$$C^*_{0,i+1} = (1 - d_i)\, C_{o,i+1}$$

$$C^*_{0i} = (1 - d_o)\, C_{oi}$$

$$C^*_{0i} = (1 - 0.186)\, 4,881$$

$$C^*_{0i} = 3,973 \qquad (48)$$

Table 20

Stress and Performance Factors for Overlay

Interval	Overlay Traffic Coverages	Base Slab			Overlay		
		SCI	E-ratio	E lb/in.^{2}	Stress lb/ in.^{2}	C_0	C_F
0	0-2,097	100	1.000	3,800,000	360	11,254	47,327
1	2,097-3,579	80	0.748	2,842,459	386	4,881	20,357
2	3,579-4,984	60	0.525	1,995,846	414	2,233	9,238
3	4,984-6,852	40	0.330	1,225,824	446	1,030	4,229
4	6,852-10,870	20	0.161	613,394	486	452	1,840
5	>10,870	0	0.020	77,554	584	97	388

This analysis is continued for each interval of traffic until the point where cracking or onset of deterioration C_0 of the overlay is reached. Table 21 shows these calculations for test Item A 2.7-60. At the end of the interval of traffic number 1 (3,579 coverages) in Table 21, the damage factor d_i shows that 37.3 percent of the overlay's capacity before the onset of deterioration has been used. The adjusted C_0 value for the next interval is 1,400 coverages, and the applied traffic is 1,405 coverages. This applied traffic is greater than the adjusted C_0 value of the overlay cracks. This is a total of 4,979 total coverages including the 3,579 coverages through interval 1 plus the 1,400 coverages in this to cracking. From this point to the end of the interval (4,984 coverages) the deterioration or loss in SCI will be the same as on the unadjusted $C_0 - C_F$ line for the interval. For this specific example, there are only five more coverages in the interval, thus resulting in the loss of only a fraction of the point in the SCI; however, this can be ignored. During all following intervals the deterioration will be the same as the interval's original $C_0 - C_F$ line during their respective traffic levels until SCI value of zero is reached. This is illustrated in Figure 35. Once cracking is predicted to start in the overlay, the loss of SCI in this example over the 1,868 coverages of interval 3 will be the same as the loss of SCI for the first 1,868 coverages past C_0 for interval 3. This brings the SCI of the overlay to 27 at the end of interval 3 or at 6,852 total coverages. Between 6,852 and 10,870 coverages the loss of SCI will be determined from the $C_0 - C_F$ relation for interval 4. As shown in Figure 35, the SCI goes from 27 to 0 after 582 coverages in interval 4. Therefore, the composite overlay will reach the SCI value of 0 after another 582 coverages or 7,427 coverages total.

Table 21

Example Overlay Damage Calculation Test Section A 2.7-60

Interval	Overlay Traffic	Applied Traffic, C_i	Overlay C_{Oi}	Damage f_i	Adjusted $C_{O,i+1}$
0	0-2097	2,097	11,254	0.186	11,254
1	2,097-3,579	1,482	4,881	0.373	3,973
2	3,579-4,984	1,405	2,233	overlay cracks	1,400
3	4,984-6,852	1,868	1,030	--	--
4	6,852-10,870	4,018	452	--	--
5	10,870+	--	97	--	--

DESIGN REQUIREMENT

The composite overlay deterioration is shown in Figure 36. The overlay begins to structurally deteriorate after 4,979 coverages and reaches an SCI value of zero after 7,427 coverages. If the overlay must carry more traffic than this, another thicker trial overlay thickness must be selected and the procedure must be repeated.

Figure 36 also shows the deterioration that would be predicted if cracking in the base slab was neglected. This is simply the behavior described by the C_O and C_F performance factors for interval 0 in Table 21. Including the effect of progressive deterioration of the base slab greatly reduces the predicted performance of the overlay.

SUMMARY

The proposed overlay design procedure is analytically more powerful than the existing empirical design procedures. It is able to include the effects of varying material properties in the overlay structure, it accounts for past traffic and the condition of the base pavement at the time of overlay, it includes the effects of progressive cracking in the base under overlay traffic, and it predicts deterioration of the pavement in terms of SCI. The proposed overlay design procedure will be used in the following sections to analyze the CE overlay test section data, and it will be compared with existing methods of design.

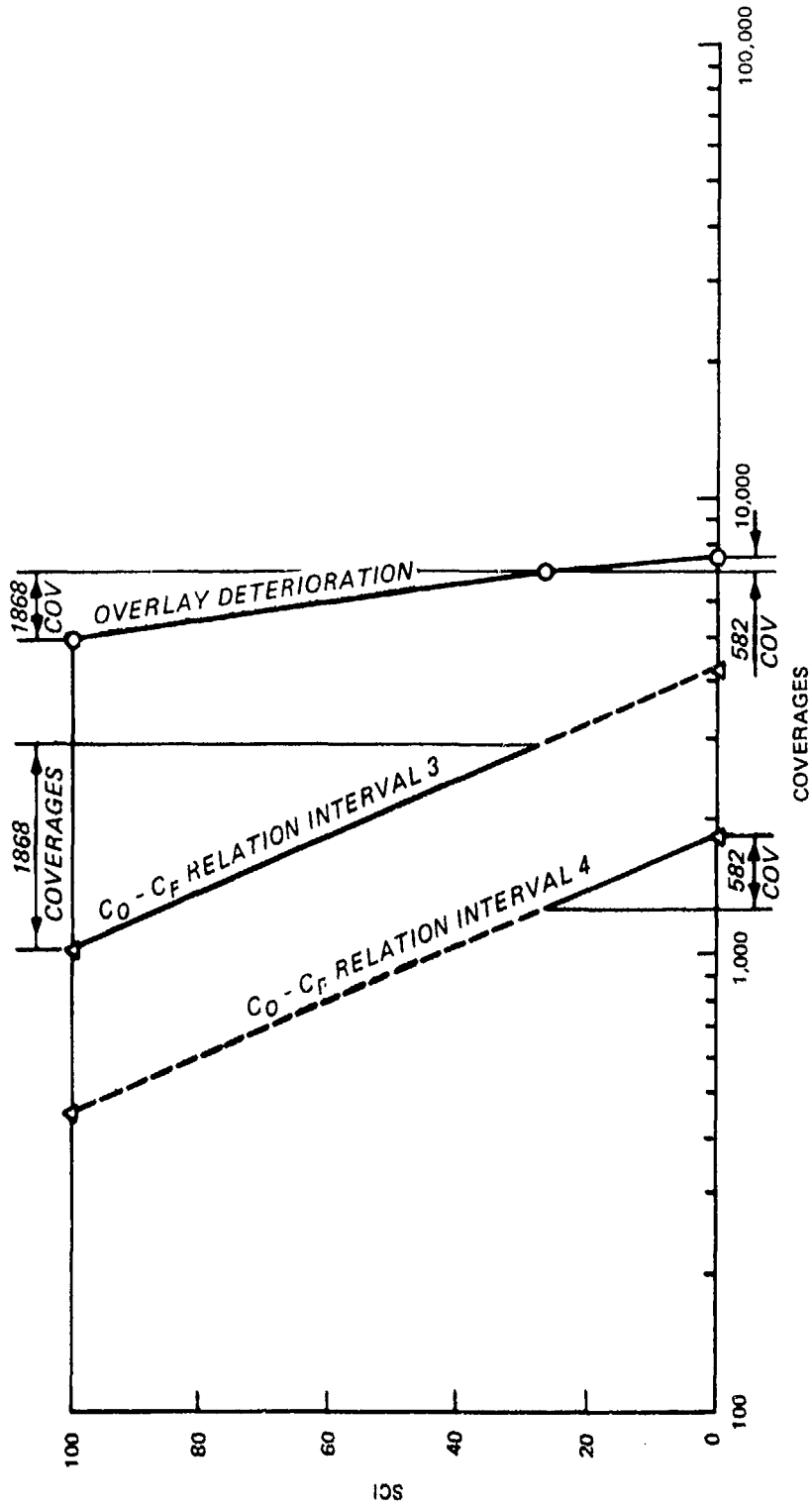

Figure 35. Construction of the deterioration of the overlay for Item A 2.7-60

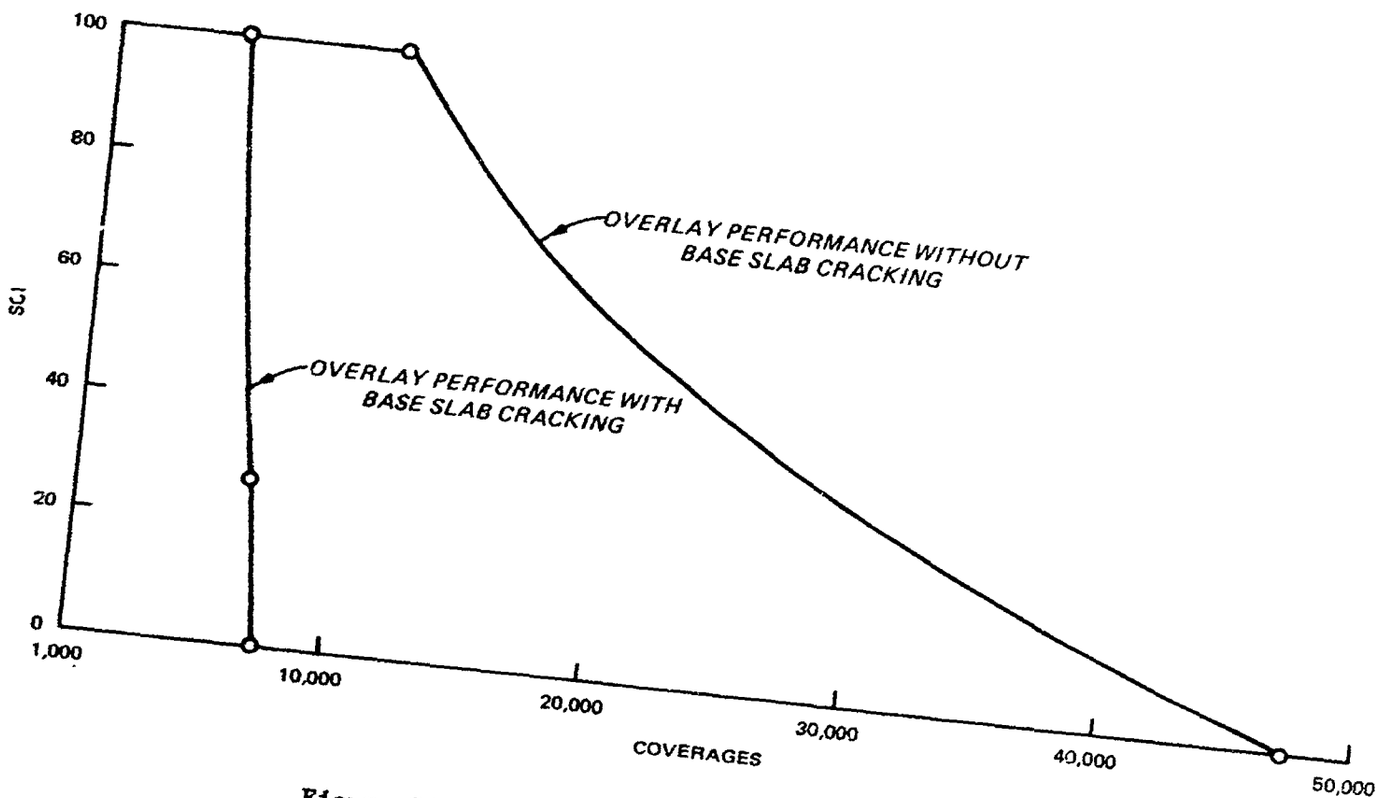

Figure 36. Overlay deterioration of Item A 2.7-60

ANALYSIS OF CE OVERLAY TEST DATA

TEST SECTION DATA

The CE tested 24 test items of rigid overlays over rigid base pavements. Table 22 is a summary of these tests. Twenty-three tests were unbonded overlays, four were partially bonded, and one was fully bonded. The quality of the data collected from these tests varied.

The unbonded test sections in Lockbourne No. 1 test used a nominal 3/4-in.-thick bond breaking layer of sand asphalt. Test Items A 2.7-60 through C 2.7-66S used a cutback asphalt cement, and Item L 1.5-60 through M 2.7-60 used an emulsified asphalt cement. The sand asphalt made with these binders did not cure adequately. When the pavement was trafficked, the sand asphalt pumped out of joints, and cracks were still soft when the overlay slabs were removed at the end of the tests. This pumping and softness of the sand asphalt bond breaking layer undoubtedly resulted in forming voids under the overlay slabs causing premature failure in the overlay. Consequently, all of these slabs would be expected to fail sooner than predicted by the models developed earlier. The Lockbourne No. 2 test items all had free joints without load transfer. Adjustment to the calculated stresses for load transfer has to be made for these overlays.

No final report was written for the Sharonville tests. Consequently, the data on performance of the test sections are very limited. No performance data were reported for Items 21 and 22. Items 23 through 28 were identified as not failing or were failed at the same stated coverage level. The SCI value of such a failure cannot be calculated from the limited available data but could be expected to be in the range of 55 to 80 as indicated in Table 6. Unpublished field records provide additional detailed descriptions of the performance of Items 69 and 70. The proposed design procedure will be used to analyze the CE overlay test sections, and the predicted overlay performance will be compared with the observed performance.

UNBONDED OVERLAYS

In Table 22 there are 19 unbonded overlay test items. The best recorded data exist for the Lockbourne Nos. 1 and 2 tests; however, the 10 unbonded test items from these tests could not be analyzed. As mentioned previously, the 3/4-in.-thick bond breaker in Lockbourne No. 1 did not cure properly, thus, the unbonded overlays all failed prematurely. Consequently, no meaningful comparison between predicted and observed behavior could be made. The Lockbourne No. 2 test items without load transfer were analyzed separately in another section. The remaining nine test items are all from the Sharonville tests. Items 21 and 22 have no recorded performance data. Items 23 and 24 did not fail after 22,000 coverages of traffic according to Mellinger[47], who also gave coverage levels at which Items 25 through 28 and 69 failed. The minutes of the meeting of the board of consultants[54] contain a diagram showing the progression of cracking and spalling for Item 69. No other data on the performance of these test items have been located.

Table 22

Summary of the CE Overlay Tests

Test Series	Test Item	Bond Condition	Slab Thickness, in. Base	Slab Thickness, in. Overlay	Traffic Coverages on Base Slab	Remarks
Lockbourne No. 1	A 2.7-60	Unbonded	5.72	7	520	3/4-in. sand asphalt bond breaker did not cure
	B 2.7-66L	Unbonded	6	7	524	Same
	C 2.7-66S	Unbonded	6	7	526	Same
	D 2.7-66	Partial	5.5	7	554	--
	E 2.7-66M	Partial	5.75	7	556	--
	F 2.7-80	Partial	8	7	554	--
	L 1.5-60	Unbonded	6	5	0	3/4-in. sand asphalt bond breaker did not cure
	L 2.5-60	Unbonded	6	5	0	Same
	M 1.7-60	Unbonded	6	7	0	Same
	M 2.7-60	Unbonded	6	7	0	Same
Lockbourne No. 2	F 12.14-100	Unbonded	10	14	0	Used nonstandard joints
	G 12.14-100	Partial	10	14	0	Same
	L 14.14-80	Unbonded	8	14	0	Same
	M 14.14-80	Unbonded	8	14	0	Same

(Continued)

Table 22 (Concluded)

Test Series	Test Item	Bond Condition	Slab Thickness, in. Base	Slab Thickness, in. Overlay	Traffic Coverages on Base Slab	Remarks
Sharonville	21	Unbonded	6	16	0	No performance data reported
	22	Unbonded	8	15	0	No performance data reported
	23	Unbonded	5.75	13.25	0	Unfailed at 22,000 coverages
	24	Unbonded	7.75	12.25	0	Unfailed at 22,000 coverages
	25	Unbonded	9.75	10.25	0	Failed at 18,500 coverages
	26	Unbonded	10	6	0	Failed at 1,200 coverages
	27	Unbonded	8	9	0	Failed at 250 coverages
	28	Unbonded	10	6	0	Failed at 230 coverages
Sharonville Heavy Load	69	Unbonded	17	15	0	Failed at 4,000 coverages
	70	Full	17	11	0	Spalling over dowel bars

Data on the subgrade for Items 23 through 28 were reported in the minutes of a meeting of the board of consultants[53]. The original subgrade was constructed at a nominal CBR of 3 to 4, but despite spraying the subgrade surface with an asphalt membrane, some unspecified amount of subgrade drying did occur. Mellinger[47] carried out his analysis of these test sections using a low modulus of subgrade reaction k value of 50 lb/in.^{2}/in. comparable with the constructed moisture content. An analysis by Monismith, Yuce, and Finn[50] used a higher k value of 125 lb/in.^{2}/in. which is representative of a condition where some drying occurred in the subgrade. Because of the uncertainty over the appropriate subgrade condition, two analyses were run for Items 23 through 28. One analysis used an elastic modulus of 12,800 psi for the subgrade, which is equivalent to the k value of 125 lb/in.^{2}/in. used by Monismith, Yuce, and Finn[50] according to the relation between k and the modulus values reported by Parker et al.[59]. The second analysis used the average CBR values at the surface and 6 in. below the surface as the subgrade was originally constructed[53]. The elastic modulus was estimated using the relation that the elastic modulus is approximately equal to 1,500 multiplied by the CBR. These two modulus values bracket the range of expected subgrade conditions expected for these test items.

Concrete strength varied considerably for Item 69. Concrete flexural strength averaged 710 and 770 psi on the east side of the test item for the overlay and the base pavements, respectively. It averaged 825 and 615 psi on the west side of the test item for the overlay and the base pavements, respectively. One analysis for this item used the average flexural strength of all concrete placed in the overlay (770 psi) and the average strength placed in the base pavement (690 psi). A second analysis used the lowest flexural strength in the overlay (710 psi) and the base pavement (615 psi).

The performance of each test item overlay was predicted using the proposed design procedures. No traffic was applied to the base pavements prior to the placement of the overlay. The results of these predictions are shown in Figures 37 to 43. Each figure shows the failure reported by Mellinger[47], which is estimated from Table 6 to have occurred at an SCI value between 55 and 80. Also, the coverage level at which the base slab would be predicted to begin deterioration or cracking is shown for Items 25, 27, 28, and 69. The overlay was predicted to start deterioration before the base slab cracking for Items 23, 24, and 26.

Items 23 and 24 did not fail with up to 22,000 coverages of traffic, and Figures 37 and 38 show agreement with this result for the higher of the two subgrade elastic moduli. Item 26 in Figure 40 also shows good agreement with the reported failure coverage level for the higher subgrade modulus value. Predictions for Items 25 and 28 in Figures 39 and 42 bracketed the reported failure levels. Predictions for Item 27 and 69 in Figures 41 and 43 were all too high. Figure 43 shows the SCI deterioration of Item 69 calculated from the cracking and spalling reported in the minutes of the meeting of the board of consultants[54]. There was some cracking at fairly low levels of traffic,

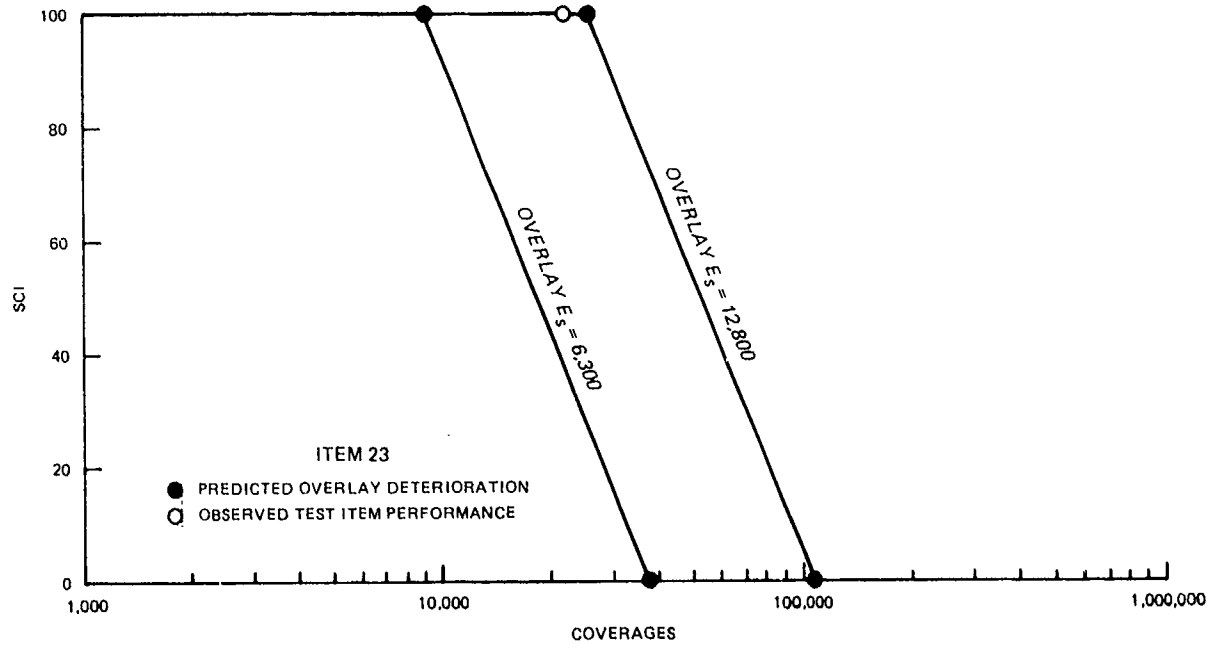

Figure 37. Performance of Item 23

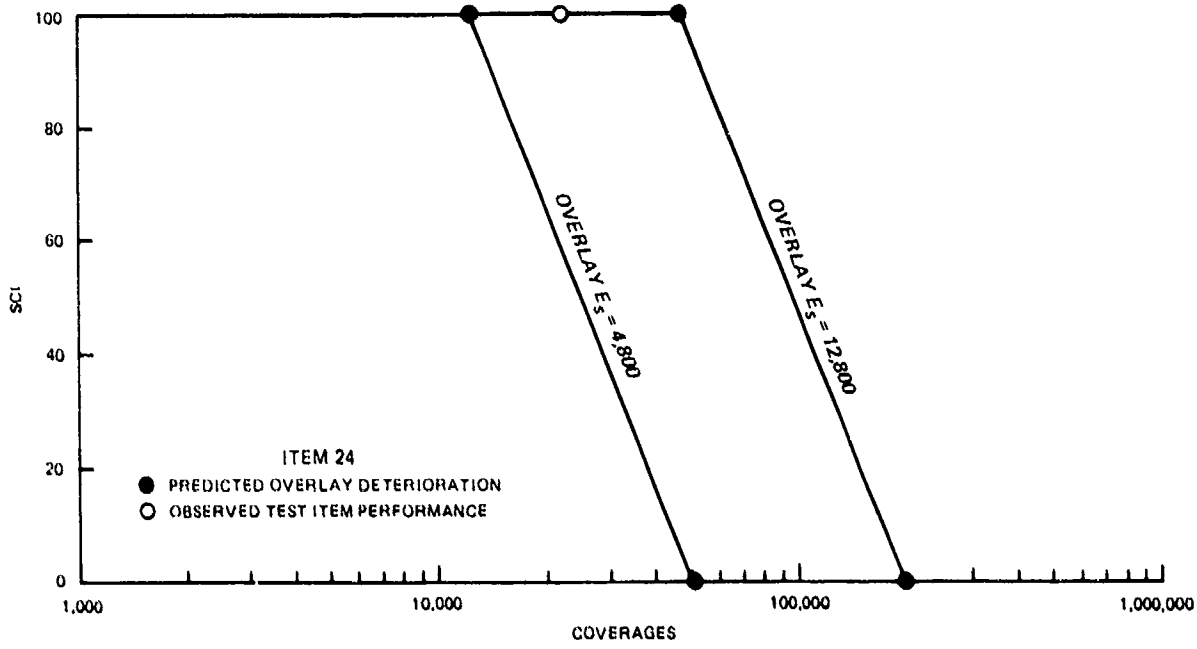

Figure 38. Performance of Item 24

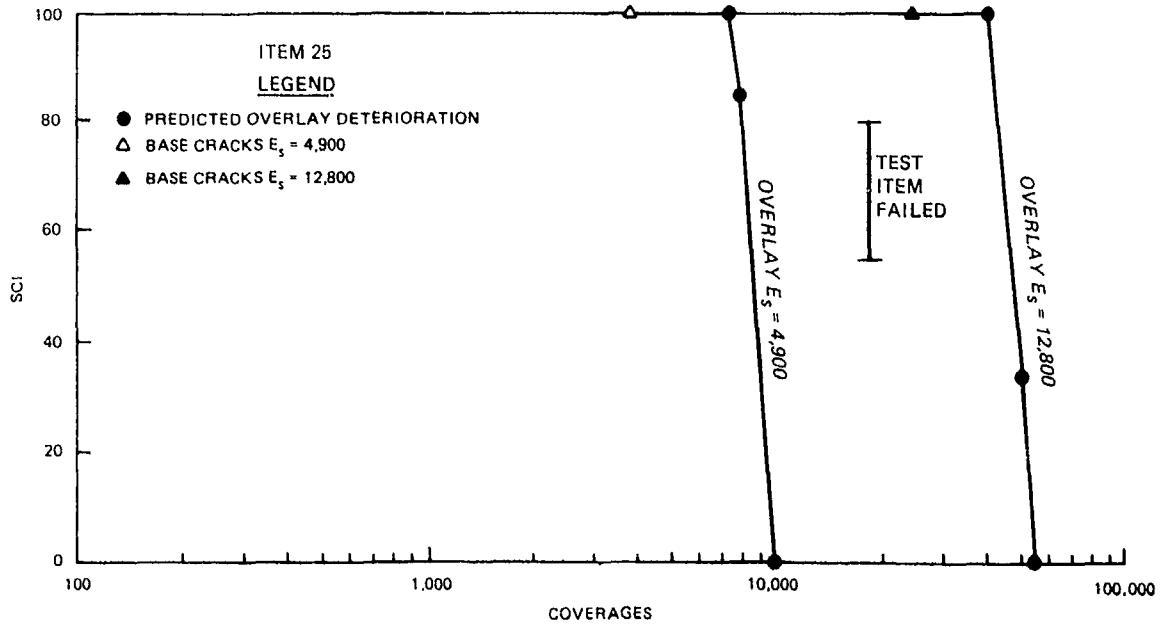

Figure 39. Performance of Item 25

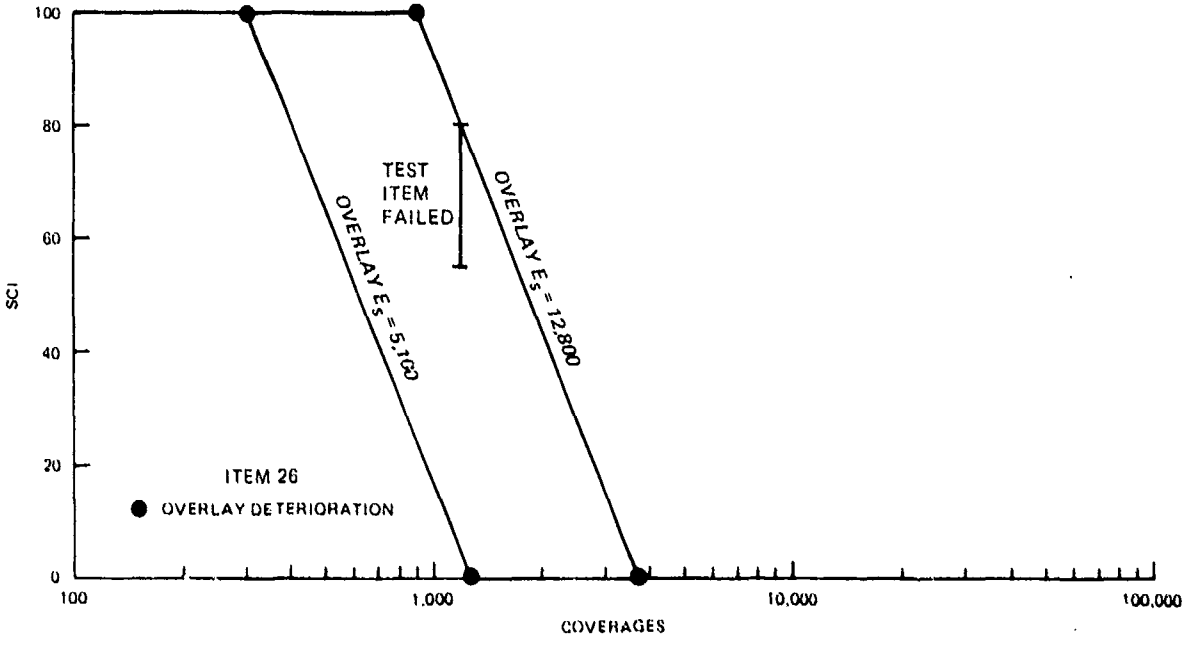

Figure 40. Performance of Item 26

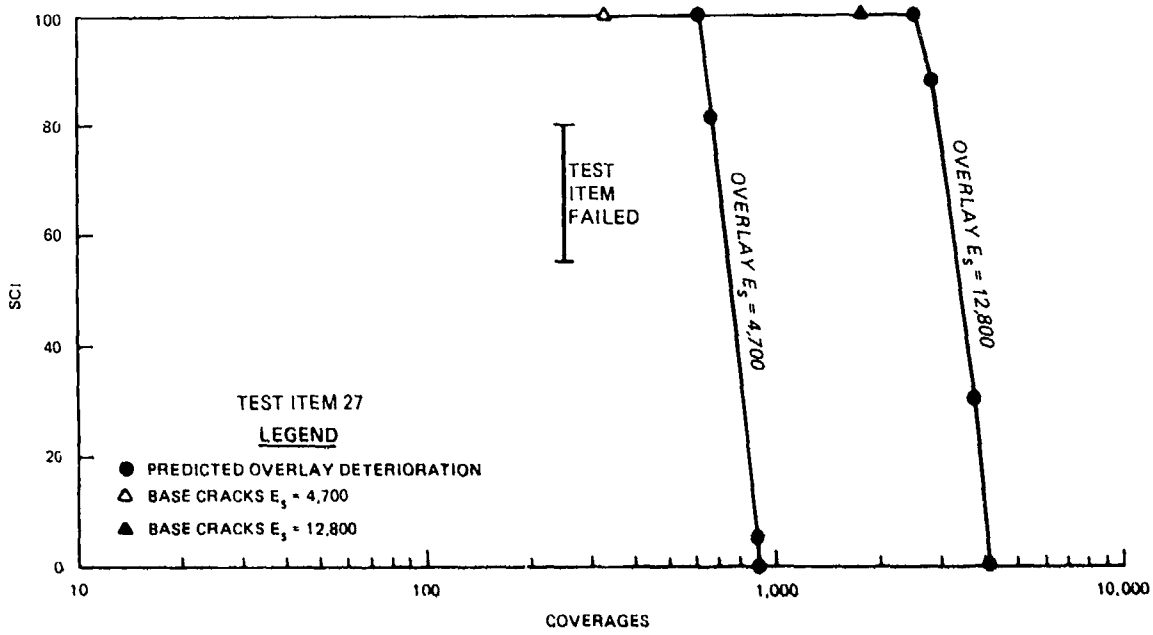

Figure 41. Performance of Item 27

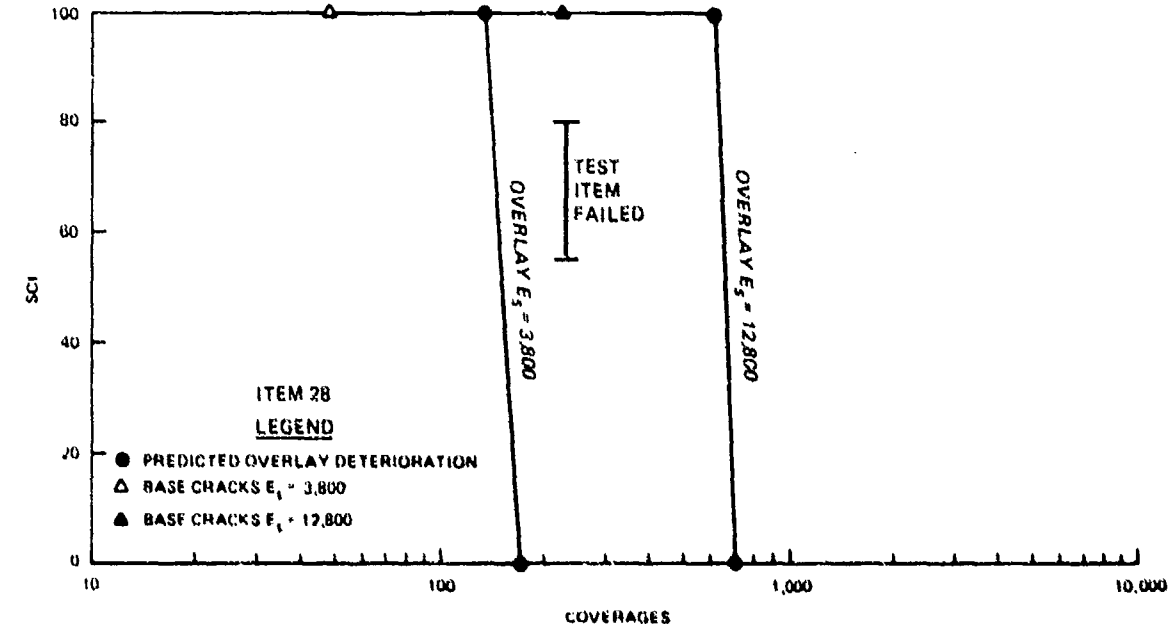

Figure 42. Performance of Item 28

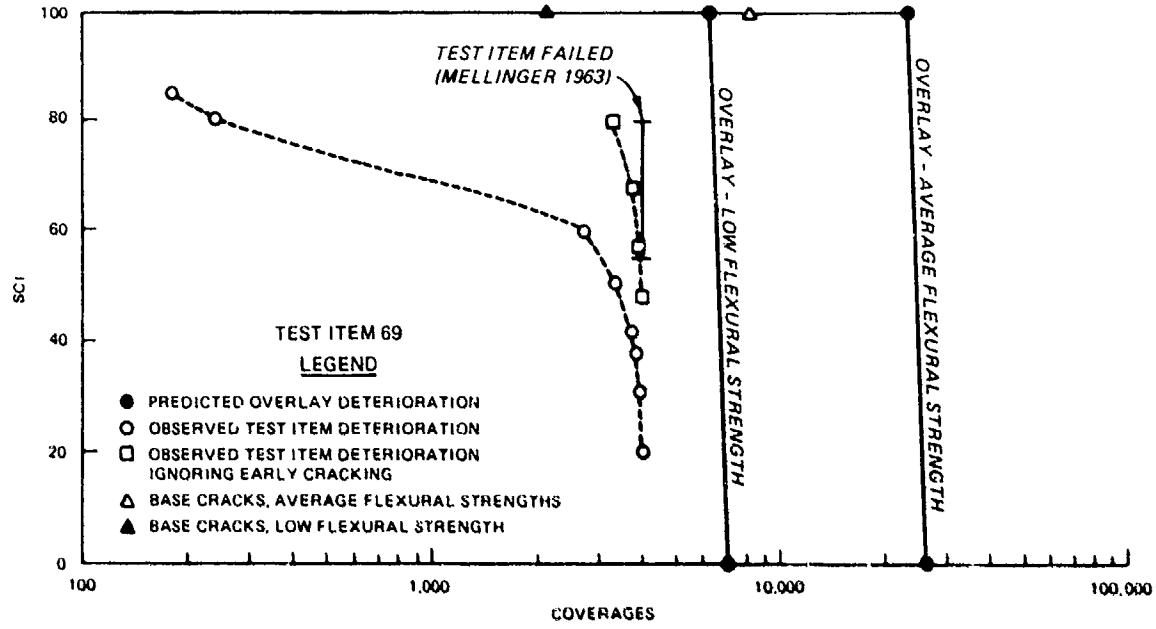

Figure 43. Performance of Item 69

which was apparently discounted by Mellinger[47] in selecting his failure level of 4,000 coverages. If this early cracking is ignored in the computation of the SCI, Mellinger's failure level and the SCI computed from the minutes of the board of consultants are in good agreement as seen in Figure 42. Table 23 shows the predicted coverage levels at which the SCI reached 70 for each test item. Except for items 27 and 69, the predicted performance is in reasonable agreement with the observed performance.

The traffic in Items 23, 24, and 26 would not be predicted to have caused deterioration in the base pavement, and no reduction was made in the base pavement modulus value in calculating the deterioration of the overlay. As shown in Figures 37, 38, and 40, the predicted deterioration in these items agreed well with the observed performance for the higher subgrade modulus values. Thus, the performance models developed are considered adequate for predicting the performance of an unbonded overlay using layered elastic theory.

The use of a reduced cracked base slab modulus at different levels of traffic for Items 25, 27, 28, and 69 was less successful. Predictions of performance for Items 25 and 28 gave reasonable agreement with the observed behavior, but the traffic predicted to cause deterioration in Items 27 and 69 was higher than observed in the test items. The inclusion of the reduced cracked slab modulus in the analysis greatly reduces the traffic required to cause deterioration in an overlay. This effect is shown in Table 24 where failure to include the reduced modulus for cracked base slab in the analysis results in greatly overpredicting the overlay traffic until deterioration starts. In the extreme example of Item 28 with the higher subgrade modulus,

Table 23

Comparison of Predicted and Observed Performance of Unbonded Overlay Test Items

Test Item	Predicted Failure Coverage Level	Observed Failure
23	14,700[a]-39,500[b]	at 22,000 unfailed[c]
24	19,000[a]-71,500[b]	at 22,000 unfailed[c]
25	8,200[a]-45,000[b]	18,500[c]
26	435[a]-1,380[b]	1,200[c]
27	700[a]-3,100[b]	250[c]
28	145[a]-640[b]	230[c]
69	6,500[d]-24,000[e]	2,400[f]-4,000[c]

[a]Coverage at which SCI is 70 in Figures 37 through 42 for lower subgrade E value.
[b]Coverage at which SCI is 70 in Figures 37 through 42 for higher subgrade E value.
[c]Coverage level at which SCI is 70 in Figure 43 for low concrete flexural strength values.
[d]Coverage level at which SCI is 70 in Figure 43 for average concrete flexural strength values.
[e]Failure level reported by Mellinger[47].
[f]Coverage at which SCI is 70 based on cracking and spalling as reported by Ohio River Division Laboratories[55].

Table 24

Effect of Including Base Slab Cracking on Predictions of Overlay Deterioration

Item	Subgrade Modulus	Predicted Onset of Deterioration, C_0		Reported Failure
		With Base Cracking	Without Base Cracking	
25	Lower	7,523	28,596	18,500
25	Higher	40,426	92,751	18,500
27	Lower	609	1,186	250
27	Higher	2,556	3,701	250
28	Lower	134	81,694	230
28	Higher	615	253,128	230
69	Average[a]	23,076	3,326,121	4,000
69	Lower[a]	6,297	812,257	4,000

[a]For Item 69, average and lower flexural strength were variables rather than subgrade elastic modulus.

the traffic, until deterioration starts, is three orders of magnitude above the reported failure of the test item. The effect of including the cracked slab in the analysis is shown graphically in Figure 44 for Item 25.

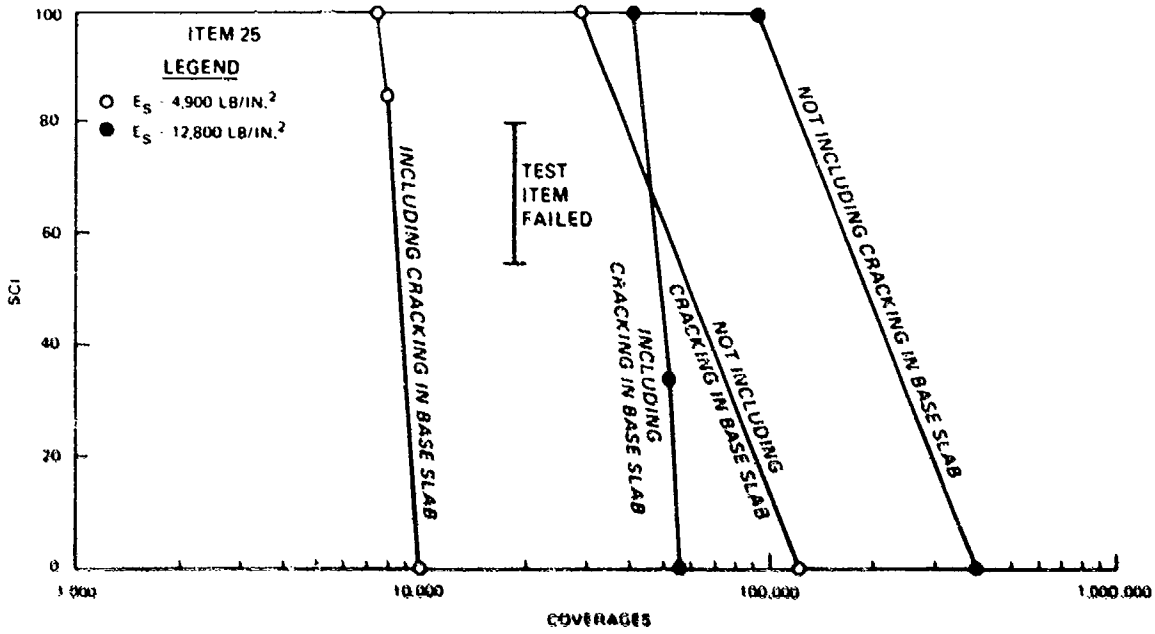

Figure 44. Effect of cracked modulus on predicted performance of Item 25

The importance and validity of including a reduced modulus to represent cracking of the base slab at different intervals of traffic are strongly supported by the results of the analysis of Items 25, 27, 28, and 69. However, the mixed success of the predictions raised the question of whether the cracked slab model is adequate. The three data points in Figure 26 that lie above the suggested AASHTO relation pull the original equation for the E-ratio upward. Figure 45 shows a revised E-ratio equation which, neglecting these three points, shows substantial agreement with the remaining data and the suggested AASHTO relation and which predicts a more rapid reduction in the cracked slab modulus as the SCI decreases.

This revised equation was used to predict the overlay deterioration of Item 25 and 69. It reduced the onset of deterioration for Item 25 with the higher modulus subgrade from 40,426 coverages to 38,872 coverages. For Item 69, it reduced the onset of deterioration using the low flexural strength values from 6,297 coverages to 5,857 coverages. These changes do not appreciably improve the agreement with the reported failures of 18,500 and 4,000 coverages. The use of a reduced modulus for cracking in the base slab greatly accelerates the predicted onset of cracking in the overlay, but it is not very sensitive to the precise form of the equation. Consequently, the original

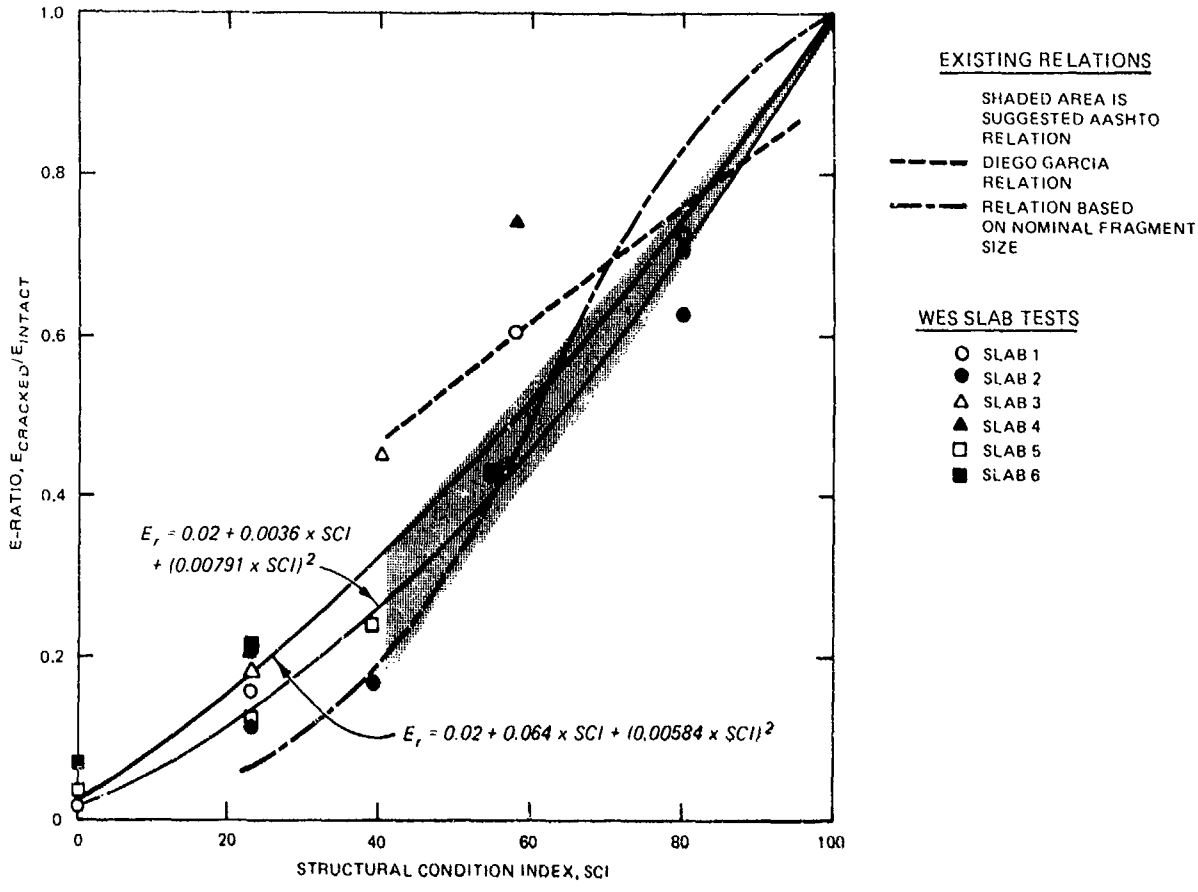

Figure 45. Revised E-ratio, SCI relationship

equation for predicting the E-ratio should remain using all of the data points.

Only 7 of the 19 unbonded overlays tested by the CE could be analyzed. Analysis of these seven overlay test items shows that predictions of performance are sensitive to the quality of the input information. Uncertainty over appropriate subgrade modulus of elasticity values and concrete flexural strengths and lack of detailed performance information on the test items hindered the analysis. Test Items 23, 24, and 26 gave good agreement between predicted and reported performance when the base slab was not predicted to crack. Thus, the layered elastic analytical model can be used with the rigid pavement performance models to predict performance of unbonded overlays that are supported by intact base slabs. The concept of using a reduced modulus for the base slab as it deteriorates under traffic was shown in the analysis of Items 25, 27, 28, and 69 to greatly reduce the predicted performance of the overlay. Without the use of this reduced modulus for the base slab, predictions of overlay deterioration are greatly in error. Using the reduced modulus for the base slab, an analysis of Items 25 and 28 gave good agreement between observed and predicted performance, but the analysis of Items 26 and 69 overpredicted the performance of the overlays. Overall performance of the seven test items support the general concept of using the layered elastic

model to analyze unbonded overlays. The models for predicting the performance of rigid pavements and for evaluating the cracked slab modulus gave reasonable results.

PARTIALLY BONDED OVERLAYS

Figure 3 shows the 12 data points that were the basis for the partially bonded overlay's 1.4 power used by the CE in their overlay design equation. Only four of these points are shown in Table 22. The remaining data points were reinforced concrete overlays. The presence of steel reinforcing in concrete pavements does not delay the onset of cracking in the pavement but changes the pattern of cracking and delays spalling and raveling. The CE used spalling of the load induced crack rather than cracking alone to define failure of reinforced pavements[63,61]. In Figure 3, the CE empirical relation between the required pavement thickness of reinforced concrete to fail by crack spalling and the pavement thickness of plain concrete required to fail by cracking were used to convert reinforced test sections to equivalent thicknesses of plain concrete. Since reinforced pavement performs differently from plain concrete, it cannot be analyzed with the models developed in this study.

Consequently, only the four partially bonded test items shown in Table 22 were analyzed. Of these four test items, traffic for Item G 12-14-100 in the Lockbourne No. 2 test series crossed free slab edges with no load transfer and is discussed in a separate section.

Crack maps of test Items D 2.7-66, E 2.7-66M, and F 2.7-80 were provided at 24, 98, 138, and 712 coverages of a 60,000-lb wheel load[51]. The SCI of each test item was calculated at these coverage levels, and the performance was predicted using the layered-elastic analytical model and cracking in the base pavement with various amounts of friction between the overlay and the base pavement. These results are shown in Figures 46, 47, and 48. The BISAR computer program expresses the bond between layers with a K factor. The fully bonded case is represented by a K of 0, the unbonded case by a K of 1,000, and intermediate bond cases between these extremes use values between 0 and 1,000. The assumptions for the various bond cases for the BISAR program were discussed earlier in this report.

For each test section, the amount of slip or friction between the overlay and the base pavement greatly affects the predicted amount of traffic the test section can withstand. For test Item D 2.7-66, the predicted onset of deterioration C_0 increases from 76 coverages for the unbonded case to 1,592 coverages for the fully bonded case. The effect of varying the friction rate K is not linear, and it becomes more pronounced as the fully bonded case is approached. Going from a K of 1,000 to a K of 750 only changed the predicted onset of deterioration from 76 to 95, whereas the change from a K of 250 to 0 changed the predicted onset of deterioration from 262 to 1,592 coverages.

Only Item D 2.7-66 provided more than one coverage level where the SCI was not 100. The two points that are less than 100 do not fit the performance model for concrete pavements and do not show the steep deterioration of the unbonded overlay in Item 69 and Figure 43. With very limited data available,

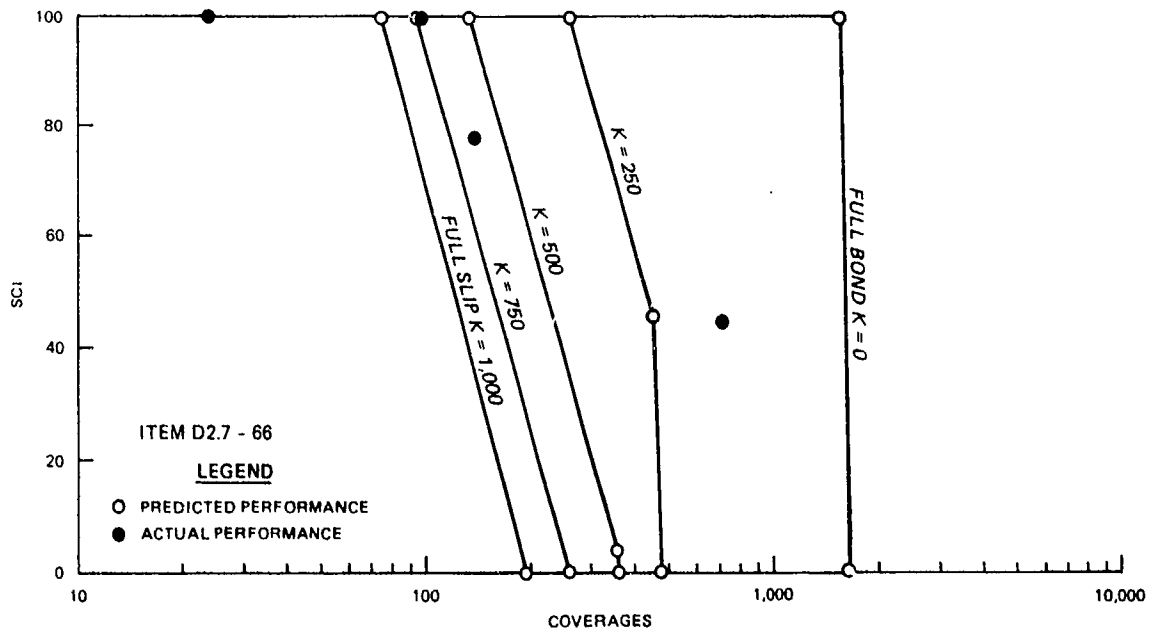

Figure 46. Performance of Item D 2.7-66

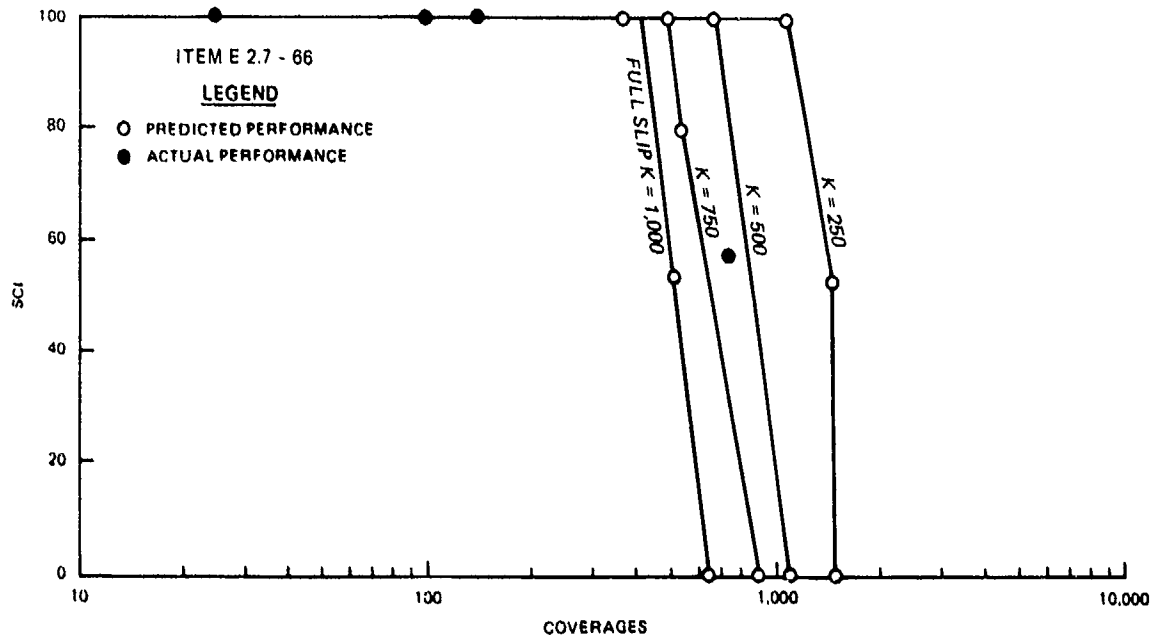

Figure 47. Performance of Item E 2.7-66M

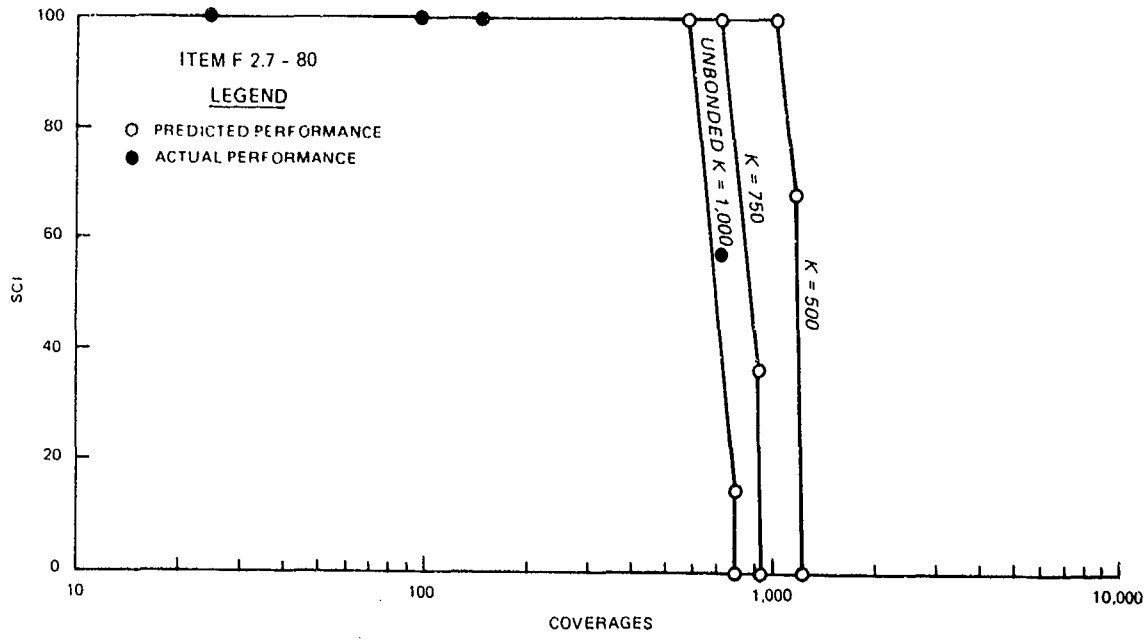

Figure 48. Performance of Item F 2.7-80

it is impossible to ascertain with certainty what form the overlay deterioration takes. However, the overlay deterioration models as calculated are reasonable, representing increased rates of deterioration as the base slab support decreases. In Item D 2.7-66, the sharp deterioration in the SCI value from 100 at 98 coverages to 78 at 138 coverages is consistent with the models. Similarly, the sharp deterioration of Item 69, once deterioration starts, supports the models. However, there is no explanation available for the initial cracking in Item 69 or for the slow deterioration between 138 and 712 coverages for Item D 2.7-66. Whether these discrepancies are caused by factors not adequately modeled in the analysis or whether there are unreported construction, material, or testing variations that contributed to this performance cannot be resolved from the limited available information. Overall these models appear to give reasonable results, but more data are needed to verify them.

Figures 46 through 48 show that the K value that gives the best agreement with the deterioration data varies from about 640 to 930. If all three test items are averaged, the K value is about 750, or if only Items E 2.7-66 and D 2.7-66 are averaged, the K value is about 660.

FULLY BONDED OVERLAYS

Item 70 of the Sharonville Heavy Load Tests was an 11-in. overlay bonded to a 17-in. base pavement. The base pavement concrete was acid etched with hydrochloric acid and thoroughly washed. Then a portland cement grout was used to bond the overlay concrete to the base concrete. This test item had

the same variations in flexural strength discussed earlier for the unbonded overlay test Item 69.

The base pavement had keyed longitudinal construction joints. The bonded overlay used doweled longitudinal construction joints over the base pavements keyed joints. Under traffic, cracking and spalling began almost immediately over the dowel bars. Despite periodic patching the test item was considered beyond salvage after 8,000 coverages.

Predictions of the fully bonded overlay performance using the layered elastic model exceeded actual traffic regardless of what combination of low or average flexural strength results was used for the overlay and the base pavement. The only deterioration reported in the test item was associated with the dowel bars, and no concrete fatigue related structural deterioration occurred.

A fully bonded overlay and base slab are essentially a monolithic structure. The layered elastic analysis can account for differences in modulus values and flexural strengths between the overlay and base pavement as well as for previous traffic fatigue damage on the base pavement. However, the value of this analysis ability for a fully bonded overlay is moot since an adequate load transfer construction joint cannot physically be built. For this reason, the CE and most other agencies require fully bonded airfield overlays to be between 2 and 5 in. thick, and their use is restricted to correction of surface smoothness or deterioration. The use of fully bonded overlays for structural upgrading of airfields requires development and testing of new construction joints. Dowels have proven unsuccessful in fully bonded overlays, and the weaker keyed joints probably will perform even more poorly. Consequently, some new method of providing load transfer across the construction joint in a fully bonded overlay must be developed.

OVERLAYS WITHOUT LOAD TRANSFER

The four test Items F 12.14-100, G 12.14-100, L 14.14-80, and M 14.14-80 in Table 22 were excluded from analysis earlier because of the substandard load transfer of the slab joints. Item F 12.14-100 was bounded by three free joints and one premolded joint-free expansion and had a contraction joint that divided the item into two slabs. Item G 12.14-100 was the same except one free joint was replaced with a keyed joint. Items L 14.14-80 and M 14.14-80 were separated from one another by a keyed joint and consisted of one slab each. The remaining joints for each slab were a free joint, a premolded joint-free expansion, and a plain butt joint. In all four test items, deterioration began as corner cracking associated with the joints that were not capable of providing load transfer to adjacent slabs. Analysis of these test items has to include the effect of these nonstandard joints.

Item G 12.14-100 was a partially bonded overlay, and the friction factor K in the BISAR program was set at 750 for the analysis. All of the other items were unbonded. These test items were constructed between 28 October and 25 November 1944. Although the same nominal concrete mixture was used for all construction, 28-day flexural strengths ranged from 570 to 915 $lb/in.^2$ Although the quality of concrete varied considerably, no differentiation was made between the base pavement and overlay concrete in each item

even though they were placed on different days. Consequently, the analysis of these test items is hindered by the lack of accurate data on the concrete. The modulus of elasticity and the flexural strength that are tabulated in Appendix D were from field cured samples for each item.

Table 25 compares the predicted performance of these four test items with the actual reported performance. All of these test items had relatively thick overlays, and the overlay began deterioration before the base pavement. The increase in stress for no load transfer from Figure 30 caused major reductions in the predicted start of deteriorations C_0 in the overlay. These reductions are typically one or two orders of magnitude, but even so, the predicted performances with no load transfer are still about an order of magnitude larger than the actual performance.

Table 25

Performance of Test Items with Substandard Load Transfer

Item	Predicted Performance: Normal Load Transfer C_0	Normal Load Transfer SCI	No Load Transfer C_0	No Load Transfer SCI	Actual Performance: Coverage	Actual Performance: SCI
F 12.14-100	7,042	100	383	100	10	71
					63	45
					1,000	11
					1,430	0
G 12.14-100	219,000	100	5,091	100	370	100
					887	71
					1,430	50
L 14.14-80	20,650	100	858	100	5	58
					1,000	0
M 14.14-80	6,908	100	377	100	36	58
					887	0

The increase in stress for substandard joints in Figure 30 greatly reduces the predicted performance of the overlays. However, the four test items all deteriorated much more rapidly than predicted. The quality of the available material data on the concrete is poor, and the value of any predictions based on it is uncertain. The available data are inadequate to allow

evaluation of the load transfer multiplier. The multiplier greatly reduces the predicted performance of the overlay, but better performance data are needed to determine if the data are adequate.

EVALUATION AND COMPARISON OF OVERLAY DESIGN PROCEDURES

DESIGN METHODS

The primary method in engineering practice today of determining the required rigid overlay thickness for airfields is the empirical CE equation. The required overlay thickness is a power relationship between the difference in the existing base pavement to be overlaid and the new equivalent pavement that would be required to support the design traffic if no base pavement existed. Differences in bond condition between the overlay and the base pavement are handled by adjusting the power used in the equation. Cracking in the base pavement before overlay and differences in flexural strength of the overlay and the base pavement are included in the analysis by adjusting the base pavement thickness.

The design method proposed in this study uses a layered-elastic analytical model to calculate stresses in the base pavement and the overlay. Deterioration of the base and the overlay in terms of the SCI is predicted using the relationships discussed earlier in this report. This deterioration is a function of the calculated stresses, the flexural strength of the concrete, and the number of stress repetitions or coverages of traffic. As the base pavement deteriorates, its support to the overlay is reduced, and this loss in support is represented by reducing the concrete modulus value of the base pavement.

The major differences in the two design approaches are summarized in Table 26. In order to evaluate these two design approaches comparative designs were prepared in the following section for a variety of design conditions.

EVALUATION

TEST CASES

The empirical power equation for overlay design uses the thickness of an equivalent new pavement to support the design traffic as input to calculate the overlay thickness required over a given thickness of base pavement. The equivalent thickness must be determined from some existing concrete pavement design procedure published by the CE, the US Navy, the FAA, or the Portland Cement Association. Any resulting overlay design will include all the assumptions and criteria of the basic design procedure used to calculate the equivalent thickness.

In order to evaluate the power equation and compare it with the proposed layered-elastic design procedure, the same criteria must be used to determine the equivalent thickness for the power equation and for the layered-elastic procedure. For this analysis, both procedures use the onset of deterioration, as determined by C_0 for the design performance criteria. The equivalent thickness input for the power equation is the thickness of pavement that develops stresses as calculated by the layered elastic theory for a given design load that will reach the onset of deterioration C_0 at the design coverage level. In this way the power equation can be compared with the proposed

Table 26

Comparison of Overlay Design Methods

Design Considerations	Corps of Engineers	Proposed Method
Analytical model	Empirical equation	Layered elastic
Failure	Cracking in 50 percent of slabs	Predict deterioration in terms of SCI
Interface conditions between overlay and base pavement	Adjust power in equation	Variable between full bond and unbonded
Material properties	Equivalent required h needed as input to empirical equation	E ν for all materials and flexural strength of concrete
Difference in strength/modulus of overlay and base pavement concrete	Adjust thickness of base pavement	Included directly in calculation of stresses and design factor
Cracking in base pavement before overlay	Reduce thickness of base pavement	Reduce E value of base concrete
Fatigue effects of traffic on uncracked base pavement	Not included	Included in terms of equivalent traffic
Cracking of base after overlay	Not applicable	Reduced E value of base as cracking progresses under traffic

layered-elastic design approach without introducing other limitations from established design procedures such as beam fatigue relationships versus field test relationships, Westergaard edge loading versus Westergaard interior loading, and reductions in thickness for high-strength subgrades.

A matrix of possible design variables is shown in Tables 27 and 28. The four aircraft shown include single, twin, and twin-tandem wheeled main gears. Their design characteristics are shown in Table 29. Soil modulus of elasticity values in Table 27 varies from 4,000 to 50,000 lb/in.^{2} representing poor to good subgrade support. Design coverage levels vary from 10,000 to 250,000. As discussed earlier, the criterion for this comparison between the CE overlay equation and the proposed design method is reaching the calculated value of C_0 at the specified design coverage level. The modulus of elasticity for concrete varies from 4 to 5 million lb/in.^{2}. The thickness of existing base pavement varies from 0.25 to 0.75 of the equivalent new pavement. In the calculations, no base pavement thickness was allowed to go below 4 in. since pavements less than 6 in. are seldom encountered, and a thickness below 4 in. would have little physical meaning.

This variation in design parameters covers the spectrum that could be expected. Twelve specific cases were selected using random numbers for analysis as shown in Tables 27 and 28. During the analysis two additional cases, 3A and 8A in the tables, were added to include a single-wheeled main gear aircraft at the 0.75 base thickness and another multiwheeled main gear aircraft at the intermediate 0.4 to 0.6 base thickness. Other than these restrictions all of the remainder of the design parameters were selected randomly for these two cases. Table 30 shows the distribution of these design parameters in the 14 specific cases analyzed.

The modulus of elasticity of concrete and the modulus of rupture or flexural strength are not independent. Therefore flexural strength was not used as a variable in Tables 27 and 28. However, there is no single, specific relation between concrete modulus of elasticity and flexural strength because concrete modulus varies depending on the aggregate and mix proportions used in the concrete. The modulus of elasticity for concrete is commonly estimated as

$$E_c = 57{,}000 \sqrt{f'_c} \tag{49}$$

where

E_c = modulus of elasticity of concrete, lb/in.^{2}

f'_c = compressive strength of concrete, lb/in.^{2}

Table 27

Design Parameters for the Overlay

Design Coverages × 10^3	E-Soil × 10^3 lb/in.^{2}	Aircraft											
		F-4C			B-727			C-141B			B-747		
		E-concrete × 10^6 lb/in.^{2}			E-concrete × 10^6 lb/in.^{2}			E-concrete × 10^6 lb/in.^{2}			E-concrete × 10^6 lb/in.^{2}		
		4.0	4.5	5.0	4.0	4.5	5.0	4.0	4.5	5.0	4.0	4.5	5.0
10	4	--	--	--	--	--	--	--	--	--	--	--	--
	10	--	--	--	--	4	--	9	--	--	--	--	--
	20	--	--	--	--	--	--	--	--	--	--	--	--
	35	--	--	1	--	--	--	--	--	--	--	--	--
	50	--	--	--	--	--	--	--	--	--	--	--	--
25	4	--	--	--	--	--	--	--	--	--	--	--	--
	10	--	2	--	--	--	--	--	--	--	--	--	--
	20	--	--	--	--	--	--	--	--	--	--	--	--
	35	--	--	--	--	--	--	--	--	--	--	--	--
	50	--	--	--	5	--	--	--	--	--	--	--	--
50	4	--	--	--	--	--	--	--	10	--	--	--	--
	10	--	--	--	--	--	--	--	--	--	--	--	--
	20	--	--	--	--	--	6	--	--	--	--	--	--
	35	--	--	--	--	--	--	--	11	--	--	--	--
	50	--	--	--	--	7	--	--	--	--	--	--	--

(Continued)

Table 27 (Concluded)

Design Coverages × 10^3	E-Soil × 10^3 lb/in.^{2}	Aircraft											
		F-4C			B-727			C-141B			B-747		
		E-concrete × 10^6 lb/in.^{2}			E-concrete × 10^6 lb/in.^{2}			E-concrete × 10^6 lb/in.^{2}			E-concrete × 10^6 lb/in.^{2}		
		4.0	4.5	5.0	4.0	4.5	5.0	4.0	4.5	5.0	4.0	4.5	5.0
75	4	--	--	--	--	--	--	--	--	12	--	--	--
	10	--	--	--	--	8A	--	--	--	--	--	--	--
	20	--	--	--	--	--	--	--	--	--	--	--	--
	35	--	3A	--	--	--	--	--	--	--	--	--	--
	50	--	--	--	--	--	--	--	--	--	--	--	--
100	4	--	--	--	--	--	--	--	--	--	--	--	--
	10	--	--	--	--	--	--	--	--	--	--	--	--
	20	--	--	--	--	--	--	--	--	--	--	--	--
	35	--	--	--	--	--	--	--	--	--	13	--	--
	50	--	--	--	--	--	--	--	--	--	--	--	--
250	4	--	--	--	--	--	--	--	--	--	--	--	--
	10	--	--	--	--	--	--	--	--	--	--	--	--
	20	--	--	--	--	--	--	--	--	--	14	--	--
	35	--	--	--	--	--	--	--	--	--	--	--	--
	50	--	--	--	--	--	--	--	--	--	--	--	--

Table 28

Design Parameters for the Base Pavement

Case No.	Base Pavement $E = 4 \times 10^6$ lb/in.^{2}					Base Pavement $E = 4.5 \times 10^6$ lb/in.^{2}					Base Pavement $E = 5.0 \times 10^6$ lb/in.^{2}				
	Thickness of Base Pavement $h_{base}/h_{equivalent}$														
	0.25[a]	0.40	0.50	0.60	0.75	0.25[a]	0.40	0.50	0.60	0.75	0.25[a]	0.40	0.50	0.60	0.75
1	--	--	--	--	--	--	--	--	--	--	--	X	--	--	--
2	X	--	--	--	--	--	--	--	--	--	--	--	--	--	--
3A	--	--	--	--	--	--	--	--	--	--	--	--	--	--	X
4	--	--	--	--	--	X	--	--	--	--	--	--	--	--	--
5	--	--	--	--	--	--	--	--	--	X	--	--	--	--	--
6	--	--	--	--	--	--	--	--	--	--	--	--	--	--	X
7	--	--	--	X	--	--	--	--	--	--	--	--	--	--	--
8A	--	--	--	--	--	--	--	--	X	--	--	--	--	--	--
9	--	--	--	--	--	--	--	--	--	X	--	--	--	--	--
10	--	--	--	--	--	--	--	--	--	--	--	X	--	--	--
11	--	--	--	--	--	X	--	--	--	--	--	--	--	--	--
12	--	--	--	--	--	--	--	--	--	--	--	--	X	--	--
13	--	--	--	--	--	--	--	--	--	--	X	--	--	--	--
14	--	--	--	X	--	--	--	--	--	--	--	--	--	--	--

[a]No base pavement allowed to go below 4 in. regardless of this ratio.

Table 29

Aircraft Characteristics

	Aircraft			
	F-4C	B-727	C-141 B	B-747
Main gear type	single	twin	twin-tandem	twin-tandem
Spacing (in., width × length)	--	38.2	32.5 × 48	44 × 58
Wheel load, lb	25,000	44,000	40,800	47,000
Tire contact area, $in.^2$	100	238	208	219
Contact pressure, $lb/in.^2$	250	185	196	215
Equivalent radius, in.	5.64	8.70	8.14	8.35

Also, flexural strength is commonly estimated from the compressive strength as

$$R = K_1 \sqrt{f'_c} \tag{50}$$

where

R = flexural strength or modulus of rupture of concrete in $lb/in.^2$

K_1 = a constant varying from 8 to 10

A variety of different modulus of elasticity and corresponding flexural strength values can be calculated from these relations. For this analysis intermediate values in the possible range of calculated values were used. Concrete with a modulus of 4 million $lb/in.^2$ was estimated to have a flexural strength of 600 $lb/in.^2$, and concrete modulus of elasticity values of 4.5 and 5 million $lb/in.^2$ were estimated to have flexural strength values of 700 and 800 $lb/in.^2$, respectively. Poisson's ratio for all concrete was assumed to be 0.15.

The Poisson's ratio for soil was assumed to vary depending on its modulus of elasticity. Soil modulus of elasticity values of 4,000 and 10,000 $lb/in.^2$ was considered representative of cohesive soils, and a Poisson's ratio of 0.4 was used for these soils. Modulus of elasticity values of 35,000 and 50,000 $lb/in.^2$ was representative of good quality cohesionless materials, and a Poisson's ratio of 0.3 was used with them. The soil with a modulus of elasticity of 20,000 $lb/in.^2$ was considered to be an intermediate

Table 30

Distribution of Design Parameters

Design Parameters	Value	Number in Sample	Percent of Total Cases
Aircraft	F-4C	3	21
	B-727	5	36
	C-141	4	29
	B-747	2	14
Design coverage levels	10,000	3	21
	25,000	2	14
	50,000	4	29
	75,000	3	21
	100,000	1	7
	250,000	1	7
Soil modulus, $lb/in.^2$	4,000	2	14
	10,000	4	29
	20,000	2	14
	35,000	4	29
	50,000	2	14
Concrete modulus for overlay, $lb/in.^2$	4.0×10^6	4	29
	4.5×10^6	7	50
	5.0×10^6	3	21
Concrete modulus for base pavement, $lb/in.^2$	4.0×10^6	3	21
	4.5×10^6	5	36
	5.0×10^6	6	43
Thickness of base pavement $h_{base}/h_{equivalent}$	0.25	4	29
	0.40	2	14
	0.50	1	7
	0.60	3	21
	0.75	4	29

soil such as a sandy clay, silty sand, or silty gravel. A Poisson's ratio of 0.35 was used for this soil.

For any case in Tables 27 and 28, the design factor required so that the onset of deterioration C_0 will be reached at the design coverage level can be determined from the following equation developed by substituting the case's required design coverage level for C_0 :

$$DF = \frac{\text{flexural strength}}{\text{calculated stress}} = 0.5234 + 0.3920 \log C_0 \qquad (51)$$

The equivalent slab is defined to have the same concrete properties as the overlay concrete for the specific case to be overlaid. For that case's flexural strength, an allowable stress level can be determined from the required design factor.

An iterative series of layered elastic calculations determined what thickness of equivalent pavement is needed to match this allowable stress level for a specific case's loading, overlay concrete properties, and subgrade properties. In all calculations an artificial stiff layer with a modulus of 1 million and a Poisson's ratio of 0.5 was placed at a depth of 20 ft as recommended by Parker et al.[59].

Once the equivalent slab thickness is determined, the thickness of the base pavement is set since each case's base thickness in Table 28 is defined as a proportion of the equivalent slab thickness. As mentioned, no base slab was allowed to be less than 4 in. regardless of the proportion shown in Table 28. Once the equivalent slab and base slab thicknesses are determined, the CE overlay thickness can be determined from the power equation.

The required overlay thickness by the proposed design method using the layered-elastic analytical model follows the same analysis technique as was outlined previously. A series of trial overlay thicknesses is analyzed for a case's specific loading, base thickness, and material properties until an overlay thickness is found that reaches C_0 at the specific case's design coverage level. If the base pavement does not reach its C_0 deterioration value within the case's design coverage level, the overlay thickness is determined simply from the C_0 value calculated from overlay stresses with full support from the base slab. If, however, the base slab reaches its C_0 before the design coverage level, the traffic is divided into intervals, and deterioration of the overlay in each interval is calculated with the reduced base support. Trial overlay thicknesses are analyzed until the C_0 in the overlay including the reduced support of the base pavement is reached at the design coverage level.

UNBONDED OVERLAY

Table 31 shows the results of these calculations for unbonded overlays for the 14 cases in Tables 27 and 28. Invariably, the required overlay thicknesses by the proposed design method are smaller than those calculated by the CE power equation. Figure 49 shows the thicknesses calculated using the proposed design approach with the CE unbonded design equation. The CE equation serves as an effective upper bound for the proposed design method solutions. As shown in Figure 5, there are distinct separate regions where stress in the overlay and base control. These regions are apparent in Figure 49 and also in Figure 50 where the ratio of base modulus of elasticity to overlay modulus of elasticity is included in the figure. This ratio reflects a difference in flexural strength as well as modulus values. In the region where cracking in the base occurs under the design traffic, the modulus ratio in Figure 50 shows a trend that increases modulus ratio. Increasing base modulus and flexural strength relative to the overlay's values result in a decrease in overlay thickness. This trend is not true of the cases where the base did not crack.

In Figure 5 it was shown that the equal rigidity definition of an equivalent slab resulted in an upper bound solution when compared with those definitions of an equivalent slab using stress in the overlay or base as the criteria for defining the equivalent slab. Similarly, the CE equation in Figures 49 and 50 serves as an upper bound for the solutions from the proposed design method.

PARTIALLY BONDED OVERLAYS

The analysis was repeated for seven of the cases in Table 31 for partially bonded overlays. Variation of the partially bonded interface K condition between 660 and 750 for four cases resulted in negligible changes in required overlay thickness. Changes varied from 0 to 0.2 in. Consequently, a K of 750 appeared to be appropriate for representing the partially bonded overlay conditions. Results of the overlay design for partially bonded conditions are shown in Table 32. Unlike the unbonded condition, the CE partially bonded equation is not an upper bound for the proposed design approach solutions.

Table 33 shows a comparison of the CE and the proposed design overlay requirements for both the bonded and partially bonded cases. Including the increased friction of partially bonded overlays in the analysis results in a decrease in required overlay thickness using the proposed design approach. However, this decrease is relatively small, 1 to 7 percent for these cases. The CE partially bonded equation reduces the required overlay thickness from 8 to 32 percent.

Figure 51 shows the unbonded and partially bonded overlay thicknesses calculated using the proposed layered elastic based approach, the CE test section data from Figure 3, and the CE design equations. The CE partially bonded equation with the 1.4 power serves as a visual best fit relation for all data regardless of bond condition, and the unbonded equation with the 2.0 power serves as an upper bound. The effect of increased friction between the overlay and the base is beneficial; however, this effect appears to be relatively

Table 31

Unbonded Overlay Results

Case	Aircraft	Equivalent Slab h_{eq} lb/in.^{2}	Overlay h_o in.	Overlay E_o lb/in.^{2}	Base Slab h_b in.	Base Slab E_b lb/in.^{2}	Subgrade E_s lb/in.^{2}	CE h_o in.
1	F-4	8.5	7.3	5.0×10^6	4.0	5.0×10^6	35,000	7.5
2	F-4	10.6	9.5	4.5×10^6	4.0	4.0×10^6	10,000	9.8
3	F-4	10.0	4.9	4.5×10^6	7.5	5.0×10^6	35,000	6.6
4	B-727	16.0	14.2	4.5×10^6	4.0	4.5×10^6	10,000	15.5
5	B-727	14.2	6.4	4.0×10^6	10.7	4.5×10^6	50,000	9.3
6	B-727	14.4	7.9	5.0×10^6	10.8	5.0×10^6	20,000	9.5
7	B-727	13.7	9.8	4.5×10^6	8.2	4.0×10^6	50,000	11.0
8	B-727	17.5	10.9	4.5×10^6	10.5	4.5×10^6	10,000	14.0
9	C-141	19.0	6.5	4.0×10^6	14.2	4.5×10^6	10,000	12.6
10	C-141	21.5	14.0	4.5×10^6	8.6	5.0×10^6	4,000	19.7
11	C-141	14.2	12.6	4.5×10^6	4.0	4.5×10^6	35,000	13.6
12	C-141	22.3	12.1	5.0×10^6	11.2	5.0×10^6	4,000	19.3
13	B-747	16.2	14.5	4.0×10^6	4.0	5.0×10^6	35,000	15.7
14	B-747	19.6	11.5	4.0×10^6	11.8	4.0×10^6	20,000	15.6

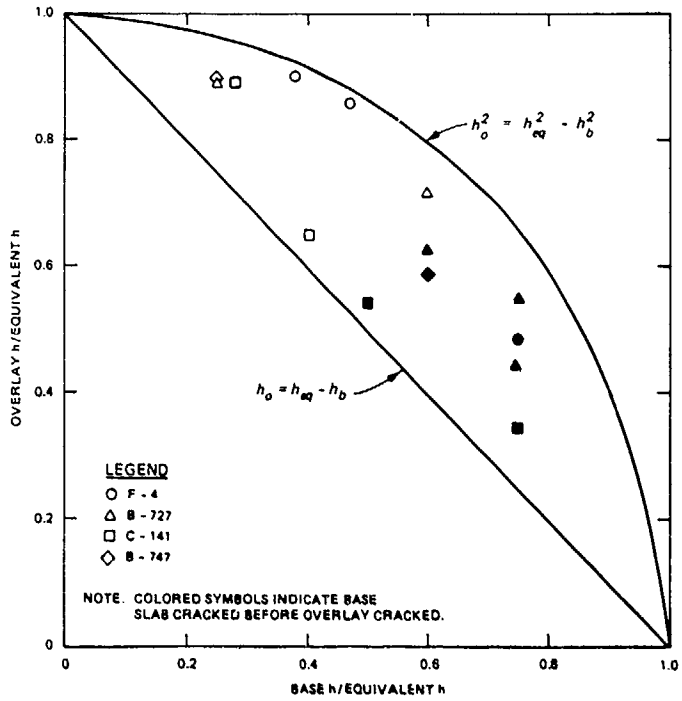

Figure 49. Comparison of proposed procedure and CE overlay design equation for unbonded overlays

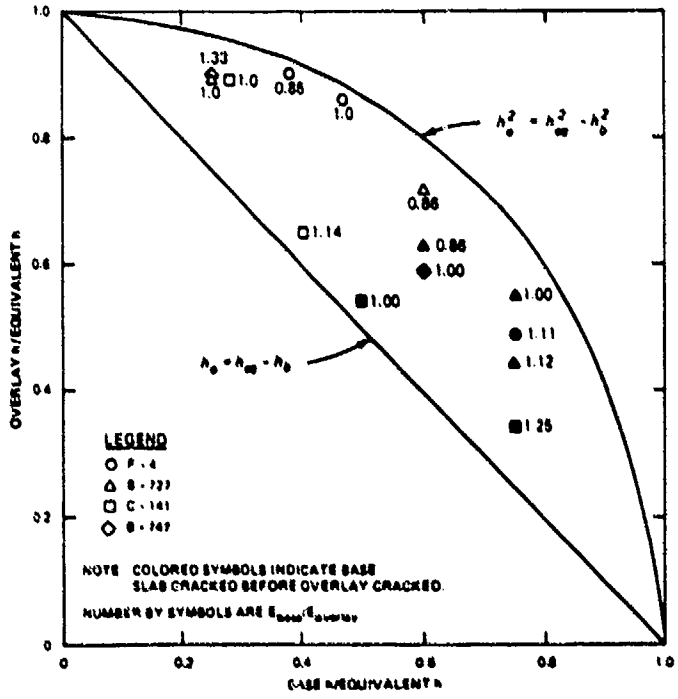

Figure 50. Effect of concrete modulus ratio on unbonded overlays

Table 32

Partially Bonded Overlay Results

Case	Aircraft	Equivalent Slab h_{eq} lb/in.^{2}	Overlay h_o in.	Overlay E_o lb/in.^{2}	Base Slab h_b in.	Base Slab E_b lb/in.^{2}	Subgrade E_s lb/in.^{2}	CE h_o in.
1	F-4	8.5	7.2	5.0×10^6	4.0	5.0×10^6	35,000	6.3
2	F-4	10.6	9.3	4.5×10^6	4.0	4.0×10^6	10,000	8.6
3	B-727	16.0	13.9	4.5×10^6	4.0	4.5×10^6	10,000	14.3
4	B-727	14.2	6.0	4.0×10^6	10.7	4.5×10^6	50,000	6.4
5	B-727	14.4	7.8	5.0×10^6	10.8	5.0×10^6	20,000	6.5
6	B-727	13.7	9.1	4.5×10^6	8.2	4.0×10^6	50,000	8.5
12	C-141	22.3	11.7	5.0×10^6	11.2	5.0×10^6	4,000	15.8

Table 33

Comparison Between Unbonded and Partially Bonded Overlay Designs

Case	Aircraft	h_b/h_{eq}	Unbonded		Partially Bonded		Percent Difference Between Unbonded and Partially Bonded	
			CE h_o, in.	LE h_o, in.	CE h_o	LE h_o, in.	LE	CE
1	F-4	0.47	7.5	7.3	6.3	7.2	1.3	16.01
2	F-4	0.38	9.8	9.5	8.6	9.3	2.1	12.2
4	B-727	0.25	15.5	14.2	14.3	13.9	2.1	7.7
5	B-727	0.75	9.3	6.4	6.4	6.0	6.2	31.2
6	B-727	0.75	9.5	7.9	6.5	7.8	1.3	31.6
7	B-727	0.60	11.0	9.8	8.5	9.1	7.1	22.7
12	C-141	0.50	19.3	12.1	15.8	11.7	3.3	18.1

Note: CE = Corps of Engineers design.
LE = Proposed design method using layered-elastic analytical model.
Percent Difference = $(h_{unbonded} - h_{partial\ bond})/h_{unbonded}$.

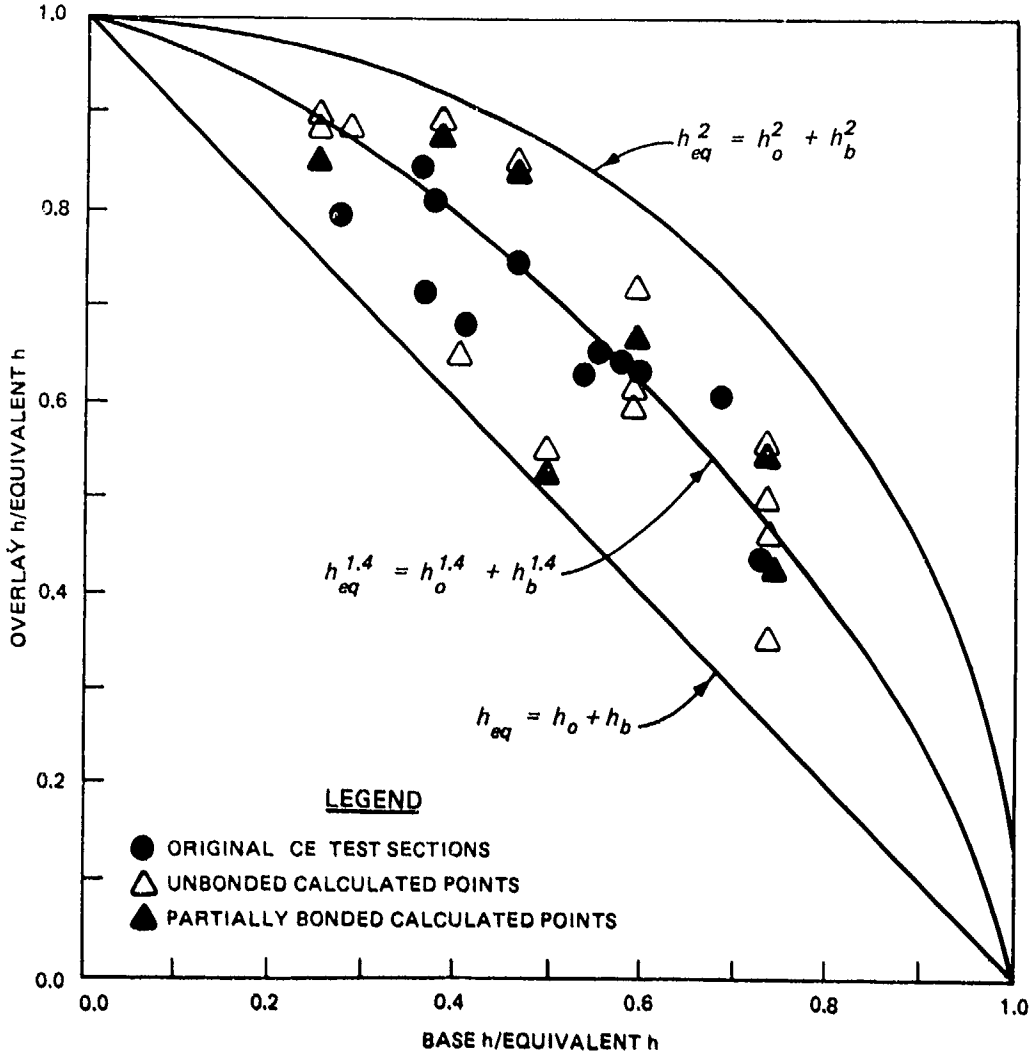

Figure 51. Comparison of unbonded and partially bonded overlay designs

small compared with other effects such as relative modulus values, strength, and loading conditions. The layered elastic model is much more powerful than the power equation for evaluating these effects; however, the CE unbonded overlay equation is an effective, simple, design method, but it is conservative. The use of the partially bonded overlay equation is not conservative; it does not adequately reflect the interaction of the various design parameters, and consequently, its continued use appears questionable.

COMPARISONS

The CE and the FAA airfield design methods have a common basis, but they differ in a variety of details such as definitions of traffic areas, thickness reduction for high-strength subgrades, and use of design factors versus percent standard thickness fatigue relationships. The WES computer programs RAD611 and R611FAA were used to develop designs for the 14 cases in Tables 27

and 28. These programs were developed specifically to be usable on IBM compatible microcomputers, and these programs are presently undergoing evaluation in CE Division and District offices as well as FAA Regional offices. The program RAD611 is an interactive program designed to follow the new Army and Air Force airfield rigid pavement design manual scheduled for printing and distribution in the fall of 1987. Similarly, R611FAA follows the existing FAA design guidance except that the adjustment for differing flexural strength in the base and the overlay is included in the computer program, although it is not in the published Advisory Circular[79].

The proposed design approach using the layered elastic model attempts to predict performance of a pavement in terms of the SCI. Some design performance levels must be selected to use with this approach to compare its required pavement thickness with the thicknesses determined for the CE and FAA approaches. The performance level used for this comparison will be the onset of deterioration C_0.

Table 34 shows the results for equivalent slab, unbonded, and partially bonded overlays determined by the proposed layered elastic based approach, the CE RAD611 program, and the FAA R611FAA program for the 14 cases in Tables 27 and 28. The subgrade modulus of elasticity values in these cases have to be converted to modulus of subgrade reaction values for use with Westergaard model based solutions. This conversion was made with the relation proposed by Parker et al.[59]. The subgrade modulus elasticity values of 4,000, 10,000, 20,000, 35,000, and 50,000 lb/in.^{2} was estimated to be equivalent to modulus of subgrade reaction values of 50, 103, 177, 274, and 361 lb/in.^{2}/in.

The proposed design method allows somewhat thinner equivalent slab thicknesses and appreciably thinner unbonded overlays. The proposed design method's added interface friction for partially bonded overlays does not reduce the overlay required thickness appreciably from the thickness required for unbonded overlays. However, both the CE and FAA design approaches greatly reduce the required overlay thickness for partially bonded overlays. In most cases, the partially bonded overlay thickness for these two approaches are approximately equal to the proposed design method's unbonded overlay thickness. Again, the partially bonded overlay equation is a best fit to data, whereas the unbonded overlay equation is a conservative upper bound. Since the partially bonded overlay equation is not always conservative and it cannot model the interactions of different parameters such as overlay and base modulus of elasticity values and load configuration, its continued use is not justified.

Figure 52 shows the results of the equivalent slab and unbonded overlay thicknesses for three design approaches. The FAA approach requires thinner pavements than the CE approach. The proposed design approach usually results in thinner equivalent slabs and always in thinner overlays. The criterion proposed by Parker et al.[59] for use with the layered elastic model is shown with the proposed design method's relations for C_0 and C_F in Figure 12. For any given coverage level the Parker et al.[57] criterion requires a lower design factor than does the relation for C_0. Consequently, their criterion

Table 34

Comparison of Overlay Design Procedure Results

Case	Aircraft	Design Procedure Thickness, in.								
		Proposed Approach			CE			FAA		
		h_{eq}	h_u	h_p	h_{eq}	h_u	h_p	h_{eq}	h_u	h_p
1	F-4	8.5	7.3	7.2	9.2	8.2	7.0	--	--	--
2	F-4	10.6	9.5	9.3	11.2	10.6	9.5	--	--	--
3A	F-4	10.0	4.9	--	10.8	6.0	7.0	--	--	--
4	B-727	16.0	14.2	13.9	17.4	16.9	15.8	16.5	16.0	14.8
5	B-727	14.2	6.4	6.0	15.2	9.4	6.2	15.3	11.3	8.9
6	B-727	14.4	7.9	7.8	15.4	11.0	7.9	15.1	10.5	7.5
7	B-727	13.7	9.8	9.1	14.3	12.3	10.0	14.9	13.0	10.7
8A	B-727	17.5	10.9	--	17.8	14.4	11.2	17.3	13.8	10.6
9	C-141	19.0	6.5	--	19.2	10.6	6.6	--	--	--
10	C-141	21.5	14.0	--	21.0	18.8	15.8	--	--	--
11	C-141	14.2	12.6	--	15.3	14.8	13.6	--	--	--
12	C-141	22.3	12.1	11.7	19.2	15.6	12.2	--	--	--
13	B-747	16.2	14.5	--	17.1	16.3	14.8	16.2	15.4	13.8
14	B-747	19.6	11.5	--	20.1	16.3	12.7	18.9	14.8	11.2

Note: h_{eq} = equivalent thickness.
h_u = unbonded overlay thickness.
h_p = partially bonded overlay thickness.

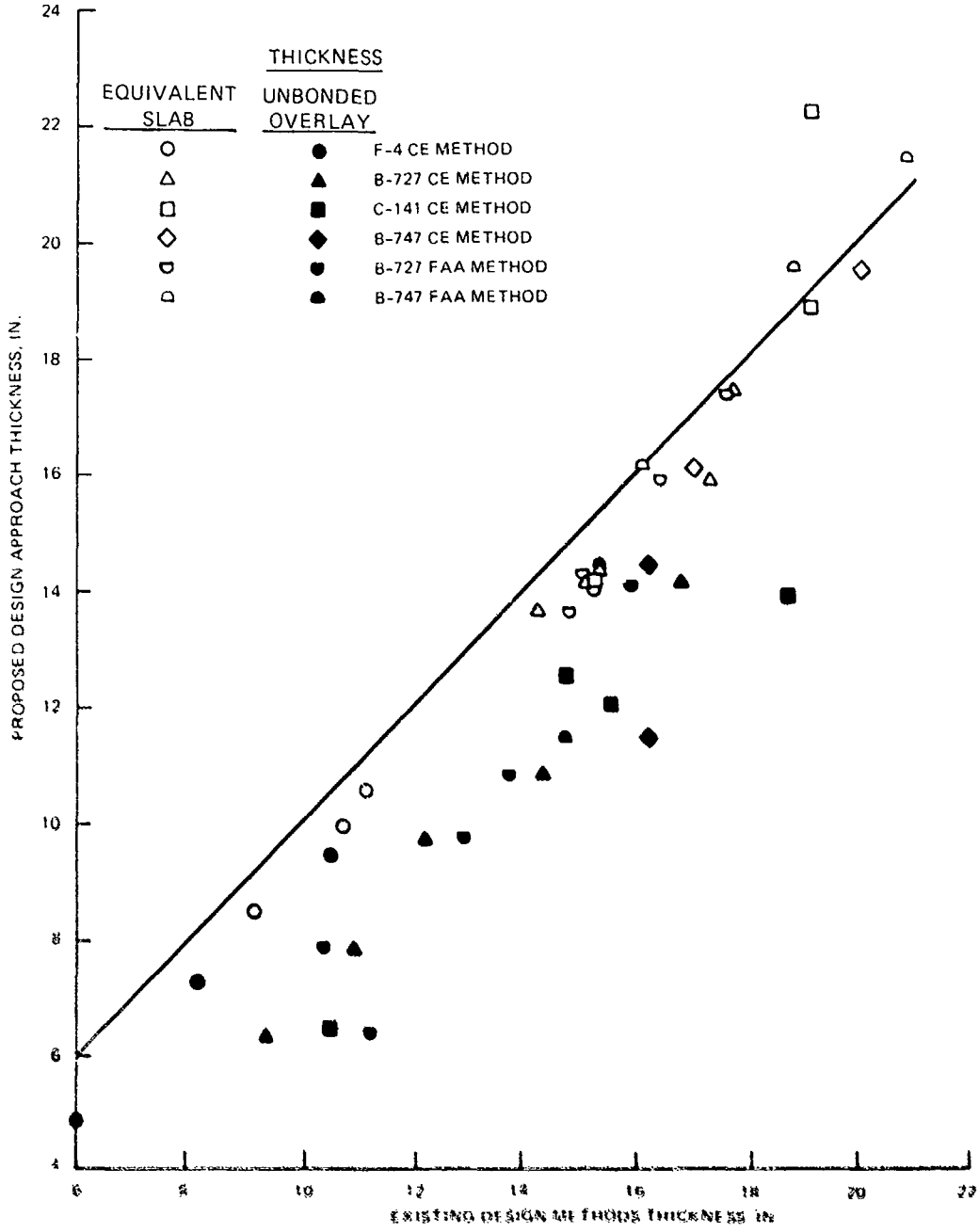

Figure 52. Comparison of proposed CE and FAA designs

for use with the layered elastic model results in a thinner pavement than does the proposed design method with C_0 as the design performance level.

The proposed design method results in pavement thicknesses that are similar to those required by existing CE and FAA design methods. Required overlay thicknesses by the proposed design method are appreciably thinner because of the improved modeling of the base pavement and the overlay. The empirical unbonded overlay equation is a conservative upper bound to the proposed design method.

EFFECT OF PREVIOUS TRAFFIC

The previous sections have treated the base pavement as being intact and undamaged by traffic before the overlay. As discussed earlier, traffic applied to the base pavement before the overlay consumes a portion of its fatigue capacity, and this effect has to be included in the analysis.

For the specific parameters of case 5 in Table 31, a 6.4-in.-thick overlay is adequate to support 25,000 coverages of a B-727 before deterioration as predicted using the relation for C_0. This prediction assumes that there has been no previous traffic. As discussed, a fatigue damage factor f could be defined as

$$f = \frac{C}{C_0} \tag{52}$$

where

f = a fatigue damage factor between 0.0 and 1.0

C = the equivalent traffic applied to the base

C_0 = the coverage level to cause the onset of deterioration in the base

In the previous analyses the base pavement has been assumed to be untrafficked, and the fatigue factor was zero. Figure 53 shows the effect of, including fatigue in the prediction, the performance of the overlay for case 5. As fatigue from traffic before the overlay is increased, the predicted coverage levels before deterioration decrease. At a fatigue factor value of 1.0, the base slab was about to start deteriorating before the overlays. Its deterioration with decreased support under the overlay traffic reduces the number of coverages to reach C_0 in the overlay by almost one-half.

If the pavement has been cracked and is deteriorating at the time of the overlay, its reduced support to the overlay has to be included in the analysis. The existing CE overlay design equations use the condition factor in Table 2 to account for the deterioration. In Figure 53 deterioration has been calculated for the overlay in case 5 for CE condition factors of 0.75, 0.50, and 0.25. The equivalent SCI values for these factors were estimated from the relationship in Figure 15 and were used to determine the initial cracked slab effective modulus for the analysis. The effect of existing structural deterioration in the base slab is very pronounced. Obviously, the inclusion of any fatigue or structural damage to the base pavement before the overlay has to be an integral part of any overlay design.

As shown previously in Table 34 and Figure 52, the existing CE and FAA design procedures result in thicker overlays. Figure 54 compares the predicted performance of the 6.4-in.-thick overlay required by the layered elastic approach and the 9.4-in.-thick overlay required by the CE design for

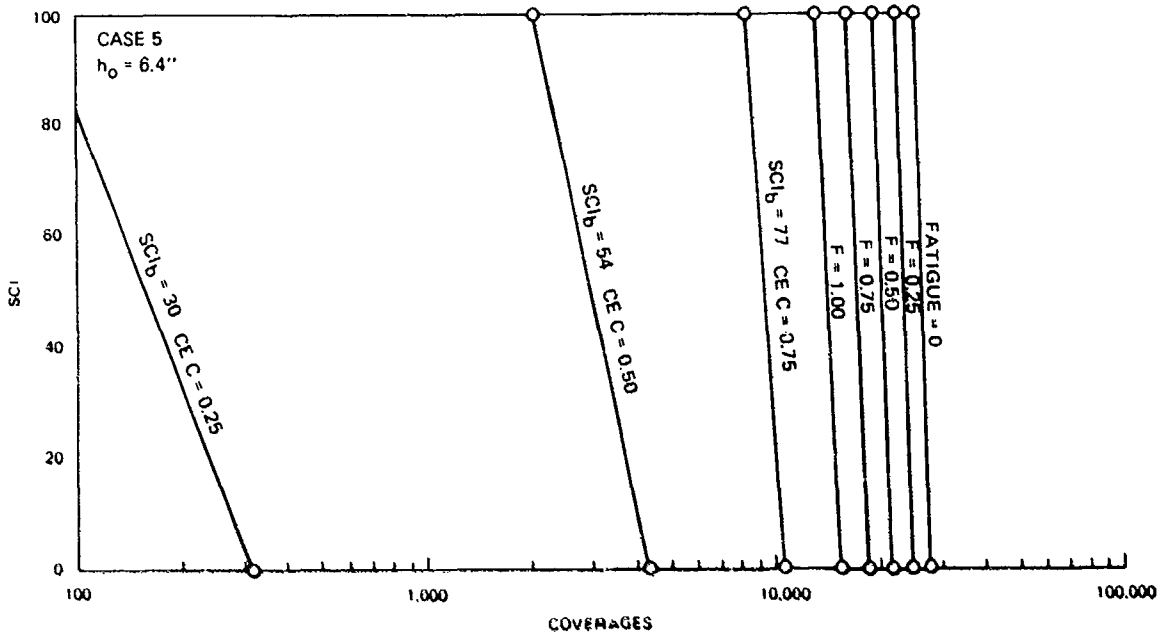

Figure 53. The effect of fatigue and initial base slab cracking on the predicted performance of the case 5 overlay

case 5. The CE design without any consideration for fatigue or structural condition of the base slab results in a predicted capacity about 20 times greater than the required 25,000 coverages. Including the effect of fatigue reduces this prediction to as little as a fourfold increase over the design coverage level. When the structural condition of the base slab before the overlay is included in the CE design using the condition factor, the predicted performance of the resulting design thickness falls between these two extremes. Although the CE overlay design procedure does not include previous fatigue damage to the base pavement, the method is sufficiently conservative that adequate capacity is provided. The additional overlay thickness required by the condition factors for cracking in the base slab before the overlay also provides adequate capacity to exceed the design coverage level.

The required increase in the overlay thickness because of the condition factor in the CE overlay equation is shown in Figure 55 along with the predicted performance of cases 4, 5, and 7. Only in case 5 did the base slab undergo a decrease in support caused by fatigue. The thickness of the pavement to support the design traffic increased from 6.4 to 7.4 in. The effect of the structural condition of the base slab at the time of the overlay is known to have very significant influence on the required thickness of overlay in Figure 55. In the specific example of case 5, the required overlay thickness almost doubled as it went from 6.4 in. to 12.7 in. to account for the condition of the base slab. As before, the CE overlay equation with the condition factor provides conservative results.

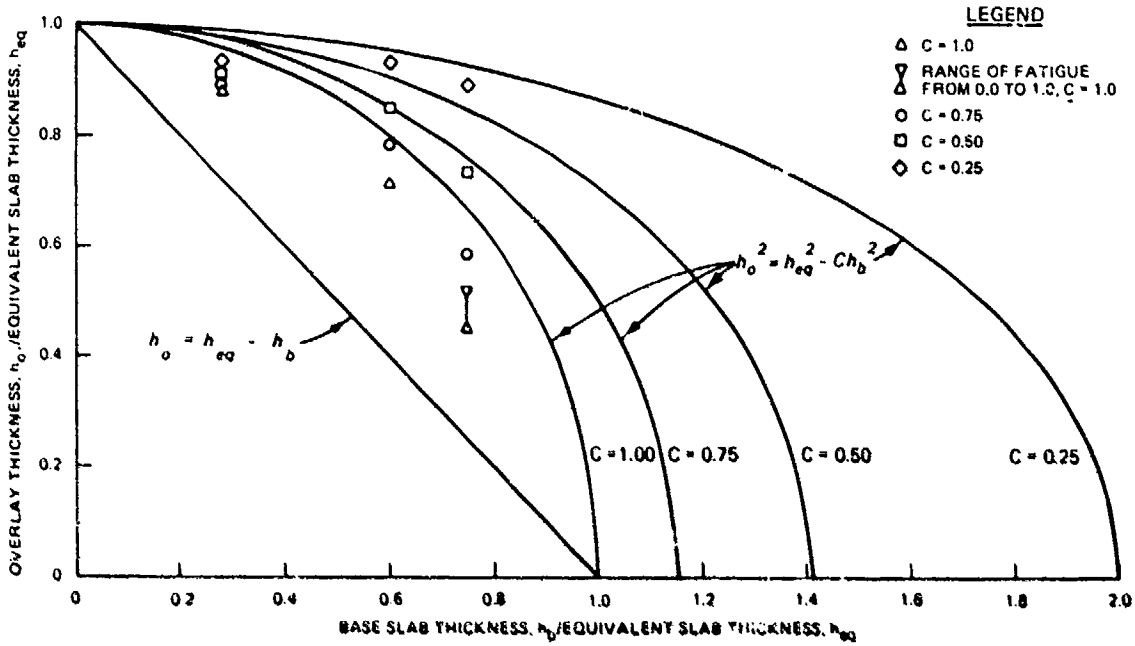

Figure 54. Comparison of the CE and the proposed design method overlay performance for case 5

The proposed overlay design approach using the layered-elastic analytical model results in thinner overlays than required by existing design approaches. Because it attempts to predict performance and more closely models the pavement structure, the proposed layered-elastic design approach requires much more accurate assessment of material properties and the structural condition of the base pavement. Factors such as fatigue damage from previous traffic that did not crack the pavement must be assessed if this approach is to be used. The conservativeness of the existing empirical approach was sufficient to allow these factors to be ignored previously. The importance of these factors is increased as the structural value of the base pavement increases.

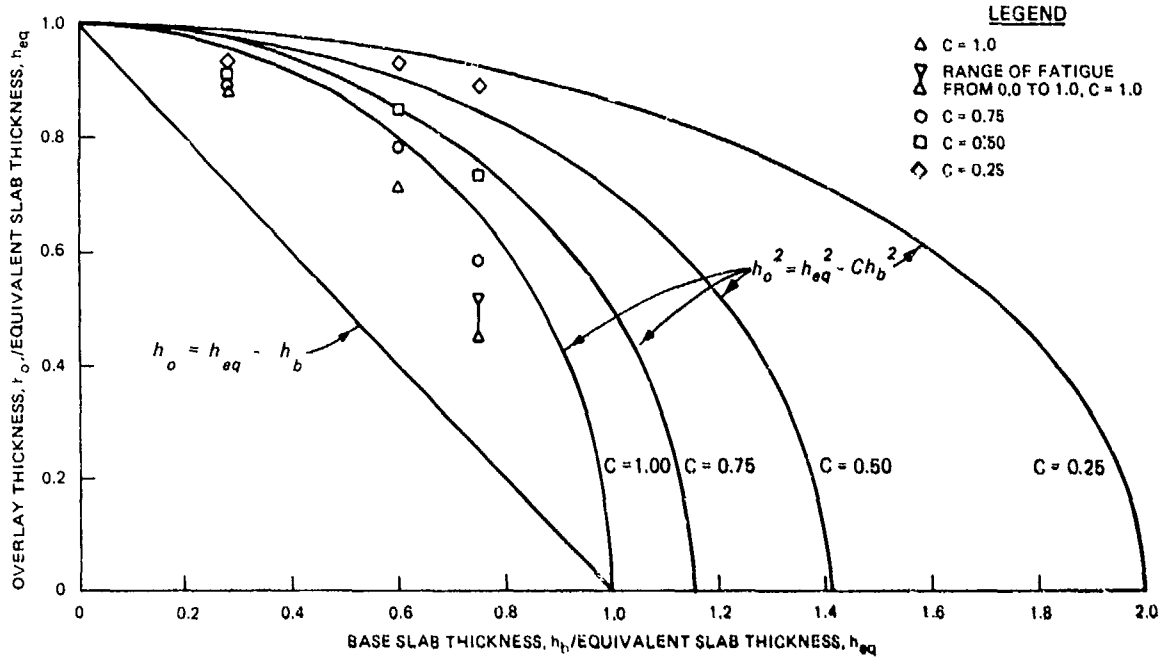

Figure 55. Effect of fatigue and initial base slab cracking on overlay relationships

EXTENSION TO FLEXIBLE OVERLAY

The proposed design procedure for rigid overlays provides a framework to consider flexible overlays as well as rigid overlays. However, the distress associated with flexible overlays is different from rigid pavements, and the proposed design procedure requires certain modifications and encounters more limitations when used with flexible overlays.

BACKGROUND

As with rigid overlays, an empirical relation developed by the CE from accelerated field tests is the most widely used design method in practice today. As with many of the rigid overlay tests, complete documentation of the flexible overlay tests was missing, but a summary of the tests and flexible overlay design method was presented by Mellinger and Sale[48].

The CE rigid and flexible overlay design methods were developed when the Air Force was upgrading existing pavements for new heavier jet aircraft. The Air Force was concerned about the potential for its new jet aircraft engines ingesting spalled concrete resulting in serious damage. Consequently, the empirical rigid overlay pavement equations were developed on the basis of initial cracking in the concrete. A similar concern did not exist over the flexible overlays for which a very different failure criterion was developed. This criterion was described by two sources.

> Mr. Turnbull (Mr. W. J. Turnbull of the Waterways Experiment Station) was interested in obtaining a realistic definition of the condition called failed by the Rigid Pavement Laboratory. He was informed that failure was usually associated with visible transient deflection on the order of 1/2 inch, and not with a nominal degree of surface rutting. He concurred that such a condition would definitely represent failure,...[53].

> The failure of a non-rigid overlay test item is determined by visual observation of the pavement surface. In the Sharonville overlay tests, large dynamic deflections and pavement displacements occurred rapidly after the first signs of visible transient deflection. Hence, failure was generally established at the number of traffic coverages corresponding to the first signs of visible deflection[48].

The CE flexible and rigid overlay design equations are often used to develop comparative designs for cost analysis of alternative pavement overlay strategies. Their very different defined levels of failure make any such comparisons ludicrous regardless of the current widespread practice of doing so. This difference in failure criteria results in anomalies such as a given pavement to be overlaid for some specified traffic requiring a certain thickness of rigid overlay. For the same conditions the flexible overlay equation will give a negative required overlay thickness. This simply reflects the difference in failure criteria.

The existing CE flexible overlay design equation is

$$t = 2.5(Fh_e - Ch_b) \quad (53)$$

where

t = thickness of flexible overlay

F = a factor less than or equal to 1.0 which accounts for cracking in the base slab charts (this factor can be found in references 24 and 78)

h_e = thickness of new concrete pavement required to support the design traffic if no base pavement existed

C = a condition factor to account for cracking in the base slab

= 1.0 if base pavement is intact or contains a small amount of structural cracking

= 0.75 if base pavement contains limited multiple cracks

= 0.50 if base pavement contains extensive multiple cracks

h_b = thickness of existing base pavement

The F factor in the above equation allows the base pavement to reach a completely failed condition (defined as a slab broken into 35 or more pieces). This extensive cracking in the base slab results in the deflection used as the failure criterion for flexible overlays. Without this F factor and with the condition factor of the base pavement equals to one, the flexible overlay equation is essentially an equivalency equation that states that 1-in. of PCC can be replaced with 2-1/2 in. of asphalt concrete (AC). Because of the problems caused by the difference in failure criteria, Chou[14] recommended that the 2.5 constant in the above equation be raised to 3.0 to increase the required thickness of flexible overlay. The existing CE flexible overlay equation does not provide the framework to develop comparative designs between flexible and rigid overlays. However, the proposed design overlay method, with certain limitations, can provide such framework.

FLEXIBLE OVERLAY DISTRESS

Any joint or crack in a rigid base pavement tends to reflect through the flexible overlay. This is because of differential movements caused by environmental effects, loads, or a combination of these factors. The problem of reflective cracking is a major research area, and summaries of the problem and recent work are presented by Treybig et al.[77] and Smith et al.[72]. At the present time there is no solution to the reflective cracking problem despite extensive work using techniques such as stress or strain relieving interlayers, geotextiles, reinforcing in the overlay, or cracking and seating of the PCC pavement prior to overlay. Also, the current research on predicting the rate and extent of reflective cracking has not advanced to the point where

the designer has a reliable method of estimating the future extent or severity of reflective cracking in a flexible overlay.

Reflective cracking starts as fine hairline cracking in the flexible overlay above joints or cracks in the underlying PCC pavement. This initial cracking can begin within a few months of the placement of the flexible overlay and with further cycles of temperature and load they propagate and widen. Initially reflective cracks are simply unsightly, but with time they deteriorate, begin to ravel, allow debris and water to enter, and are a continuous maintenance problem. Table 35 shows the PCI values for a pavement containing only reflective cracking from underlying pavement joints at the indicated density and severity levels as calculated using the PCI procedure of the FAA[80]. Reflective cracking from cracks in the underlying pavement rather than joints is computed as a separate distress type and has somewhat higher deduct values (hence lower overall PCI) than the joint reflective cracking in Table 35. Since reflective cracking appears to be unavoidable, even because

Table 35

PCI Values for Joint Reflective Cracking

	Severity		
Density, %	Low[a]	Medium[b]	High[c]
10	73	64	46
25	64	47	26
50	56	36	13
75	52	31	6
100	50	28	3

[a]Cracks have little or no spalling and a width of 1/4 in. or less.
[b]Cracks are moderately spalled with some loose particles. Crack width is greater than 1/4 in., or light random cracking exists near the crack or at the corners of intersecting cracks.
[c]Cracks are severely spalled with loose or missing particles.

of joints alone, and the extent of reflective cracking cannot be predicted at the present time, all flexible overlays can be expected to exhibit distress from reflective cracking. As indicated in Table 35 the evaluated condition of the pavement can be significantly affected by reflective cracking. The proposed design procedure will select thicknesses of flexible overlay to withstand structural loadings, but it will not prevent reflective cracking. Since reflective cracking seems to be eventually unavoidable in flexible overlays, one criterion for design of flexible overlays would be to avoid any cracking or deterioration in the concrete base pavement after the flexible overlay is placed.

If cracking and seating are used for the base pavement prior to overlay, it might be reasonable to treat the base pavement as having an SCI of 0 and the appropriate reduced modulus could be used to represent this layer in analysis. This is a new construction technique, and field data is required to validate any proposed design concepts such as this.

AC subjected to repeated loading will, like PCC, exhibit fatigue cracking. However, fatigue cracking is not a normal distress mechanism observed in flexible overlays. Nevertheless, any analysis of a flexible overlay should also check this possibility. The WES has used a layered elastic asphalt fatigue criterion based on work by Heukelom and Klomp[27] as follows:

$$\varepsilon_{all} = 10^{-A} \tag{54}$$

where

ε_{all} = allowable asphalt tensile strain

$$A = \frac{N + 2.665 \log(E/14.22) + 0.392}{5}$$

N = log (coverages)

E = modulus elasticity of asphalt concrete, lb/in.^{2}

The visible deflection criterion used in developing the CE empirical flexible overlay design equation suggests that subgrade failure may be an important factor in flexible overlay performance. Consequently, subgrade performance should also be checked for flexible overlay design. A criterion used by the WES for subgrade strain in layered elastic analysis is based on work by Barker and Brabston[7] and is determined by

$$\varepsilon_{sa} = \frac{A}{\left(\frac{N}{10,000}\right)^{1/B}} \tag{55}$$

where

ε_{sa} = allowable vertical subgrade strain

$A = 0.000247 + 0.000245 \log E_s$

N = Cycles of strain or coverages

$B = 0.0658\ E_s^{0.559}$

E_s = subgrade modulus (lb/in.^{2})

Rutting is a common distress in flexible overlays. However, this is primarily dependent on the quality of the AC and construction used for the overlay and is best controlled by material and construction specifications. Therefore, flexible overlay rutting is not analyzed directly in the proposed design approach.

Because of the eventual reflective cracking that will probably occur from any cracks forming in the base pavement, a conservative approach to flexible overlay design is to select the flexible overlay thickness so that no cracking is caused in the base pavement (i.e., C_o for the base pavement after adjustment for equivalent traffic prior to overlay is not reached during the design life of the overlay). This approach would not be feasible, for example, if a flexible overlay was planned for a pavement that was already exhibiting distress. In this case some reflective cracking from this distress would have to be expected, and the flexible overlay thickness should be selected so that further loss in SCI of the base pavement through the design life of the overlay is minimal. When the base slab has been cracked by previous traffic, allowable asphalt tensile stain and the subgrade vertical strain should be checked.

OVERLAY BEHAVIOR

Case 6 from Tables 27 and 28 will be used to illustrate the proposed design procedure's application to flexible overlays. For this case an existing 10.8 in. concrete base pavement with a modulus of 5,000,000 lb/in.^{2} and a flexural strength of 800 lb/in.^{2} is to be overlaid to support 50,000 coverages of a B-727. The subgrade has an elastic modulus of 20,000 lb/in.^{2}. The equivalent new slab to support this traffic is 14.4 in. The AC modulus will be assumed to be 250,000 lb/in.^{2}, and the Poisson's ratio will be assumed to be 0.45. From the equations given earlier the allowable AC tensile strain for 50,000 coverages is 5.24×10^{-4} in./in. and the allowable subgrade strain is 1.18×10^{-3}.

Table 36 shows the effect of the deterioration of the base slab for several overlay thicknesses between 2 and 14 in. The 9.8 in. (rounded to the nearest 0.1 in.) overlay will protect the base slab against deteriorating during the 50,000 design coverages and would be the design using the criteria for the proposed design method. The 8.2 in. thickness would be the design using the CE flexible overlay equation. For this specific case, strain in the AC and subgrade never became a concern. Even after the SCI of the base reaches 0 neither of these parameters reaches a value that would cause deterioration within another 50,000 coverages. Reflective cracking from deterioration of the base slab is the primary potential distress for the flexible overlay.

Figure 56 shows the base slab deterioration for several flexible overlay thicknesses for case 6 and also shows the AC tensile strain and subgrade vertical strain as the base slab deterioration. The AC strain begins in compression and turns into tension for this specific case and example overlay thicknesses only after the base slab has undergone significant deterioration. Table 36 shows this usually occurs when the base slab reaches an SCI value of

Table 36

Stresses and Strains for the Case 6 Flexible Overlay

Thickness of Asphalt Concrete, in.	Base Slab		Strain[a]		Predicted Base Slab Performance	
	SCI	Tensile Stress, lb/in.^{2}	Asphalt Concrete	Vertical Subgrade	C_o	C_F
2.0	100	481	-7.76×10^{-5}	-3.21×10^{-4}	808	3,319
	80		-9.48×10^{-5}	-3.68×10^{-4}		
	60		-1.20×10^{-4}	-4.28×10^{-4}		
	40		-1.58×10^{-4}	-5.08×10^{-4}		
	20		-2.26×10^{-4}	-6.25×10^{-4}		
	0		-1.67×10^{-4}	9.9×10^{-4}		
4.0	100	439	-6.38×10^{-5}	-3.00×10^{-4}	2,058	8,531
	80		-7.57×10^{-5}	-3.40×10^{-4}		
	60		-5.42×10^{-5}	-3.90×10^{-4}		
	40		-1.12×10^{-4}	-4.54×10^{-4}		
	20		-1.32×10^{-4}	-5.41×10^{-4}		
	0		$+2.05 \times 10^{-4}$	-7.95×10^{-4}		
6.0	100	402	-5.29×10^{-5}	-2.79×10^{-4}	5,514	23,077
	80		-6.10×10^{-5}	-3.14×10^{-4}		
	60		-7.02×10^{-5}	-3.55×10^{-4}		
	40		-7.90×10^{-5}	-4.07×10^{-4}		
	20		-7.35×10^{-5}	-4.75×10^{-4}		
	0		$+3.18 \times 10^{-4}$	-6.59×10^{-4}		
8.2	100	365	-4.38×10^{-5}	-2.57×10^{-4}	18,033	76,378
	80		-4.88×10^{-5}	-2.86×10^{-4}		
	60		-5.36×10^{-5}	-3.21×10^{-4}		
	40		-5.50×10^{-5}	-3.62×10^{-4}		
	20		-3.61×10^{-5}	-4.16×10^{-4}		
	0		$+3.29 \times 10^{-4}$	-5.49×10^{-4}		

(Continued)

[a]The plus sign (+) denotes tension; the minus (-) sign denotes compression.

Table 36 (Concluded)

Thickness of Asphalt Concrete, in.	Base Slab		Strain		Predicted Base Slab Performance	
	SCI	Tensile Stress, lb/in.^{2}	Asphalt Concrete	Vertical Subgrade	C_o	C_F
9.8	100	340	-3.83×10^{-5}	-2.04×10^{-4}	46,472	198,712
	80		-4.19×10^{-5}	-2.26×10^{-4}		
	60		-4.44×10^{-5}	-2.52×10^{-4}		
	40		-4.25×10^{-5}	-2.82×10^{-4}		
	20		-1.88×10^{-5}	-3.19×10^{-4}		
	0		$+3.21 \times 10^{-5}$	-3.80×10^{-4}		
12	100	308	-3.30×10^{-5}	-2.22×10^{-4}	195,354	874,458
	80		-3.52×10^{-5}	-2.44×10^{-4}		
	60		-3.60×10^{-5}	-2.69×10^{-4}		
	40		-3.19×10^{-5}	-2.99×10^{-4}		
	20		-6.64×10^{-6}	-3.37×10^{-4}		
	0		$+2.85 \times 10^{-4}$	-4.20×10^{-4}		
14	100	282	-2.90×10^{-5}	-2.06×10^{-4}	797,505	3,508,870
	80		-3.03×10^{-5}	-2.24×10^{-4}		
	60		-3.00×10^{-5}	-2.46×10^{-4}		
	40		-2.47×10^{-5}	-2.71×10^{-4}		
	20		$+5.52 \times 10^{-7}$	-3.04×10^{-4}		
	0		$+2.56 \times 10^{-4}$	-3.71×10^{-4}		

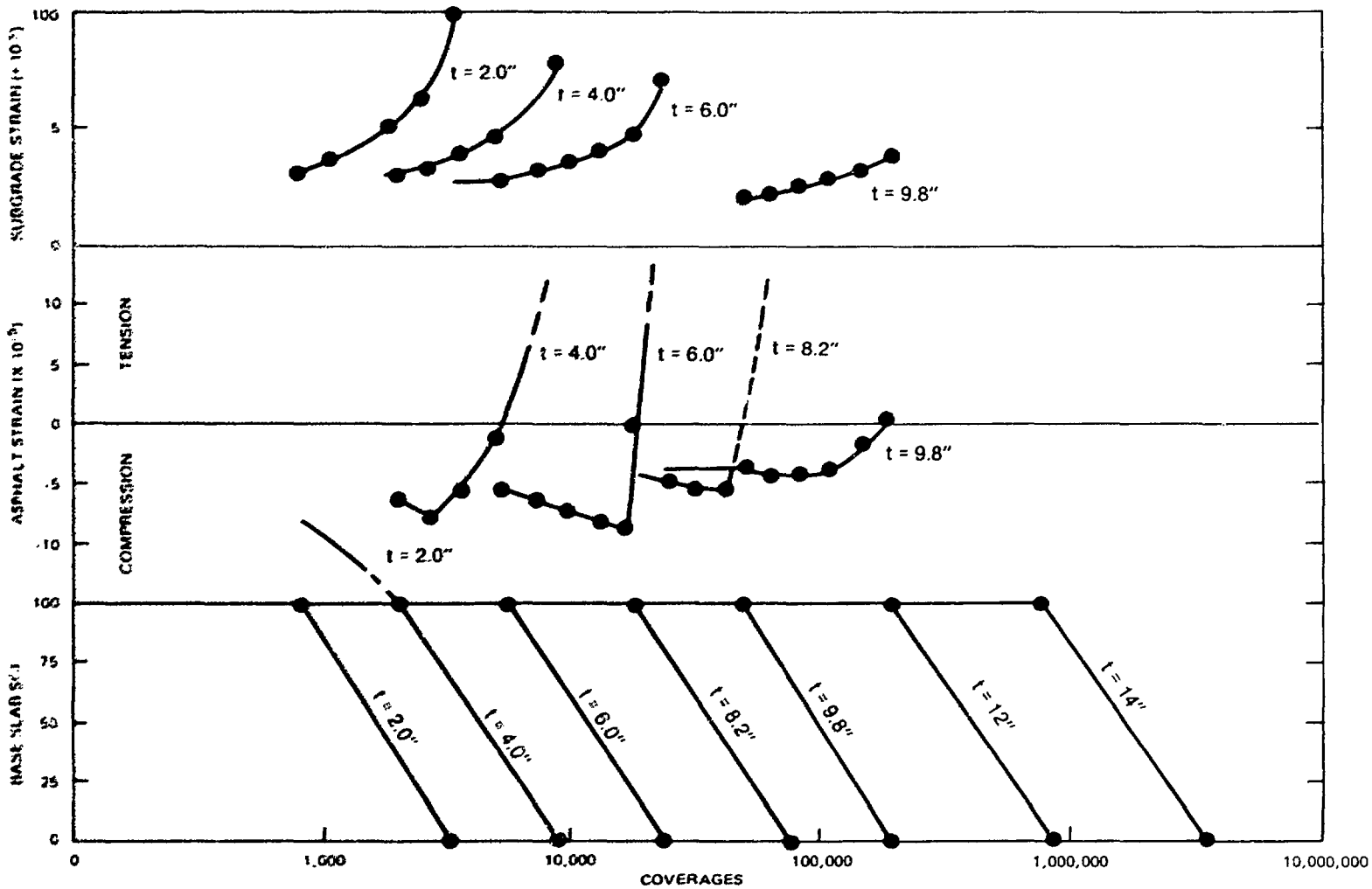

Figure 56. Base slab deterioration and resulting strains in the AC

20 or 0. The subgrade strain steadily increases as the base slab deteriorates. At no time do either AC tensile strain or subgrade vertical strain reaches the limiting values given earlier. This may not always be true, thus these parameters need to be checked in each flexible overlay design. Analysis of these parameters would follow the same procedures discussed earlier for calculating the onset of cracking (composite C_o value) in the rigid overlay. During each interval of traffic the damage from AC or subgrade strain would have to be calculated as is done in Table 21 for PCC damage.

For an initial undamaged base pavement, a 9.8 in. flexible overlay would just be starting to allow deterioration in the base pavement after the design 50,000 coverages of the B-727 for case 6. The only distress that would exist at the end of the design traffic would be whatever flexible overlay reflective cracking developed from the underlying joints plus any durability, environmental, or construction related distress. The 8.2 in. overlay thickness calculated from the CE flexible overlay equation would allow deterioration of the base pavement to start at 18,033 coverages (Table 36), and the base SCI would be 29 at the end of the 50,000 design coverages (Figure 56). Significant cracking from this amount of base slab could be expected to reflect through the flexible overlay.

Pavements are often overlaid after they have undergone some pavement damage. Because of the problem of reflective cracking, this damage will eventually reappear in the flexible overlay. Under the proposed design procedure a thickness of overlay can be selected that will minimize further deterioration of the base pavement. Table 37 shows the final base SCI value at the end of 50,000 coverages for initial base SCI values of 25 to 75. The 9.8 in.-thick overlay shows a large decrease in SCI value after 50,000 coverages when used on any of the three deteriorated pavements in Table 37. Considerable reflective cracking damage could be expected under these conditions. The 12 in. flexible overlay suffers far less base damage at the end of the design traffic than did the 9.8 in. overlay, but the 14 in. overlay essentially prevents any further damage to the base slab. Consequently, for a pavement that has undergone structural deterioration prior to the overlay (i.e., SCI <100) the 14 in. overlay offers the design that will minimize damage for case 6 under the 50,000 design coverages.

Table 37 shows that the rigid and flexible CE overlay C factors are defined differently from one another for the same base pavement SCI. This simply reflects the differences in failure criterion and performance to be expected from these overlay types under the existing CE design approach. The proposed design procedure can be extended as described to include flexible overlays. However, analytical models to describe the progression and severity of reflective cracking are beyond the current state-of-the-art, and therefore the ability to predict the flexible pavement deterioration is very limited. With the proposed design method a thickness of AC overlay is selected to prevent cracking from developing in an existing base pavement after overlay or at least to minimize further cracking in an already cracked based pavement after overlay. Strain in the AC and subgrade are also checked against allowable valuables, but they normally will not control flexible overlay design.

Table 37

Effect of Initial Base SCI on the Performance of Case 6 Flexible Overlays

Initial Base SCI	Approximate Equivalent CE C Factor		Thickness in.	Equivalent Traffic[b]	Base SCI After 50,000 or More Coverages
	Rigid[a]	Flexible			
75	0.73	1.00	9.8	66,827	37
			12.0	284,152	64
			14.0	1,155,026	72
50	0.46	0.75	9.7	96,097	21
			12.0	413,314	42
			14.0	1,672,824	48
25	0.19	0.50	9.8	138,187	4
			12.0	601,187	20
			14.0	2,422,751	24

[a]Calculated from $C = -0.076 + 1.073 \frac{SCI}{100}$.

[b]Equivalent traffic on the overlay that would develop the initial base SCI given in the first column.

EVALUATION

Table 38 shows the design parameters for the 14 cases from Tables 27 and 28 along with randomly selected AC modulus values for a flexible overlay. Allowable PCC tensile stresses, AC tensile strains, and subgrade vertical strains based on the criteria given in the preceding sections are shown in Table 39 for each case. Comparative designs were prepared for each of these 14 cases using the proposed design procedures and CE flexible overlay equation. The CE designs were made using the WES computer program RAD611. The results are shown in Figure 57. For case 5 the CE flexible overlay equation requires a negative overlay thickness compared with the 5.0 in. overlay required by the proposed design procedure to protect the base from cracking. This again illustrates the extreme failure criterion used by the CE flexible overlay procedure. For thick flexible overlays the proposed design procedure would require thinner overlays than the CE equations. For thinner overlays the proposed method tends to require thicker overlays than the CE method. There are some very extreme differences between the overlays required by these methods (e.g., for case 2 the proposed method requires 15.1 in., and the CE method requires 21.6 in.; for case 4 the proposed method requires 21.2 in., and the CE method requires 37.3 in.; for case 9 the proposed method requires 15.5 in., and the CE method requires 3.3 in.).

There is not a consistent basis for comparison between the proposed design method and the CE flexible overlay method. The CE thickness calculations in Figure 57 include all the inconsistencies of the empirical CE flexible overlay equation and all the assumptions of the CE rigid pavement design method which are used in developing the equivalent new pavement thickness. The flexible overlay failure criterion is of doubtful validity today.

Table 38

Flexible Overlay Design Parameters

Case	Aircraft	Design Coverages	Equivalent Slab, h, in.	Base Slab		Flexible Overlay ($lb/in.^2$)			Subgrade
				h in.	E_b $lb/in.^2$	150,000	250,000	350,000	E, $lb/in.^2$
1	F-4	10,000	8.5	4.0	5.0×10^6			X	35,000
2	F-4	25,000	10.6	4.0	4.0×10^6		X		10,000
3A	F-4	75,000	10.0	7.5	5.0×10^6	X			35,000
4	B-727	10,000	16.0	4.0	4.5×10^6		X		10,000
5	B-727	25,000	14.2	10.7	4.5×10^6			X	50,000
6	B-727	50,000	14.4	10.8	5.0×10^6		X		20,000
7	B-727	50,000	13.7	8.2	4.0×10^6		X		50,000
8A	B-727	75,000	17.5	10.5	4.5×10^6			X	10,000
9	C-141	10,000	19.0	14.2	4.5×10^6	X			10,000
10	C-141	50,000	21.5	8.6	5.0×10^6			X	4,000
11	C-141	50,000	14.2	4.0	4.5×10^6	X			35,000
12	C-141	75,000	22.3	11.2	5.0×10^6			X	4,000
13	B-747	110,000	16.2	4.0	5.0×10^6		X		35,000
14	B-747	250,000	19.6	11.8	4.0×10^6			X	20,000

Table 39

Portland Cement Concrete, Asphalt Concrete, and Subgrade Criteria

Case	Concrete Base Slab Flexural Strength, lb/in.	Required Design Factor[a]	Allowable Stress, lb/in.^{2} [b]	Allowable Strain, in./in.[c]	Allowable Subgrade Strain, in./in.[d]
1	800	2.091	383	6.04×10^{-4}	1.36×10^{-3}
2	600	2.247	267	6.02×10^{-4}	1.1×10^{-3}
3A	800	1.434	329	6.34×10^{-4}	1.25×10^{-3}
4	700	2.091	335	7.23×10^{-4}	1.33×10^{-3}
5	700	2.247	311	5.03×10^{-4}	1.35×10^{-3}
6	800	2.365	338	5.24×10^{-4}	1.18×10^{-3}
7	600	2.365	254	5.24×10^{-4}	1.32×10^{-3}
8A	700	2.434	288	4.04×10^{-4}	1.03×10^{-3}
9	700	2.091	335	9.49×10^{-4}	1.23×10^{-3}
10	800	2.365	338	4.38×10^{-4}	8.91×10^{-4}
11	700	2.365	296	6.88×10^{-4}	1.29×10^{-3}
12	800	2.434	329	4.04×10^{-4}	8.39×10^{-4}
13	800	2.438	322	4.56×10^{-4}	1.23×10^{-3}
14	600	2.639	227	3.17×10^{-4}	1.07×10^{-3}

[a] Design Factor = $0.5234 + 0.390 \log C_o$.

C_o = onset of deterioration in base slab set equal to design coverage level.

[b] Allowable stress in PCC base slab equals flexural strength divided by design factor.

[c] From preceding section:

$$\varepsilon_{all} = 10^{-A}$$

$$A = \frac{N + 2.665 \log (E/14.22) + 0.392}{5}$$

[d] From preceding section:

$$\varepsilon_{sa} = \frac{\frac{A}{N}}{10{,}000}^{1/B}$$

$$A = 0.000247 + 0.000245 \log E_s$$

$$B = 0.0658 E_s^{0.0559}$$

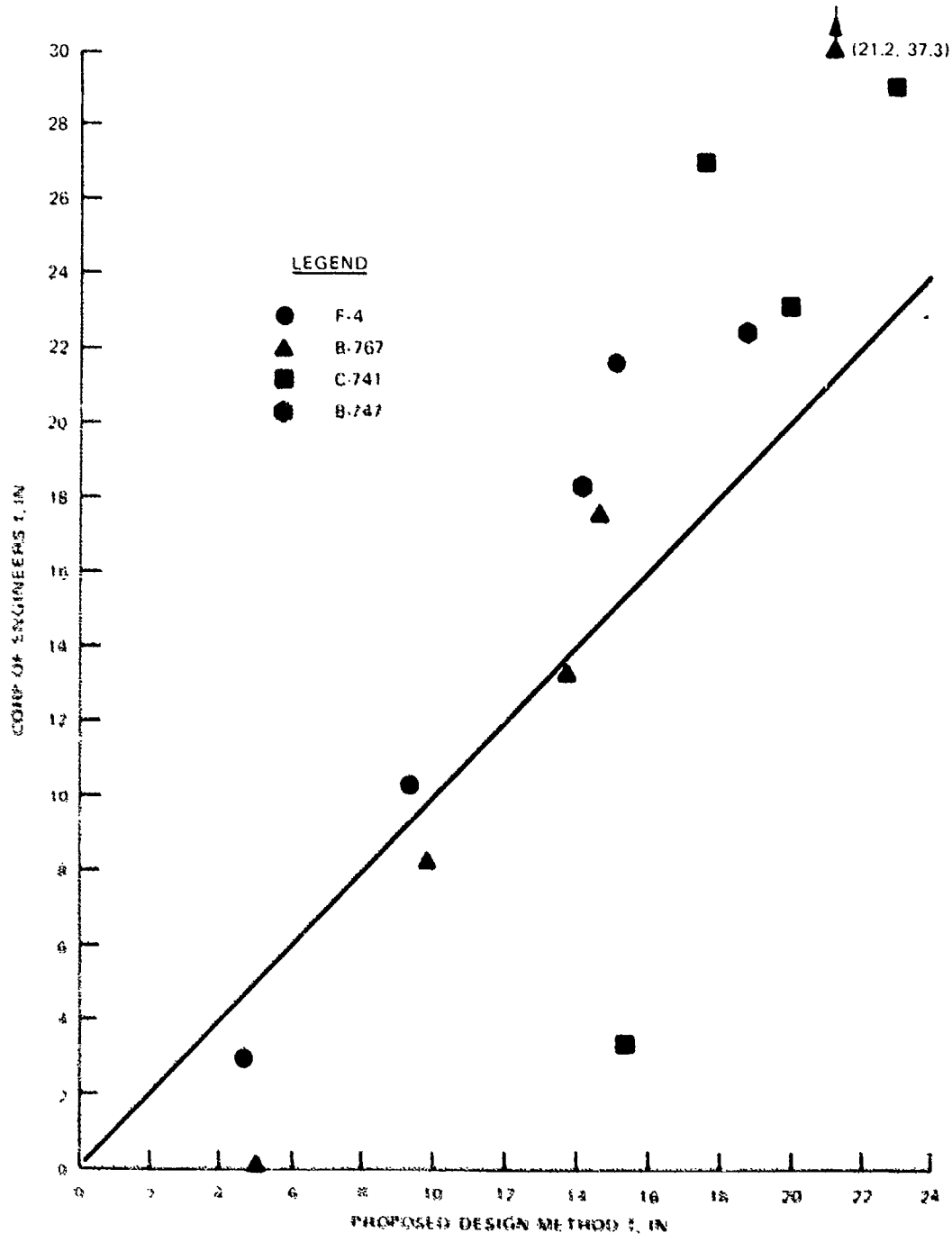

Figure 57. Comparison of overlay thicknesses required by the proposed design method and the CE design method

Table 40 summarizes some of the differences between the empirical CE method and the proposed design methods. The basis and approach between the design methods are very different, and the differences shown in Figure 57 are not surprising in light of the variations in assumptions and criteria involved.

The results in Figure 57 suggest that the proposed design procedure wil generally require approximately the same or thicker overlays under conditions where the CE design procedure would require about 14 in. or less of overlay. With thicker overlays the proposed method would require thinner overlays than the CE design procedure.

In order to compare the CE flexible overlay equation with the proposed method the thicknesses required by the flexible overlay equation were recalcu lated using the CE overlay equation, but the equivalent thickness from layere elastic calculated stresses and a failure defined as C_o from Tables 31 or 3 were used with the CE equation. This puts the comparison on a similar failur basis and removes differences caused by rigid and flexible pavement factor differences or failure criteria differences, CE reductions in thickness for high-strength subgrades, or stress calculation differences between the Wester gaard and layered elastic analytical models. Also, an additional six cases were evaluated. These cases were case 2 with the base pavement set equal to 0.1, 0.6, and 0.9 times the equivalent slab thickness and designated as case 2B, 2C, and 2D, respectively. The other three new cases were case 4 wit the base slab thickness set equal to 0.1, 0.5, and 0.9 times the equivalent slab thickness and designated as case 4B, 4C, and 4D.

As shown in Figure 58 the redefinitions of equivalent slab thickness reduced the CE calculated overlay thickness. The pattern in Figure 58 is ver similar to that in Figure 57. The proposed design method requires thicker or approximately the same overlay thickness when the CE required thickness is about 14 to 16 in. and thinner overlays otherwise.

The CE unbonded equation for rigid overlays was a conservative upper bound for the layered elastic solutions, and the derivation of the cubic form of this equation based on a definition of equal rigidity found that the thick nesses of the overlay could be adjusted by the ratio of modulus value to account for material differences between the overlay and base pavement. This suggests that a conservative upper bound solution to the layered-elastic flex ible overlay solutions may take the form of

$$h_e^2 = h_b^2 + B\ t^2 \qquad (56$$

where

h_e = equivalent new pavement thickness

h_b = existing base pavement thickness

B = modular ratio

= E AC/E PCC

t = required thickness of AC overlay

Table 40

Comparison Between CE Flexible Overlay Design Procedure and the Proposed Design Procedure

Design Considerations	Corps of Engineers	Proposed Method
Analytical model	Empirical equation	Layered elastic model
Failure	Visual deflection in test sections	Onset of cracking in base slab or minimize additional cracking in base slab Limit tensile strain in AC Limit vertical strain in subgrade
Material properties	Equivalent required h needed as input to empirical equation	Include elastic modulus and Poisson's ratio for each layer Include flexural strength of concrete used to limit cracking Include allowable AC and subgrade strain as functions of modulus and repetitions
Cracking in base pavement before overlay	Existing pavement thickness is reduced	Modulus of concrete reduced in calculations
Reflective cracking and rutting in the flexible overlay	Not included	Not included

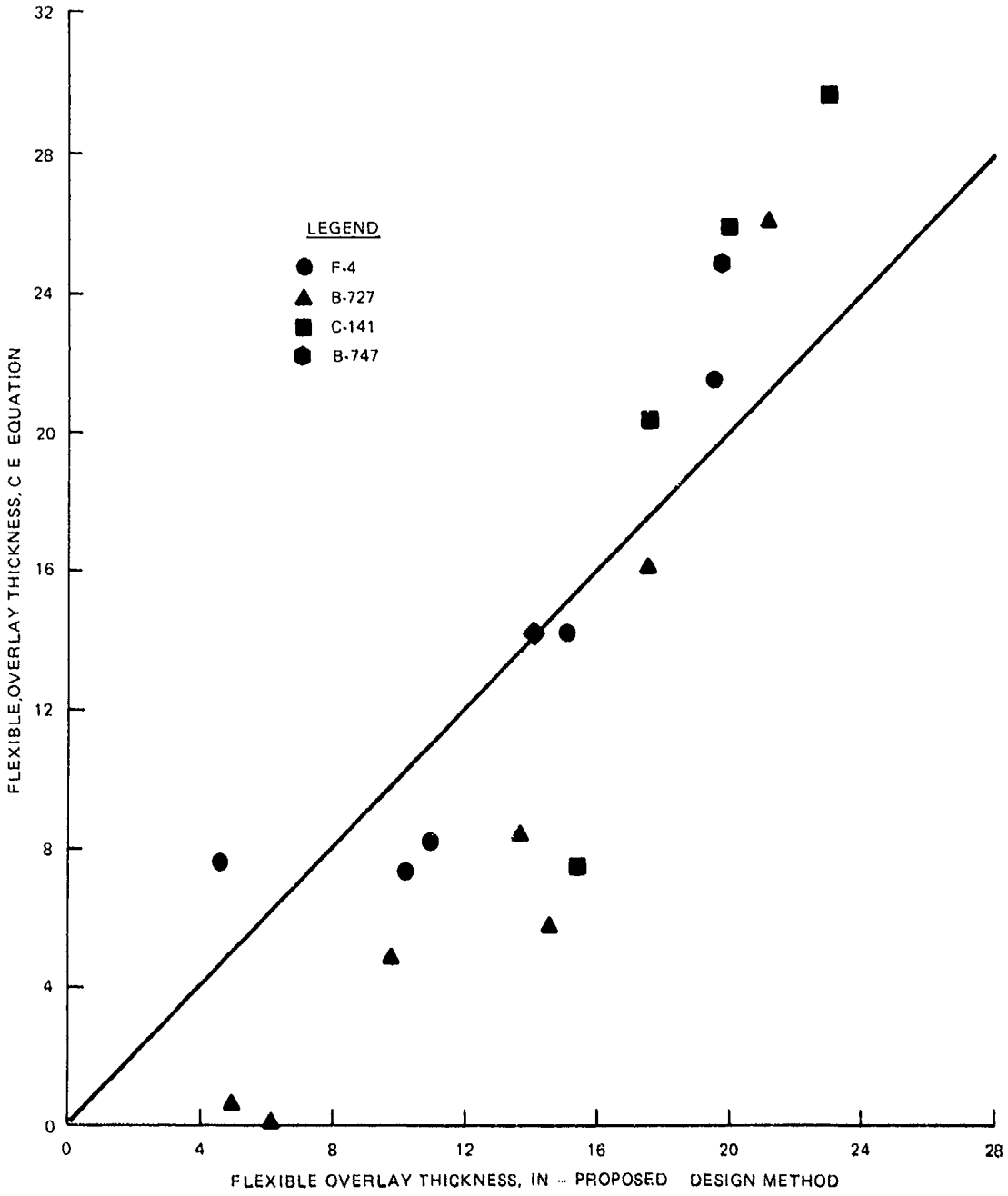

Figure 58. Comparison of proposed design procedure and CE design equation with layered elastic equivalent slab thickness

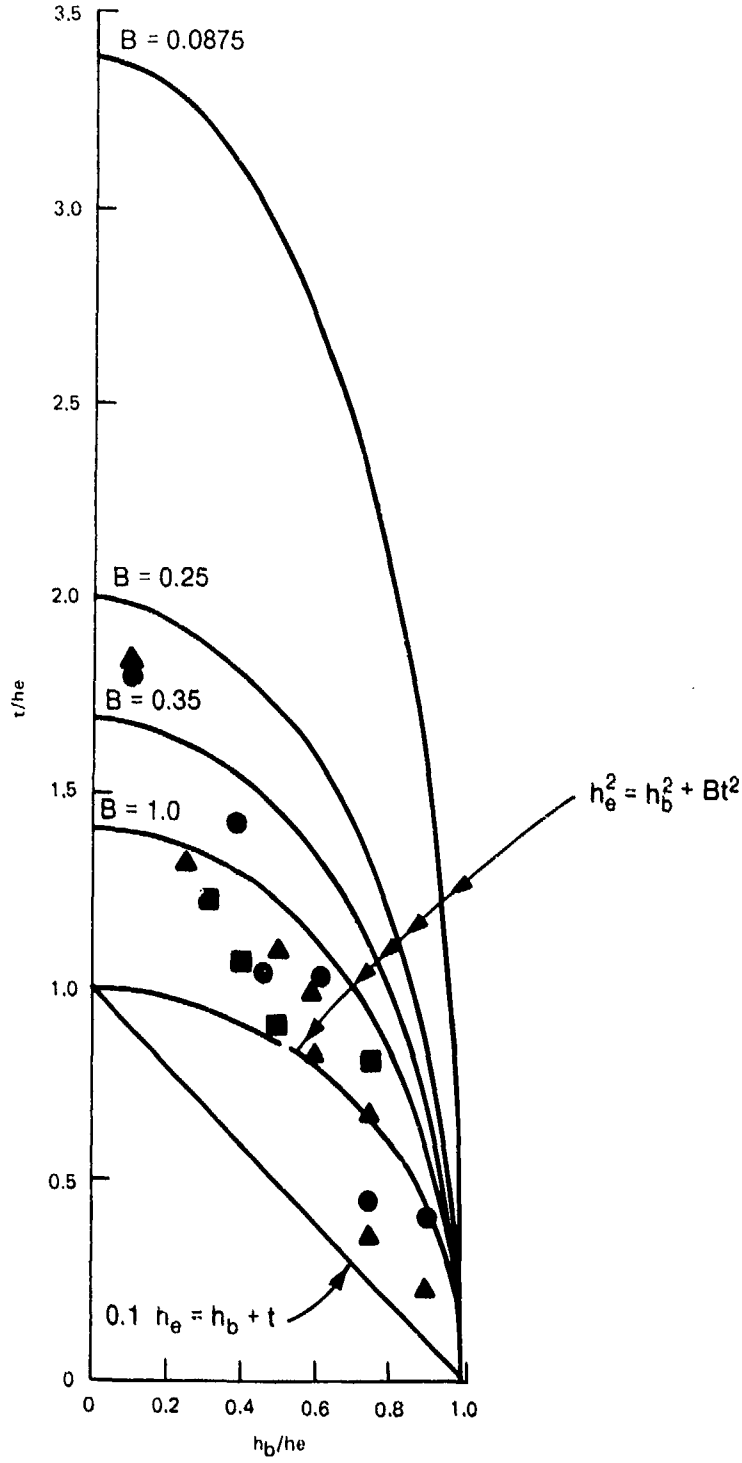

Figure 59. Power equation with varying values of B

The ratio of AC modulus to PCC modulus for 20 cases that were analyzed could vary between 0.0300 and 0.0875. As shown in Figure 59 the use of B set equal to 0.0875 is much too conservative to be usable. Smaller values of the E ratio are in further error. Curves with other B values are shown in Figure 59. A conservative upper bound solution to the proposed design method results can be found with this equation if B is allowed to vary with the ratio of h_b/h_e as shown in Table 41.

Table 41

Appropriate Values of B for a Conservative Flexible Overlay Solution

Proposed Equation	h_b/h_e	B
$h_e^2 = h_b^2 + B\ t^2$	≥0.5	0.50
	≥0.25, <0.5	0.35
	<0.25	0.25

Note: h_e = equivalent new pavement thickness.
h_b = existing pavement thickness.
t = AC overlay thickness.

This form of the power equation is not very satisfactory, and a variety of regression equations were also evaluated. Attempts to include the effect of modulus value in the equation were not successful. The best of these attempts was

$$t/h_e = 1.819 - 1.656 \frac{h_b}{h_e} + 0.723\ (E_a/E_c) \qquad (57)$$

where

t = thickness of AC overlay

h_e = thickness of equivalent new pavement

h_b = thickness of existing base pavement

E_a = modulus of elasticity of the AC in the overlay

E_c = modulus of elasticity of the PCC in the base pavement

However, as shown in Figure 60 there is no significant change caused by the modulus ratio within the ranges for the 20 flexible overlays examined.

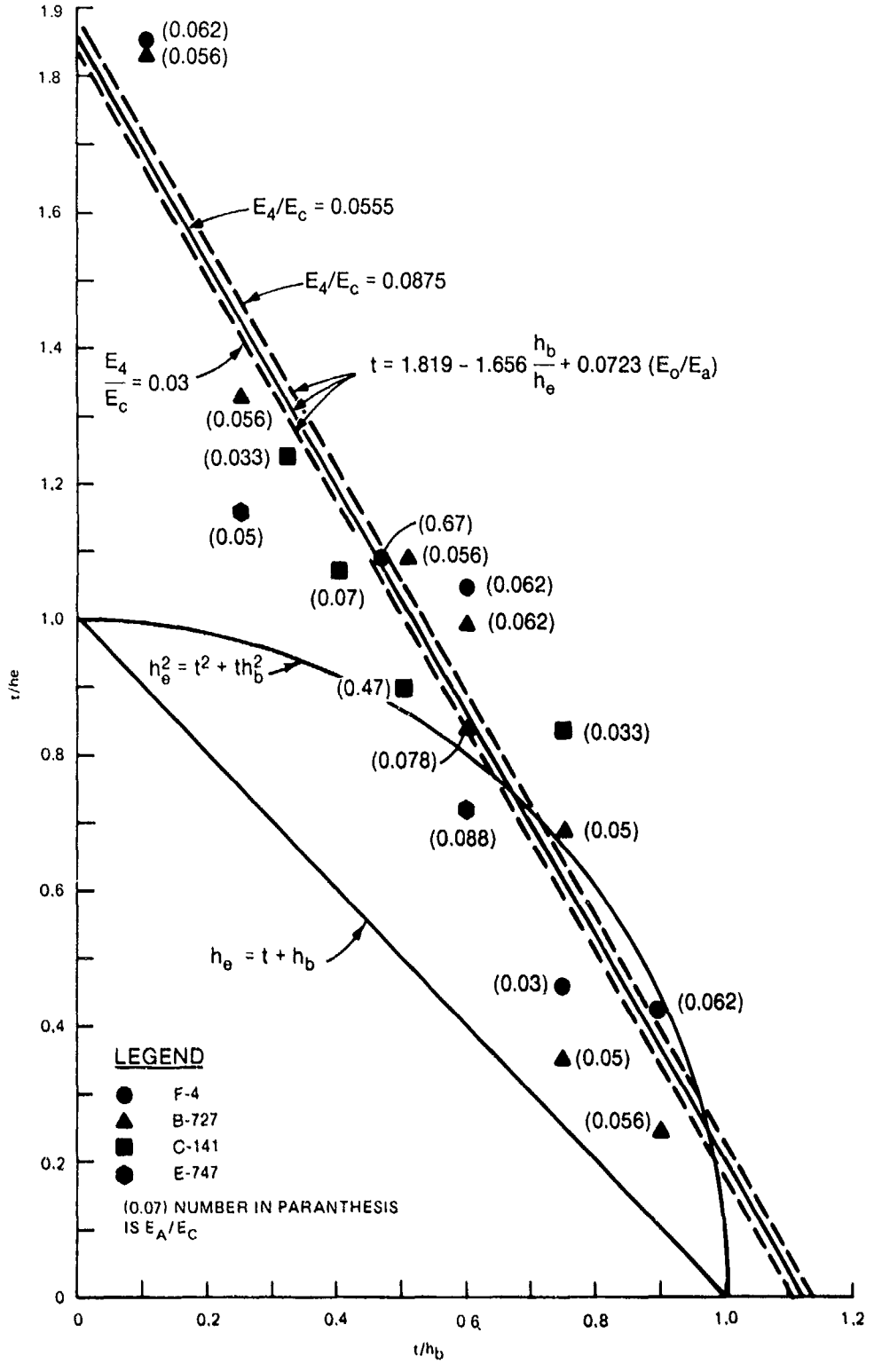

Figure 60. Flexible overlay equation with modular ratio term

The modulus ratio E_a/E_c in the above equation has little real effect. Therefore, several linear regression forms were examined with a single independent variable. The most promising of these was

$$t/h_e = 1.853 - 1.645\ (h_b/h_e) \qquad (58$$

$$r^2 = 0.84$$

Standard error of estimate = 0.1805

The variables in the equation are defined in equation 57. This equation is almost identical to the one plotted in Figure 60 with the E_a/E_c is equal to 0.555. This form of the equation is not always conservative as was the CE unbonded equation for rigid overlays or as it was modified in Table 41 for flexible overlays. Also, when the base thickness equals the equivalent thickness for new pavement, the equation would still require a flexible overlay of 0.208 of the equivalent slab thickness. Since by definition the equivalent slab can support all of the design traffic, this equation is not consistent a the ratio of h_b/h_{eg} approaches 1.0.

The basis or data for the flexible C factor (note that this is different from the rigid pavement C factor in Table 2) with CE flexible overlay design equation was not presented by Mellinger and Sale[48]. In Figure 61 the CE flexible overlay equation is shown for various F and C factors. The F factor may vary for 0.4 to 1.0, and it is the factor that representing the base slab reaching complete failure. The F factor is a function of the subgrade k and number of coverages. The F factor for the 20 cases considered in this section varied from 0.77 to 0.96. It is this factor that leads to the anomalies in the CE flexible overlay equation that causes calculation of negative flexible overlay thicknesses in certain circumstances

The C factor has a major impact on the required overlay thickness in Figure 61. The previously given power and overlay regression equations can also use a C factor in the same manner as the CE equation. For example the overlay regression equation would become

$$\frac{t}{h_e} = 1.853 - 1.645\ C\ \frac{h_b}{h_e} \qquad (59$$

In Figure 62 this equation is plotted with the CE flexible overlay equation. The C factor values for the above regression equation were selected to be numerically equal to the rigid pavement C factor values that correspond wit the flexible C factor values in Table 37. From Table 37 it appears that th flexible pavement C factor of 1.0 corresponds to the rigid pavement C factor values of 1.0 and 0.73 used with the overlay regression equation. The flexible C factor of 0.75 corresponds to the rigid factor of 0.46, and 0.5(

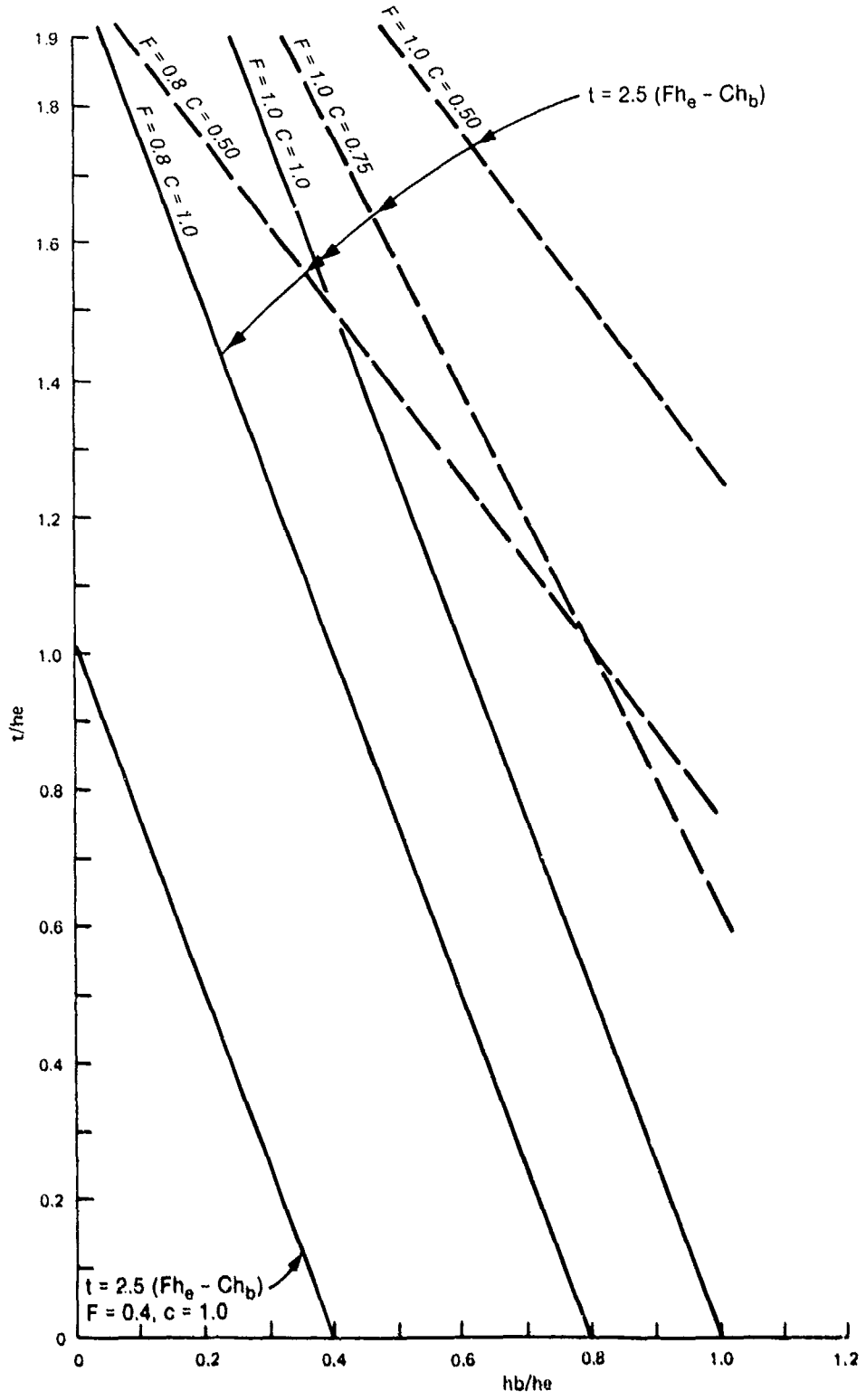

Figure 61. CE flexible overlay equation for varying C and F values

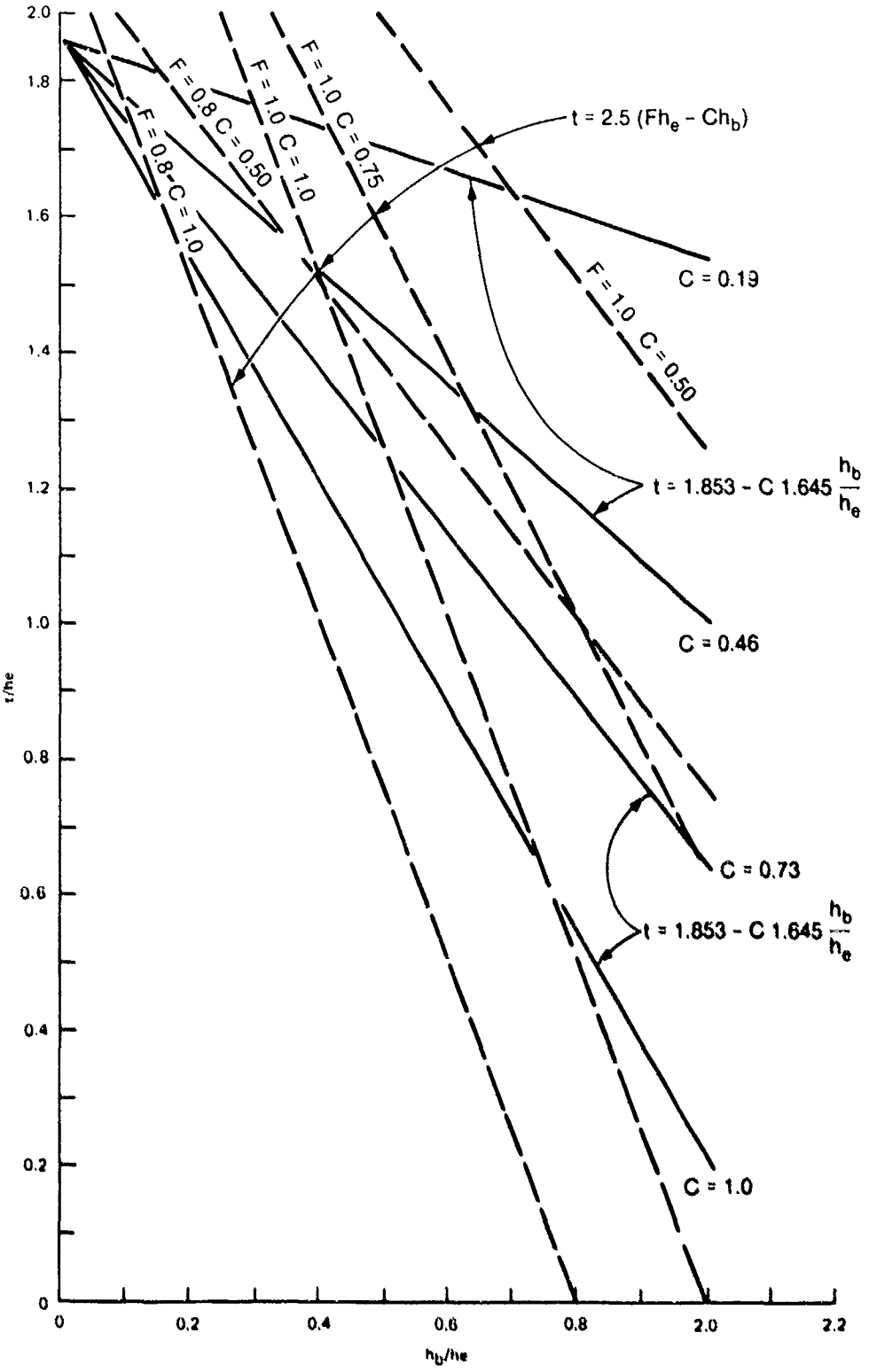

Figure 62. Comparison between CE flexible overlay equation and the overlay regression equation

corresponds to the rigid factor of 0.19. The use of the F factor complicates the analysis, but in general it appears that the rigid overlay C factor determined from Table 2 or Figure 15 can be used with the overlay regression equation to conservatively account for the condition of the base slab. For example, for a CE flexible F of 1.0 and C of 1.0 the regression equation would require a thicker overlay than the CE equation whenever h_b/h_e was greater than 0.75 for a rigid C value of 1.0. Similarly, the regression equation would require a greater overlay thickness than the CE equation whenever h_b/h_e was greater than 0.51 for a rigid C of 0.73. However, F is almost always less than 1.0, and for an F of 0.8, the regression equation would require a greater flexible overlay thickness for h_b/h_e value greater than 0.17 for a rigid C factor of 1.0 or greater than 0.12 for a rigid C factor of 0.75. If a rigid pavement overlay C factor is used as a multiplier for the B factor in the power equation in Table 41, the results compare conservatively with the CE flexible overlay equation in Figure 61.

The basis for the C factors used with the CE rigid and flexible overlay equations is not documented or adequately supported by data. They are based more on judgement, are highly subjective, and have caused considerable confusion in the part. Because of the lack of precision in their definition and weak basis, a single C factor selected by a reproducible method such as Figure 15 could be used for all of these equations. It can be used conservatively with the overlay regression or power equation presented in this section.

SUMMARY

The proposed design method can be extended to include flexible overlays over rigid pavements. However, the current limited ability to predict the extent and severity of reflective cracking makes it impossible to predict performance with the proposed design procedure as was done for rigid overlays with the proposed design procedure.

The thickness of flexible overlay is selected to prevent an uncracked base pavement from cracking, to minimize any further cracking in a base slab that was cracked prior to overlaying, and to avoid exceeding the allowable AC tensile strain and subgrade vertical strain. The allowable subgrade vertical strain will not be exceeded.

The existing CE flexible overlay equation is based on a failure criterion that is unrelated to other pavement criterion and which does not seem to be appropriate for current airfield design practice. Because of its empirical nature and unique failure criterion, the CE flexible overlay equation cannot be used to develop comparative designs. Also, peculiar and unrealistic results can be obtained. Consequently, the CE flexible overlay design equation is not recommended for further use.

Two simple equations were developed for possible use when the proposed design method was not used or to obtain an initial estimate of trial overlay thickness for the proposed design method. One is a power equation similar to the CE unbonded overlay equation, and it is presented in Table 41. It is con-

servative and probably most appropriate for use when h_b/h_e is 0.50 or greater. The other equation is the overlay regression equation. It is a least square linear regression equation and is not always conservative. It also is not consistent when h_b/h_e reaches 1.0. Both the power equation and the regression equation can conservatively use the condition C factor from Figure 15 to account for structural cracking in the base pavement. These are both empirical equations with all the inherent limitations of such equations. However, they are based on protecting the base slab from cracking, and therefore, they use a failure criterion related to the one used in the proposed design procedure.

CONCLUSIONS AND RECOMMENDATIONS

CONCLUSIONS

A proposed new overlay design and analysis procedure has been presented for rigid airport pavements. It predicts pavement deterioration in terms of an SCI varying between 0 and 100. The basis for the procedure is the layered elastic analytical model. Effects of fatigue damage to the base pavement, progressive cracking in the base pavement, and substandard load transfer at the pavement joints are included in the analysis.

The proposed new overlay design procedure required thinner overlays than existing design procedures. This reduction in required thickness is particularly true for thick base pavements that contribute significantly to the structural capacity of the overlay and base pavement system. The difference is mainly caused by the proposed design procedure's improved modeling of the base pavements contribution to the system compared with the existing empirical design procedures.

The proposed new overlay design procedure usually required thicker flexible overlay thicknesses for conditions where the current CE flexible overlay design procedure required up to about 16 in. of flexible overlay. For greater CE required thicknesses, the proposed design method required thinner overlays.

The proposed design procedure predicts pavement performance and therefore requires accurate material, structural condition, and fatigue characterization of the pavement.

The existing CE unbonded rigid overlay design equation is a conservative upper bound to the solutions from the proposed design procedure. Consequently, it remains as a simple conservative design method. The CE partially bonded rigid overlay equation is not conservative, and its continued use is highly questionable and subject to further study.

The proposed design approach using the BISAR computer program is capable of handling any degree of interface condition from frictionless to fully bonded. A fully bonded overlay may have major problems in constructing a satisfactory joint capable of adequate load transfer if a thick overlay is used. Therefore, the fully bonded overlay for airfields is generally limited to a thin overlay of 2 to 5 in. thick to correct surface deficiencies and provide limited structural improvement of the pavement. The limited data on the overlays normally referred to as partially bonded suggest that there is increased friction or bonding which improves their performance compared to unbonded overlays. However, accurately characterizing the appropriate friction level to use in design is difficult.

Models to predict reflective cracking in flexible overlays have not been developed, and therefore, the proposed design approach for flexible overlays protects against additional cracking in the base pavement, fatigue cracking caused by AC tensile strain, and excessive subgrade vertical strain. Consequently, the proposed design approach cannot predict the performance of flexible overlays as it can for rigid overlays or rigid pavements.

The BISAR computer program was used to calculate layered elastic stresses for this study. Other layered elastic computer programs may be used if they provide stress solutions of the same accuracy as the BISAR program. Most of these programs can only handle the fully bonded and unbonded overlays because they lack models for intermediate levels of friction.

The proposed design procedure gives reasonable results and provides general agreement with the available data. However, the data upon which the proposed and existing design procedures are based are very limited. Major efforts are needed to develop new trafficking data and to collect field performance data for overlays.

The proposed design procedure predicts structural deterioration of a pavement from load induced stresses. There are other causes of deterioration in pavements that must be addressed separately.

The proposed design procedure is analytically much more powerful than the existing empirical procedures and allows direct analysis of the effects of a variety of design parameters such as material properties or interface friction. However, load characterization, major simplifications of material properties, and simple assumptions concerning time-dependent effects such as variation in load transfer or temperature are needed to simplify the problem to a point where analytical solutions are feasible. The analytical solutions should be tempered and adjusted with judgment and experience.

RECOMMENDATIONS

The proposed design procedure and the existing overlay design procedures are based on limited data. A program of full-scale test sections and field monitoring of in-service parameters and overlays are needed. Some specific areas that require further work are validating the proposed rigid performance model from in-service pavements, determining if any factors affect the structural deterioration besides the design factor, gathering more data on the effective cracked slab model, validating or improving the load transfer adjustment, determining appropriate friction levels to use in analysis of unbonded and partially bonded overlays, developing other models to include durability and pumping related deterioration, and extending the improved design method to include flexible overlay reflective cracking models.

The proposed design approach should be used to study the optimal point for pavement rehabilitation and to compare rehabilitation strategies (e.g., should an overlay try to protect the base pavement from further cracking or should it be more cost effective to allow the base to crack with a thinner overlay).

The effective cracked slab model should be investigated as a method of designing overlays for crack and seat construction.

A long-term assessment and monitoring of load transfer in rigid airfield pavements are needed to determine the actual values and variability of this parameter.

REFERENCES

1. Ahlvin, R. G., Ulery, H. H., Hutchinson, R., and Rice, J. 1971. "Multiple Wheel Heavy Gear Load Tests," Technical Report S-71-17, US Army Engineer Waterways Experiment Station, Vicksburg, Miss.

2. American Association of State Highway and Transportation Officials (AASHTO). 1986. "AASHTO Guide for Design of Pavement Structures," American Association of State Highway and Transportation Officials, Washington, DC.

3. American Concrete Institute. 1967 (Aug). "Design of Concrete Overlays for Pavements," Title No. 64-80, ACI Journal, Detroit, Mich.

4. _____. 1981. "Considerations for Design of Concrete Structures Subjected to Fatigue Loading," ACI 215R-74 revised 1981, ACI Manual of Concrete Practice, Detroit, Mich.

5. Arms, L., Aaron, H., and Palmer, L. 1958. "Design of Concrete Overlays for Pavements," Proceedings, American Concrete Institute, Vol 55, Detroit, Mich.

6. Barenberg, E. J., and Smith, R. E. 1979. "Longitudinal Joint Systems in Slip-Formed Rigid Pavements, Vol I - Literature Survey and Field Inspection," Report No FAA-RD-79-4-I, Department of Transportation, Federal Aviation Administration, Washington, DC.

7. Barker, W. R., and Brabston, W. N. 1975. "Development of a Structural Design Procedure for Flexible Airport Pavements," Technical Report S-75-17, US Army Engineer Waterways Experiment Station, Vicksburg, Miss.

8. Benture, A., and Mindess, S. 1986. "The Effect of Concrete Strength on Crack Patterns," Cement and Concrete Research, Vol 16, Pergamon Press Ltd., United Kingdom.

9. Brown, D. N., and Thompson, O. O. 1973. "Lateral Distribution of Aircraft Traffic," Miscellaneous Paper S-73-56, US Army Engineer Waterways Experiment Station, Vicksburg, Miss.

10. Burmister, D. M. 1943. "The Theory of Stresses and Displacements in Layered Systems," Proceedings, Highway Research Board, Washington, DC.

11. Bush, A. J. 1980. "Nondestructive Testing for Light Aircraft Pavements; Phase II: Development of the Nondestructive Evaluation Methodology," Report No. FAA-RD-80-9-II, Department of Transporation, Federal Aviation Administration, Washington, DC.

12. Carey, W. N., and Irick, P. E. 1960. "The Pavement Serviceability Performance Concept," Highway Research Bulletin No. 250, Highway Research Board, Washington, DC.

13. Cauwelaert, F. V., Lequeux, M., and Delaunois, P. 1986. "Computer Programs for the Determination of Stresses and Displacements in a Four Layered System with Fixed Bottom," Centre De Recherches De L'Institute Superieur Industriel Catholique Du Hainaw, MONS, Belgium.

14. Chou, Y. T. 1983. "Investigation of the FAA Overlay Design Procedure for Rigid Pavements," Report No. FAA-PM-83-22, Department of Transportation, Federal Aviation Administration, Washington, DC.

15. Chou, Y. T., and Huang, Y. H. 1981. "A Computer Program for Slabs with Discontinuities on Layered Elastic Solids," Second International Conference on Concrete Pavement Design, Purdue University, West Lafayette, Ind.

16. Crawford, J., and Katona, M. 1975. "State-of-the-Art for Predictions of Pavement Response," Contract Report S-75-8, US Army Engineer Waterways Experiment Station, Vicksburg, Miss.

17. Domenichini, L., and Marchionna, A. 1981. "Influence of Stress Range on Plain Concrete Pavement Fatigue Design," Second International Conference on Concrete Pavement Design, Purdue University, West Lafayette, Ind.

18. Dorman, G. M. and Klomp, A. G. J. 1964. "Stress Distribution and Dynamic Testing in Relation to Road Design," Shell Bitumin No. 18, Shell Oil Company, London, U.K.

19. Grau, R. W. 1979. "Evaluation of Drilled and Grouted-In-Place Dowels for Load Transfer of Portland Cement Concrete, Tyndall Air Force Base, Florida," Technical Report GL-79-11, US Army Engineer Waterways Experiment Station, Vicksburg, Miss.

20. Green, J. L. 1978. "Literature Review - Elastic Constants for Airport Pavement Design," Report No. FAA-RD-76-138, Department of Transportation, Federal Aviation Administration, Washington, DC.

21. Hammitt, G. M. 1974. "Concrete Strength Relationships," Miscellaneous Paper S-74-30, US Army Engineer Waterways Experiment Station, Vicksburg, Miss.

22. Harr, M. E. 1977. Mechanics of Particulate Media, A Probabilistic Approach, McGraw-Hill, Inc., N.Y.

23. Headquarters, Department of the Army. 1958. "Rigid Airfield Pavements," EM 1110-45-303, Washington, DC.

24. _____. 1979. "Rigid Pavements for Airfields Other Than Army," Technical Manual 5-824-3/AFM 88-6, Chapter 3, Washington DC.

25. Headquarters, Department of the Navy. 1973. "Airfield Pavements," Design Manual NAVFAC DM-21, Washington, DC.

26. _____. 1985. "Condition Survey Procedures, Navy and Marine Corps Airfield Pavements," NAFAC Interim Guide, Naval Facilities Engineering Command, Alexandria, Va.

27. Heukelom, W., and Klomp, A. 1964. "Road Design and Dynamic Loading," Proceedings, Association of Asphalt Paving Technologists, Vol 33.

28. HoSang, V. A. 1975. "Field Survey and Analysis of Aircraft Distribution on Airport Pavements," Report No. FAA-RD-74-36, Department of Transportation, Federal Aviation Administration, Washington, DC.

29. Huang, Y. H. 1985. "A Computer Package for Structural Analysis of Concrete Pavements," Third International Conference on Concrete Pavement Design and Rehabilitation, Purdue University, West Lafayette, Ind.

30. Huang, Y. H., and Wang, S. T. 1973. "Finite Element Analysis of Concrete Pavements and Its Implication for Rigid Pavement Design," Highway Research Record No. 466, Transportation Research Board, Washington, DC.

31. Hutchinson, R. 1982. "Resurfacing with Portland Cement Concrete," Synthesis of Highway Practice, No. 99, Transportation Research Board, Washington, DC.

32. Hutchinson, R., and Wathen, T. 1962. "Strengthening Existing Airport Pavements," Air Transport Journal, Vol 88, AT1, American Society of Civil Engineers, New York.

33. Hutchinson, R., and Vedros, P. 1977. "Performance of Heavy-Load Portland Cement Concrete (Rigid) Airfield Pavements," First International Conference on Concrete Pavement Design, Purdue University, West Lafayette, Ind.

34. Ioannides, A. M., Thompson, M. R., and Barenberg, E. J. 1985a. "The Westergaard Solutions Reconsidered," 1985 Annual Conference of the Transportation Research Board, Washington, DC.

35. _____. 1985b. "Finite Element Analysis of Slabs-on-Grade Using a Variety of Support Models," Third International Conference on Concrete Pavement Design and Rehabilitation, Purdue University, West Lafayette, Ind.

36. Jones, A. 1962. "Tables of Stresses in Three-Layered Elastic Systems," Highway Research Bulletin No. 342, Highway Research Board, Washington, DC.

37. Jong, D. L. D., Peutz, M. G. F., and Korswagen, A. R. 1973. "Computer Program BISAR, Layered Systems Under Normal and Tangential Surface Loads," External Report AMSR 0006.73, Kloninklÿke/Shell Laboratorium, Amsterdam, Netherlands.

38. Kesler, C. 1970. "Fatigue and Fracture of Concrete," Lecture No. 8, Stanton Walker Lecture Series on the Materials Sciences, National Sand and Gravel Association/National Ready Mixed Concrete Association, Silver Springs, Md.

39. Kohn, S. 1985. "Evaluation of the FAA Design Procedures for High Traffic Volume Rigid Pavements," Third International Conference on Concrete

Pavement Design and Rehabilitation, Purdue University, West Lafayette, Ind.

40. Kreger, W. C. 1967. "Computerized Aircraft Ground Flotation Analysis-Edge Loaded Rigid Pavement," EER-FW-572, General Dynamics, Fort Worth, Tex.

41. Lambiotte, D. 1972. "Airfield Pavement Evaluation, Royal Thai Navy Station, Ban U-Tapao Airfield, Thailand," Technical Note N-1244, Naval Civil Engineering Laboratory, Port Hueneme, Calif.

42. Lambiotte, D., and Chapman, M. 1969. "Airfield Pavement Evaluation, Royal Thai Navy Station, Ban U-Tapao Airfield, Thailand," Technical Note N-1058, Naval Civil Engineering Laboratory, Port Hueneme, Calif.

43. Ledbetter, R. H. 1976. "Pavement Response to Aircraft Dynamic Loads; Compendium," Technical Report S-75-11, Vol III, US Army Engineer Waterways Experiment Station, Vicksburg, Miss.

44. Lyons Associates, Inc. 1982. "Pavement Study: Upgrade of Runway 13-31, US Naval Support Facility, Diego Garcia, B.I.O.T.," Prepared for US Navy under USN Contract No. N62742-82-C-0007.

45. Majidzadeh, K., Ilves, G. J., and Skylut, H. 1985. "RISC - A Mechanistic Method of Rigid Pavement Designs," Third International Conference on Concrete Pavement Design and Rehabilitation, Purdue University, West Lafayette, Ind.

46. Martin, R. 1973. "Design Considerations for Resurfacing Pavements with Concrete," Highway Research Record, No. 434, Highway Research Board, Washington, DC.

47. Mellinger, F. 1963. "Structural Design of Concrete Overlays," Title No. 60-15, Journal, Vol 60, No. 2, American Concrete Institute, Detroit, Mich.

48. Mellinger, F. and Sale, J. 1956. "The Design of Non-Rigid Overlays for Concrete Airfield Pavement," Journal of the Air Transport Division, Vol 82, No. A72, American Society of Civil Engineers, N.Y.

49. Miner, M. 1945. "Cumulative Damage in Fatigue," Transactions, Vol 67, American Society of Mechanical Engineers, N.Y.

50. Monismith, C. L., Yuce, R., and Finn, F. N. 1981. "Investigation of Overlays for Rigid Pavement," (in preparation) US Army Engineer Waterways Experiment Station, Vicksburg, Miss.

51. Ohio River Division Laboratories. 1946. "Lockbourne No. 1 Test Track, Final Report," US Army Corps of Engineers, Mariemont, Ohio.

52. _____. 1950. "Lockbourne No. 2; Experimental Mat: Final Report," US Army Corps of Engineers, Mariemont, Ohio.

53. Ohio River Division Laboratories. 1954. "Minutes of the Meeting of the Board of Consultants to Review the Military Investigation Program of the Rigid Pavement Laboratory, 24, 25 August 1954," US Army Corps of Engineers, Mariemont, Ohio.

54. _____. 1959a. "Minutes of the Meeting of the Board of Consultants, Joint Conference on Military Investigational Program, 12 February 1959," US Army Corps of Engineers, Mariemont, Ohio.

55. _____. 1959b. "Field Tests of Doweled Joint Performance," US Army Corps of Engineers, Mariemont, Ohio.

56. Older, C. 1924. "Highway Research in Illinois," Transactions, Vol 87, American Society of Civil Engineers, N.Y.

57. Packard, R. G. 1984. "Computer Program for Airport Pavement Design," Portland Cement Association, Skokie, Ill.

58. _____. 1973. "Design of Concrete Airport Pavement," Engineering Bulletin 050.03P, Portland Cement Association, Skokie, Ill.

59. Parker, F., Barker, W., Gunkel, R, and Odom, E. 1979. "Development of a Structural Design Procedure on Rigid Airport Pavements," Technical Report GL-79-4, US Army Engineer Waterways Experiment Station, Vicksburg, Miss.

60. Peutz, M. G. F., Kempen, H. P. M. V., and Jones, A. 1968. "Layered Systems Under Normal Surface Loads," Highway Research Record, No. 228, Highway Research Board, Washington, DC.

61. Philippe, R. R. 1948. "Use of Reinforcement in Concrete Pavement," Proceedings, Vol 28, Highway Research Board, Washington, DC.

62. Pickett G., and Ray, G. 1951. "Influence Charts for Concrete Pavements," Transactions, Vol 116, American Society of Civil Engineers, N.Y.

63. Rollings, R. S. 1981. "Corps of Engineers Design Procedures for Rigid Airfield Pavements," Second International Conference on Concrete Pavement Design, Purdue University, West Lafayette, Ind.

64. _____. 1985. "Review of Rigid Airfield Design," Pavement Design Seminar, University of New South Wales, Duntroon, Australia.

65. Sale, J., and Hutchinson, R. 1959. "Development of Rigid Pavement Design Criteria for Military Airfields," Journal of the Air Transport Division, Vol 85, AT3, American Society of Civil Engineers, N.Y.

66. Sawan, J. S., and Darter, M. I. 1979. "Structural Design of PCC Shoulders," Transportation Research Record, No. 725, Washington, DC.

67. Schiffman, Robert L. 1962. "General Analysis of Stresses and Displacements in Layered Elastic Systems," International Conference on the Structural Design of Asphalt Pavements, University of Michigan, Ann Arbor, Mich.

68. Scrivner, F. 1962. "Structural Deterioration of Test Pavements: Rigid," The AASHO Road Test, Special Report 73, Highway Research Board, Washington, DC.

69. Shahin, M., Darter, M., and Kohn, S. 1976. "Development of a Pavement Maintenance Management System, Vol I: Airfield Pavement Condition Rating," Technical Report No. AFCEC-TR-76-27, US Air Force Civil Engineering Center, Tyndall Air Force Base, Fla.

70. _____. 1977a. "Development of a Pavement Maintenance Management System, Vol III: Maintenance and Repair Guidelines for Airfield Pavements," CEEDO TR-77-44, US Air Force Civil and Environmental Engineering Development Office, Tyndall Air Force Base, Fla.

71. _____. 1977b. "Development of a Pavement Maintenance Management System, Vol V: Proposed Revision of Chapter 3, AFR93-5," Technical Report No. CEEDO-TR-77-44, US Air Force Civil and Environmental Engineering Development Office, Tyndall Air Force Base, Fla.

72. Smith, R. E., Palmier, R. P., Darter, M. I., and Lytton, R. L. 1986. "Pavement Overlay Design Procedures and Assumptions," FHWA/RD-85/006TU008, three volumes, Federal Highway Administration, Washington, DC.

73. Tayabji, S., and Okamoto, P. 1985. "Thickness Design of Concrete Resurfacing," Third International Conference on Concrete Pavement Design and Rehabilitation, Purdue University, West Lafayette, Ind.

74. Tepfers, R. 1979 (Aug). "Tensile Fatigue Strength of Plain Concrete," Journal, American Concrete Institute, Detroit, Mich.

75. Tepfers, R., and Kutti, T. 1979 (May). "Fatigue Strength of Plain, Ordinary and Lightweight Concrete," Journal, American Concrete Institute, Detroit, Mich.

76. Terzaghi, K. 1955. "Evaluation of Coefficients of Subgrade Reaction," Geotechnique, Vol 5, No. 4, United Kingdom.

77. Treybig, H., McCullough, B., Smith, P, and Quintus, H. V. 1977. "Overlay Design and Reflection Cracking Analysis for Rigid Pavements: Vol 1, Development of New Design Criteria," Report No. FHWA-RD-77-6, Vol 1, Federal Highway Administration, Washington, DC.

78. US Army Engineer Rigid Pavement Laboratory. 1943. "Final Report on the Dynamic Loading of Concrete Test Slabs - Wright Field Slab Tests," US Army Corps of Engineers, Mariemont, Ohio.

79. US Department of Transportation, Federal Aviation Administration. 1978. "Airport Pavement Design and Evaluation," Advisory Circular 150/5320-6C, Washington, DC.

80. _____. 1980. "Procedure for Condition Survey of Civil Airports," Report No. FAA-RD-80-55, Department of Transportation, Federal Aviation Administration, Washington, DC.

81. Vesic, A. S., and Saxena, S. K. 1969. "Analysis of Structural Behavior of Road Test Rigid Pavements," Highway Research Record, No. 291, Highway Research Board, Washington, DC.

82. Westergaard, H. M. 1926. "Stresses in Concrete Pavements Computed by Theoretical Analysis," Public Roads, Vol 7, No. 2, Pork Ridge, Ill.

83. _____. 1948. "New Formulas for Stresses in Concrete Pavements of Airfields," Transactions, Vol 113, American Society of Civil Engineers, N.Y.

84. Witczak, M. W. 1976. "Pavement Performance Models: Repeated Load Fracture of Pavement Systems," Contract Report S-76-15, Vol I, US Army Engineer Waterways Experiment Station, Vicksburg, Miss.

85. Witczak, M. W., Uzan, J., and Johnson, M. 1983. "Development of Probabilistic Rigid Pavement Design Methodologies for Military Airfields," Technical Report GL-83-18, US Army Engineer Waterways Experiment Station, Vicksburg, Miss.

BIBLIOGRAPHY

Burns, C. D., Rone, C. L., Brabston, W. N., and Ulery, H. H. 1974. "Comparative Performance of Structural Layers in Pavement Systems," Technical Report S-74-8, US Army Engineer Waterways Experiment Station, Vicksburg, Miss.

Grau, R. W. 1972. "Strengthening of Keyed Longitudinal Construction Joints in Rigid Pavements," Miscellaneous Paper S-72-43, US Army Engineer Waterways Experiment Station, Vicksburg, Miss.

Huntington District. 1951. "Specifications for Constructions of Overlay Test Track, Sharonville Engineer Depot, Sharonville, Ohio," US Army Corps of Engineers, Huntington, W. Va.

_____. 1953. "Specification for Construction of Overlay Test Track No. 2," US Army Corps of Engineers, Huntington, W. Va.

_____. 1957. "Specifications for Construction of Heavy Load Test Tracks at Sharonville, Ohio," US Army Corps of Engineers, Huntington, W. Va.

Ohio River Division Laboratories. 1944. "Design and Construction Report Lockbourne Test Track," US Army Corps of Engineers, Mariemont, Ohio.

_____. No date. "Lockbourne No. 1, Test Track Lockbourne Army Air Base-Photographs," US Army Corps of Engineers, Mariemont, Ohio.

_____. 1945. "Report of Reconstruction Lockbourne Test Track," US Army Corps of Engineers, Mariemont, Ohio.

_____. 1950. "Final Report Lockbourne No. 2 Experimental Mat," US Army Corps of Engineers, Mariemont, Ohio.

_____. 1954. "Overlay Test Track, Sharonville, Ohio, Report of Construction," US Army Corps of Engineers, Mariemont, Ohio.

_____. No date. "Photographs of Sharonville No. 1 and 2," US Army Corps of Engineers, Mariemont, Ohio.

_____. No date. "Overlay Test Track, Sharonville, Representative Photographs," US Army Corps of Engineers, Mariemont, Ohio.

_____. 1958. "Ohio River Division Laboratory Participation in Joint Conference on Military Investigational Programs," US Army Corps of Engineers, Mariemont, Ohio.

_____. 1959. "Weekly Progress Reports 20 Feb 1957 - Sept 1959," US Army Corps of Engineers, Mariemont, Ohio.

_____. 1961. "Heavy-Load Test Tracks, Report of Construction," Technical Report 4-17, US Army Corps of Engineers, Mariemont, Ohio.

US Army Engineer Waterway Experiment Station. 1953. "Subgrade Preparation for Overlay Test Track No. 2, Sharonville, Ohio," US Army Corps of Engineers, Vicksburg, Miss.

Walthen, T. R. 1959. "Heavy Load Investigation Consultants Briefing," Ohio River Division Laboratories, US Army Corps of Engineers, Mariemont, Ohio.

APPENDIX A

CORPS OF ENGINEERS RIGID PAVEMENT

TEST SECTION DATA

Table A1

Material Properties for Lockbourne No. 1 Test Sections

Item	Concrete Surface			Base Course			Subgrade		
	h, in.	E × 10^6 lb/in.^{2}	h in.	Type	E lb/in.^{2a}	ν	Type	E lb/in.^{2a}	ν
A 1.60	5.72	3.8	--	--	--	--	Silty clay	16,000	0.4
A 2.60	5.72	3.8	--	--	--	--	Silty clay	16,000	0.4
B 1.66L	5.50	3.8	6	Loose gravel	6,700	0.3	Silty clay	9,500	0.4
B 2.66L	5.50	3.8	6	Loose gravel	6,700	0.3	Silty clay	9,500	0.4
C 1.66S	5.50	3.8	6	Sand	10,000	0.3	Silty clay	4,900	0.4
C 2.66S	5.50	3.8	6	Sand	10,000	0.3	Silty clay	4,900	0.4
D 1.66	5.50	3.8	6	Sand and gravel	10,000	0.3	Silty clay	4,900	0.4
D 2.66	5.50	3.8	6	Sand and gravel	10,000	0.3	Silty clay	4,900	0.4
E 1.66M	5.75	3.8	6	Crushed stone	18,000	0.3	Silty clay	6,000	0.4
E 2.66M	5.75	3.8	6	Crushed stone	18,000	0.3	Silty clay	6,000	0.4
F 1.80	7.75	3.8	--	--	--	--	Silty clay	4,100	0.4
F 2.80	7.75	3.8	--	--	--	--	Silty clay	4,100	0.4
K 1.100	9.44	3.8	--	--	--	--	Silty clay	8,200	0.4
K 2.100	9.44	3.8	--	--	--	--	Silty clay	8,200	0.4

(Continued)

[a]Estimated from Log E = 1.415 + 1.284 log k = modulus of subgrade reaction.[57]

Table A1 (Concluded)

Item	Concrete Surface			Base Course			Subgrade		
	h, in.	$E \times 10^6$ lb/in.^{2}	h in.	Type	E lb/in.^{2}	ν	Type	E lb/in.^{2}	ν
N 1.86	8.0	3.8	6	Sand and gravel	10,000	0.3	Silty clay	4,900	0.4
N 2.86	8.0	3.8	6		10,000	0.3	Silty clay	4,900	0.4
O 1.06	9.46	3.8	6	Sand and gravel	10,000	0.3	Silty clay	4,900	0.4
O 2.06	9.46	3.8	6	Sand and gravel	10,000	0.3	Silty clay	4,900	0.4
P 1.812	7.58	3.8	12	Sand and gravel	15,000	0.3	Silty clay	3,200	0.4
P 2.812	7.58	3.8	12	Sand and gravel	15,000	0.3	Silty clay	3,200	0.4
Q 1.1012	9.44	3.8	12	Sand and gravel	15,000	0.3	Silty clay	3,900	0.4
Q 2.1012	9.44	3.8	12	Sand and gravel	15,000	0.3	Silty clay	3,900	0.4
R 1.612	5.88	3.77	60	Sand and gravel	59,800	0.3	Silty clay	5,800	0.4
R 2.612	5.67	3.53	60	Sand and gravel	59,800	0.3	Silty clay	5,800	0.4
S 1.66	5.83	3.77	66	Sand and gravel	55,800	0.3	Silty clay	5,800	0.4
S 2.66	5.69	3.53	66	Sand and gravel	55,800	0.3	Silty clay	5,800	0.4
T 1.60	5.63	3.77	72	Sand and gravel	51,800	0.3	Silty clay	5,800	0.4
T 2.60	5.68	3.53	72	Sand and gravel	51,800	0.3	Silty clay	5,800	0.4
U 1.60	5.83	3.8	72	Sand	23,000	0.3	Silty clay	5,800	0.4
U 2.60	5.83	3.8	72	Sand	23,000	0.3	Silty clay	5,800	0.4

Table A2

Performance for Lockbourne No. 1 Test Sections

Item	Coverages	SCI	C_O [a]	C_F [b]	Slabs Analyzed	Load kip Single Wheel Load (SWL)
A 1.60	18	80	13	59	NE, SE	37
	59	0				
	94	0				
A 2.60	294	93	225	10,084	SE	20
	520	78				
B 1.66L	14	55	3	96	NW, SW	37
	56	13				
	91	3				
	225	0				
B 2.66L	76	86	59	522	SW	20
	298	42				
	388	0				
C 1.66S	15	93	13	92	NE, SE	37
	56	23				
	91	2				
	225	0				
C 2.66S	78	78	54	599	SE	20
	300	42				
	390	17				
	526	0				
D 1.66	20	55	6	104	NW, SW	37
	56	28				
	91	0				

(Continued)

[a] Calculated onset of deterioration, DF = 0.5234 + 0.3924 Log C_o.

[b] Calculated absolute failure (SCI = 0) DF = 0.2967 + 0.3881 Log C_F. DF = design factor = flexural strength ÷ calculated stress.

(Sheet 1 of 4)

Table A2 (Continued)

Item	Coverages	SCI	C_O	C_F	Slabs Analyzed	Load kip Single Wheel Load (SWL)
D 2.66	300	100	289	3,776	SE	20
	390	86				
	526	78				
E 1.66M	21	100	50	212	NE, SE	37
	57	100				
	92	45				
	226	0				
E 2.66M	556	100	--	--	SE	20
F 1.80	111	55	70	195	NW, SW	37
	195	0				
	287	0				
F 2.80	550	100	--	--		20
K 1.100	412	78	259	1,995	NW, SW	37
	722	44				
	982	42				
	1,482	12				
K 2.100	42	42	1	1,435	SW	60
	722	12				
	982	0				
N 1.86	107	100	105	284	NW, SW	37
	191	36				
	283	3				
N 2.86	6	100	6	32	NW, SW	60
	16	39				
	32	0				
O 1.06	418	93	347	1,606	NE, SE	37
	728	45				
	988	27				
	1488	11				

(Continued)

(Sheet 2 of 4)

Table A2 (Continued)

Item	Coverages	SCI	C_0	C_F	Slabs Analyzed	Load kip Single Wheel Load (SWL)
O 2.06	42	100	41	155	NE, SE	60
	80	45				
	138	11				
	205	0				
P 1.812	106	100	--	--	NW, SW	37
	272	93				
	1,148	0				
P 2.812	6	42	--	--	NW, SW	60
	190	0				
Q 1.1012	457	100	--	--	NE, SE	37
	988	100				
	1,487	93				
Q 2.1012	42	100	36	209	NE, SE	60
	80	5				
	138	13				
	205	13				
R 1.612	105	100	217	557	NW, SW	37
	262	80				
	492	13				
	1,022	0				
R 2.612	1.5	58	1.0	4.2	NW, SW	60
	19	26				
	42	0				
S 1.66	90	93	222	549	NE, SE	37
	271	78				
	497	11				
	1,027	0				
S 2.66	1.5	25	1.0	42	NE, SE	60
	19	17				
	42	0				

(Continued)

Table A2 (Concluded)

Item	Coverages	SCI	C_O	C_F	Slabs Analyzed	Load kip Single Wheel Load (SWL)
T 1.60	87	86	215	559	NW, SW	37
	268	77				
	494	13				
	1,184	0				
T 2.60	19	100	19	137	NW, SW	60
	42	58				
	138	0				
U 1.60	81	100	123	488	NE, SE	37
	262	45				
	488	0				
U 2.60	1.5	12	1.0	42	NE, SE	60
	19	2				
	42	0				

Table A3

Material Properties for Lockbourne No. 2 Test Section and Modification

	Concrete Surface			Base Course			Subgrade		
Item	h, in.	$E \times 10^6$ lb/in.^{2}	h in.	Type	$E \times 10^3$ lb/in.^{2} [a]	ν	Type	$E \times 10^3$ lb/in.^{2} [a]	ν
E-2	15	4.0	72	Sand and gravel	16,000	0.3	Silty clay	6,600	0.4
E-6	20.26	4.0	--	--	--	--	Silty clay	9,300	0.4
M 1	12	4.12	--	--	--	--	Silty clay	4,400	0.4
M 2	15	4.12	--	--	--	--	Silty clay	4,400	0.4
M 3	20	4.12	--	--	--	--	Silty clay	4,400	0.4

[a] Estimated from Log E = 1.415 + 1.285 log k = modulus of subgrade reaction.[57]

Table A4

Performance for Lockbourne No. 2 Test Section and Modification

Item	Coverages	SCI	C_O [a]	C_F [b]	Slabs Analyzed	Load
E-2	1,430	78	1,280	2,241	D 10.150	150-kip SWL
	2,023	16				
E-6	500	98	1,040	52,554	F and G 7.20; F, G, H, I, and J 8.2	150-kip SWL
	1,000	96				
	1,430	91				
	1,725	89				
	2,023	82				
M 1	125	91	93	353	R, S, and Q 0.120, 1.120, and 2.120	150-kip twin-tandem
	144	83				Wheel Spacing: 31.25 × 62.75
	150	57				
	154	56				
	169	49				
	188	35				
	235	18				
	324	15				
	384	0				

(Continued)

[a] Calculated onset of deterioration DF = 0.5234 + 0.3920 Log C_o.

[b] Calculated absolute failure (SCI = 0) DF = 0.2967 + 0.3881 log C_F. DF = Design Factor = flexural strength ÷ calculated stress.

Table A4 (Concluded)

Item	Coverages	SCI	C_O	C_F	Slabs Analyzed	Load
M 2	29	95	1,693	6,774	U and V 0.150, 1.150, and 2.150	150-kip twin-tandem
	1,500	92				
	2,000	88				
	2,204	81				
M 3	2,204	100	--	--	X and Y 0.200, 1.200 and 2.200	150-kip twin-tandem

Table A5

Material Properties for Sharonville Heavy Load and Multiple Wheel Heavy Gear Load Tests

Item	Concrete Surface		Base Course			Subgrade		
	h, in.	$E \times 10^6$ lb/in.^{2}	h in.	Type	$E \times 10^3$ lb/in.^{2} [a]	Type	$E \times 10^3$ lb/in.^{2} [a]	ν
72	28	4.2	4	Sand	Not modeled	CL-CH clay	6,000	0.4
73	24	4.2	4	Sand	Not modeled	CL-CH clay	6,000	0.4
1-C5	10	6.0	--	--	--	CH clay	7,500	0.4
2-C5	12	6.0	--	--	--	CH clay	7,500	0.4
2-DT	12	6.0	--	--	--	CH clay	7,500	0.4
3-C5	14	6.0	--	--	--	CH clay	7,500	0.4
3-DT	14	6.0	--	--	--	CH clay	7,500	0.4
4-C5	8	6.0	--	--	--	CH clay	7,500	0.4

[a] Estimated from Log E = 1.415 + 1.284 log k = modulus of subgrade reaction.[57]

Table A6

Performance for Sharonville Heavy Load and Multiple Wheel Heavy Gear Load Tests

Item	Coverages	SCI	C_O [a]	C_F [b]	Load
72	1,000	85	420	147,210	325-kip twin-tandem
	1,260	82			
	1,440	79			Tire spacing 31.25 × 62.75 in.
	3,700	63			
73	1,000	89	668	7,054	325-kips twin-tandem
	1,200	68			
	1,650	58			
	2,115	55			
1-C5	112	92	150	936	360-kip
	192	85			12-wheel C-5 gear assembly
	251	81			
	288	56			
	592	26			
2-DT	40	93	128	476	166-kip dual-tandem
	150	86			
	290	43			Wheel spacing 44 × 58 in.
	410	8			
3-DT	150	8	177	960	166-kip dual-tandem
	260	78			
	410	45			Wheel spacing 44 × 58 in.
	530	43			
	680	17			
4-C5	180	80	1o5	258	325-kip
	240	16			12-wheel C-5 gear assembly

[a] Calculated onset of deterioration DF = 0.5234 + 0.3924 Log C_o.

[b] Calculated absolute failure (SCI = 0) DF = 0.2967 + 0.3881 Log C_F. DF = design factor = flexural strength ÷ calculated stress.

Table A7

Material Properties for Keyed Longitudinal Joint Study and Soil Stabilization Pavement Study

	Concrete Surface		Base Course				Subgrade		
Item	h, in.	$E \times 10^6$ lb/in.^{2}	h in.	Type	E lb/in.^{2a}	ν	Type	$E \times 10^3$ lb/in.^{2a}	ν
KLJS-1	8	6.0	24	Clayey, gravelly sand	20,000	0.3	CH clay	7,500	0.4
KLJS-2	11	6.0	--	--	--		CH clay	7,500	0.4
KLJS-3	10	6.0	4	Sand	7,500	0.3	CH clay	7,500	0.4
KLJS-4	10	6.0	6	Cement stabilized	250,000	0.2	CH clay	7,500	0.4
SSPS-3	15	6.0	6	Bituminous stabilized	b	0.4	CH clay	7,500	0.4
SSPS-4	15	6.0	6	Cement stabilized	200,000	0.2	CH clay	7,500	0.4

[a] Estimated from Log E = 1.415 + 1.284 log k = modulus of subgrade reaction.[57]
[b] E = 200,00 in Lane 1 under 200-kip gear load.
E = 100,000 in Lane 2 under 240-kip gear load.

Table A8

Performance for Keyed Longitudinal Joint Study and Soil Stabilization Pavement Study

Item	Coverages	SCI	C_O [a]	C_F [b]	Load
KLJS 1-C5	54	68	16	683	360-kip
	144	38			C-5 gear assembly
	344	30			
	504	0			
KLJS 3-C5	144	85	292	783	360-kip
	344	80			C-5 gear assembly
	504	52			
	688	9			
KLJS 3-C5	22	80	11	395	360-kip
	116	45			C-5 gear assembly
	164	15			
	364	3			
KLJS 4-DT	320	78	228	1094	166-kip dual-tandem
	630	34			
	880	23			
	950	1			
SSPS 3-200	200	84	937	4258	200-kip dual-tandem
	1770	60			
	2050	52			
	3000	12			
	4460	3			
SSPS 4-200	1770	74	1179	5934	200-kip dual-tandem
	4660	20			
	5220	0			

(Continued)

[a] Calculated onset of deterioration DF = 0.5234 + 0.3924 Log C_o.

[b] Calculated absolute failure (SCI = 0) DF = 0.2967 + 0.3881 Log C_F. DF = design factor = flexural strength ÷ calculated stress.

Table A8 (Concluded)

Item	Coverages	SCI	C_O	C_F	Load
SSPS 4-240	40	80	22	377	240-kip dual-tandem
	100	42			
	200	27			
	350	1			

Table A9

Calculated Stresses and Design Factors

Test Section	Item	Flexural Stress lb/in.^{2}	Layered Elastic Stress, lb/in.^{2}	Design Factor
Lockbourne No. 1	A 1.60	780	599	1.302
	A 2.60	740	405	1.827
	B 1.66 C	780	759	1.028
	B 2.66 C	740	504	1.468
	C 1.66 S	780	853	0.914
	C 2.66 S	740	558	1.326
	D 1.66	780	877	0.889
	D 2.66	740	572	1.294
	E 1.66 M	780	771	1.012
	E 2.66 M	740	505	1.465
	F 1.80	780	625	1.248
	F 2.80	740	396	1.869
	K 1.100	780	410	1.902
	K 2.100	735	570	1.290
	N 1.86	780	560	1.383
	N 2.86	735	785	0.936
	O 1.06	780	458	1.703
	O 2.06	735	647	1.136
	P 1.812	780	632	1.234
	P 2.812	735	883	0.832
	Q 1.1012	780	465	1.677
	Q 2.1012	735	659	1.115
	R 1.612	780	332	2.349
	R 2.612	735	381	1.929
	S 1.66	780	344	2.267
	S 2.66	735	381	1.929
	T 1.60	780	364	2.143
	T 2.60	735	397	1.851
	U 1.60	780	527	1.480

(Continued)

Table A9 (Concluded)

Test Section	Item	Flexural Stress lb/in.^{2}	Layered Elastic Stress, lb/in.^{2}	Design Factor
	U 2.60	735	651	1.129
	E-2	680	574	1.185
	E-6	700	397	1.763
	M 1	725	600	1.208
	M 2	725	446	1.626
	M 3	725	295	2.458
Sharonville heavy load	72	800	319	2.508
	73	800	401	1.995
Multiple wheel	1-C5	725	580	1.250
Heavy gear load	2-C5	800	473	1.691
	2-DT	700	566	1.234
	3-C5	660	396	1.675
	3-DT	700	461	1.518
	4-C5	775	735	1.054
Keyed longitudinal joint study	1-C5	905	656	1.380
	2-C5	730	522	1.399
	3-C5	810	580	1.397
	4-C5	860	522	1.648
	4-DT	860	643	1.338
Soil stabilization pavement study	3-200	900	463	1.944
	4-240	900	564	1.596
	4-200	870	463	1.879
	4-240	870	555	1.568

APPENDIX B

SLAB TEST DATA

Figure B1. Crane and headache ball used to crack slabs

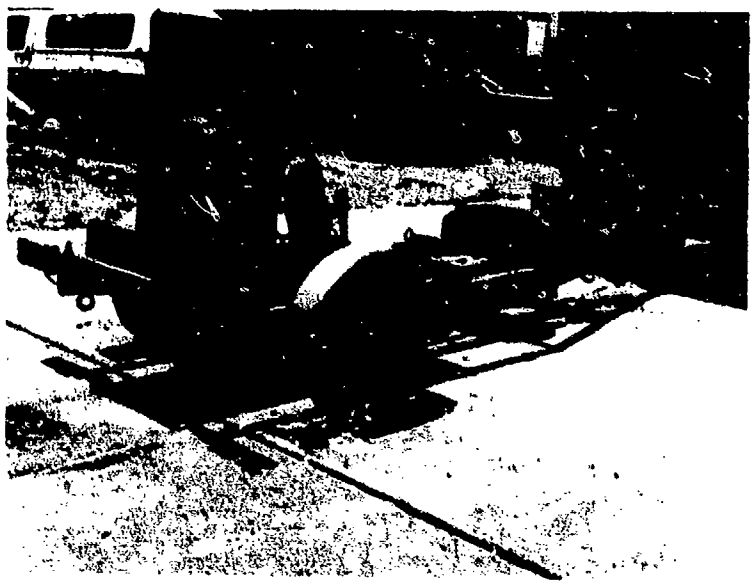

Figure B2. Dynatest falling weight deflectometer, Model 8000

Figure B3. Initial condition, Slab 1

Figure B4. Initial condition, Slab 2

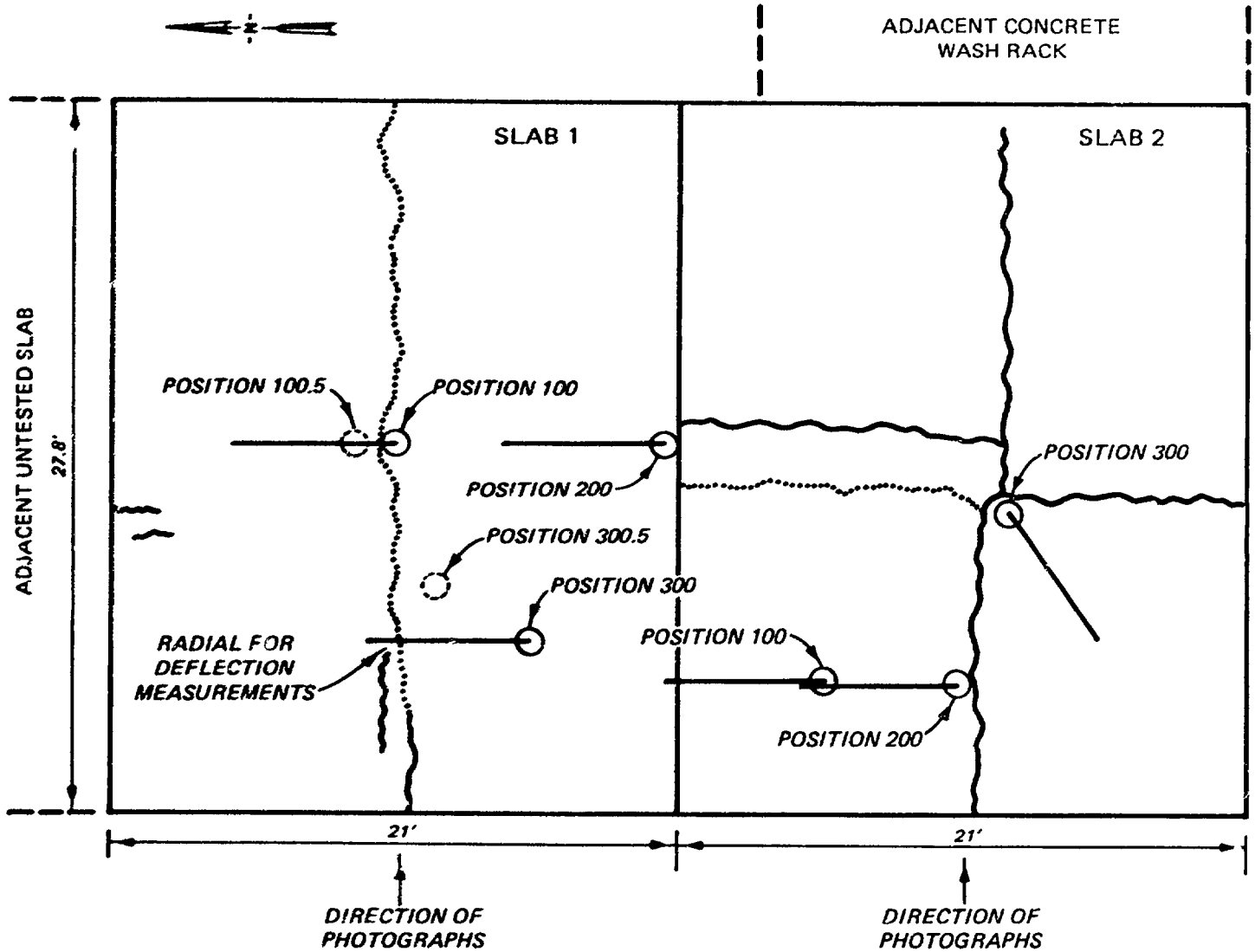

Figure B5. Initial cracking for Slabs 1 and 2

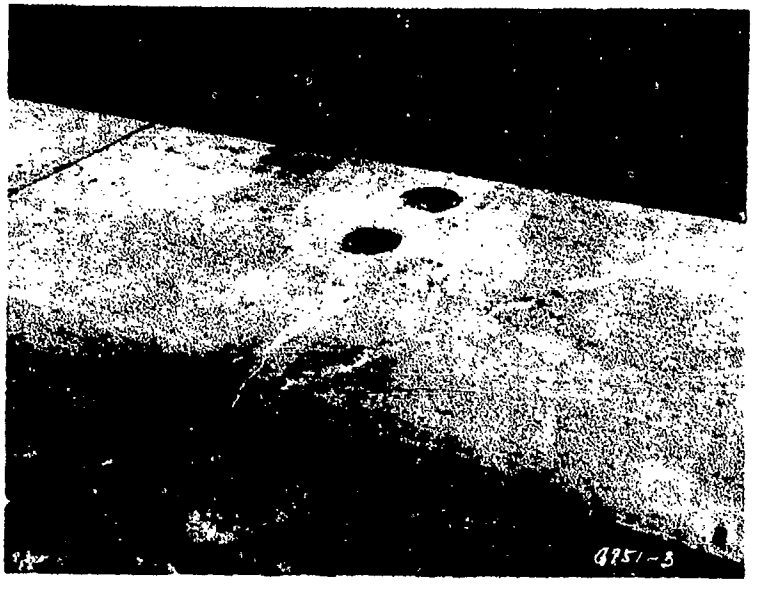

Figure B6. Initial cracking, Slab 1, SCI = 80

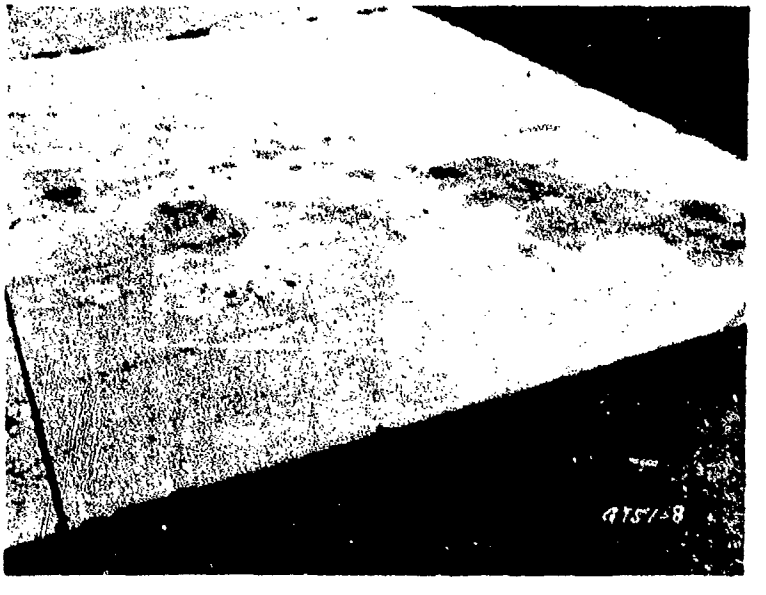

Figure B7. Initial cracking, Slab 2, SCI = 80

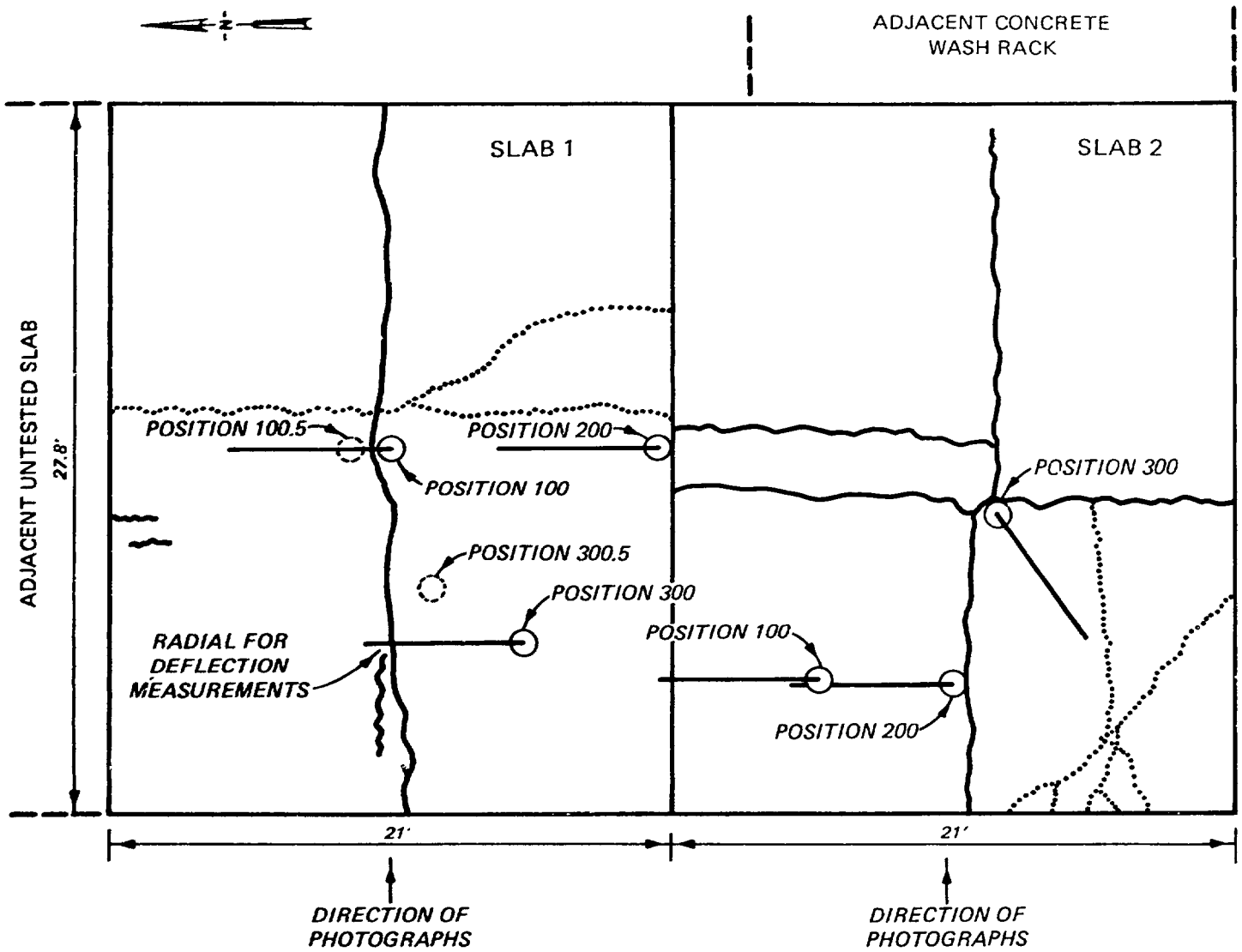

Figure B8. Second cracking for Slabs 1 and 2

Figure B9. Second cracking, Slab 1, SCI = 58

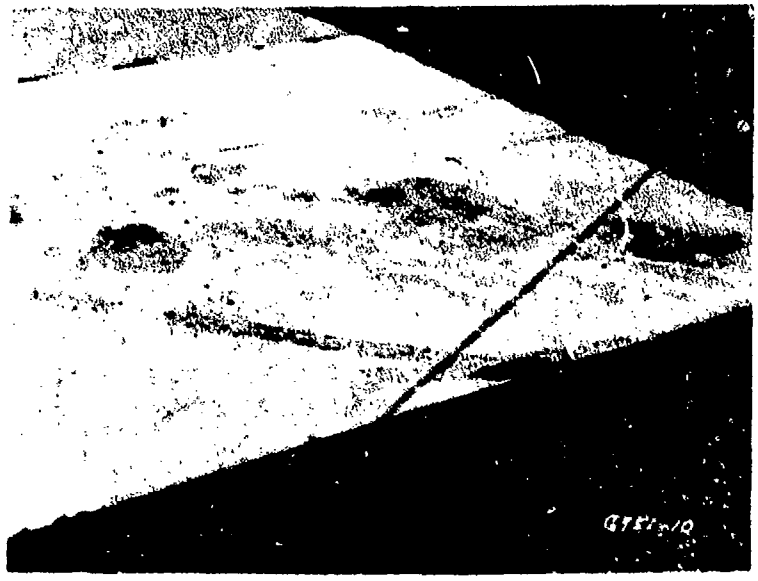

Figure B10. Second cracking, Slab 2, SCI = 80 at position 100

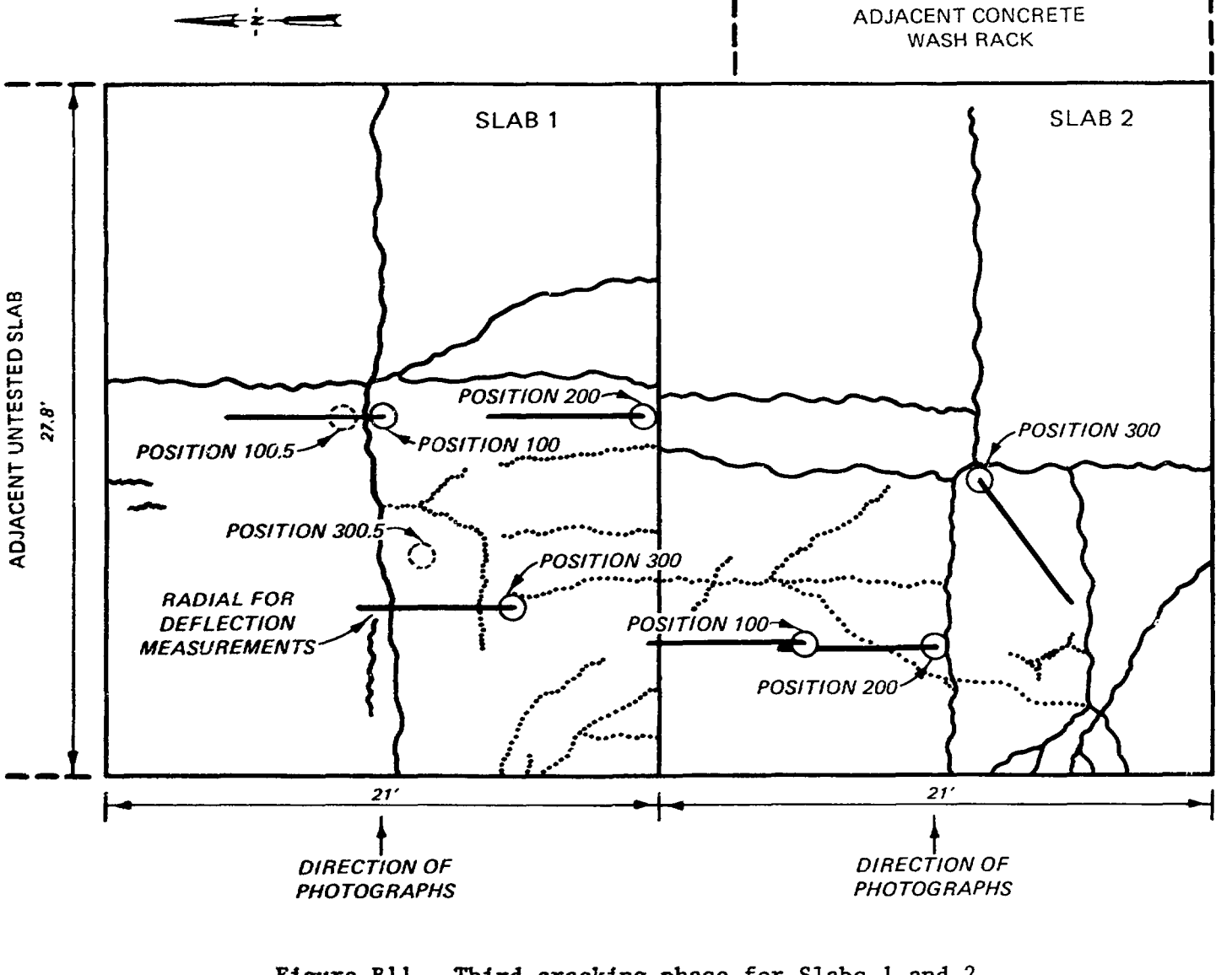

Figure B11. Third cracking phase for Slabs 1 and 2

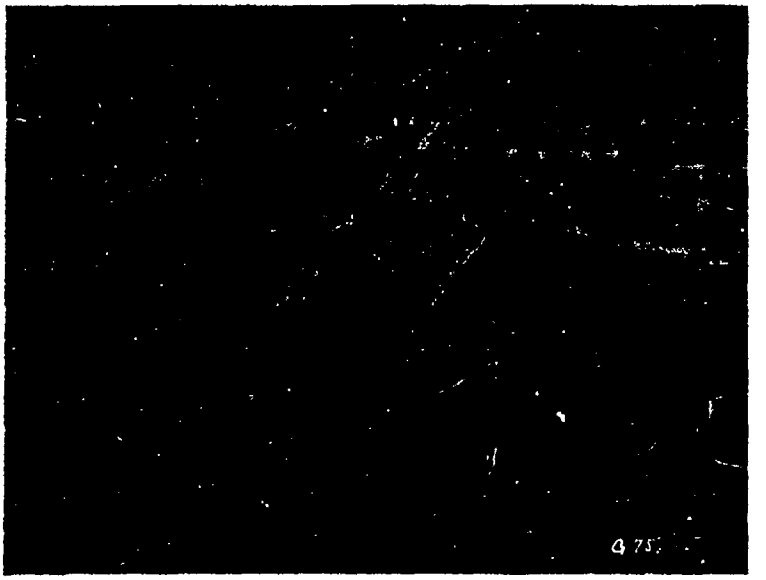

Figure B12. Third cracking, Slab 1, SCI = 23

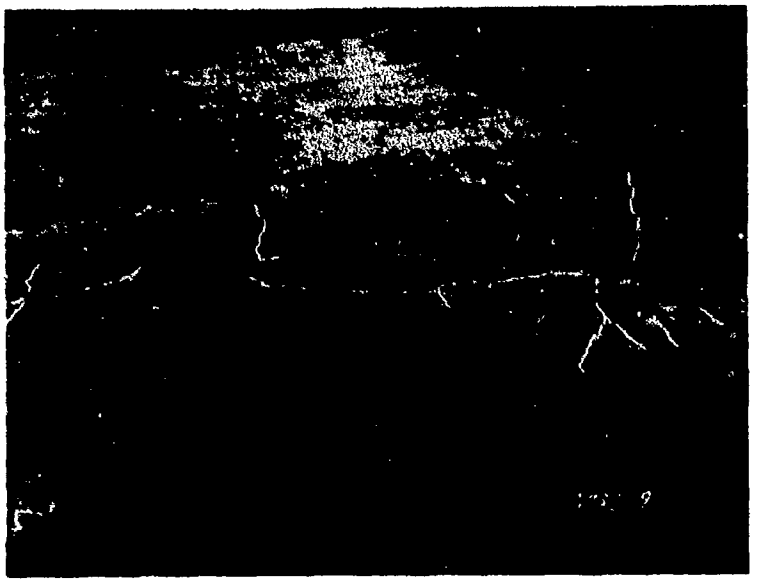

Figure B13. Third cracking, Slab 2, SCI = 39

Figure B14. Fourth cracking, Slab 1, SCI = 0

Figure B15. Slab 1 next morning (additional visible cracks compared with B13)

Figure B16. Fourth cracking, Slab 2, SCI = 23

Figure B17. Initial condition, Slab 3

Figure B18. Initial condition, Slab 4

Figure B19. First cracking, Slab 3, SCI = 39

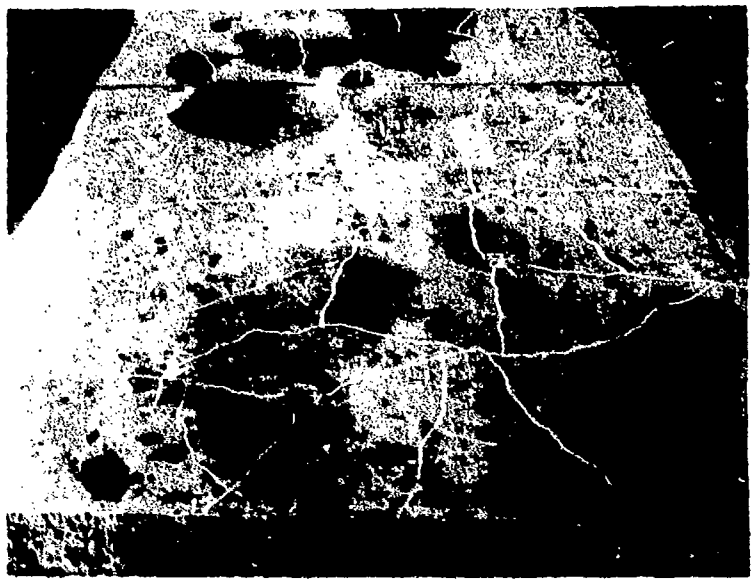

Figure B20. Second cracking, Slab 3, SCI = 23

Figure B21. First cracking, Slab 4, SCI = 58

Figure B22. Second cracking, Slab 4, SCI = 23

Figure B23. Initial conditions, Slab 5

Figure B24. Initial conditions, Slab 6

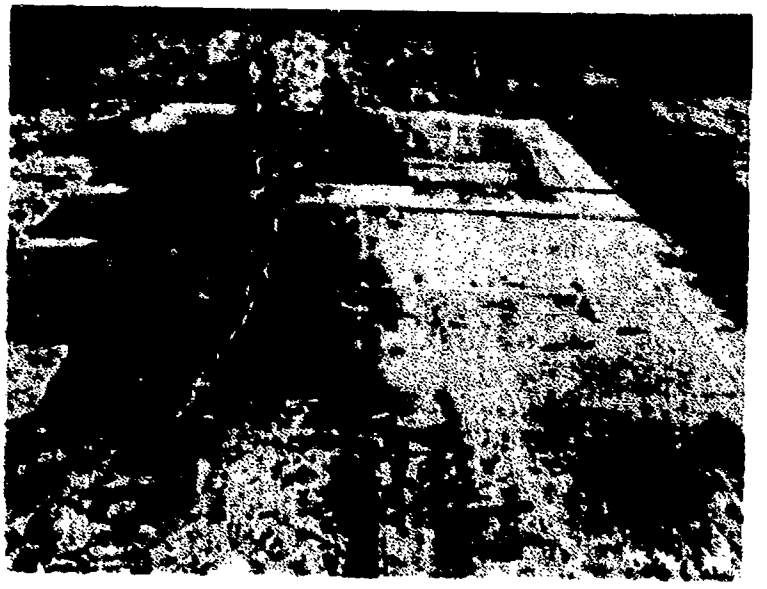

Figure B25. First cracking, Slabs 5 and 6, SCI = 39 and 55

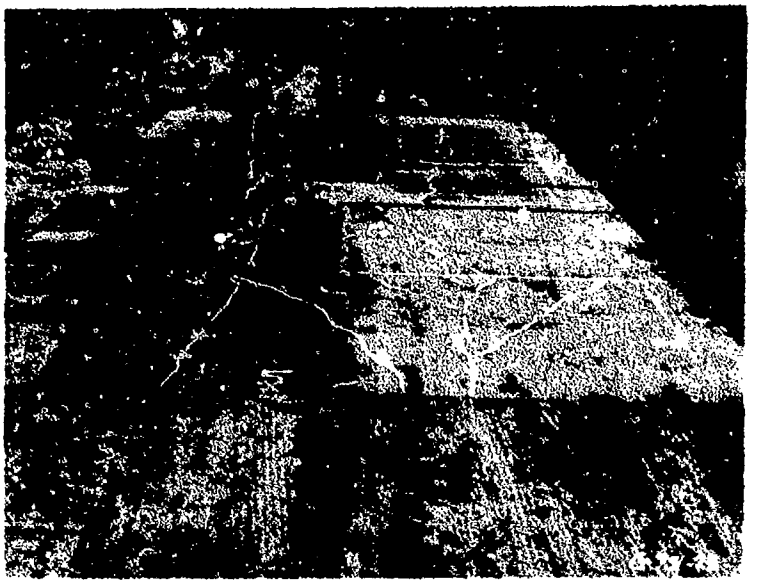

Figure B26. Second cracking, Slabs 5 and 6, SCI = 23

Figure B27. Third cracking, Slabs 5 and 6, SCI = 0

Table B1

Falling Weight Results, Slab 1, Position 100

Position[a]	Load[b] lb	Deflection, × 10^{-3} in.						
		D_0[c]	D_{12}[c]	D_{24}[c]	D_{36}[c]	D_{48}[c]	D_{60}[c]	D_{72}[c]
100	22,278	28.0	24.6	18.9	14.0	10.3	7.7	5.7
100	22,421	26.9	23.6	18.0	13.5	10.0	7.5	5.6
100	22,405	27.1	23.4	18.0	13.5	10.0	7.5	5.6
100	22,437	27.3	23.6	18.0	13.5	10.0	7.5	5.6
101	22,071	45.7	47.2	30.2	20.7	14.1	9.5	6.7
101	22,389	42.7	41.7	28.3	19.4	13.1	9.0	6.3
101	22,357	42.6	40.7	28.3	19.3	13.0	8.9	6.3
101	22,373	42.6	40.4	28.3	19.2	13.0	8.9	6.3
102	13,109	67.2	55.6	31.9	19.0	11.6	7.4	5.0
102	13,109	67.2	55.0	32.0	19.1	11.7	7.4	5.0
102	13,141	67.3	54.8	32.2	19.3	11.7	7.5	5.0
102	13,125	67.2	54.4	32.4	19.2	11.7	7.4	5.0
103	13,093	65.7	56.0	32.2	19.0	11.5	7.7	5.0
103	13,173	64.0	52.2	31.1	18.2	11.1	7.4	4.9
103	13,125	64.4	52.4	31.2	18.2	11.0	7.4	4.9
103	13,093	64.6	52.3	31.3	18.2	10.8	7.3	4.9
104	7,627	79.3[d]	64.0	32.0	16.7	7.2	3.3	2.6
104	7,770	80.9[d]	63.7	32.4	16.8	7.6	3.4	2.6
104	7,818	82.0[d]	65.0	32.5	16.9	7.5	3.4	2.5
104	7,850	83.0[d]	64.4	32.7	17.0	7.5	3.4	2.6
104	8,215	84.9[d]	63.1	29.6	15.3	7.3	3.0	2.5
104	8,326	84.6[d]	63.2	29.9	15.4	7.4	3.1	2.6
104	8,358	85.6[d]	64.3	30.4	15.6	7.4	3.2	2.6
104	8,390	86.5[d]	65.0	30.8	15.7	7.5	3.1	2.6

[a] Third digit in position number shows cracking level (i.e., 100 initial condition, 101 first cracking, and 102 second cracking).
[b] Measured on plate.
[c] Sensor location D_0 at center of plate, D_{12} at 12 in. from center of plate, and D_{24} at 24 in. from center of plate.
[d] Overranged sensor maximum capacity of 75 × 10^{-3} in.

Table B2

Falling Weight Results, Slab 1, Position 100.5

Position[a]	Load[b] lb	Deflection, $\times 10^{-3}$ in.						
		D_0[c]	D_{12}[c]	D_{24}[c]	D_{36}[c]	D_{48}[c]	D_{60}[c]	D_{72}[c]
101.5	22,278	39.7	32.8	23.7	16.8	11.7	8.2	5.9
101.5	22,294	39.2	32.4	23.3	16.6	11.5	8.1	5.8
101.5	22,294	39.4	32.3	23.4	16.6	11.4	8.1	5.8
101.5	22,294	39.4	32.2	23.5	16.6	11.4	8.1	5.8
102.5	13,538	61.8	42.6	26.0	16.1	10.7	6.7	4.6
102.5	13,570	61.5	42.6	26.0	16.1	10.2	6.7	4.6
102.5	13,538	61.7	42.8	26.1	16.2	10.4	6.7	4.6
102.5	13,538	61.9	43.1	26.2	16.3	10.4	6.7	4.6
103.5	13,808	45.5	35.6	22.4	14.4	9.1	6.1	4.3
103.5	13,872	45.2	34.7	22.2	14.2	9.3	6.1	4.4
103.5	13,856	45.4	34.8	22.3	14.1	9.3	6.1	4.4
103.5	13,840	45.5	34.8	22.3	14.3	9.0	6.0	4.3
104.5	7,484	65.6	45.8	25.0	9.1	3.8	3.7	2.8
104.5	7,548	66.5	46.8	25.6	9.3	3.8	3.8	2.8
104.5	7,580	67.0	47.3	25.9	9.4	3.6	3.7	2.8
104.5	7,611	68.1	48.1	26.5	9.6	3.6	3.8	2.9

[a] Third digit in position number shows cracking level (i.e., 100 initial condition, 101 first cracking, and 102 second cracking).
[b] Measured on plate.
[c] Sensor location D_0 at center of plate, D_{12} at 12 in. from center of plate, and D_{24} at 24 in. from center of plate.

Table B3

Falling Weight Results, Slab 1, Position 200

Position[a]	Load[b] lb	Deflection, $\times 10^{-3}$ in.						
		D_0[c]	D_{12}[c]	D_{24}[c]	D_{36}[c]	D_{48}[c]	D_{60}[c]	D_{72}[c]
200	23,025	32.6	26.3	19.6	14.6	9.8	7.9	5.7
200	23,501	31.0	25.0	18.7	14.1	9.6	7.6	5.6
200	23,517	31.5	25.2	18.8	14.0	9.7	7.7	5.6
200	23,470	32.0	25.5	19.0	14.1	9.8	7.6	5.6
201	22,087	48.0	37.0	26.3	18.8	12.5	9.3	6.5
201	22,119	47.5	36.2	25.9	18.4	12.3	9.2	6.5
201	22,119	54.4	36.1	26.1	18.5	12.4	9.3	6.5
201	22,039	48.2	36.2	26.3	18.7	12.4	9.3	6.5
202	13,967	43.5	32.0	21.4	14.8	10.0	6.8	4.9
202	14,047	41.8	30.8	20.6	14.3	9.8	6.1	4.9
202	14,031	42.2	31.1	20.7	15.6	9.8	6.0	5.1
202	14,015	42.4	31.3	20.9	14.4	9.6	5.5	5.4
202	18,369	56.3	41.9	27.8	19.3	12.6	9.1	6.7
202	18,337	57.0	42.6	28.3	19.4	12.7	8.8	6.9
202	18,337	57.8	43.0	28.7	20.7	12.8	9.3	6.9
202	18,369	58.5	43.4	28.9	20.0	13.0	9.4	7.0
202	21,483	67.9	50.4	33.5	22.9	15.7	10.9	8.3
202	21,563	68.6	51.1	33.8	23.6	15.8	11.0	8.3
202	21,563	69.8	51.5	33.9	23.3	16.1	11.1	8.3
202	21,610	70.4	51.7	34.1	23.5	16.1	11.1	8.3
203	18,591	44.3	35.4	24.8	16.1	10.3	7.3	5.4
203	18,639	40.2	32.4	22.2	15.0	9.8	7.1	5.4
203	18,655	40.3	32.3	22.1	15.0	9.4	7.1	5.5
203	18,639	40.6	32.5	22.2	15.0	9.6	7.1	5.5
203	21,388	52.2	42.2	26.3	17.8	11.7	8.4	6.5
203	21,420	51.9	40.2	26.7	16.7	10.3	6.9	6.3
203	21,404	52.6	41.9	26.9	17.6	12.2	8.5	6.2
203	21,356	53.0	41.1	27.0	17.7	12.3	8.5	6.1

(Continued)

[a] Third digit in position number shows cracking level (i.e., 100 initial condition, 101 first cracking, and 102 second cracking).
[b] Measured on plate.
[c] Sensor location D_0 at center of plate, D_{12} at 12 in. from center of plate, and D_{24} at 24 in. from center of plate.

Table B3 (Concluded)

Position	Load lb	Deflection, $\times 10^{-3}$ in.						
		D_0	D_{12}	D_{24}	D_{36}	D_{48}	D_{60}	D_{72}
204	8,374	19.3	17.8	14.2	9.8	6.1	3.7	2.6
204	8,453	18.9	17.5	14.0	9.8	6.1	3.7	2.7
204	8,422	18.9	17.5	14.0	9.8	6.1	3.7	2.8
204	8,422	19.0	17.6	14.1	9.8	6.1	3.7	2.8
204	14,094	35.2	31.9	24.8	16.9	10.4	6.4	4.8
204	14,158	35.0	31.9	24.6	16.8	10.4	6.5	5.0
204	14,142	35.2	32.0	24.8	16.9	10.4	6.5	5.0
204	14,142	35.4	32.3	24.8	16.9	10.4	6.5	5.0
204	21,515	59.3	54.1	40.2	27.4	16.4	10.2	8.1
204	21,595	59.2	53.0	40.2	27.4	16.1	2.8	8.3
204	21,610	59.5	53.1	39.9	27.6	14.9	8.6	8.4
204	21,595	59.8	53.5	41.4	27.2	15.1	8.1	8.4
204	13,475	65.4	48.3	29.2	13.5	7.4	4.8	7.2
204	13,522	65.0	47.8	29.3	13.6	7.6	4.8	4.8
204	13,554	65.2	47.9	29.4	13.8	7.5	4.9	5.2
204	13,554	65.2	47.9	29.4	13.9	7.6	4.9	4.9

Table B4

Falling Weight Results, Slab 1, Position 300

Position[a]	Load[b] lb	Deflection, × 10^{-3} in.						
		D_0[c]	D_{12}[c]	D_{24}[c]	D_{36}[c]	D_{48}[c]	D_{60}[c]	D_{72}[c]
300.0	21,912	30.4	26.6	20.2	15.3	11.2	8.2	6.0
300.0	21,976	30.2	26.0	20.0	14.9	11.0	8.1	5.9
300.0	21,992	30.4	26.2	20.0	14.9	11.0	8.7	5.9
300.0	21,992	30.6	26.2	20.0	14.9	11.0	8.1	5.9
301.0	22,262	35.4	33.7	26.3	20.0	14.1	10.3	4.8
301.0	22,262	34.5	32.8	25.7	19.6	13.9	10.2	4.2
301.0	22,167	34.6	33.1	25.9	19.6	14.0	10.1	4.0
301.0	22,055	34.7	33.3	26.0	19.6	14.1	10.1	2.1
302.0	21,849	36.5	35.7	27.5	20.7	14.8	10.6	7.7
302.0	21,912	36.4	33.5	26.5	20.2	14.4	10.3	7.8
302.0	21,896	37.1	33.2	26.4	20.0	14.4	10.1	7.7
302.0	21,881	36.9	33.1	26.5	20.2	14.4	10.3	7.8
303.0	21,642	66.3	57.8	42.6	29.6	18.7	11.1	7.8
303.0	21,817	61.7	55.7	40.3	29.1	18.1	11.3	8.1
303.0	21,833	61.6	53.9	40.6	27.9	18.0	11.3	8.1
303.0	21,849	61.6	51.2	40.9	27.9	18.1	11.3	8.1
304.5	7,595	43.2	36.1	19.0	11.4	7.8	5.3	3.4
304.5	7,627	43.3	35.8	18.8	11.2	7.7	5.3	3.5
304.5	7,675	44.0	36.6	19.2	11.4	7.8	5.4	3.5
304.5	7,691	44.3	37.1	19.3	11.4	7.9	5.3	3.4
304.0	8,088	60.3	42.1	21.1	11.7	6.2	3.4	2.6
304.0	8,120	60.5	42.2	21.3	11.8	6.3	3.4	2.7
304.0	8,136	60.6	42.3	21.3	11.9	6.3	3.5	2.7
304.0	8,120	60.5	42.2	21.3	11.8	6.3	3.4	2.7
304.5	8,072	38.8	34.4	16.6	9.5	6.5	4.8	3.2
304.5	8,088	38.7	34.1	16.8	9.6	6.7	4.8	3.2
304.5	8,024	38.9	34.5	17.1	9.7	6.7	4.8	3.2
304.5	8,009	39.2	34.9	17.2	9.8	6.7	4.8	3.2
304.5	13,220	75.6	66.7	35.1	18.9	12.6	8.5	5.7
304.5	13,205	75.7	66.2	35.4	19.0	12.6	8.6	5.7
304.5	13,220	75.9	66.3	35.2	19.1	12.6	8.7	5.7
304.5	13,220	76.1	67.0	35.4	19.3	12.8	8.7	5.8

[a] Third digit in position number shows cracking level (i.e., 100 initial condition, 101 first cracking, and 102 second cracking).
[b] Measured on plate.
[c] Sensor location D_0 at center of plate, D_{12} at 12 in. from center of plate, and D_{24} at 24 in. from center of plate.

Table B5

Falling Weight Results, Slab 2, Position 100

Position[a]	Load[b] lb	Deflection, × 10^{-3} in.						
		D_0[c]	D_{12}[c]	D_{24}[c]	D_{36}[c]	D_{48}[c]	D_{60}[c]	D_{72}[c]
100	22,246	26.7	24.2	19.4	14.9	10.9	7.6	5.4
100	22,246	26.0	23.4	18.8	14.5	10.7	7.5	5.5
100	22,294	26.1	23.5	18.9	14.6	10.7	7.6	5.5
100	22,278	26.2	23.5	18.9	14.6	10.7	7.6	5.6
1,000	23,025	26.3	24.2	19.1	14.9	11.5	9.0	6.8
1,000	23,009	26.3	23.8	18.9	14.8	11.6	9.0	6.8
1,000	22,913	26.3	23.7	19.0	14.9	11.6	9.0	6.9
1,000	22,897	26.4	23.6	19.1	15	11.5	9.0	6.9
101	22,516	30.2	27.0	21.9	17.1	12.8	9.5	7.1
101	22,484	29.5	26.3	21.5	16.7	12.6	9.4	7.2
101	22,389	29.6	26.4	21.5	16.8	12.6	9.5	7.2
101	22,357	29.6	26.4	21.5	16.8	12.6	9.5	7.2
102	22,135	32.6	31.1	22.6	17.6	13.2	9.8	7.4
102	22,135	30.2	27.8	22.3	17.4	13.0	9.8	7.4
102	22,151	30.2	27.6	22.3	17.4	13.0	9.8	7.5
102	22,135	30.2	27.4	22.3	17.4	13.1	9.7	7.4
103	21,706	52.8	48.8	34.3	25.1	17.9	12.4	8.9
103	21,896	49.7	43.9	32.8	24.1	17.2	12.2	9.1
103	21,896	49.6	43.9	32.7	24.1	17.3	12.3	9.2
103	21,881	49.7	43.9	32.8	24.1	17.2	12.3	9.3
104	21,769	61.1	49.9	34.1	23.2	15.5	10.4	7.7
104	21,881	57.0	47.0	32.8	22.7	15.3	10.6	8.0
104	21,881	56.9	46.7	32.9	22.7	15.5	10.7	8.1
104	21,896	57.1	46.9	33.1	22.8	15.6	10.7	8.1

[a] Third digit in position number shows cracking level (i.e., 100 initial condition, 101 first cracking, and 102 second cracking).

[b] Measured on plate.

[c] Sensor location D_0 at center of plate, D_{12} at 12 in. from center of plate, and D_{24} at 24 in. from center of plate.

Table B6

Falling Weight Results, Slab 2, Position 200

Position[a]	Load[b] lb	Deflection, × 10^{-3} in.						
		D_0[c]	D_{12}[c]	D_{24}[c]	D_{36}[c]	D_{48}[c]	D_{60}[c]	D_{72}[c]
200	22,516	28.8	24.2	19.4	15.5	10.7	8.7	6.6
200	22,548	27.1	24.1	19.3	15.2	10.8	8.7	6.7
200	22,437	27.2	24.0	19.2	15.1	11.5	8.7	6.7
200	22,389	27.4	24.1	19.3	15.2	11.5	8.7	6.7
2,000	22,818	28.4	27.4	19.6	15.0	10.9	8.5	6.4
2,000	22,850	27.0	24.9	19.7	15.0	11.1	8.6	6.5
2,000	22,802	26.7	25.0	19.6	15.0	11.2	8.6	6.5
2,000	22,770	26.1	26.1	19.6	15.0	11.3	8.6	6.5
201	22,500	30.0	26.1	20.7	16.2	12.2	9.2	6.9
201	22,453	29.4	25.6	20.4	16.1	12.2	9.3	7.0
201	22,532	29.4	25.8	20.4	16.1	12.3	9.3	7.0
201	22,580	29.4	25.6	20.6	16.2	12.4	9.3	7.0
202	22,754	34.3	29.4	23.1	17.9	13.5	10.1	7.5
202	22,723	33.3	28.3	22.4	17.3	13.1	9.8	7.2
202	22,611	33.4	28.2	22.4	17.3	13.1	9.8	7.3
202	22,564	33.5	28.5	22.4	17.3	13.1	9.8	7.3
203	21,769	61.2	53.6	40.7	29.8	21.5	15.0	10.7
203	21,896	58.4	50.7	39.8	29.3	21.5	15.4	11.0
203	21,928	58.7	50.7	40.4	29.4	21.6	15.5	11.1
203	21,896	58.9	50.9	39.8	29.5	21.6	15.6	11.1
204	18,432	51.5	45.0	33.5	24.3	16.2	11.5	7.9
204	18,575	49.4	43.5	32.0	23.4	14.8	11.3	7.8
204	18,560	49.6	42.0	31.9	23.4	13.8	11.4	7.8
204	18,560	49.8	42.9	32.0	23.5	13.0	11.5	7.8
204	21,753	60.2	50.6	41.1	28.1	19.9	13.6	9.4
204	21,785	59.6	50.9	39.1	28	19.9	13.7	9.4
204	21,785	59.9	51.3	38.6	28.3	20.0	13.7	9.5
204	21,769	60.2	51.2	38.8	28.4	20.0	13.7	9.5

[a] Third digit in position number shows cracking level (i.e., 100 initial condition, 101 first cracking, and 102 second cracking).
[b] Measured on plate.
[c] Sensor location D_0 at center of plate, D_{12} at 12 in. from center of plate, and D_{24} at 24 in. from center of plate.

Table B7

Falling Weight Results, Slab 2, Position 300

Position[a]	Load[b] lb	Deflection, × 10^{-3} in.						
		D_0[c]	D_{12}[c]	D_{24}[c]	D_{36}[c]	D_{48}[c]	D_{60}[c]	D_{72}[c]
300	22,357	30.6	25.2	19.6	15.1	10.4	8.7	6.5
300	22,421	27.7	24.6	19.0	14.8	9.4	8.5	6.4
300	22,421	27.9	24.2	19.1	14.8	9.3	8.5	6.4
300	22,437	28.0	24.4	19.1	15.0	10.6	8.5	6.5
3,000	22,405	27.8	24	18.9	14.7	11.3	8.3	6.3
3,000	22,516	27.4	23.7	18.9	13.8	9.7	8.2	6.3
3,000	22,532	27.4	23.5	18.3	14.1	8.9	8.3	6.3
3,000	22,532	27.5	23.9	18.0	14.1	9.8	8.2	6.0
301	22,024	42.9	37.2	25.4	18.6	13.5	9.9	7.4
301	22,230	41.0	34.1	24.3	17.8	13.0	9.7	7.2
301	22,278	41.2	33.5	24.2	17.7	12.9	9.6	7.1
301	22,325	41.5	33.4	24.3	17.7	13.0	9.6	7.2
302	21,372	61.0	58.3	47.3	38.3	30.2	24.6	17.8
302	21,563	57.7	54.1	44.8	36.4	28.9	23.3	17.1
302	21,626	60.3	53.9	45.0	36.7	28.8	23.3	17.2
302	21,626	58.1	53.7	45.0	37.1	28.4	23.4	17.2
303	21,007	80.2	74.6	62.8	50.5	35.1	25.6	17.2
303	21,181	75.1	69.7	59.3	49.4	36.2	26.3	17.8
303	21,197	75.7	69.8	59.8	50.0	38.9	26.3	18.0
303	21,102	76.1	70.5	60.3	50.4	39.4	26.5	18.1
303	18,226	66.0	61.7	53.9	43.8	33.2	23.8	16.0
303	18,242	66.1	62.3	53.0	44.2	33.6	24.1	16.1
303	18,210	66.1	61.5	53.1	44.3	33.1	24.0	16.1
303	18,242	66.3	61.5	53.2	44.4	32.8	24.1	16.2
304	21,245	76.7	71.5	59.1	43.6	24.8	16.0	10.5
304	21,420	72.6	69.6	58.2	44.3	51.4	16.9	11.0
304	21,404	73.2	69.6	59.4	45.5	27.3	17.2	11.1
304	21,404	73.6	70.3	59.7	45.7	28.0	17.0	11.0

[a] Third digit in position number shows cracking level (i.e., 100 initial condition, 101 first cracking, and 102 second cracking).
[b] Measured on plate.
[c] Sensor location D_0 at center of plate, D_{12} at 12 in. from center of plate, and D_{24} at 24 in. from center of plate.

Table B8

Falling Weight Results, Slab 3, Position 100

Position[a]	Load[b] lb	Deflection, $\times 10^{-3}$ in.						
		D_0[c]	D_{12}[c]	D_{24}[c]	D_{36}[c]	D_{48}[c]	D_{60}[c]	D_{72}[c]
100	22,802	21.2	19.9	15.7	12.0	8.3	6.5	4.8
100	22,993	21.0	19.1	15.4	11.9	6.9	6.5	4.8
100	22,977	21.1	19.2	15.5	12.0	7.0	6.5	4.8
100	23,009	21.1	19.1	15.7	11.9	7.4	6.5	4.8
101	22,659	30.0	34.7	19.8	14.6	10.3	7.5	5.2
101	22,786	28.8	28.8	19.2	14.2	10.1	7.3	5.2
101	22,786	28.7	28.5	19.2	14.2	10.1	7.3	5.2
101	22,786	28.6	28.5	19.1	14.2	10.1	7.3	5.2
102	22,325	41.4	43.7	26.3	19.7	14.0	9.9	6.7
102	22,437	38.7	39.3	23.8	18.0	13.1	9.4	6.4
102	22,421	38.6	38.9	24.0	17.4	13.0	9.3	6.4
102	22,437	38.6	38.8	22.4	17.4	12.9	9.2	6.3

[a] Third digit in position number shows cracking level (i.e., 100 initial condition, 101 first cracking, and 102 second cracking).
[b] Measured on plate.
[c] Sensor location D_0 at center of plate, D_{12} at 12 in. from center of plate, and D_{24} at 24 in. from center of plate.

Table B9

Falling Weight Results, Slab 3, Position 200

Position[a]	Load[b] lb	Deflection, × 10^{-3} in.						
		D_0[c]	D_{12}[c]	D_{24}[c]	D_{36}[c]	D_{48}[c]	D_{60}[c]	D_{72}[c]
200	21,944	37.6	29.5	20.4	13.8	9.6	7.0	5.2
200	22,437	38.6	29.9	20.7	14.1	9.6	7.0	5.1
200	22,405	39.8	30.5	21.0	14.3	9.6	7.1	5.0
200	22,437	40.7	31.0	21.4	14.4	9.6	7.2	5.2
201	13,713	65.9	36.6	17.8	8.3	5.6	4.6	3.6
201	13,729	65.6	36.7	17.7	8.3	5.9	4.7	3.7
201	13,761	65.6	36.1	16.8	8.6	5.1	4.7	3.7
201	13,729	65.6	36.2	17.0	8.5	5.9	4.7	3.7
202	13,634	68.3	38.2	18.0	9.6	5.3	4.4	3.7
202	13,650	69.4	38.2	18.3	9.9	5.5	4.5	3.7
202	13,618	68.0	38.0	18.3	9.6	5.5	4.4	3.6
202	13,618	67.9	38.0	18.4	9.7	5.5	4.4	3.6

[a] Third digit in position number shows cracking level (i.e., 100 initial condition, 101 first cracking, and 102 second cracking).
[b] Measured on plate.
[c] Sensor location D_0 at center of plate, D_{12} at 12 in. from center of plate, and D_{24} at 24 in. from center of plate.

Table B10

Falling Weight Results, Slab 3, Position 300

Position[a]	Load[b] lb	Deflection, × 10^{-3} in.						
		D_0[c]	D_{12}[c]	D_{24}[c]	D_{36}[c]	D_{48}[c]	D_{60}[c]	D_{72}[c]
300	22,580	28.8	26.1	18.0	12.1	8.5	6.6	4.9
300	22,659	28.3	24.6	16.7	12.1	7.8	6.6	5.0
300	22,611	28.4	24.5	17.1	12.7	8.3	6.7	5.0
300	22,627	28.4	24.9	17.3	12.0	8.1	6.7	5.0
301	22,389	37.5	32.4	21.7	13.9	9.2	6.5	4.7
301	22,468	35.9	30.9	21.1	13.5	9.1	6.6	4.9
301	22,421	36.0	30.4	21.1	13.4	9.1	6.7	4.9
301	22,389	36.3	30.7	20.9	13.5	9.1	6.6	4.9
302	22,246	47.9	45.0	27.2	14.1	9.2	7.2	5.5
302	22,310	44.0	40.2	25.4	14.0	9.4	7.4	5.6
302	22,294	44.4	39.8	25.3	14.1	9.5	7.5	5.7
302	22,278	44.8	39.7	25.0	14.1	9.6	7.5	5.7

[a] Third digit in position number shows cracking level (i.e., 100 initial condition, 101 first cracking, and 102 second cracking).
[b] Measured on plate.
[c] Sensor location D_0 at center of plate, D_{12} at 12 in. from center of plate, and D_{24} at 24 in. from center of plate.

Table B11

Falling Weight Results, Slab 4, Position 100

Position[a]	Load[b] lb	Deflection, x 10^{-3} in.						
		D_0[c]	D_{12}[c]	D_{24}[c]	D_{36}[c]	D_{48}[c]	D_{60}[c]	D_{72}[c]
100	22,850	18.0	16.0	12.9	10.1	7.4	5.9	4.3
100	22,961	17.8	15.9	12.8	10.0	7.6	5.8	4.3
100	22,929	17.8	15.9	12.8	10.0	7.6	5.8	4.3
100	22,897	17.9	15.9	12.8	10.0	7.6	5.9	4.4
101	22,310	38.0	32.4	22.9	16.3	11.2	8.1	5.4
101	22,532	35.5	29.3	22.0	15.6	10.7	7.9	5.3
101	22,516	35.4	28.9	21.6	15.5	10.7	7.8	5.2
101	22,516	35.4	28.8	21.5	15.5	10.6	7.8	5.2
102	21,912	50.1	45.0	28.4	16.7	10.7	7.9	5.7
102	21,928	46.8	40.9	27.4	16.3	10.4	7.8	5.7
102	21,912	46.8	40.6	27.4	16.3	10.4	7.8	5.7
102	21,912	46.8	40.6	27.4	16.1	10.4	7.8	5.7

[a] Third digit in position number shows cracking level (i.e., 100 initial condition, 101 first cracking, and 102 second cracking).
[b] Measured on plate.
[c] Sensor location D_0 at center of plate, D_{12} at 12 in. from center of plate, and D_{24} at 24 in. from center of plate.

Table B12

Falling Weight Results, Slab 4, Position 200

Position[a]	Load[b] lb	Deflection, × 10^{-3} in.						
		D_0[c]	D_{12}[c]	D_{24}[c]	D_{36}[c]	D_{48}[c]	D_{60}[c]	D_{72}[c]
200	22,246	51.4	38.9	25.0	16.1	10.4	6.9	5.0
200	22,310	51.3	38.5	24.7	16.1	10.4	7.0	5.0
200	22,262	52.0	38.9	24.6	16.3	10.6	7.0	5.0
200	22,262	52.4	38.8	24.6	16.4	10.6	7.0	5.1
201	21,499	72.4	52.7	32.1	16.8	11.5	8.0	5.4
201	21,674	66.7	47.7	29.6	15.8	11.0	7.9	5.6
201	21,595	66.4	47.7	29.7	15.7	10.9	7.8	5.7
201	21,610	66.8	48.1	29.8	15.5	10.9	7.9	5.6
202	18,051	74.9	53.2	29.3	9.9	5.6	4.6	4.1
202	18,115	74.0	52.6	29.6	10.1	5.8	4.6	4.1
202	18,051	75.9	52.7	29.7	10.0	5.8	4.3	4.0
202	18,115	75.2	53.1	29.9	10.2	5.8	4.3	4.1

[a] Third digit in position number shows cracking level (i.e., 100 initial condition, 101 first cracking, and 102 second cracking).
[b] Measured on plate.
[c] Sensor location D_0 at center of plate, D_{12} at 12 in. from center of plate, and D_{24} at 24 in. from center of plate.

Table B13

Falling Weight Results, Slab 4, Position 300

Position[a]	Load[b] lb	Deflection, × 10^{-3} in.						
		D_0[c]	D_{12}[c]	D_{24}[c]	D_{36}[c]	D_{48}[c]	D_{60}[c]	D_{72}[c]
300	22,818	20.7	18.3	14.1	10.6	7.3	5.8	4.4
300	22,770	20.4	18.0	14.0	10.5	7.5	5.7	4.4
300	22,770	20.5	17.9	14.1	10.6	7.5	5.8	4.4
300	22,739	20.6	17.9	14.0	10.6	7.6	5.8	4.4
301	22,484	23.6	20.9	16.3	12.1	8.7	6.2	4.7
301	22,580	22.8	20.2	15.8	11.8	8.5	6.2	4.7
301	22,564	22.7	20.2	15.8	11.8	8.5	6.2	4.8
301	22,468	22.8	20.1	15.8	11.8	8.5	6.3	4.8
302	21,960	40.2	37.2	26.3	16.1	9.2	6.1	4.7
302	21,976	35.2	31.7	23.8	15.2	9.2	6.3	4.8
302	21,960	35.1	31.5	23.9	15.1	8.9	6.3	4.8
302	22,008	35.2	31.5	23.7	15.2	8.9	6.3	4.9

[a] Third digit in position number shows cracking level (i.e., 100 initial condition, 101 first cracking, and 102 second cracking).
[b] Measured on plate.
[c] Sensor location D_0 at center of plate, D_{12} at 12 in. from center of plate, and D_{24} at 24 in. from center of plate.

Table B14

Falling Weight Results, Slab 5, Position 100

Position[a]	Load[b] lb	Deflection, × 10^{-3} in.						
		D_0[c]	D_{12}[c]	D_{24}[c]	D_{36}[c]	D_{48}[c]	D_{60}[c]	D_{72}[c]
100	20,371	4.3	4.0	3.7	3.3	3.0	2.6	2.3
100	20,466	4.2	4.0	3.7	3.3	3.0	2.6	2.4
100	20,419	4.3	4.0	3.7	3.3	2.9	2.6	2.3
100	20,419	4.3	4.0	3.7	3.3	3.0	2.6	2.4
1,000	21,213	4.8	4.3	3.9	3.5	3.1	2.7	2.3
1,000	21,134	4.6	4.2	3.8	3.4	3.0	2.6	2.3
1,000	21,150	4.6	4.2	3.8	3.4	3.0	2.6	2.3
1,000	21,118	4.4	4.3	3.8	3.4	3.0	2.6	2.2
101	20,482	9.4	8.2	7.0	5.8	4.8	3.9	2.9
101	20,546	9.1	8.0	6.[illegible]	5.6	4.5	3.8	2.8
101	20,466	9.1	8.0	6.9	5.7	4.6	3.8	2.8
101	20,562	9.2	8.0	6.9	5.8	4.7	3.8	2.9
102	20,721	13.7	11.2	9.4	7.8	5.9	4.9	3.6
102	20,784	13.1	10.7	9.0	7.5	5.9	4.8	3.5
102	20,641	12.9	10.6	9.0	7.4	5.4	4.7	3.4
102	20,530	14.6	10.5	9.0	7.4	5.2	4.7	3.4
1,020	20641	13.6	15.4	9.8	8.1	6.6	5.1	3.8
1,020	20705	13.5	15.3	9.8	8.1	6.5	5.1	3.8
1,020	20689	13.7	15.4	9.8	8.1	6.5	5.2	3.8
1,020	20641	13.8	15.6	9.8	8.1	6.5	5.1	3.8
103	20053	29.7	34.7	14.1	9.4	7.5	5.8	4.4
103	20069	27.6	31.9	13.3	9.3	7.5	5.9	4.5
103	20021	27.6	31.7	13.2	9.3	7.5	5.9	4.5
103	20069	27.7	31.7	13.2	9.2	7.4	5.9	4.5

[a] Third digit in position number shows cracking level (i.e., 100 initial condition, 101 first cracking, and 102 second cracking).
[b] Measured on plate.
[c] Sensor location D_0 at center of plate, D_{12} at 12 in. from center of plate, and D_{24} at 24 in. from center of plate.

Table B15

Falling Weight Results, Slab 5, Position 200

Position[a]	Load[b] lb	Deflection, × 10^{-3} in.						
		D_0[c]	D_{12}[c]	D_{24}[c]	D_{36}[c]	D_{48}[c]	D_{60}[c]	D_{72}[c]
200	22,071	10.1	8.5	7.4	6.4	5.1	4.4	3.5
200	22,214	9.9	8.4	7.5	6.5	4.4	4.0	3.5
200	22,071	7.2	8.4	7.6	6.5	4.8	3.5	2.3
200	21,881	7.3	8.4	7.6	6.4	4.9	3.5	3.1
2,000	20,435	9.4	8.3	7.2	6.2	5.3	4.5	3.5
2,000	20,816	9.3	8.1	7.0	6.1	4.9	4.5	3.5
2,000	20,736	9.2	8.1	7.1	6.1	5.2	4.4	3.5
2,000	20,768	9.2	8.1	7.0	6.1	5.2	4.3	3.5
201	20,657	16.8	14.2	11.5	8.8	6.5	4.6	3.5
201	20,625	16.3	13.9	11.1	8.6	6.4	4.6	3.6
201	20,625	16.3	13.8	11.1	8.6	6.3	4.6	3.7
201	20,657	16.4	13.9	11.2	8.6	6.4	4.6	3.7
202	20,403	23.8	19.6	15.7	12.0	8.3	5.3	3.9
202	20,530	22.3	18.6	14.8	11.4	8.1	5.3	4.1
202	20,450	22.3	18.6	14.8	11.4	8.0	5.3	4.1
202	20,498	22.4	18.7	14.8	11.4	8.1	5.5	4.1
2,020	20,180	22.2	18.7	13.5	10.8	7.1	4.4	4.0
2,020	20,498	22.2	18.1	14.0	10.8	7.1	4.4	4.3
2,020	20,546	22.3	18.5	14.6	10.7	7.2	4.4	4.3
2,020	20,546	22.4	18.5	14.6	10.7	7.2	4.4	4.4
203	19,386	64.2	49.4	28.9	16.5	8.7	5.9	3.7
203	19,513	58.0	35.0	28.3	15.7	8.5	6.4	4.5
203	19,449	57.7	41.1	24.5	15.4	9.2	6.7	4.6
203	19,449	57.4	42.2	27.0	15.4	9.2	6.7	4.8

[a] Third digit in position number shows cracking level (i.e., 100 initial condition, 101 first cracking, and 102 second cracking).
[b] Measured on plate.
[c] Sensor location D_0 at center of plate, D_{12} at 12 in. from center of plate, and D_{24} at 24 in. from center of plate.

Table B16

Falling Weight Results, Slab 5, Position 300

Position[a]	Load[b] lb	Deflection, × 10^{-3} in.						
		D_0[c]	D_{12}[c]	D_{24}[c]	D_{36}[c]	D_{48}[c]	D_{60}[c]	D_{72}[c]
300	27,680	8.2	7.8	7.2	6.8	6.4	5.9	5.4
300	27,394	8.3	7.4	7.2	7.0	5.9	6.1	5.5
300	27,251	8.2	7.5	7.2	7.0	6.1	5.9	5.4
300	27,220	8.1	7.5	7.0	7.0	5.2	5.9	5.4
3,000	20,879	5.7	5.4	5.0	4.6	4.3	3.9	3.5
3,000	20,943	5.6	5.2	4.9	4.5	4.2	3.8	3.4
3,000	20,895	5.6	5.2	4.9	4.5	4.1	3.8	3.4
3,000	20,879	5.6	5.2	4.9	4.5	4.2	3.8	3.4
301	20,911	9.6	9.5	8.0	6.7	5.4	4.4	3.5
301	20,975	9.6	9.4	8.0	6.7	5.4	4.4	3.4
301	20,848	9.6	9.4	8.0	6.7	5.5	4.4	3.4
301	20,832	9.6	9.5	8.0	6.7	5.4	4.4	3.4
302	19,878	22.8	12.6	10.5	8.6	5.8	5.0	3.6
302	19,831	22.2	12.6	10.4	8.7	6	5.0	3.7
302	19,783	22.4	12.6	10.5	8.2	6.8	5.0	3.8
302	19,783	22.6	12.6	10.5	8.3	6.9	5.1	3.8
3,020	19,862	23.8	13.0	10.8	8.7	6.9	5.2	3.7
3,020	19,878	24.0	13.0	10.8	8.7	6.9	5.2	3.7
3,020	19,831	24.2	13.0	10.8	8.7	6.9	5.2	3.8
3,020	19,767	24.4	13.0	10.8	8.8	6.9	5.2	3.7
303	19,354	41.9	19.7	13.1	10.9	8.3	5.8	4.2
303	19,608	39.1	18.9	11.4	11.0	8.1	6.0	4.3
303	19,561	39.1	18.7	11.7	10.9	8.3	6.1	4.4
303	19,561	39.1	18.6	11.9	11.0	8.1	6.1	4.4

[a] Third digit in position number shows cracking level (i.e., 100 initial condition, 101 first cracking, and 102 second cracking).
[b] Measured on plate.
[c] Sensor location D_0 at center of plate, D_{12} at 12 in. from center of plate, and D_{24} at 24 in. from center of plate.

Table B17

Falling Weight Results, Slab 6, Position 100

Position[a]	Load[b] lb	Deflection, × 10^{-3} in.						
		D_0[c]	D_{12}[c]	D_{24}[c]	D_{36}[c]	D_{48}[c]	D_{60}[c]	D_{72}[c]
100	20,975	3.7	3.6	3.5	3.4	3.3	3.3	3.3
100	20,705	3.8	3.6	3.5	3.4	3.3	3.3	3.2
100	20,657	3.8	3.6	3.5	3.4	3.3	3.3	3.2
100	20,498	3.7	3.5	3.5	3.4	3.2	3.2	3.1
1,000	20,975	3.9	3.7	3.6	3.4	3.3	3.1	3.0
1,000	20,991	3.9	3.7	3.6	3.4	3.2	3.1	3.0
1,000	21,070	3.9	3.7	3.6	3.4	3.3	3.1	3.0
1,000	21,007	3.9	3.7	3.6	3.4	3.3	3.1	3.0
101	20,546	6.5	6.1	5.5	5.0	4.3	3.9	3.4
101	20,625	6.4	6.0	5.4	4.9	4.3	3.8	3.4
101	20,625	6.4	6.0	5.4	5.0	4.3	3.9	3.4
101	20,578	6.3	5.9	5.4	4.9	4.3	3.8	3.4
102	20,546	9.3	8.8	7.7	6.6	5.5	4.4	3.5
102	20,466	8.9	8.5	7.4	6.3	5.3	4.3	3.4
102	20,578	8.9	8.5	7.4	6.3	5.3	4.3	3.4
102	20,562	8.9	8.5	7.4	6.3	5.3	4.3	3.4
103	20,403	17.2	14.6	11.7	9.2	7.6	5.5	4.1
103	20,419	16.5	14.0	11.2	8.9	7.2	5.4	4.0
103	20,387	16.5	14.0	11.2	9.0	7.3	5.4	4.1
103	20,323	16.6	15.0	11.3	9.0	7.2	5.4	4.1

[a] Third digit in position number shows cracking level (i.e., 100 initial condition, 101 first cracking, and 102 second cracking).
[b] Measured on plate.
[c] Sensor location D_0 at center of plate, D_{12} at 12 in. from center of plate, and D_{24} at 24 in. from center of plate.

Table B18

Falling Weight Results, Slab 6, Position 200

Position[a]	Load[b] lb	Deflection, × 10^{-3} in.						
		D_0[c]	D_{12}[c]	D_{24}[c]	D_{36}[c]	D_{48}[c]	D_{60}[c]	D_{72}[c]
200	20,879	7.7	6.4	5.5	4.7	4.1	3.5	2.9
200	20,800	7.6	6.4	5.4	4.7	4.0	3.4	2.9
200	20,752	7.6	8.7	5.5	4.6	3.9	3.4	2.8
200	20,530	7.5	7.1	5.5	4.7	3.9	3.4	2.9
201	20,546	10.2	8.6	7.2	5.9	5.0	4.3	3.5
201	20,562	9.5	8.1	6.8	5.6	4.9	4.2	3.6
201	20,466	9.5	8.1	6.8	5.6	4.8	4.2	3.5
201	20,482	9.5	8.1	6.9	5.8	4.8	4.2	3.5
202	20,149	13.4	10.7	8.2	5.9	5.0	4.2	3.5
202	20,021	12.4	10.0	7.8	5.7	4.8	4.3	3.5
202	19,799	12.3	10.0	7.9	5.9	4.9	4.3	3.5
202	19,799	12.3	10.2	7.8	5.8	4.6	4.2	3.5
203	20,260	23.4	19.0	14.2	9.1	6.7	4.8	3.5
203	20,180	21.5	17.8	13.6	9.1	6.7	5.2	3.5
203	20,021	21.4	17.7	13.7	9.1	6.8	5.1	3.6
203	20,037	21.6	17.8	13.7	9.3	6.7	5.2	3.6

[a] Third digit in position number shows cracking level (i.e., 100 initial condition, 101 first cracking, and 102 second cracking).
[b] Measured on plate.
[c] Sensor location D_0 at center of plate, D_{12} at 12 in. from center of plate, and D_{24} at 24 in. from center of plate.

Table B19

Falling Weight Results, Slab 6, Position 300

Position[a]	Load[b] lb	Deflection, × 10^{-3} in.						
		D_0[c]	D_{12}[c]	D_{24}[c]	D_{36}[c]	D_{48}[c]	D_{60}[c]	D_{72}[c]
301	20,466	6.5	6.2	5.5	4.9	4.3	3.9	3.5
301	20,530	6.5	6.1	5.5	4.8	4.3	3.9	3.5
301	20,514	6.4	6.1	5.4	4.8	4.3	3.9	3.5
301	20,593	6.4	6.1	5.4	4.8	4.2	3.9	3.5
302	20,307	10.5	9.3	8.4	7.2	5.8	5.2	4.4
302	20,180	10.2	8.9	8.0	6.9	5.6	5.0	4.2
302	20,133	10.2	9.1	8.0	6.9	5.9	5.2	4.4
302	20,164	10.2	8.8	8.0	6.9	5.4	5.1	4.1
303	19,926	27.0	18.0	14.5	11.2	8.3	6.2	4.7
303	19,894	25.4	17.4	14.0	11.0	7.9	6.2	4.4
303	19,910	25.5	17.3	14.1	10.9	8.1	6.1	4.7
303	19,878	25.7	17.3	13.2	10.9	7.8	6.2	4.4

[a] Third digit in position number shows cracking level (i.e., 100 initial condition, 101 first cracking, and 102 second cracking).
[b] Measured on plate.
[c] Sensor location D_0 at center of plate, D_{12} at 12 in. from center of plate, and D_{24} at 24 in. from center of plate.

APPENDIX C

WESTERGAARD AND LAYERED ELASTIC STRESS CALCULATIONS

Table C1

Stresses Calculated From Corps of Engineers Test Sections[59]

Test	Item	Layered Elastic Stress, lb/in.^{2}	Westergaard Edge Stress, lb/in.^{2}
Lockbourne No. 1	A-1	405	836
	A-2	599	1,215
	B-1	504	1,035
	B-2	759	1,527
	C-1	558	1,051
	C-2	853	1,553
	D-1	572	1,035
	D-2	877	1,527
	E-1	505	907
	E-2	771	1,331
	F-1	396	700
	F-2	625	1,072
	K-3	570	973
	K-2	410	729
	N-2	564	945
	N-3	785	1,248
	O-2	458	759
	O-3	647	1,019
	P-2	632	961
	P-3	883	1,249
	Q-2	465	699
	Q-3	659	925
	U-2	527	1,091
	U-3	651	1,327
	A-Rec	390	601
Lockbourne No. 2	E-1	629	1,061
	E-2	574	961

(Continued)

Table C1 (Continued)

Test	Item	Layered Elastic Stress, lb/in.^{2}	Westergaard Edge Stress, lb/in.^{2}
	E-3	663	1,043
	E-4	642	943
	E-5	454	764
	E-6	397	673
	E-7	312	529
	M-1	600	959
	M-2	446	724
	M-3	295	485
Lockbourne No. 3	--	976	1,785
Sharonville Channelized	57	315	596
	58	373	692
	59	394	780
	60	416	872
	61	349	717
	62	274	571
Sharonville Heavy	71	249	479
	72	319	621
	73	401	780
MWHGL	1-C5	580	1,093
	2-C5	473	843
	3-C5	394	680
	4-C5	735	1,352
	2-D7	566	1,039
	3-D7	461	849
KLJS	1-C5	656	996
	2-C5	522	855
	3-C5	580	1,017
	4-C5	522	768
	4-D7	643	945

(Continued)

Table C1 (Concluded)

Test	Item	Layered Elastic Stress, lb/in.^{2}	Westergaard Edge Stress, lb/in.^{2}
SSPS	3-200	463	828
	3-240	564	993
	4-200	463	784
	4-240	555	941

Table C2

Calculated Westergaard and Layered Elastic Stresses for Different Aircraft and Subgrade Conditions

Aircraft	Subgrade k, lb/in.^{2}/in.[a]	Pavement Thickness, in.	Westergaard Stress, lb/in.^{2}	Layered Elastic Stress, lb/in.^{2}
B-707	50	6	3,123	1,420
	50	10	1,591	834
	50	30	322	187
	50	40	199	121
	200	6	2,125	714
	200	10	1,166	459
	200	30	257	129
	200	40	165	87
	400	6	1,758	499
	400	10	966	325
	400	30	228	101
	400	40	147	70
B-727	50	6	2,335	1,210
	50	10	1,150	639

(Continued)

[a] Value of subgrade E for layered elastic calculations estimated from k using relation of Parker et al.[59].

(Sheet 1 of 4)

Table C2 (Continued)

Aircraft	Subgrade k, lb/in.^{2}/in.	Pavement Thickness, in.	Westergaard Stress, lb/in.^{2}	Layered Elastic Stress, lb/in.^{2}
B-727	50	30	201	126
	50	40	122	79
	200	6	1,675	661
	200	10	866	399
	200	30	172	94
	200	40	106	61
	400	6	1,404	473
	400	10	740	296
	400	30	156	79
	400	40	98	52
B-747	50	6	2,774	1,510
	50	10	1,550	894
	50	30	329	207
	50	40	214	132
	200	6	1,843	791
	200	10	1,047	489

(Continued)

Table C2 (Continued)

Aircraft	Subgrade k, lb/in.^{2}/in.	Pavement Thickness, in.	Westergaard Stress, lb/in.^{2}	Layered Elastic Stress, lb/in.^{2}
B-747	200	30	261	140
	200	40	170	93
	400	6	1,511	586
	400	10	852	351
	400	30	225	109
	400	40	151	74
C-141	50	6	2,782	1,460
	50	10	1,497	850
	50	30	306	187
	50	40	194	120
	200	6	1,781	722
	200	10	1,041	471
	200	30	244	130
	200	40	160	88
	400	6	1,413	498
	400	10	842	331
	400	30	218	103
	400	40	142	71

(Continued)

Table C2 (Concluded)

Aircraft	Subgrade k, lb/in.^{2}/in.	Pavement Thickness, in.	Westergaard Stress, lb/in.^{2}	Layered Elastic Stress, lb/in.^{2}
F-4	50	6	1,377	898
	50	10	613	395
	50	30	90	54
	50	40	53	31
	200	6	1,091	653
	200	10	506	305
	200	30	82	44
	200	40	49	25
	400	6	958	535
	400	10	455	260
	400	30	78	39
	400	40	47	23

APPENDIX D

CORPS OF ENGINEERS RIGID OVERLAY TEST SECTION DATA

Table D1

Overlay Material Properties

Test Series	Test Item	Flexural Strength, lb/in.^{2}		Elastic Modulus × 10^6 lb/in.^{2}		Subgrade Elastic Modulus lb/in.^{2}
		Base	Overlay	Base	Overlay	
Lockbourne No. 1	A 2.7-60	740	760	3.8	3.8	16,000
	D 2.7-66	740	760	3.8	3.8	4,900[a]
	E 12.14-100	740	760	3.8	3.8	6,000[b]
	F 2.7-80	760	760	3.8	3.8	4,100
Lockbourne No. 2	F 12.14-100	735	735	4.0	4.0	16,880
	G 12.14-100	735	735	4.0	4.0	17,580
	L 14.14-80	735	735	4.0	4.0	26,500
	M 14.14-80	735	735	4.0	4.0	19,700
Sharonville	23	775	840	4.4	4.8	6,300-12,000
	24	775	840	4.4	4.8	4,800-12,000
	25	775	840	4.4	4.8	4,900-12,800
	26	775	840	4.4	4.8	5,100-12,800
	27	775	840	4.4	4.8	4,700-12,800
	28	775	840	4.4	4.8	3,800-12,800
Sharonville Heavy Load	69	615-770	710-825	4.4	4.4	9,600
	70	615-770	710-825	4.4	4.4	9,600

[a]Overlaid by a 6-in. base with an E of 10,000 lb/in.^{2}.
[b]Overlaid by a 6-in. base with an E of 18,000 lb/in.^{2}.

Table D2

Observed Field Deterioration Data

Item	Coverages	SCI
D 2.7-66	138	78
	712	45
E 2.7-66	138	100
	712	58
F 2.7-80	138	100
	712	58
F 12.14-100	10	71
	63	45
	1,000	11
	1,430	0
G 12.14-100	10	100
	370	100
	887	71
	1,430	50
L 14.14-80	5	58
	1,000	0
M 14.14-80	36	58
	807	0
69	180	85
	240	80
	2,750	60
	3,310	51
	3,750	42
	3,810	38
	3,940	31
	4,630	20

Table D3

Base Slab Stress Calculations for Unbonded Overlays

Item	Subgrade E, lb/in.^{2}	After Overlay		
		Stress, lb/in.^{2}	C_o	C_F
23	12,800	229	2×10^7	9×10^7
23	6,300	263	1.5×10^6	6.7×10^6
24	12,800	277	634,056	2.8×10^6
24	4,800	326	53,621	229,609
25	12,800	345	24,851	105,596
25	4,900	402	3,827	15,957
26	12,800	372	9,537	40,136
26	5,100	444	1,311	5,408
27	12,800	430	1,830	7,577
27	4,700	513	330	1,343
28	12,800	536	226	914
28	3,800	656	48	190
69[a]	9,600	335	2,228	9,242
69[b]	9,600	335	8,301	34,885

[a] Low flexural strength values used in analysis.
[b] Average flexural strength values used in analysis.

Table D4

Overlay Stress Calculations for Unbonded Overlays

Item	Subgrade E, lb/in.^{2}	Overlay Traffic Coverages	Base		Overlay		
			E-Ratio	E, lb/in.^{2}	Stress, lb/in.^{2}	C_O	C_F
23	12,800	0-2 × 10^7	1.000	4,400,000	373	25,687	109,178
23	6,300	0-1.5 × 10^6	1.000	4,400,000	405	9,032	37,991
24	12,800	0-634,056	1.000	4,400,000	357	46,473	198,712
24	4,800	0-53,621	1.000	4,400,000	395	12,296	51,877
25	12,800	0-24,851	1.000	4,400,000	340	92,751	399,356
		24,851-38,758	0.748	3,291,268	374	24,795	105,353
		38,758-51,764	0.525	2,310,980	413	7,134	29,934
		51,764-69,133	0.330	1,450,639	459	2,154	8,932
		69,133-105,596	0.161	710,245	518	633	2,593
		105,596+	0.020	89,800	649	96	385
25	4,900	0-3,827	1.000	4,400,000	370	28,596	121,678
		3,827-5,933	0.748	3,291,268	410	7,785	32,697
		5,933-7,894	0.525	2,310,980	456	2,312	9,593
		7,894-10,503	0.330	1,450,639	512	708	2,903
		10,503-15,957	0.161	710,249	588	204	825
		15,957+	0.020	89,800	760	31	121

(Continued)

Table D4 (Continued)

Item	Subgrade E, lb/in.^{2}	Overlay Traffic Coverages	Base E-Ratio	Base E, lb/in.^{2}	Overlay Stress$_2$ lb/in.^{2}	Overlay C_O	Overlay C_F
26	12,800	0-9,537	1.000	4,400,000	499	910	3,741
26	5,100	0-1,3112	1.000	4,400,000	517	310	1,260
27	12,800	0-1,830	1.000	4,400,000	437	3,701	15,429
		1,830-2,831	0.748	3,291,268	477	1,436	5,929
		2,831-3,762	0.525	2,310,980	521	599	2,454
		3,762-4,998	0.330	1,450,639	572	258	1,046
		4,998-7,557	0.161	710,245	636	108	435
		7,557+	0.020	89,800	777	26	105
27	4,700	0-330	1.000	4,400,000	486	1,186	4,886
		330-508	0.748	3,291,268	533	484	1,978
		508-672	0.525	2,310,980	587	207	837
		672-892	0.330	1,450,639	652	89	359
		892-1,343	0.161	710,245	738	37	147
		1,343+	0.020	89,800	933	9	36
28	12,800	0-226	1.000	4,400,000	318	253,128	1.1×10^6
		226-347	0.748	3,291,268	382	18,809	79,698
		347-459	0.525	2,310,980	467	1,792	7,416

(Continued)

Table D4 (Continued)

Item	Subgrade E, lb/in.^{2}	Overlay Traffic Coverages	Base E-Ratio	Base E, lb/in.^{2}	Overlay Stress$_2$ lb/in.^{2}	Overlay C_O	Overlay C_F
28		459-607	0.330	1,450,639	584	216	874
		607-914	0.161	710,245	760	31	121
		914+	0.020	89,800	1,170	3	12
28	3,800	0-48	1.000	4,400,000	343	81,694	351,304
		48-73	0.748	3,291,268	418	6,184	25,910
		73-96	0.525	2,310,980	518	633	2,593
		96-127	0.330	1,450,639	661	81	324
		127-190	0.161	710,245	884	12	48
		190+	0.020	89,800	1,460	1	5
69[a]	6,900	0-2,228	1.000	4,400,000	250	812,257	3.6×10^6
		2,228-3449	0.748	3,291,268	283	116,114	501,080
		3,449-4584	0.525	2,310,980	325	17,290	73,199
		4,584-6,093	0.330	1,450,639	377	2,945	12,249
		6,093-9,242	0.161	710,245	454	451	1,841
		9,242+	0.020	89,800	653	27	109
69[b]	9,600	0-8,301	1.000	4,400,000	250	3.3×10^6	14.8×10^6
		8,301-12,903	0.748	3,291,268	283	403,399	1.8×10^6

(Continued)

[a] Low flexural strength values used in analysis.
[b] Average flexural strength values used in analysis.

Table D4 (Concluded)

Item	Subgrade E, lb/in.^{2}	Overlay Traffic Coverages	Base		Overlay		
			E-Ratio	E, lb/in.^{2}	Stress$_2$ lb/in.^{2}	C_O	C_F
69[b]		12,903-17,193	0.525	2,310,980	325	51,139	218,876
		22,912-34,886	0.161	710,245	454	980	4,033
		34,886+	0.020	89,800	653	47	188

[a] Low flexural strength values used in analysis.
[b] Average flexural strength values used in analysis.

Table D5

Calculated Composite Unbonded Overlay Deterioration

Item	Subgrade E, lb/in.^{2}	Coverages	SCI	Remarks
23	12,800	25,687	100	Base did not crack
		109,178	0	
23	6,800	9,032	100	Base did not crack
		37,991	0	
24	12,800	46,473	100	Base did not crack
		198,712	0	
24	4,800	12,296	100	Base did not crack
		51,877	0	
25	12,800	40,426	100	--
		51,764	34	
25	4,900	55,162	0	
		7,357	100	--
26	12,800	7,894	85	
		9,926	0	
		910	100	Base did not crack
		3,791	0	
26	5,100	310	100	Base did not crack
		1,260	0	
26	12,800	2,556	100	--
		2,831	88	
		3,762	28	
		4,105	0	
27	4,700	609	100	--
		672	81	
		892	5	
		901	0	
28	12,800	615	100	--
		706	0	

(Continued)

Table D5 (Concluded)

Item	Subgrade E, lb/in.^{2}	Coverages	SCI	Remarks
28	3,800	134	.00	--
		170	0	
69[a]	9,600	6,297	100	--
		7,687	0	
69[b]	9,600	23,067	100	--
		26,128	0	

[a] Low flexural strength values used in analysis.
[b] Average flexural strength values used in analysis.

Table D6

Base Slab Stress Calculations for Partially Bonded Overlays

Item	Bond K Factor	Before Overlay					After Overlay		
		Stress, lb/in.^{2}	C_O	C_F	SCI	Equivalent Traffic	Stress, lb/in.^{2}	C_O	C_F
D 2.7-66	1,000	549	127	511	42	385	529	171	692
	750	549	127	511	42	403	526	179	725
	500	549	127	511	42	444	520	197	799
	250	549	127	511	42	570	505	253	1,026
	0	549	127	511	42	1,957	442	862	3,543
E 2.7-66	1,000	485	361	1,469	100	301	495	301	1,223
	750	485	361	1,469	100	317	492	317	1,391
	500	485	361	1,469	100	354	486	354	1,441
	250	485	361	1,469	100	462	472	462	1,884
F 2.7-80	1,000	381	4,164	17,379	100	27	519	200	812
	750	381	4,164	17,379	100	31	510	232	942
	500	381	4,164	17,379	100	40	495	301	1,223

Table D7

Overlay Stress Calculations for Partially Bonded Overlays

Item	Bond K Factor	Overlay Traffic Coverages	Base		Overlay		
			E-Ratio	E, lb/in.^{2}	Stress, lb/in.^{2}	C_O	C_F
D 2.7-66	1,000	0-70	0.330	1,252,824	596	83	332
		70-307	0.161	613,394	661	40	158
		307+	0.020	77,554	821	11	42
	750	0-74	0.330	1,252,824	565	125	503
		74-322	0.161	613,394	635	52	209
		322+	0.020	77,554	816	11	43
	500	0-81	0.330	1,252,824	519	251	1,020
		81-335	0.161	613,394	600	79	316
		335+	0.020	77,554	809	12	45
	250	0-104	0.330	1,252,824	443	1,100	4,528
		104-456	0.161	613,394	542	175	706
		456+	0.020	77,554	801	12	48
	0	0-362	0.330	1,252,824	248	3×10^6	13×10^6
		362-1,586	0.161	613,394	413	2,286	9,485
		1,586+	0.020	77,554	790	13	52
E 2.7-66	1,000	0-157	0.748	2,842,459	468	642	2,629
		157-306	0.525	1,995,846	506	314	1,275

(Continued)

Table D7 (Continued)

Item	Bond K Factor	Overlay Traffic Coverages	Base		Overlay		
			E-Ratio	E, lb/in.^{2}	Stress, lb/in.^{2}	C_O	C_F
E 2.7-66		306-502	0.330	1,252,824	552	150	607
		502-922	0.161	613,394	614	66	266
		922+	0.020	77,554	768	15	61
	750	0-166	0.748	2,842,459	437	1,263	5,208
		166-323	0.525	1,995,846	476	547	2,236
		323-530	0.330	1,252,824	523	235	955
		530-974	0.161	613,394	590	89	359
		974+	0.020	77,554	763	16	63
E 2.7-66	500	0-185	0.748	2,842,459	391	4,201	17,532
		185-360	0.525	1,995,846	430	1,491	6,160
		360-592	0.330	1,252,824	480	506	2,066
		592-1,087	0.161	613,394	555	144	581
		1,087+	0.020	77,5542	756	17	67
	250	0-242	0.748	842,459	310	82,968	356,836
		242-471	0.525	1,995,846	351	15,430	65,251
		471-774	0.330	1,252,824	407	2,681	11,142
		774-1,423	0.161	613,394	499	355	1,445
		1,423+	0.020	77,554	748	18	71

(Continued)

Table D7 (Concluded)

Item	Bond K Factor	Overlay Traffic Coverages	Base		Overlay		
			E-Ratio	E, lb/in.^{2}	Stress, lb/in.^{2}	C_O	C_F
F 2.7-80	1,000	0-174	1.000	3,800,000	322	48,511	207,517
		174-278	0.748	2,842,459	367	8,863	37,270
		278-377	0.525	1,995,846	420	1,910	7,907
		377-507	0.330	1,252,824	488	434	1,771
		507-785	0.161	613,394	586	94	378
		785+	0.020	77,554	817	11	43
F 2.7-80	750	0-202	1.000	3,800,000	293	191,327	115,815
		202-323	0.748	2,842,459	336	27,225	115,786
		323-437	0.525	1,995,846	388	4,588	19,167
		437-588	0.330	1,252,824	455	843	3,462
		588-911	0.161	613,394	554	146	589
		911+	0.020	77,554	809	12	45
	500	0-261	1.000	3,800,000	251	2.4×10^6	10.0×10^6
		261-418	0.748	2,842,459	291	212,449	922,393
		418-567	0.525	1,995,846	341	22,406	95,104
		567-763	0.330	1,252,824	407	2,681	11,142
		763-1,183	0.161	613,394	511	288	1,169
		1,183+	0.020	77,554	798	12	49

Table D8

Calculated Composite Partially Bonded Overlay Deterioration

Item	Bond K Factor	Coverages	SCI
D 2.7-66	1,000	76	100
		194	0
	750	95	100
		252	0
	500	134	100
		355	4
		357	0
	250	262	100
		456	46
		479	0
	0	1,592	100
		1,631	0
E 2.7-66	1,000	362	200
		502	53
		640	0
	750	481	100
		530	86
		781	0
	500	661	100
		1,087	1
		1,088	0
	250	1,088	100
		1,423	53
		1,460	0
F 2.7-80	1,000	571	100
		785	15
		793	0

(Continued)

Table D8 (Concluded)

Item	Bond K Factor	Coverages	SCI
F 2.7-80	750	707	100
		911	37
		929	0
		1,029	100
		1,183	69
		1,213	0